Electrochemical and corrosion behavior of electrodeposited Zn, Zn-Ni alloy and Zn-Ni-TiO_2 composite coatings

by

©Shams Anwar

A thesis submitted to the School of Graduate Studies
in partial fulfillment of the requirements for the degree of

Doctor of Philosophy (Ph.D.) in Oil and Gas Engineering

Faculty of Engineering & Applied Science
Memorial University of Newfoundland

October 2020

St. John's, Newfoundland and Labrador, Canada

ABSTRACT

Corrosion is one of the main causes of structural deterioration in process industries. It often causes process equipment failure and ruptures, which lead to severe safety problems, such as environmental pollution or even fatalities. To address this problem, one approach is to provide a preventive barrier-coating. This thesis investigates the electrochemical and corrosion behavior of the electrodeposited zinc, zinc-nickel alloys, and zinc-nickel-oxide composites. The negative reduction potential of Zn/Zn^{2+} electrode offer significant challenge to be electroplated. It also has high propensity liberate hydrogen gas. The complexation of zinc and nickel ions by complexing agent (ammonium citrate, potassium citrate and ethylene-diamine-tetra-acetic acid (EDTA)) stabilized the bath, which can extend the pH of nickel hydroxide and zinc oxide for electroplating purposes. The systematic design of the Zn-Ni alloy electroplating has been conducted using a five-variable experimental plan comprised of four steps: (1) a two-level fractional factorial design (FFD), (2) a response surface design the steepest ascent analysis, (3) a central composite design (CCD), and (4) corrosion behaviour test to optimize the factors in Zn-Ni deposition. After design of experiment, the optimum conditions were found to be a Zn/Ni molar concentration ratio 0.66, a plating temperature of 28^0C, an electroplating current density of $60mA/cm^2$, an electroplating time of 13 minutes, and a citrate concentration of 0.062 mol/l. From the corrosion behaviour test of step-4 was found that the films with higher intensity of γ-$NiZn_3$, γ-Ni_2Zn_{11}, and γ-Ni_3Zn_{22} phases exhibited better corrosion resistance. The pure Zn, Zn-Ni alloy and Zn-Ni-nanoTiO_2 composite electroplated samples were deposited from citrate and non-citrate bath under the various level of deposition conditions from baths containing potassium and ammonium citrate were studied. Zn-Ni deposit obtained at $60mA/cm^2$ from citrate bath exhibited lower corrosion current (I_{corr}), and less negative corrosion potential (E_{corr}) compared to pure Zn and Zn-Ni alloy coatings from the non-citrate bath. Crystallite size of Zn-Ni coating deposited from citrate bath is 35.40 nm, and Ni content

of the coating is 8.3 wt%. Zn-Ni films with smaller grain size with uniform coating had increased impedance modulus and improved corrosion resistance. The electrochemical behavior of samples shown that Zn-Ni alloy with the incorporation of 0.003 mol/l of Titania (TiO_2) nanoparticles exhibited noble E_{corr} and less I_{corr} values led to increasing impedance modulus with a less coarse, compact and stronger uniform coating of 25.84 nm grain size. The chemical composition result showed that the Zn-Ni-0.003 mol/l of TiO_2 coating electrodeposited from citrate bath at various immersion tests reduced dezincification in the coating. The most significant anticorrosion products for Zn-Ni alloy electroplating are simonkolleite, hydrozincite, zincite, and wulfingite.

Additionally, Zn-Ni alloy deposited from a chloride bath containing EDTA was also investigated in this study. Polarization tests demonstrated that the Zn-Ni alloy deposited from 0.119 mol/l of EDTA bath at 20mA/cm^2 current density exhibited lower I_{corr} and more positive E_{corr} values. At 24 hours of immersion time, the samples exhibit higher corrosion resistance leads to the formation of stronger anticorrosion layers.

Finally, the pitting corrosion behavior of Zn-Ni alloy coatings in NaCl solutions with different chloride concentrations and pH were investigated. The pitting behavior in acidic solution with low chloride concentration was found to be significantly different from that in the neutral solution with high chloride concentration. Electrochemical analysis indicates that the corrosion behavior of the samples immersed at 0.35 mol/l of NaCl and pH = 3.0 have low impedance values in comparison to the samples immersed at 0.35 mol/l of NaCl and pH = 7.0 samples. Exclusive large pit morphology due to corrosion in acidic (pH 3.0) and low chloride concentration (0.35 mol/l) was observed.

The comprehensive experimental study developed the processes for enhancing the corrosion resistant and mechanical properties of the Zn, Zn-Ni alloy and Zn-Ni-TiO_2 composite coatings and investigate the stability of the electroplating baths.

ACKNOWLEDGEMENT

In the name of Allah, the Most Beneficent and the Most Merciful. All praise be to Allah alone, the Sustainer of all the worlds, most Compassionate, ever Merciful, and I send salutations upon His noble prophet Muhammad peace be upon him.

I could not have accomplished this work as presented here had it not been for the expert support and constant encouragement from my supervisors Dr. Faisal Khan, Dr. Yahui Zhang and Dr. Susan Caines. Their enormous research experience and knowledge have brought me to think seriously on the problem I have taken up in this thesis. Also, their diverse interests helped me think over a problem with different perspectives. I would always remember the way they guided me through all this process. It has been a pleasure working under their supervision.

I would also like to thank all of my fellow colleagues at Centre for Risk Integrity and Safety Engineering (C-RISE) at Memorial University of Newfoundland, for their valuable help and suggestions for improving this work. Thanks to the Natural Science and Engineering Council of Canada (NSERC) and the Canada Research Chair (CRC) Tier I Program for their financial support. Thanks to Dr. John Shirokoff, Dr. Erika Merschrod, Dr. Wanda Aylward, Dr. David Grant and Steve Steel for giving me an opportunity to work in their labs and use their laboratory equipments.

In the last, I would like to extend my deepest and sincere thanks to my elders, my father, my mother, and sisters for their moral support. I know without their love, conviction and prayers I would never be able to perform this scholarly activity.

Table of Contents

List of Figures

List of Tables

Authorship Statement

This thesis is a manuscript format thesis. Each chapter of the thesis is either published or submitted in a peer-reviewed relevant journal. The full bibliographic citation and contributions of the authors in each paper are presented below:

Chapter-3

Shams Anwar, Yahui Zhang, Faisal Khan*, Susan Caines *(2019)* "Optimization of Zinc-Nickel Film Electrodeposition for Better Corrosion Resistant Characteristics**"** Canadian Journal of Chemical Engineering, 1–14, 2019.

The first author (Shams Anwar) did the experiments, analyzed the experimental results and wrote the first draft of the manuscript. Co-authors, Drs. Khan and Zhang conceptualize the problem, provided financial and technical support in conducting the experiments and helped in analyzing the data and also helped in revising the manuscript. Dr. Susan Caines, the co-author, provided technical guidance and also provided valuable feedback in improving the manuscript. She also assisted in analyzing the data. All co-authors reviewed the final version of the manuscript and approved its submission. Dr. David Grant assisted in conducting the scanning electron microscopy (SEM) and energy dispersive spectroscopy (EDS) of the Zn-Ni samples. Dr. Wanda Aylward helped in the x-ray diffraction methods.

Chapter-4

Shams Anwar, Yahui Zhang, Faisal Khan*_(2018)_ "Electrochemical Behaviour and Analysis of Zn and Zn-Ni Alloy Anti-corrosive coatings Deposited from Citrate Baths" RSC advance, 28861-28873, 8, 2018.

The first author (Shams Anwar) conducted the experiments, collected relevant data, analyzed the, and wrote the first draft of the manuscript. Coauthors, Drs. Faisal Khan and Yahui Zhang, conceptualize the problem, provided financial and technical support in conducting the experiments, helped in analyzing the data and also helped in revising the manuscript. Dr. David Grant assisted in conducting the scanning electron microscopy (SEM) and energy dispersive spectroscopy (EDS) of the Zn-Ni samples. Dr. Wanda Aylward helped in the x-ray diffraction methods. Dr. Erika Merschrod assisted in conducting the atomic force microscopy (AFM) of the coated and uncoated samples.

Chapter-5

Shams Anwar, Yahui Zhang, Faisal Khan* *(2020)* "EDTA stabilized bath for electrodeposition of Zn-Ni alloy coatings and corrosion resistant analysis in 3.5 wt.% NaCl solutions" Materials Today Proceedings, 28, 532-537, 2020

The first author (Shams Anwar) conducted the experiments, collected relevant data, analyzed the, and wrote the first draft of the manuscript. Co-authors, Drs. Faisal Khan and Yahui Zhang, conceptualize the problem, provided financial and technical support in conducting the experiments, helped in analyzing the data and also helped in revising the manuscript. Dr. David Grant assisted in conducting the scanning electron microscopy (SEM) and energy dispersive spectroscopy (EDS) of the Zn-Ni samples. Dr. Wanda Aylward helped in the x- ray diffraction methods. Dr. Erika Merschrod helped in conducting the atomic force microscopy (AFM) of the coated and uncoated samples.

Chapter-6

Shams Anwar, Yahui Zhang, Faisal Khan* *(2020)* "Electrodeposition of Zn-Ni alloy and Zn-Ni-TiO_2 nano-composite corrosion resistance coatings from ammonium citrate stabilize baths" is published in Process Safety and Environmental Protection, 141, 366-379, 2020.

The first author (Shams Anwar) conducted the experiments, collected relevant data, analyzed the, and wrote the first draft of the manuscript. Co-authors, Drs. Faisal Khan and Yahui Zhang, conceptualize the problem, provided financial and technical support in conducting the experiments, helped in analyzing the data and also helped in revising the manuscript. Dr. David Grant assisted in conducting the scanning electron microscopy (SEM) and energy dispersive spectroscopy (EDS) of the Zn-Ni samples. Dr. Wanda Aylward helped in the x- ray diffraction methods. Dr. Erika Merschrod helped in conducting the atomic force microscopy (AFM) of the coated and uncoated samples.

Chapter-7

Shams Anwar, Faisal Khan*, Susan Caines, Yahui Zhang *(2020)* "Effect of chloride and pH the micro-mechanism of Zn-Ni alloy pitting corrosion in NaCl Solution" is published in Canadian Journal of Chemical Engineering

The first author (Shams Anwar) did the experiments, analyzed the experimental results and wrote the first draft of the manuscript. Co-authors, Drs. Khan and Zhang conceptualize the problem, provided financial and technical support in conducting the experiments and helped in analyzing the data and also helped in revising the manuscript. Dr. Susan Caines, coauthor, provided technical guidance and also provided valuable feedback in improving the manuscript. She also assisted in analyzing the data. All coauthors reviewed the final version of the

manuscript and approved its submission. Dr. David Grant assisted in conducting the scanning electron microscopy (SEM) and energy dispersive spectroscopy (EDS) of the Zn-Ni sample.

1.0 INTRODCUCTION

1.1 General Background

There are several mechanisms for structural damage in process equipment/components during the operative lifespan. Corrosion is the most common destruction mechanism in the process industries resulted in metal loss, cracks, localized corrosion, and degradation of material properties [1][2]. Corrosion is a common issue which leads to the cracking and rupturing of the pipelines, equipment, and platforms[3]. In offshore oil and gas production and transportation, fabricated steels are the most used materials to construct the platforms, pipelines, and marine structures, which have a high possibility of severe hazardous incidents because of corrosion. One of the most reliable and industrial transporting procedures to transfer crude oils is the subsea pipeline. However, it has a chance of leakage and rupture due to internal and external pipe corrosion[4]. According to the statistics of the World Corrosion Organization (WCO), the global annual cost of corrosion is around $US 2.4 trillion (3% of the world's GDP)[5].

The significant factors affecting the corrosion of offshore and marine steel machinery or industries are summarized in Table 1.1 [6][7][8][9]. They are classified into three different categories: (1) Physical factors (2) Chemical factors and (3) Biological factors.

Table 1.1. Factors affecting corrosion in offshore and marine environments

Physical Factors	**Chemical Factors**	**Biological Factors**
Temperature	pH	Fouling
Strong velocity	Salinity	Bacterial growth
Suspended Silt	Dissolved oxygen	Oxygen consumption
Air bubbles	Carbon dioxide	Biomass
Pressure depth	Hydroxide ions	Oxygen generation
Surface wetting	Halogen ions	Pollutants

Humidity	Sulphur dioxide	Carbon dioxide consumption
Atmospheric Condition	Carbonate solubility	
Sample thickness	Water hardness	
Duration of exposure	Chemical equilibrium	
Total dissolved solid (TDS)		

Corrosion can give rise to severe safety problems or even disasters in commercial practices. Some major offshore and marine process industries accidents caused by corrosion are summarized in Table 1.2 [10] [11][12] [13].

Table 1.2. The major accidents reported due to corrosion

Accident name and place	**Types of corrosion**	**Date**	**Killed/ Injured**	**Descriptions**
Ekofisk Norway (Weld Failure, Offshore Platform)	**Corrosion**	**March 27, 1980**	**123 killed**	The broken bracing leads to broke other five bracing due to overload and the vertical column connected with the cracked bracings became separated from the platform. The inquiry revealed that the *corrosion* caused a fatigue crack that had propagated from the second fillet near the hydrophone mounted to one of the horizontal bracings.
Norco Louisiana-US	**Erosion-Corrosion**	**May 5, 1988**	**4 killed, 20 injured, 4500 evacuated**	The elbow failed at de-propanizer column piping system in a fluid catalytic cracking (FCC) unit due to *corrosion*. The most severe damage was the exploded FCC unit. Loss of **USD 254,700,000/336,000,000.**
Umm Said Qatar (Weld Failure, Gas Processing Plant)	**Corrosion**	**April 3, 1997**	**3 killed**	A refrigerated propane tank containing 236,000 barrels of C_3H_8 at 7.2^0C is ruptured at the weld due to *corrosion*. It took one week

				to completely extinguish and discontinue the fire. Loss of **USD 76,350,000/179,000,000.**
Martinez California US	**Corrosion**	**February 23, 1999**	**4 killed, 1 injured**	The origination of leakage and fire occurred from a heat exchanger. The fin-fan cooler of heat transfer tube was *corroded*. Corrosion was caused by insufficient re-design of heat exchanger changing service.
Mina Al-Ahmadi Kuwait Refinery	**Erosion-Corrosion**	**June 25, 2000**	**5 killed, 50 injured**	A condensate line failed, between an NGL plant and refinery. The failed pipe was an old pipe that deteriorated due to erosion-*corrosion* and lack of regular inspection and maintenance. **Loss of USD 412,000,000/ 433,000,000.**
Carlsbad New Mexico US	**Pitting-Corrosion**	**August 19, 2000**	**12 killed**	A 50-years old natural gas transmission pipeline ruptured. The investigation reported that pitting *corrosion* was the main cause for failure. The pipeline operator was fined USD 15,500,000 for legal fines and USD 86,000,000 for pipeline modifications. **Loss of USD 100,000,000.**
Mihama Japan, Power Plant	**Erosion-Corrosion**	**August 9, 2004**	**6 killed, 5 injured**	The steam of pressurized water reactor (PWR) exploded due to failed piping system. The pipe section ruptured due to *localized metal loss* in the cross-sectional area of the piping. Unfortunately, the pipe thickness was not checked for 27 years due to oversights.

A number of corrosion protection methods have been implemented to improve the life span of steel structures/machinery against corrosion and rusting[14]. The anti-corrosion coating is a common and effective approach for preventing the steel structures from corrosion. Electrodeposition is one of the most widely applied technologies for the fabrication of corrosion resistant metallic coatings due to high technological feasibility and economic viability. The thin layer of coating can provide a reasonable barrier between the steels and exposure environment. Due to its high reductive property, zinc is employed as a sacrifice anode in conventional corrosion-resistant methods[15]. One of the ways to improve the corrosion resistant properties of zinc coating is to make alloying with Fe, Cu and Ni. According to the literature[15][16], zinc alloy coatings such as Zn-Ni, Zn-Cu and Zn-Fe alloy films are often used to provide excellent corrosion resistance and maintain strong mechanical properties for steel equipment. They have better corrosion resistance compared to pure zinc coating[15][16]. An alternate process to increase more corrosion resistant property of the zinc and nickel coating to introduce Zn-Ni composite coating in which Zn-Ni incorporated with TiO_2[55][56][57], Al_2O_3[58], ZrO_2[59], SiO_2[60][61], Fe_2O_3[62][63][64] and SiC[65] to further enhance the corrosion resistance and mechanical properties of the coating[19][66][67][68][69]. The inclusions of composite materials have to increase various properties of the alloy coatings such as dispersion hardening, high-temperature oxidation resistance, self-lubricity, wear resistance and corrosion resistance[17][18]. Therefore, the coatings of zinc, zinc-nickel alloys, and zinc-nickel-oxide composites are commonly employed for anti-corrosion purposes[18][19]. The most preferred metallic coating method is the electrodeposition, and it is one of the most technologically feasible, economically viable and widely applied technology for the fabrication of corrosion resistant metallic coatings.

1.2 Problem Statement and Purpose of Investigation

A main sources of structural deterioration, equipment failure and safety problems in offshore and marine systems is corrosion [20][21]. Anti-corrosion electroplating is a practical approach for protecting steel structures/machinery against corrosion [21]. Zinc-nickel alloy coatings are extensively employed in anti-corrosion purposes. Electrodeposition is one of the most widely applied technologies for the fabrication of corrosion resistant metallic coatings due to high technological feasibility and economic viability [22][23]. The electrodeposition of zinc and zinc alloy has been extensively used to reduce corrosion attack on steel. Recently, Zn-Ni alloy coating has increased in interest compared to pure Zn coating [24][16]. Pure zinc coating are unsatisfactory because they have the lowest anti-corrosion property to protect steel, and the plated surface achieved by the zinc coating is unacceptable under severe atmospheric corrosion conditions [25]. The challenge in electroplating is to develop stable electrolytes to deposit a Zn-Ni coating on steel. The application of zinc and its alloy for providing better anti-corrosion property to the steel structures has been growing globally as an alternative to toxic and costly cadmium coatings [26].

An alternate process to increase corrosion resistance of the zinc and nickel coating is to introduce Zn-Ni composite coating. The inclusions of composite materials increase various properties of the alloy coatings such as dispersal toughening, high-temperature oxidation resistance, self-lubricity, wear and corrosion resistance [17][18]. The literature confirm the successful co-deposition of TiO_2, Al_2O_3, ZrO_2, SiO_2, Fe_2O_3 and SiC to enhance corrosion resistance and mechanical properties of the Zn-Ni alloy coating [18][27][23][28]. The incorporation of composite materials on the Zn-Ni surface refine the crystal size and shape, and increase the corrosion resistance, micro hardness and wear resistance property. Among the composite nanomaterials, titanium dioxide (TiO_2) for the generation of composite coatings has

received the most attention. Successful results have been reported on the co-deposition of TiO_2 with Ni, Cu, Zn and Ag metals [17]. Incorporation of TiO_2 enhances the hardness, wear and corrosion resistance property of the coatings [29].

1.3 Current state of the knowledge and the gaps

After a comprehensive review on the Zn, Zn-Ni alloy and Zn-Ni nano-composite anti-corrosion coating. The current electroplated alloy and composite samples has some weakness. These weaknesses are: (1) The electroplated baths are not stable to coat uniform coating. (2) No systematic design of experiment study was found for Zn-Ni alloy deposited from a citrate and EDTA baths, that includes optimum parameter conditions and hydrogen evolution reaction (HER) suppression to improve corrosion resistant properties of the coating. (3) There is no systematic study specifically for comparing Zn-Ni alloy and Zn-Ni-TiO_2 deposited from citrate bath, optimum TiO_2 (titania) concentration. (4) The study of corrosion and pitting mechanism of Zn-Ni and Zn-Ni-TiO_2 samples is not observed by the short-time lab scale Atlantic Ocean seawater immersion tests, and the electrochemical measurements analysis is tested. (5) There is no study on main corrosion products for Zn-Ni alloy coatings immersed in the short-time lab scale Atlantic Ocean seawater.

The current study is not an attempt to address all the gaps and recommendations, but to contribute significant knowledge to this area of research.

1.4 Objectives

The objectives of this research are:

i) To examine the stability of Zn, Zn-Ni and Zn-Ni nano-composite plating baths and suppression of hydrogen evolution reaction (HER).

ii) To conduct design of experiment study to identify best conditions for Zn-Ni alloy deposition and also the best complexing agent.

iii) To study the effects of plating variables such as bath composition, cathodic current density, morphological texture and anti-corrosion property for better corrosion resistance Zn-Ni applications.

iv) To study the effect of chloride concentration and pH on the Zn-Ni pitting corrosion in the NaCl solution.

v) To Analyze the corrosion resistance behavior by the chemical composition, phase formation, and microstructure (including surface morphology, grain size, coating thickness and density) of the deposited film and identify the main factors controlling the corrosion resistant properties of Zn-Ni and Zn-Ni-TiO_2 films.

1.5 Thesis Format

The research work presented in this thesis has been published or submitted to peer-reviewed journal.

An outline of each chapters is presented below:

Chapter-1 highlights the significant factors affecting the corrosion and process industries accidents due to the corrosion. This chapter also discussed the primary information about the development and application of Zn, Zn-Ni alloy and Zn-Ni composite coatings and the objectives of the research work.

Chapter-2 provides a detailed literature review related to the present work. The intention of the review is to deliver information on the coating process and characteristics, morphology, electrochemical analysis, corrosion behaviour, mechanical properties, pitting corrosion behaviour and suppression of hydrogen evolution reactions. This literature review is followed by six chapters containing the journal articles (four published and two under submission).

Chapter-3 presents an article published in the *Canadian Journal of Chemical Engineering,* entitled **"Optimization of Zinc-Nickel film electrodeposition for better corrosion resistant characteristics**". This paper comprised the extensive experimental design and optimization procedures for Zn-Ni alloy electroplating. The conditions were found to be a Zn/Ni molar concentration ratio 0.66, a plating temperature of 28^0C, an electroplating current density of 60mA/cm^2, an electroplating time of 13 minutes, and a citrate concentration of 0.062 mol/l.

Chapter-4 presents an article published in the *RSC advance*, entitled **"Electrochemical behavior and analysis of Zn and Zn-Ni alloy anti-corrosive coatings deposited from citrate baths"**. In this chapter the effects of plating variables such as bath composition, pH and current density on the coating composition, morphology, corrosion and mechanical property were systematically investigated. The stability of the electroplating bath studied through a stability diagram or Pourbaix diagram. Electrochemical behavior of the deposition bath on steel plates were studied by cyclic voltammetry (CV). Potentiodynamic polarization measurement (Tafel) and EIS were carried out to evaluate the corrosion protection performance of the Zn-Ni alloy coatings.

Chapter-5 presents an article published in the *Materials Today Proceedings* entitled with entitled **"EDTA stabilized bath for electrodeposition of Zn-Ni alloy coatings and corrosion resistant analysis in 3.5 wt.% NaCl solutions"**. In this work, the electrodeposition of Zn-Ni alloy film on steel substrate from a chloride bath containing ethylene-diamine-tetra-acetic acid (EDTA) was investigated in this study. The immersion test including the electrochemical analysis has been performed to find the better corrosion resistant performance of the coated samples.

Chapter-6 presents an article published in the *Process safety and Environmental Protection* with entitled "**Electrodeposition of Zn-Ni alloy and Zn-Ni-TiO_2 nano-composite corrosion**

resistance coatings from ammonium citrate stabilize bath". This research work prepared the Zn-Ni-nanoTiO_2 composite coatings and examined the electrochemical and corrosion behavior analysis of the coated samples. The study also analyzes the most significant corrosion products for Zn-Ni alloy electroplating are simonkolleite, hydrozincite, zincite, and wulfingite.

Chapter-7 presents an article published in the *Canadian Journal of Chemical Engineering* with entitled **"Effect of chloride and pH the micro-mechanism of Zn-Ni alloy pitting corrosion in NaCl solution**". In this work the pitting corrosion behavior of Zn-Ni alloy coatings in NaCl solutions with different chloride concentrations and pH were investigated using an optical microscope, potentiodynamic polarization (Tafel slopes), electrochemical impedance spectroscopy (EIS) and scanning electron microscopy (SEM) integrated with energy dispersive spectroscopy (EDS).

Chapter-8 presents the conclusions of this work and the contribution to the original knowledge respectively.

References

[1] M. Khalifa, F. Khan, and M. Haddara, "Inspection sampling of pitting corrosion," *Insight Non-Destructive Test. Cond. Monit.*, vol. 55, no. 6, pp. 290–296, 2013.

[2] M. Khalifa, F. Khan, and M. Haddara, "A methodology for calculating sample size to assess localized corrosion of process components," *J. Loss Prev. Process Ind.*, vol. 25, no. 1, pp. 70–80, 2012.

[3] M. G. Stewart and A. Al-Harthy, "Pitting corrosion and structural reliability of corroding RC structures: Experimental data and probabilistic analysis," *Reliab. Eng. Syst. Saf.*, vol. 93, no. 3, pp. 373–382, 2008.

[4] Y. Yang, F. Khan, P. Thodi, and R. Abbassi, "Corrosion induced failure analysis of subsea pipelines," *Reliab. Eng. Syst. Saf.*, vol. 159, no. November 2016, pp. 214–222, 2017.

[5] J. C. Velázquez, J. A. M. Van Der Weide, E. Hernández, and H. H. Hernández, "Statistical modelling of pitting corrosion: Extrapolation of the maximum pit depth-growth," *Int. J. Electrochem. Sci.*, vol. 9, no. 8, pp. 4129–4143, 2014.

[6] M. Schumacher, *Seawater corrosion handbook/edited by M. Schumacher*. 1979.

[7] M. P. Ryan, D. E. Williams, R. J. Chater, B. M. Hutton, and D. S. McPhail, *Why stainless steel corrodes*, vol. 415, no. 6873. 2002.

[8] S. Ahmad and A. U. Malik, "Corrosion behavior of some conventional and high alloy stainless steels in gulf seawater," *J. Appl. Electrochem.*, vol. 31, pp. 1009–1016, 2001.

[9] M. Ahammed and R. E. Melchers, "Probabilistic analysis of underground pipelines subject to combined stresses and corrosion," *Eng. Struct.*, vol. 19, no. 12, pp. 988–994, 1997.

[10] M. H. Wood, A. L. Vetere Arellano, and L. Van Wijk, *Corrosion - Related Accidents in*

Petroleum Refineries. 2013.

[11] A. Mcgillivray, J. Hare, and H. Hill, "Offshore hydrocarbon releases Offshore hydrocarbon releases 2001-2008," 2008.

[12] A. International, *Friction, Lubrication, and Wear Technology*. ASM Handbook, 1992.

[13] A. International, *Standard Guide for Examination and Evaluation of Pitting Corrosion*. 2005.

[14] O. S. I. Fayomi and A. P. I. Popoola, "An Investigation of the Properties of Zn Coated Mild Steel," *Int. J. Electrochem. Sci*, vol. 7, pp. 6555–6570, 2012.

[15] R. Fratesi, G. Roventi, G. Giuliani, and C. R. Tomachuk, "Zinc-cobalt alloy electrodeposition from chloride baths," *J. Appl. Electrochem.*, vol. 27, no. 9, pp. 1088–1094, 1997.

[16] I. H. Karahan and H. S. Güder, "Electrodeposition and properties of Zn, Zn–Ni, Zn–Fe and Zn–Fe–Ni alloys from acidic chloride–sulphate electrolytes," *Trans. IMF*, vol. 87, no. 3, pp. 155–158, 2009.

[17] S. Myagmarjav *et al.*, "Characterization of the Ni-Zn/TiO_2 Nanocomposite Synthesized by the Liquid-Phase Selective-Deposition Method," *Mater. Trans.*, vol. 45, no. 7, pp. 2035–2038, 2004.

[18] J. Fustes, A. Gomes, and M. I. Da Silva Pereira, "Electrodeposition of Zn-TiO_2 nanocomposite films-effect of bath composition," *J. Solid State Electrochem.*, vol. 12, no. 11, pp. 1435–1443, 2008.

[19] M. M. Momeni, S. Hashmizadeh, M. Mirhosseini, A. Kazempour, and S. A. Hosseinizadeh, "Preparation, characterisation, hardness and antibacterial properties of Zn–Ni–TiO2 nanocomposites coatings," *Surf. Eng.*, vol. 32, no. 7, pp. 490–494, 2016.

[20] M. Shourgeshty, M. Aliofkhazraei, and A. Karimzadeh, "Study on functionally graded

Zn–Ni–Al_2O_3 coatings fabricated by pulse-electrodeposition," *Surf. Eng.*, vol. 35, no. 2, pp. 167–176, 2019.

[21] K. Vathsala and T. V. Venkatesha, "Zn-ZrO_2 nanocomposite coatings: Elecrodeposition and evaluation of corrosion resistance," *Appl. Surf. Sci.*, vol. 257, no. 21, pp. 8929–8936, 2011.

[22] N. Lotfi, M. Aliofkhazraei, H. Rahmani, and G. B. Darband, *Zinc–Nickel Alloy Electrodeposition: Characterization, Properties, Multilayers and Composites*, vol. 54, no. 6. 2018.

[23] O. Hammami, L. Dhouibi, P. Berçot, E. M. Rezrazi, and E. Triki, "Study of Zn-Ni alloy coatings modified by Nano-SiOparticles incorporation," *Int. J. Corros.*, vol. 2012, 2012.

[24] C. M. Kumar, P. Kumar, T. V. Venkatesha, K. Vathsala, and K. O. Nayana, "Electrodeposition and corrosion behavior of Zn-Ni and Zn-Ni-Fe2O3coatings," *J. Coatings Technol. Res.*, vol. 9, no. 1, pp. 71–77, 2012.

[25] T. Jin, F. mei Kong, R. qin Bai, and R. liang Zhang, "Anti-corrosion mechanism of epoxy-resin and different content Fe_2O_3 coatings on magnesium alloy," *Front. Mater. Sci.*, vol. 10, no. 4, pp. 367–374, 2016.

[26] R. Winand *et al.*, "Electrodeposition and corrosion behavior of Zn-Ni and Zn-Ni-Fe2O3coatings," *Electrochim. Acta*, vol. 20, no. 3, pp. 1227–1232, 2011.

[27] J. P. T. W.X.Chen, "Electroless preparation and tribological properties of Ni-P-CNT composite coating under lubricated condition," *Surf. Coatings Technol.*, vol. 160, pp. 68–73, 2002.

[28] B. M. Praveen and T. V. Venkatesha, "Electrodeposition and Corrosion Resistance Properties of Zn-Ni/TiO_2 Nano composite Coatings," *Int. J. Electrochem.*, vol. 2011, pp. 1–4, 2011.

[29] C. Zhao, Y. Yao, and L. He, "Electrodeposition and characterization of Ni-W/ZrO_2 nanocomposite coatings," *Bull. Mater. Sci.*, vol. 37, no. 5, pp. 1053–1058, 2014.

[30] D. Blejan, D. Bogdan, M. Pop, A. V. Pop, and L. M. Muresan, "Structure, morphology and corrosion resistance of Zn-Ni-TiO_2 composite coatings," *Optoelectron. Adv. Mater. Commun.*, vol. 5, no. 1, pp. 25–29, 2011.

[31] Q. Zhao, Y. Liu, and C. Wang, "Development and evaluation of electroless Ag-PTFE composite coatings with anti-microbial and anti-corrosion properties," *Appl. Surf. Sci.*, vol. 252, no. 5, pp. 1620–1627, 2005.

[32] K. Makise *et al.*, "Estimations of superconducting fluctuation effects in amorphous MoRu and MoRe alloy thin films," *Mater. Res. Express*, vol. 5, p. 096406, 2018.

[33] B. M. Praveen and T. V. Venkatesha, "Electrodeposition and properties of Zn-nanosized TiO_2 composite coatings," *Appl. Surf. Sci.*, vol. 254, no. 8, pp. 2418–2424, 2008.

[34] D. R. Tobergte *et al.*, "Electroplating of Nanocrystalline CoFeNi Soft Magnetic Thin Films from a Stable Citrate-Based Bath," *J. Chem. Inf. Model.*, vol. 53, no. 9, pp. 1189–1194, 2013.

[35] T. V. Venkatesha, S. K. Rajappa, and B. M. Praveen, "Chemical treatment of zinc surface and its corrosion inhibition studies," *Bull. Mater. Sci.*, vol. 31, no. 1, pp. 37–41, 2008.

[36] C. C. Lin and C. M. Huang, "Zinc-nickel alloy coatings electrodeposited by pulse current and their corrosion behavior," *J. Coatings Technol. Res.*, vol. 3, no. 2, pp. 99–104, 2006.

[37] V. G. Roev, R. A. Kaidrikov, and A. B. Khakimullin, "Zinc – Nickel Electroplating from Alkaline Electrolytes Containing Amino Compounds," vol. 37, no. 7, pp. 756–759, 2001.

[38] R. Fratesi and G. Roventi, “Corrosion resistance of Zn-Ni alloy coatings in industrial production,” *Surf. Coat. Technol.*, vol. 82, pp. 158 – 164, 1996.

[39] T. Tsuru, S. Kobayashi, T. Akiyama, H. Fukushima, S. K. Gogia, and R. Kammel, “Electrodeposition behaviour of zinc-iron group metal alloys from a methanol bath,” *J. Appl. Electrochem.*, vol. 27, no. 2, pp. 209–214, 1997.

[40] S. Shivakumara, U. Manohar, Y. Arthoba Naik, and T. V. Venkatesha, “Influence of additives on electrodeposition of bright Zn-Ni alloy on mild steel from acid sulphate bath,” *Bull. Mater. Sci.*, vol. 30, no. 5, pp. 455–462, 2007.

[41] A. Vlasa, S. Varvara, A. Pop, C. Bulea, and L. M. Muresan, “Electrodeposited Zn-TiO_2 nanocomposite coatings and their corrosion behavior,” *J. Appl. Electrochem.*, vol. 40, no. 8, pp. 1519–1527, 2010.

2.0 LITERATURE REVIEW

Preamble

The literature review is divided into six sections namely 1) Zn-Ni alloy electroplating process: this section discusses about the plating procedures followed in the literature, 2) stability of electroplating bath: this section discuss about the different stabilizing electroplating bath used in the Zn-Ni alloy study, 3) morphology, phase and composition of Zn-Ni alloy deposits, 4) electrodeposition of Zn-Ni alloy and Zn-Ni/solid composite coatings, 5) electrochemical and mechanical behavior of the deposits, 6) pitting corrosion behavior of Zn-Ni alloy electroplating.

2.1 Zn-Ni alloy electroplating process

For the many years' zinc has been used as a sacrificial anode to protect steel structures from corrosion. The demand of the better corrosion resistant product in the modern industry led to enhance the properties of the zinc coating by making it into the Zn-based alloys with longer life to survive in the rigorous environmental condition. Such as pure Zn and Zn-Ni alloy-based metal can be electroplated on to the steel specimens for both alkaline and acid bath solutions. A common industrial practice to electroplated steel/iron components is Rack and Barrel plating[1].

Rack plating process is usually applied for the steel components with larger length and bigger diameter whereas, Barrel process is used for the smaller components. In a Rack process, the components are placed on the separate racks with individual connections and then electrodeposited. In the Barrel process, components are immersed in a bulk solution with a large rotating barrel and the linings of the barrel is sued as the anode. The Zn-Ni electroplating bath conditions for acid and alkaline solutions are shown in Table 2.1[2].

Table 2.1. Zn-Ni electroplating bath conditions for acid and alkaline solutions[2]

Parameter	Acid Baths (g/l)		Alkaline bath (g/l)
	Rack	**barrel**	
Zinc Chloride	130	120	-
Zinc metal	-	-	8
Nickel chloride	130	110	-
Nickel metal	-	-	1.6
Potassium chloride	230	-	-
pH	5-6	5-6	
Temperature (^{0}C)	24-30	35-40	23-26
Cathode current density (A/dm^2)	0.1-4	0.5-3	2-10
Anodes	Zinc and nickel separately, eventually with separate rectifiers	Mix: nickel plated steel 70%- zinc 30%	

Electrodeposition processes are extensively used in industry of large variety of metallic coatings, ranging from technological to decorative applications. An experimental setup of electrodeposition is requiring an appropriate vessel and two conducting electrodes such as working electrode (WE) where the metallic layer is deposited, and a counter/auxiliary electrode (CE) immersed in bath solution containing the metal ions to be deposited. Sometimes, a third electrode called reference electrode (RE) is used to measure more accurate potential at the electrode[3]. The schematic diagram of the electrodeposition process is shown in Figure 2.1[3].

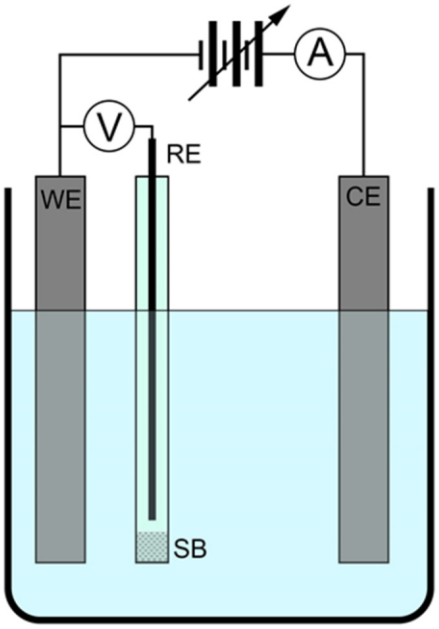

Figure 2.1 Schematic diagram of the electrochemical cell [3]

2.2 Stability of electroplating bath

2.2.1 Development of alkaline baths

There are various types of the electroplating bath used in the electrodeposition process to attain the uniformity, corrosion resistant and mechanical properties of the coatings in which Feng et al. (2015) developed an alkaline bath (Table 5) and prepared nano-crystalline Zn-Ni alloy coatings on carbon steel substrates. 5, 5'-dimethyl hydantoin (DMH) was employed as the complexing agent, while, coumarin (CA) and vanillin (VL) were used as additives. The hardness and corrosion resistance of the coating increased as the Ni contents in deposit increased[4]. The optimum conditions for Zn-Ni plating from the alkaline bath are shown in Table 2.2.

Table 2.2. The optimum bath composition and process parameters[4]

Bath composition and process parameter	Optimum values
$ZnSO_4.7H_2O$ (g/l)	70
$NiSO_4.6H_2O$ (g/l)	30
5,5′-dimethylhydantoin (DMH) (g/l)	140
$Na_4P_2O_7.10H_2O$(g/l)	40
K_2CO_3 (g/l)	95
Additives (g/l)	0.04
pH	9-10
Cathode current density (A/dm^2)	1, 2, 3, 4, 5
Temperature (^0C)	20, 30, 40, 50, 60
Agitation speed (rpm)	0, 200, 600, 1000, 1400

2.2.2 Development of citrate baths

As mentioned in chapter-1, the addition of citrates can improve the stability of Zn-Ni plating baths, whereas, there are few kinds of literature related to being published. Some baths other than Zn-Ni with the addition of citrates have been developed. The authors have prepared Zn-Ni samples in the citrate bath and observed the stability of the bath and suppressed hydrogen evolution reaction lead to decrease the corrosion current (I_{corr}).

Silva et al. (2010) electroplated Zn-Cu coating on mild steel substrate from an electrolyte containing sodium citrate and additives, such as benzotriazole and cysteine. The coatings exhibited excellent anti-corrosion performance [5]. The bath composition and process parameters employed in the experiments are shown in Table 2.3.

Table 2.3. The optimum bath compositions and process parameters [5]

Bath composition and process parameter	Optimum values
$CuSO_4.5H_2O$ (mol/l)	0.02
$ZnSO_4.7H_2O$ (mol/l)	0.20
$Na_3C_5H_6O_7$ (mol/l)	1.0
Benzotriazole (mol/l)	0.001
Current density (A/m^2)	10,20,30,60
Stirring speed (rpm)	300
pH	6.59,6.52,6.77

2.2.3 Development of EDTA baths

The addition of complexing agent leads to stabilize the bath solution. However, there are few works of literature related to being published on the EDTA containing bath for Zn-Ni and other than Zn-Ni plating have been reported. The authors have prepared Zn-Ni plating deposited from EDTA bath and discussed the optimum conditions for plating. As the EDTA concentration increases in the bath solution, observed to attain the stability of the bath and suppressed hydrogen evolution reaction lead to decrease the corrosion current (Icorr). Depending on the quality of the additive used in the bath, it can form complexes with metal ions and inhibits metal nucleation by adsorbing on the cathodic surface [6]. Different complexing agents have been introduced, such as amine [7], ethylene-diamine [8], tartrate[9], tri-ethanolamine [10], sodium acetate and citrate [11]. Ethylenediaminetetraacetic acid (EDTA) is favourable to the environment and is readily soluble in an aqueous medium. EDTA is used in several industrial applications because it has a high ability to bind the metal cations [12]. Research has been done on Zn-Ni plating deposited from EDTA bath in which Bajat et al. [13] studied the behaviour of Zn-Ni plating in a chloride bath with EDTA as a complexing

agent by applying a direct and pulse current. It was shown that Zn-Ni alloy electroplated by pulse current exhibited better anti-corrosive properties.

The influence of plating current density on the Zn-Ni coating was reported by Shivakumara et al. [14] They prepared a Zn-Ni coating by the electrodeposition method for the steel in a sulphate bath with EDTA as a complexing agent. 15g/l of EDTA in the bath solution exhibited a uniform and bright coating with a cathodic current density range of 0.2-5.5A/dm^2. An increase in the concentration above 15g/l, no improvement in the coating was observed. Similarly Soare et al. [15] studied the behaviour of Zn-Ni-P alloy coating from a sulphate bath containing EDTA as the complexing agent. The deposition parameters were optimized such as concentration of EDTA was 15g/l, zinc sulphate 30g/l, pH 2, current density 1.0-2.0 A/dm^2 and at a temperature between 25^0C to 40^0C. The SEM and optical microscopy result showed that a thin film with a fine grain deposits and excellent adhesion to the steel substrate were exhibited in the presence of EDTA. EDTA also enhanced the anti-corrosion property of the Zn-Ni alloy coatings. Zohdy [12] observed that plating reactions are slowed down by the inclusion of EDTA. Moreover, the inhibition efficiency increases with an increase of the EDTA concentration. The morphological result revealed that the plated surface of the carbon steel was non-uniform and covered with corrosion products in the absence of EDTA. Whereas, in the presence of EDTA, the surface of plated carbon steel was homogeneous.

Fashu et al. [16] observed the electrochemical behaviour, morphological structure and anti-corrosion property of Zn-Ni alloy film deposited from EDTA and NH_4Cl. The electrochemical result revealed that increasing the concentration of EDTA led to an increase in Zn content and a decrease in Zn when NH_4Cl was used. They also noted that the Zn-Ni deposited from EDTA provide less anti-corrosion property in comparison to NH_4Cl.

Conde et al. (2011) developed an alkaline electrolyte based on ethylene diamine tetraacetic acid (EDTA) as a complexing agent, and electrodeposited Zn-Ni coatings on 4340 high strength steels at pH equal to 13.6. The optimum corrosion protective properties of Zn-Ni coating achieved at 15mA/cm^2 current density and stirring speed of 800 rpm, exhibiting highly compact and uniform deposition (Table 2.4). The hydrogen deposition is suppressed in the alkaline bath[17].

Table 2.4. The optimum bath compositions and process parameters[17]

Bath composition and process parameter	**Optimum values**
ZnO (g/l)	13
$NiSO_4.6H_2O$ (g/l)	4.5
NaOH (g/l)	150
Diethylenetriamine (g/l)	3.5
Current density (mA/cm^2)	15,25,35
Stirring speed (rpm)	500-800
pH	13.6

2.2.4 Development of fluoroborate baths

Bapu et al. [18] employed a fluoroborate (H_3OBF_4) bath (Table 2.5) and investigated zinc-nickel electroplating on mild steel for better corrosion protection. They found that zinc content increased with current density and was maximum at 10 A/dm^2. A rough and coarse deposit was observed at low pH due to the evolution of hydrogen. The desired coating composition was obtained at pH 3.5. The effect of temperature was significant because when the bath temperature was decreased, then the diffusion rate of nickel ions may slow down in comparison to zinc ions[18]. Su et al.[19] also electrodeposited Ni, Fe, and Ni–Fe alloy coatings from fluoroborate baths[19].

Table 2.5. The optimum bath compositions and process parameters[18]

Bath composition and process parameter	Optimum values
Nickel fluoroborate (g/l)	60
Zinc fluoroborate (g/l)	75
Boric acid (g/l)	40
Current density (A/dm^2)	8-10
Temperature (^0C)	50
pH	3.5

2.3 Research Challenge - Development of stable baths for Zn containing coatings

Due to the negative reduction potential of Zn/Zn^{2+} electrode. Zn is more difficult to be electrodeposited than hydrogen gas[30]

Zn^{2+} (aq) + 2e $\longrightarrow$ Zn (s) $\quad E_{Zn/Zn^{2+}} = -0.762$ v

$2H^{+}$ (aq) +2e $\longrightarrow$ H_2 (g) $\quad E_{Zn/Zn^{2+}} = 0.000$ v

The hydrogen ions in the solution will be deposited prior to zinc as H^+ ions have a more positive reduction potential under the standard state. To overcome and modify this problem the higher pH bath electroplating is preferable. Generally, high pH bath (alkaline) is not stable. Therefore, most of the electroplating is developed as an acidic bath. The major problem, to use of acidic bath is the hydrogen evolution reaction is occurring in the electrolyte and exhibiting non-uniform less corrosive resistant coatings. To electrodeposit Zn-containing coatings with suitable composition and microstructure, which lead to ideal corrosion resistant and mechanical properties, the development of long duty stable plating bath is vital. To suppress hydrogen deposition and stabilize the plating baths, alkalis and complexing agents (e.g., acetate, tartrate and citrate) were added into the baths for ideal Zn, Zn-Ni and Zn-Ni/solid composite electrodeposition, which resulted in improved corrosion resistant property, uniformity, thickness, and enhanced hardness of the plated films [30][31][32][33][34][35].

The Pourbaix diagrams of Zn, Ni and Zn-Ni plating baths (composition listed in Table 2.6) are calculated by authors using OLI Analyzer Studio software and demonstrated in Figures 2.2, 2.3 and 2.4. For single zinc electrodeposition, the natural bath pH is around 4.0, by adding alkali to increase the pH above 4.0 but below 8.5 (without the precipitation of ZnO), the hydrogen deposition will be suppressed at a great extent; for single nickel electrodeposition, the natural bath pH is around 4.2, by adding alkali to increase the pH above 4.2 but below 6.4 (without the precipitation of $Ni(OH)_2$), the hydrogen deposition will be suppressed; for Zn-Ni co-deposition, the natural bath pH is around 4.1, by adding alkali to increase the pH above 4.1 but below 6.4 (without the precipitation of $Ni(OH)_2$), the hydrogen deposition will also be suppressed. Therefore, theoretically, increasing the bath alkalinity leads to less hydrogen evolution and more uniform deposits. Arrow line indicates the pH, precipitate region is shown by brackets, in which red colour line shows the indication of ZnO whereas, the green line shows the $Ni(OH)_2$.

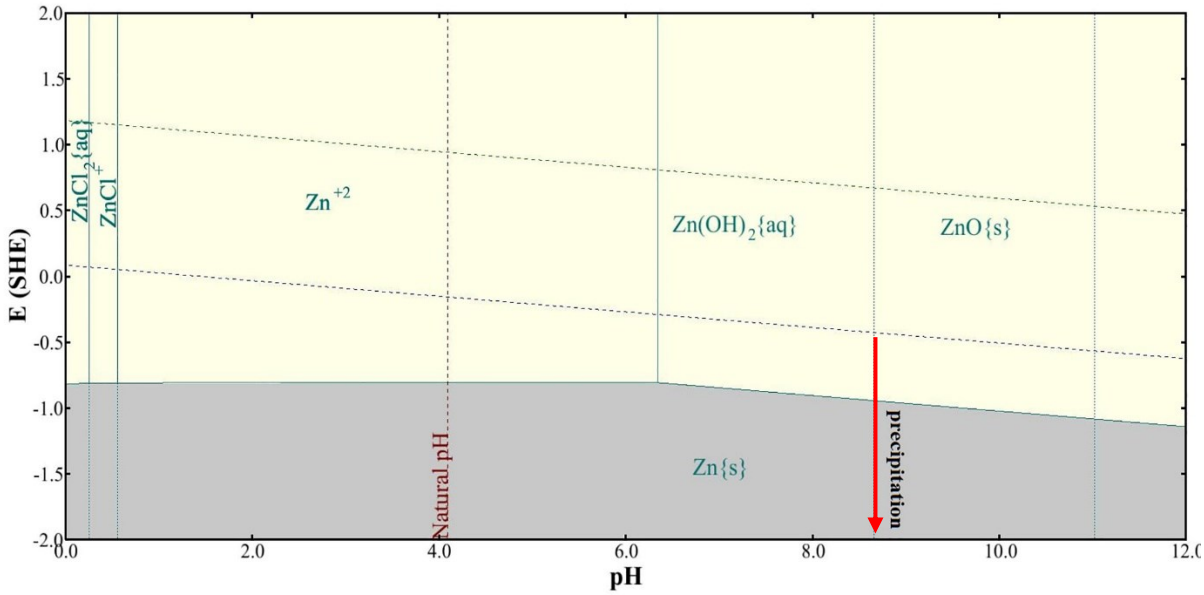

Figure 2.2 The Pourbaix diagram for Zn plating bath (The dashed line 'a' and 'b' refers to the equilibrium lines for $H+/H_2$ and $(O_2+H_2O)/OH-$ respectively, same for the following figures) lines for H^+/H_2 and $(O_2+H_2O)/OH^-$ respectively, same for the following figures)

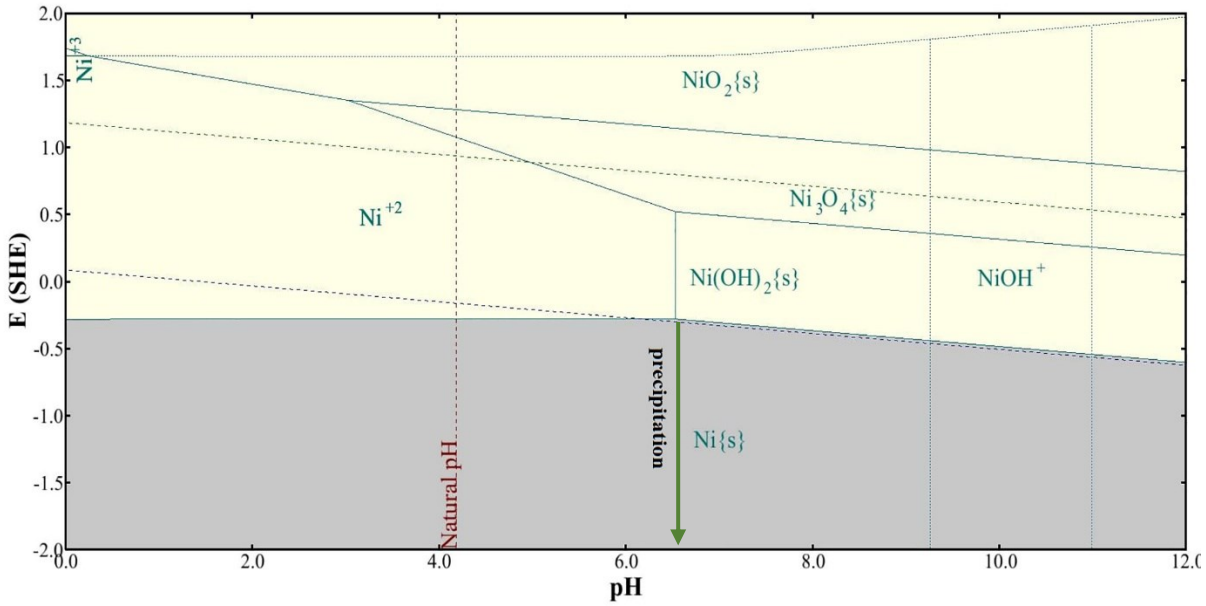

Figure 2.3 The Pourbaix diagram for Ni plating bath

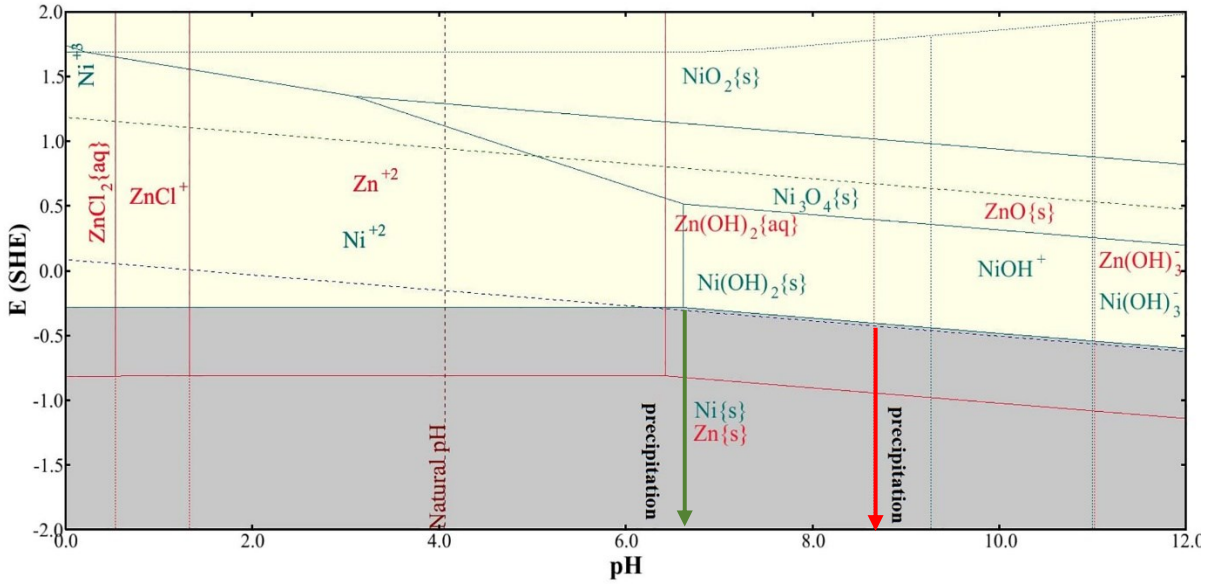

Figure 2.4 The Pourbaix diagram for Zn-Ni plating bath

To stabilize the plating baths and obtain improved corrosion resistant property of the coatings, complexing agents, e.g., EDTA, citrate, acetate and fluoroborate, were employed by researchers[31][36][37][38][39][40][41][42]. The Pourbaix diagrams of Zn-Ni plating baths with EDTA, citrate, and acetate addition (bath composition listed in Table 2.6) are calculated by authors using OLI software and shown in Figures 2.5, 2.6, 2.7 It can be seen, with the addition of EDTA, citrate, and acetate, the precipitation of nickel hydroxide ($Ni(OH)_2$) is extended to pH 7.2, 7.2, and 8.8, respectively. Similarly, the precipitation of zinc oxide (ZnO)

is extended to pH 8.8, 9.5 and 9.0 respectively. A summary on the precipitate(s) and precipitating pH of the Zn, Ni, and Zn-Ni plating baths with and without complexing agent addition is shown in Table 2.6. From Figures. 2.5 and 2.6, it is apparent that citrate and EDTA have the strongest complexing power for Zn ions, followed by Ni ions. Therefore, $Zn[C_6H_5O_7]$ (aq) and $Ni[C_6H_5O_7]$ (aq) contribute to stabilizing the Zn-Ni elements in the bath solution. The calculation of Pourbaix diagrams demonstrates that the bath stability can be improved with the addition of complexing agents. The similar result has been studied and reported by Zhang et al.[36].

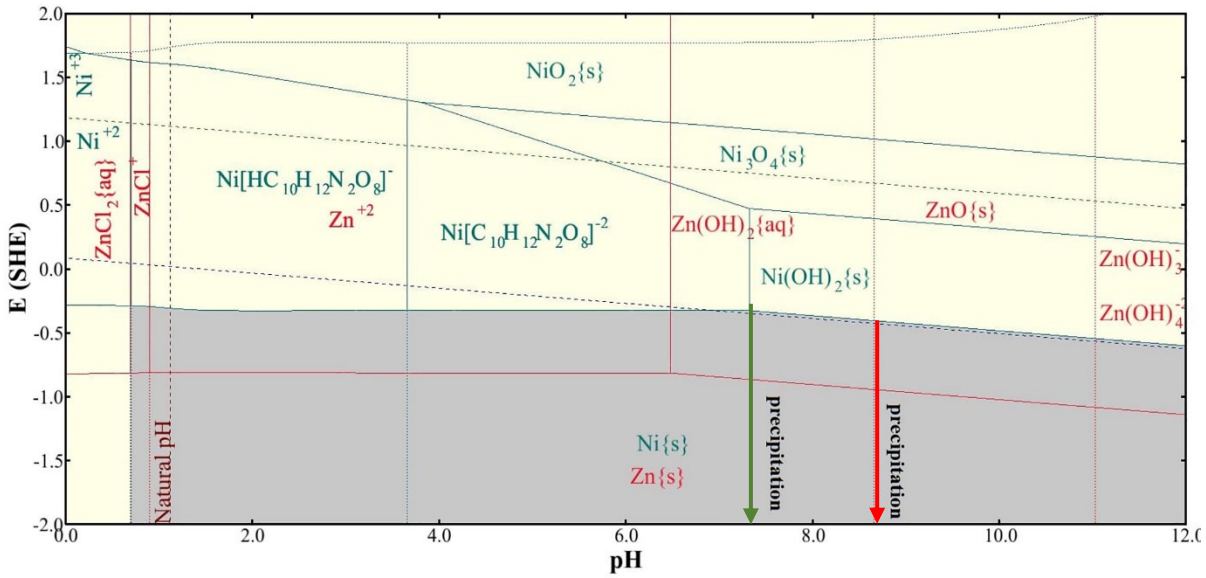

Figure 2.5 The Pourbaix diagram for Zn-Ni alloy with EDTA plating bath

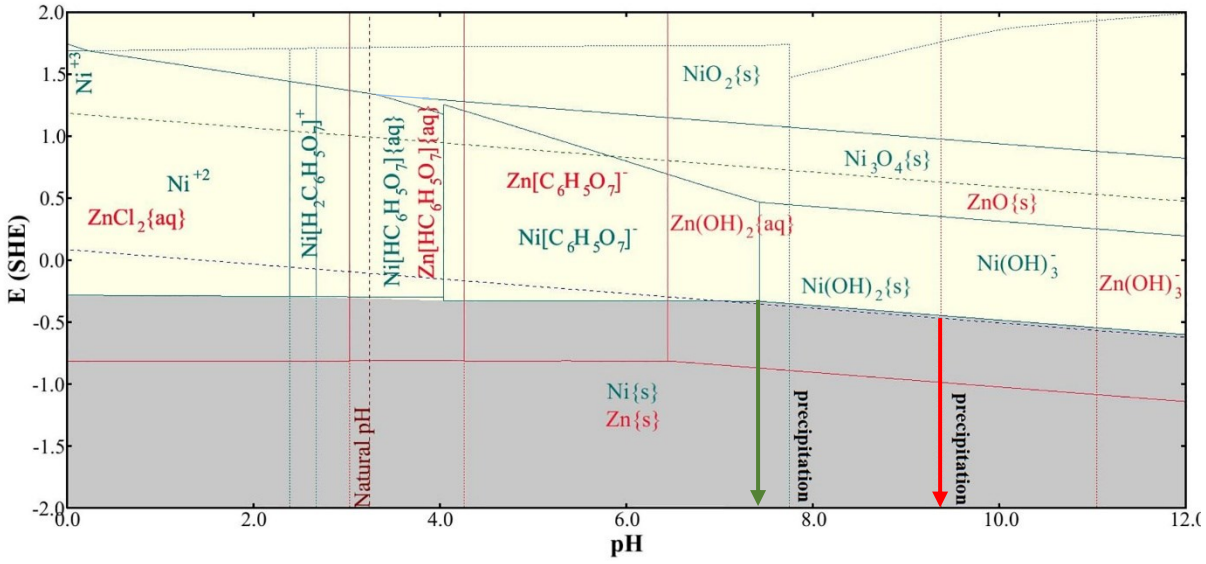

Figure 2.6 The Pourbaix diagram for Zn-Ni alloy with citrate plating bath

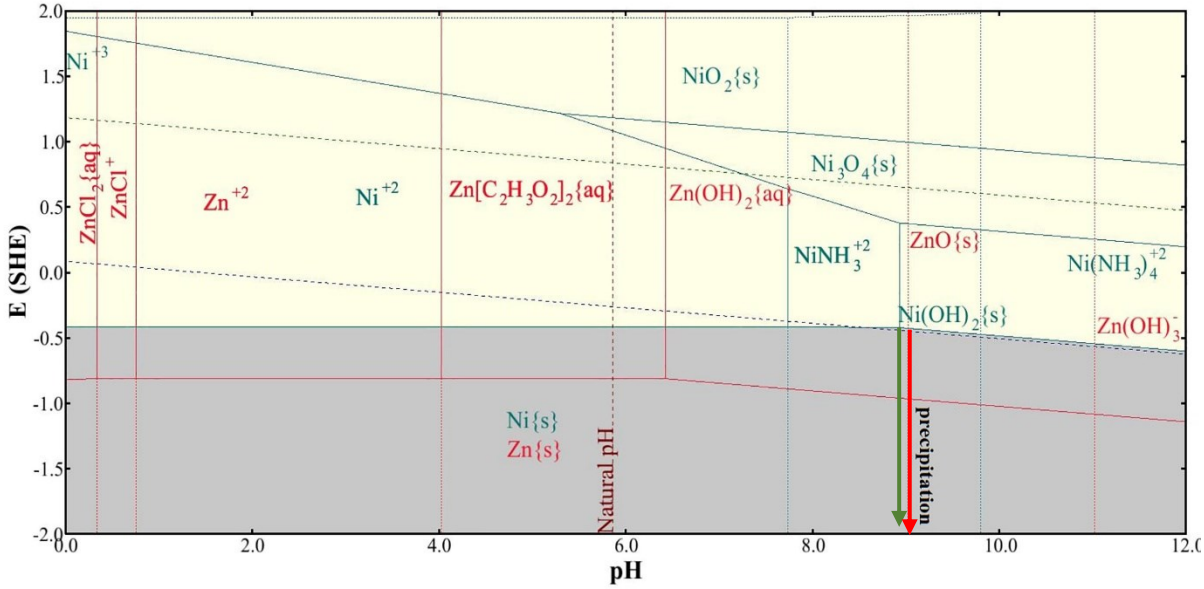

Figure 2.7 The Pourbaix diagram for Zn-Ni alloy with ammonium acetate plating bath

Table 2.6. The stability of specific baths calculated using OLI software

Serial. No.	Molar Concentration of bath composition (mol/l)	Coatings	Precipitates	Precipitating pH
1.	0.32 $ZnCl_2.1H_2O$ 0.32 H_3BO_3	Zn	ZnO	8.6
2.	0.21 $NiCl_2.6H_2O$ 0.32 H_3BO_3	Ni	$Ni(OH)_2$	6.8
3.	0.3 $ZnCl_2.1H_2O$ 0.21 $NiCl_2.6H_2O$ 0.32 H_3BO_3	Zn-Ni	ZnO $Ni(OH)_2$	8.7 6.8

4.	0.32 $ZnCl_2.1H_2O$ 0.21 $NiCl_2.6H_2O$ 0.32 H_3BO_3 0.228 EDTA	Zn-Ni	ZnO $Ni(OH)_2$	8.8 7.2
5.	0.32 $ZnCl_2.1H_2O$ 0.21 $NiCl_2.6H_2O$ 0.32 H_3BO_3 0.228 $K_3C_6H_5O_7$	Zn-Ni	ZnO $Ni(OH)_2$	9.5 7.2
6.	0.32 $ZnCl_2.1H_2O$ 0.21 $NiCl_2.6H_2O$ 0.32 H_3BO_3 0.228 $C_2H_7NO_2$	Zn-Ni	ZnO $Ni(OH)_2$	9.0 8.8

2.4 Morphology, phase and composition of Zn-Ni alloy deposits

The structure of pure zinc coating is conventional hexagonal close packed structure (HCP) and the Zn-Ni alloy electrodeposits differs from this structure. Several researches have been carried out to find that there is a phase transformation in Zn-Ni alloys concerning to the compositions[20] [21] [22]. It was reported by Bories et al.[21] and Bruet et al.[22] that the phase achieved from Zn-Ni alloy electrodeposits are distinct from the equilibrium phase diagram. The comparable explanation is shown in Figure 2.8 a) and b).

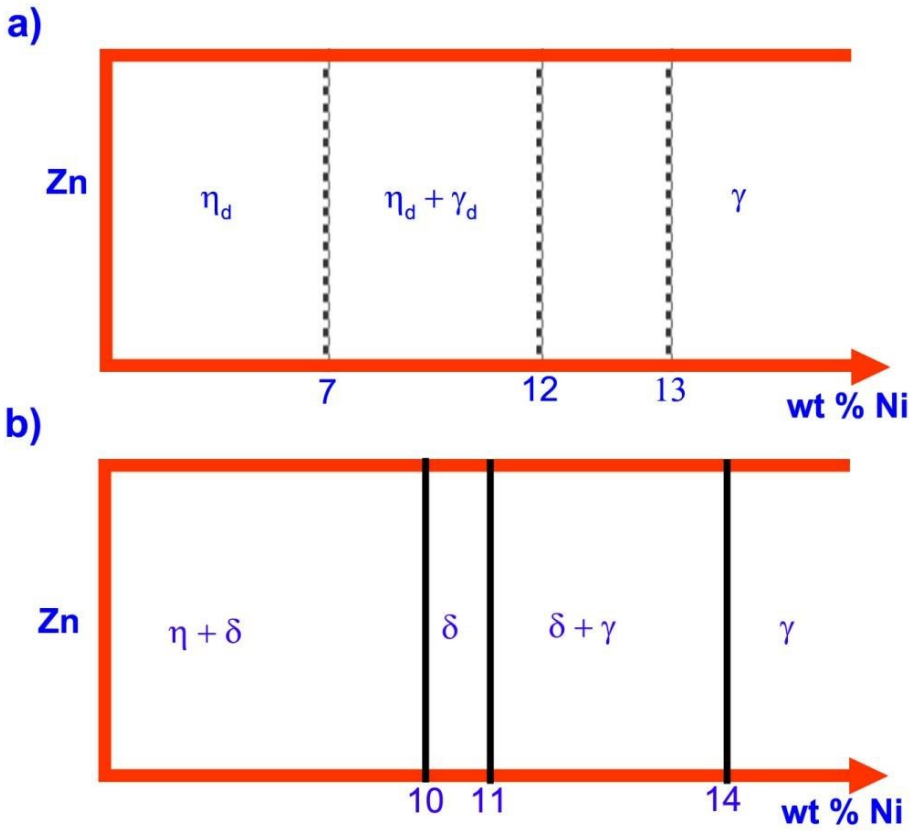

Figure 2.8 Phase orientation achieved from Zn-Ni alloy a) electrodeposition process [21] [22] and b) from equilibrium phase diagram [22].

In the process of Zn-Ni electrodeposition, the crystal structure keeps as HCP from 0-7% Ni. The addition of Ni in the Zn matrix changed the Zn lattice by decreasing the "c" axis quickly and increasing the "a" axis slowly. It is observed from Figure 2.3 a) that on the zinc rich side solution (η_d phase) is developed with the maximum solubility of Ni is 7.4. A cubic, non-stoichiometric, intermetallic phase, γ_d is formed at 7.4% Ni composition in the Zn-Ni alloy. As the percentage of Ni component increase (12.5%) in the Zn matrix led to increase the volume of the γ_d phase. At Ni 12 to 13%, the γ_d and, γ co-exist. When the Ni content greater than 13%, the lattice parameter decreases to the equivalent to the equilibrium phase diagram, which is identified as γ. The incorporation of Ni in the Zn matrix changes the surface morphology of the electroplating[21][22][23]. Pure Zn alloying with 2.8% Ni causes the replacement of Zn atom with Ni resulted in smaller grain size with isotropic shapes. At the 7.4% Ni content, the shape of the grained changed to the hexagonal, owing to change in orientation in pyramid planes.

Furthermore, at 13% Ni contents resulted in fine grain and uniform distribution of materials with lessened surface roughness and more surface coverages.

There are several researches on the morphology and phase have been reported with the incorporation of metal oxide (TiO_2) in the Zn-Ni matrix. A. Gomes et al.[24] has prepared Zn–Ni–TiO_2 and Zn–TiO_2 nanocomposites by Galvano static cathodic square wave deposition. The metallic grain size decreases in the presence of the TiO_2 nanoparticles. This fact is mainly related to modifications of the nucleation and growth of the metallic crystallites in the presence of the semiconducting particles, as mentioned before. Similarly, a decrease of the metal particle size caused by occlusion of semiconducting nanoparticles was observed for Ni–TiO_2 nanocomposites. The Morphological and structural studies of the coatings after immersion for 24 h in the Na_2SO_4 solutions are characterized (Zn–Ni deposit) by a globular morphology, and the Zn deposits are formed by compact and hexagonal grains randomly oriented.

The intensity of the diffraction peaks of the corrosion products is higher for the Zn– Ni–TiO_2 and Zn–TiO_2 nanocomposites than for the pure metallic electrodeposits, because of a higher amount of corrosion products (and/or thicker layer) formed on the composite surfaces.

Vlasa et al.[25] has examined the Coating on steel substrate and the corrosion behaviour of Zn–TiO_2 nanocomposite coatings by using two types of TiO_2 nanoparticles [Alfa Aesar (AA) 99.9%, 32 nm, Anatase and Degussa (D) 99.5%, 21 nm mixture of rutile and anatase]. Morphological and structural analysis result shown that by increasing the TiO_2 concentration in the plating bath, the nanoparticles show a distinct tendency to form conglomerates in solution due to their high surface energy and to the more intense interactions between the particles.

At high TiO_2 concentrations, the particles agglomerate and a decreasing incorporation trend is noticed. The XRD peaks are narrow, the grain size of the metallic matrix was estimated from the width of (110) diffraction line. Thus, the grain size of the composite deposits was proved to be smaller (19.89 nm for Zn-5 g L^{-1} TiO_2, 19.14 nm for Zn-10 g L^{-1} TiO_2) than that of the

pure Zn coatings (20.35 nm). The topographic images of the surface obtained by AFM (Atomic force Microscope) measurements for composite coatings obtained from solutions containing different concentrations of TiO_2 (D) suggest a non-linear dependence of the deposit uniformity on TiO_2 concentration in the plating bath. The presence of TiO_2 (D) nanoparticles embedded in the zinc matrix makes the composite coatings more corrosion-resistant.

One of the main reasons to increase the anti-corrosion performance of the coated sample while immersing in the corrosive solvent is the formation of corrosion products. This was evidence that the corrosion products act as a barrier against diffusion leads to decrease the corrosion rate of the coated sample. The composition of the corrosion products layer has a significant impact on the corrosion resistant properties of the Zn-Ni alloys. The principal corrosion products in moisture environments are zinc oxide (ZnO) and zinc hydroxide ($Zn(OH)_2$)[26]. Moreover, due to the standard components of carbon dioxide in the air, the appearance of smithsonite ($ZnCO_3$) and hydrozincite ($Zn_5(CO_3)_2(OH)_6$) was feasible. However, the ($Zn_5(OH)_8Cl_2.H_2O$) was the most favorable component formed in the hydrophilic solution, and it contains high chloride (Cl^-) contents. However, the simonkolleite was contemplated as an active-passive layer and during the Zn alloy corrosion, the layer solubility of Zn alloy since their low solubility and solidity[27][28]. It was affirmed that the corrosion resistant properties of Zn-Ni alloy electroplating dependent on the formation of corrosion products. Hence, it was requiring doing the analysis and observe the corrosion product process and the constrained effect of their film during the corrosion mechanism was happen.

2.5 Electrodeposition of Zn-Ni alloy and Zn-Ni/solid composite coatings

2.5.1 Electrodeposition of Zn-Ni alloy coatings

Due to the excellent corrosion resistant property of nickel, Zn-Ni alloy coatings are used extensively in industry as they have a high degree of corrosion protection for steels[29], especially in automobile industry[30][31]. Zn-Ni alloys possess better mechanical and

excellent thermal properties compared to pure Zn and other Zn alloys[32][9]. The 10-15% Ni contents in Zn-Ni alloys can enhance corrosion protection to steels, and these Zn-Ni alloys are used as an alternative for cadmium coating in the automotive industry[33]. Zn-Ni alloys with 15–22% Ni contents exhibit low hydrogen embrittleness and numerous applications in the aeronautical industry. Researchers investigated the effects of electroplating conditions such as bath concentrations, acidic/basic, plating current density on the coating composition, texture and anti-corrosion properties.

Abou-Krisha [34] observed the potential for Zn, Ni, and Zn-Ni alloy deposition from a sulfate bath at different conditions. Zn deposition was observed to start at -1.14V, which is close to Zn-Ni alloy coating at -1.12V, and the Ni deposition started at -0.85V and then rapidly grow with more negative potential. Therefore, Ni deposits at a lower potential, Zn deposits at a higher potential, and Zn-Ni alloy deposits at medium potential because Ni deposition is strongly inhibited in the presence of Zn^{+2}, whereas, Zn deposition is induced with the presence of Ni^{+2}. The plated Zn-Ni alloys exhibited better corrosion resistance than pure Zn coating.

Faid et al. [35] studied the electrodeposition of Zn-Ni coating on a mild steel substrate from a sulfate bath under different deposition potentials. They observed that the content of nickel in the deposit was increased by applying a more negative deposition potential. Moreover, the electrochemical analysis revealed that the Zn-Ni coating obtained at the most negative deposition potential exhibited the best corrosion resistance.

Gavrila et al. [31] studied the corrosion behavior of Zn-Ni coating electrodeposited on steel from a neutral saline solution under different preparation conditions (e.g., the composition of the bath, the current density of electrodeposition, degassing and chromate passivation). The optimum bath compositions and process parameters are shown in Table 2.7.

Table 2.7. The optimum bath compositions and process parameters[31]

Bath composition and process parameter	Optimum values
Zinc sulphate (mol/l)	0.2
Nickel sulphate (mol/l)	0.2
Sodium sulphate (mol/l)	0.1
Boric acid (mol/l)	0.4
Temperature (^{0}C)	Room
Plating time (sec)	600
Deposition potential (V)	-1.2, -1.25, -1.3
pH	4
Current density (mA/cm^2)	5

Fashu et al. [36] studied the vital electrodeposition parameters, such as temperature, deposition voltage and bath composition, on the properties of Zn-Ni films deposited from chlorine-chloride-urea baths. Electrochemical analysis indicated that the Zn-Ni coating deposited from the 0.45 mol/l of Zn and 0.05 mol/l of Ni bath at 55 ^{0}C and 0.8V, which exhibited dense, smooth and crack free morphology with ideal Zn content, showed highest corrosion resistance compared with Zn-Ni coatings obtained from other baths with different Zn-Ni compositions.

Assaf et al. [37] analysed the significance of current density (0.5-40 mA/cm^2) on the experimental behaviour of zinc-nickel-manganese alloy coating deposited on steel. It is reported that an increase in the plating current density favored the higher contents of nickel and manganese in the deposit, and higher nickel content showed higher corrosion resistance and cathodic current efficiency.

Additional Zn based alloy coatings for the corrosion protection purpose have also been explored by researchers but have fewer commercial applications. Guan and Peng [38] electroplated Cu-Zn-Bi films on steel. Abou-Krisha et al. [39] studied the electrodeposition of

Zn-Co-Fe alloy coatings on different substrates such as high purity copper, iron, AISI 4340 steel and 304-stainless steel from a sulfate bath composed of $ZnSO_4$, $CoSO_4$, $FeSO_4$, Na_2SO_4, and H_2SO_4.

2.5.2 Electrodeposition of Zn-Ni/solid composite coatings

An alternate process to increase more corrosive resistant property of the zinc and nickel coating is to introduce Zn-Ni composite coating. The inclusions of composite materials have to increase various properties of the alloy coatings such as dispersion hardening, high-temperature oxidation resistance, self-lubricity, wear and corrosion resistance[40][41]. A number of past literature appears to the co-deposition of TiO_2, Al_2O_3, ZrO_2, SiO_2, Fe_2O_3 and SiC for enhancing the corrosion resistant and mechanical properties of the Zn-Ni alloy coating[41][42][43][44]. The incorporation of composite materials on the Zn-Ni surface refine the crystal size and shape, and increase the corrosion resistance, microhardness and wear resistance property.

2.5.3 Electrodeposition of Zn–Ni/Al_2O_3 composite coatings

Zheng and An [45] prepared Zn-Ni/Al_2O_3, coatings using an ultrasound horn in the electrolyte. They found that increasing the ultrasonic power from 0 to 0.7 W/cm^2 would improve the Al_2O_3 content in the coating from 4.5 to 8.9 wt. % and could reduce the agglomeration of the Al_2O_3 particles. The best-operating conditions for the Zn-Ni/Al_2O_3 composite coatings are shown in Table 2.8.

Table 2.8. The optimum bath compositions and process parameters [45]

Bath composition	Optimum values
$NiCl_2.6H_2O$ (g/l)	120
$ZnCl_2$ (g/l)	60
KCl (g/l)	120
NH_4Cl (g/l)	100
NaAc (g/l)	30

Temperature (^{0}C)	35
Current density (A/dm^2)	4
pH	4

Ghaziof and Gao [46] studied the behaviour of sol-enriched Zn–Ni/Al_2O_3 composite coatings on mild steel. Authors have prepared apparent Al_2O_3 sol and incorporate with the acidic zinc-nickel electrolyte to produce Zn–Ni/Al_2O_3 composite coatings. The morphological texture of the composite coatings possessed refined crystals with higher hardness as compared to the pure zinc-nickel alloy coatings. The experimental result revealed that higher stirring speed showed uniform coating with smaller grain size and slightly higher hardness. The operating conditions for plating the Zn-Ni/Al_2O_3 coating on mild steel are shown in Table 2.9.

Table 2.9. The optimum value of bath compositions and process parameters [46]

Bath composition and process parameter	**Quantity**
$ZnSO_4.7H_2O$ (g/l)	35
$NiSO_4.6H_2O$ (g/l)	35
$NaSO_4$ (g/l)	80
Al_2O_3 sol (for composite coating) (mol/l)	6
Current density (mA/cm^2)	80
Agitation speed (rpm)	1200
Time (min)	10

2.5.4 Electrodeposition of Zn-Ni/TiO_2 composite coatings

The large availability and superior characteristics have made a significant impact on the various application of the nanoparticle, now a day they are generally used in composite coating for achieving better anti-corrosion and mechanical properties of the alloy coatings. Among the composite nanomaterials, titanium dioxide (TiO_2) for the generation of composite coatings has received the most attention. The successful result has been reported on the co-

deposition of TiO_2 with Ni, Cu, Zn and Ag metals[40]. Incorporation of TiO_2 enhances the hardness, wear and corrosion resistance property of the coatings[47].

Praveen and Venkatesha [41] prepared Zn-Ni/TiO_2 composite coatings on mild steel and analyzed the effect and behaviour of titanium dioxide (TiO_2) nanoparticles on coating corrosion properties. The optimum bath composition and process parameters are shown in Table 2.10. The titanium dioxide particles were prepared using the sol-gel method. The polarization curve revealed that the anodic and cathodic potentials shift toward a more positive and negative direction, respectively. The more negative cathodic potential reduced the hydrogen reduction process and the corrosion rate. The Zn-Ni/TiO_2 composite coating had superior corrosion inhibiting property than the Zn-Ni alloy coating.

Table 2.10. The optimum value of bath compositions and process parameter[41]

Bath composition and process parameter	**Quantity**
$ZnSO_4$ (g/l)	160
$NiSO_4$ (g/l)	16
Na_2SO_4 (g/l)	40
H_3BO_3 (g/l)	12
Cetyl trimethyl ammonium bromide (CTAB) (g/l)	1.5
TiO_2(g/l)	3
Current density (A/dm^2)	2.0
Temperature (K)	300
pH	4.0

There are various types of the titanium dioxide (TiO_2) combined with Zn-Ni matrix has been studied by several authors in which Vlasa et al. [47] prepared Zn–TiO_2 nanocomposite coatings and observed the corrosion behaviour of the coating on a steel substrate. In this study, authors have used two different types of TiO_2 nanoparticles in which Anatase-TiO_2 (Alfa Aesar (AA) 99.9%, 32 nm,) and Degussa-TiO_2 (99.5%, 21 nm mixture of rutile and anatase). They found

that the porous Zn-TiO_2 nanocomposite coatings exhibit higher corrosion resistance as compared to the pure Zn coatings and is strongly affected by the TiO_2 crystal structure and molar concentration. Kumar et al. [48] prepared the composite coating with the rutile (is a mineral composed primarily of TiO_2) TiO_2 nanoparticles (size ≤ 100nm). The Electrochemical Impedance Spectroscopy (EIS) measurements have found that in 0.25 g/L samples of ammonium sulphate solution shows coating obtained from 6 g/L of rutile TiO_2 nanoparticles (D_2) has higher impedance modulus than other coatings. It is concluded that the successfully generated Zn-TiO_2 composite coatings on mild steel from bath solution containing 2, 6, and 10 g/L of rutile TiO_2 nanoparticles. The percentage of TiO_2 content for D_2 provides condense and uniform surface to the D_2 deposit. As seen from the above literature on a different type of Zn-Ni-TiO_2, there are several experimental studies have been implemented on the Zn-Ni and Zn-Ni-TiO_2 under various operating conditions. To the best of the author's knowledge, there is no systematic study specifically for comparing Zn-Ni alloy and Zn-Ni-TiO_2 deposited from citrate bath, optimum TiO_2 concentration and challenge to suppress the hydrogen evolution reaction (HER) to improve corrosion resistant properties of the coating. Therefore, to fulfil this gap, the authors have studied the experimental research on the Zn-Ni and Zn-Ni with Titania TiO_2 deposited from citrate bath is investigated. The electrochemical behaviour of Zn-Ni and Zn-Ni-TiO_2 deposit from citrate bath reveals that Zn-Ni with the incorporation of 0.003 mol/l of Titania TiO_2 nanoparticles at 60mA/cm^2 plating current density exhibited lower corrosion current (I_{corr}). This increases impedance modulus and corrosion resistance with fine and stronger uniform coating (of 25.84 nm of grain size).

2.5.5 Electrodeposition of Zn–Ni/Fe_2O_3 composite coatings

Kumar et al. [49] electrodeposited Zn–Ni/Fe_2O_3 thin films on a mild steel substrate using Zn-Ni alloy plating solution with dispersed nano-sized Fe_2O_3 particles. The Tafel plot revealed that the Zn–Ni/Fe_2O_3 composite coating possessed more positive corrosion potential

and lower corrosion current, which indicate that the composite coating acquired higher corrosion resistance than the Zn–Ni alloy coating. EIS measurements demonstrated that the composite film possessed higher polarization resistance than the alloy film. Thus, the Zn–Ni/Fe_2O_3 composite coating had excellent corrosion resistant property. Similar work has been finished by Jin et al. [50], they prepared an anti-corrosive Zn–Ni/Fe_2O_3 coating on a magnesium alloy substrate with the optimum content of iron oxide from a 3.5 wt. % NaCl solution. The potentiodynamic polarization result revealed that increasing Fe_2O_3 contents in the bath led to more positive corrosion potential and lowered corrosion current density for the coating, i.e., better anti-corrosive properties; whereas when the Fe_2O_3 content in the coating was more than 5.0 wt.%, the anti-corrosion properties went down conversely.

2.4.6 Electrodeposition of Zn-Ni/SiO_2 composite coatings

Hammami et al. [51] reported the incorporation of SiO_2 nanoparticles into the Zn-Ni alloy coating electrodeposited on steel in order to improve surface properties. The results revealed that a high percentage of Ni and 1.54% of silica were deposited in the coated film. The composite coating exhibited a higher value of hardness and thermally stable up to 200^0C at 24 hours. Electrochemical tests revealed that the coating possessed higher corrosion resistance due to higher Ni content, uniform morphology and incorporated silica nanoparticles.

2.6 Electrochemical and mechanical behavior of the deposits

Zinc coating is broadly used for the protection of steel structures and process equipment from corrosion. Significant efforts have been made to increase the corrosion resistant properties of steel in harsh environment [52][43]. Zinc coatings usually form alloys with Fe, Co, and Ni. According to the literature[53][54], zinc alloy coatings such as Zn-Ni, Zn-Co, and Zn-Fe can result in higher corrosion resistance compared to pure zinc coating. Currently, Zn-Ni alloy coatings become a crucial, eco-friendly substitute for toxic cadmium coating[27]. An alternate approach to improve corrosion resistant and mechanical properties of zinc-nickel alloy coatings

is to introduce Zn-Ni composite coatings. The inclusion of composite material can improve various properties of the alloy coatings such as dispersal toughening, high-temperature oxidation resistance, self-lubricity, wear, and corrosion resistance[41]. Co-deposition of TiO_2, Al_2O_3, ZrO_2, SiO_2, Fe_2O_3 and SiC for enhancing the corrosion resistant and mechanical properties of the Zn-Ni alloy coating were studied [41][42][43][44]. The incorporation of composite materials on the Zn-Ni surface refine the crystal size and shape, which increase the corrosion resistance, microhardness, and wear resistance property. Among the composite nanomaterials, titanium dioxide (TiO_2) has been attain more attention in the recent years. Successful results have been reported on the co-deposition of TiO_2 with Ni, Cu, Zn and Ag metals.

Fayomi and Popoola [55] studied the corrosion resistance properties and mechanical behaviour of zinc coating on a mild steel substrate by applying polarization measurement and Vickers micro-hardness tester. Three zinc coating samples were electrodeposited by different potential (0.6-1.0V), and the corrosion resistance, wear resistance and microhardness of the coated mild steel samples were measured[55][56][57]. The electrochemical analysis revealed that the mild steel sample without zinc coating had a higher corrosion rate (41mm/year) than the samples with zinc coating, which leads to decrease in the corrosion rate[55]. Durodola et al. (2011) evaluated the corrosion behaviour of Zn-coated steel and without coated in which the result revealed that the coated steel plates achieved higher corrosion resistant properties in the corrosive medium (seawater and chloride environment) as compared to without coated steel [58].

Li et al.[59] investigated the effect of nanocrystallization of Zn coatings electrodeposited from a dilute NaCl bath on their corrosion-wear resistant property. It was observed that reduced grain size led to improved corrosion-wear resistance of the Zn coatings.

Higher mechanical strength and surface stability possessed by nanocrystalline Zn coatings enhanced the corrosion resistant property[59].

Kumar et al. [48] prepared the composite coating with the rutile (is a mineral composed primarily of TiO_2) TiO_2 nanoparticles (size $\leq$ 100nm). They performed a test on Electrochemical work station as Potentio-dynamic polarization curves for Zn coating as D_0 and Zn-TiO_2 composite Coatings are D_1, D_2, and D_3. It is found that the lowest I(corr) of D_2 is due to the incorporation of TiO_2 nanoparticles with zinc matrix, where the incorporated TiO_2 particles decreases the active surface area or anodic sites in zinc coating, which are responsible for corrosion. This higher Icorr and more negative Ecorr of D_3 could suggest an acceleration of the corrosion process, which may be due to chemical heterogeneities generated in the zinc matrix by the incorporation of agglomerated TiO_2 particles. The Electrochemical Impedance Spectroscopy (EIS) measurements has found that in 0.25 g/L samples of ammonium sulphate solution shows coating obtained from 6 g/L of rutile TiO_2 nanoparticles (D_2) has higher impedance modulus than other coatings.

2.7 Pitting corrosion behavior of Zn-Ni alloy electroplating

Pitting is one of the most common and localized corrosion, which occurs at the sites of local failure of the passive layers[61][62]. It is an intensive and destructive surface attack and can cause the equipment failure by penetration. At the microscopic level, pits nucleate and are mostly obscured by the corrosion products. Therefore, pitting is one of the most detrimental and indiscernible forms of corrosion[63][64].

There are several study has been done on the pitting corrosion of the metal alloy on the steel surface, and one of the studies conducted an experiment on the Cu-Ni alloy pitting corrosion and has been reported by Jin et al.[65] at various exposure times in the marine environment (30^0C). It is revealed that the coated sample showed slight pits at one week in comparison to the months of the marine exposure. The pitting areas are small, and the Cu matrix is still

apparent. Although some white and gray corrosion products gradually exhibited on the coated surface. Moreover, E_{corr} values shifted to the positive direction, and I_{corr} turned to the negative for the extension of the exposure time.

Electrochemical and morphological analyses of Zn and Zn alloy pitting corrosion have been studied by Miao et.al.[66] Pitting corrosion behavior of Zn and Zn alloy was examined using cyclic voltammetry and potential scan technique in the presence of 0.10 – 0.90 mol/l of NaCl over a pH range of 2 to 12. Zinc hydroxy chloride complexes were the principal element of a passive layer formed during the span of passivation which makes the passive layer considerably stable over a more extended period in the pH range of 2 to 12. However, increasing the concentration of chloride ions lead to break the passive layer and propagate the pit growth on the zinc surface.

2.8 Novelty and contribution

This research attempts to overcome the gaps identified in Chapter 1 and Chapter 2 by taking the following steps:

The research articles and connections to the research objectives and associated tasks and block diagram of the overall research is presented in Table 2.11 and Figure 2.9.

Table 2.11. Papers and connections to the research objectives and associated tasks

Papers as chapters	*Research objectives*	*Associated task*
Chapter-3: experimental design and optimization for Zn-Ni alloy electroplating	• To determine the key factor influencing Zn-Ni alloy electroplating • Optimization of Zn-Ni films	• Experimental plan comprised of four steps: • Two-level fractional factorial design (FFD) • Response surface design the steepest ascent analysis • Central composite design (CCD) • Corrosion behaviour test to optimize the factors in Zn-Ni deposition.
Chapter-4 (a) and 4 (b): Electrochemical behaviour and analysis of Zn and Zn-Ni coatings from potassium citrate baths	• To study the electrochemical behaviour of pure Zn and Zn–Ni alloy coatings from citrate and non-citrate baths • To determine the stability of the electrolyte baths	• Bath stability by using Pourbaix diagram • Corrosion current and potential calculation from potentiodynamic polarization method • Impedance and electrical circuit evaluation by using electrochemical impedance spectroscopy. • Hardness test by using Vicker microhardness method.
Chapter-5: Zn-Ni alloy coatings and corrosion resistant analysis in 3.5 wt.% NaCl solutions from EDTA bath	• Zn-Ni plating from EDTA bath at various operating conditions	• Bath stability by using Pourbaix diagram • Morphological analysis of the Zn-Ni coating • crystalline phase and orientation studied by XRD • Corrosion current and potential calculation from potentiodynamic polarization method • Impedance and electrical circuit evaluation by using electrochemical impedance spectroscopy.
Chapter-6: Zn-Ni alloy and Zn-Ni-TiO_2 nano-composite corrosion resistance coatings from ammonium citrate	• Zn-Ni alloy and Zn-Ni-TiO_2 under different operating settings • formation of corrosion products on the coated samples • Titania TiO_2 electrodeposited from ammonium citrate bath	• Potentiodynamic polarization results studied from Tafel slopes • Impedance measurement and electrical circuit evaluation conducted by EIS method • Compositions of corrosion products analyzed using EDS method • Morphological analysis of the coatings • corrosion behaviour studies at various exposure time by using Atlantic Ocean sea water
Chapter-7: **e**ffect of chloride and pH the micro-mechanism of Zn-Ni alloy pitting corrosion in NaCl solution	• Electrochemical and morphological analysis of Zn-Ni pitting corrosion by using experimental design method	• Zn-Ni alloy coatings in NaCl solutions with different chloride concentrations and pH by using: • Potentiodynamic polarization (Tafel slopes), electrochemical impedance spectroscopy (EIS) and scanning electron microscopy (SEM) integrated with energy dispersive spectroscopy (EDS). The design of the experiment with three-level fractional factorial design (FFD)

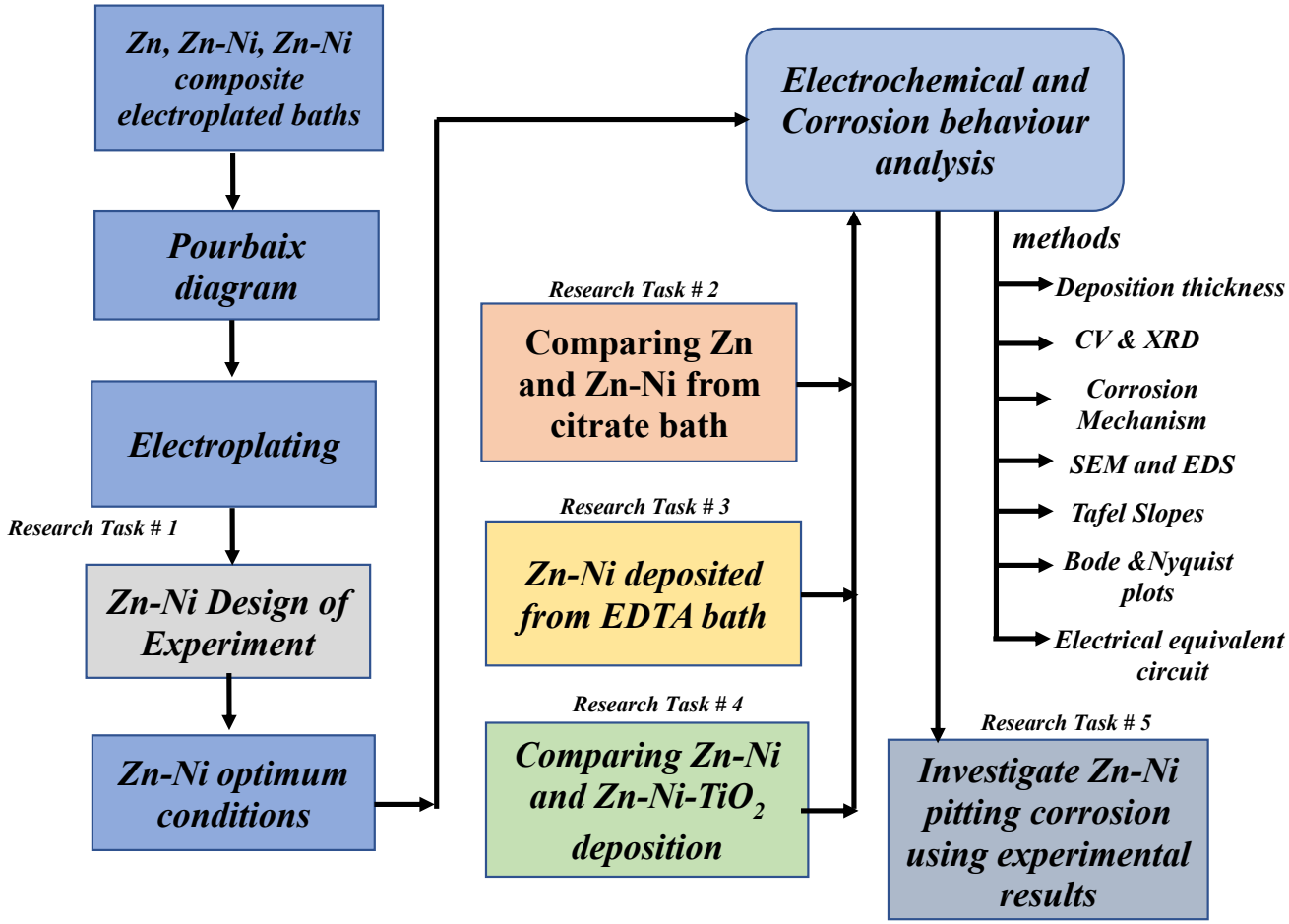

Figure 2.9 Block diagram of the overall research tasks

- As seen from the literature, several experimental studies have been completed on Zn-Ni deposited from non-citrate and citrate baths at various operating conditions. No systematic design of experiment study was found for Zn-Ni alloy deposited from a citrate bath, that includes optimum parameter conditions and hydrogen evolution reaction (HER) suppression to improve corrosion resistant properties of the coating. To study the design of experiments of Zn-Ni alloy deposited from citrate bath lead to finding the optimum conditions for Zn-Ni electroplating to enhance the corrosion-resistant properties of the coating.
- The continuous studies for pure Zn and Zn-Ni alloy coating on steel substrates to improve corrosion resistance using potassium citrate as a complexing agent. The effects of plating variables such as bath composition and current density on coating composition, morphology

and corrosion property were investigated. The stabilized bath also studied from the pourbaix diagram. The equivalent electrical circuits obtained from the experimental fitted data of Nyquist and Bode plot also demonstrated the Zn-Ni deposited from citrate in comparison to the pure Zn and Zn-Ni from the non-citrate bath. The effect of an optimum operating parameter on deposit character and their corrosion behaviour was observed and discussed.

- Another experimental study to examine the stability behaviour of the EDTA bath has conducted. Zn-Ni plating from EDTA bath at various operating conditions, there was no systematic study found to determine the optimal concentration of EDTA, plating current density, and bath composition. To fulfill the knowledge gap, research was needed to find the operating conditions at various levels.
- The next experimental study has been conducted on the comparison of Zn-Ni alloy and composite coatings. Experimental analyses have been carried out on Zn-Ni alloy and Zn-Ni-TiO2 under different operating settings; there was less study found to compare Zn-Ni alloy and composite coatings deposited from ammonium citrate bath at optimum TiO_2 concentration. Therefore, to fulfil this knowledge gap, the research was needed to find the optimum conditions for the Zn-Ni alloy and Zn-Ni nanosized Titania TiO_2 electrodeposited from ammonium citrate bath. The most significant corrosion products and phase orientation for Zn-Ni alloy electroplating are also examined.
- The last study for this research work is conducted on the pitting corrosion behaviour of Zn-Ni alloy. Electrochemical and morphological analyses of pitting corrosion have been implemented on Zn-Ni alloy coated samples. However, less systematic studies have been conducted to investigate the pitting corrosion behaviour of Zn-Ni alloy coating on mild steel. In this paper, the effects of chloride and pH on the pitting-mechanism of Zn-Ni alloy coatings in NaCl solutions have been investigated and analyzed. An optical microscope and scanning

electron microscope (SEM) was used to measure the pits' depth/diameter and visualization of pits' behaviour.

References

[1] B. J.H and N. S., *Handbook of bolts and bolted joints*. New York: M. Dekker., 1998.

[2] W. R., *Electrodeposition of Zinc and Zinc Alloys. Modern Electroplating:* John Wiley & Sons, Inc.

[3] W. Giurlani *et al.*, "Electroplating for Decorative Applications: Recent Trends in Research and Development," *Coatings*, vol. 8, 260, pp. 1–25, 2018.

[4] Z. Feng, Q. Li, J. Zhang, P. Yang, H. Song, and M. An, "Electrodeposition of nanocrystalline Zn-Ni coatings with single gamma phase from an alkaline bath," *Surf. Coatings Technol.*, vol. 270, pp. 47–56, 2015.

[5] F. L. G. Silva, D. C. B. Do Lago, E. D'Elia, and L. F. Senna, "Electrodeposition of Cu-Zn alloy coatings from citrate baths containing benzotriazole and cysteine as additives," *J. Appl. Electrochem.*, vol. 40, no. 11, pp. 2013–2022, 2010.

[6] A. P. Abbott, J. C. Barron, G. Frisch, K. S. Ryder, and A. F. Silva, "The effect of additives on zinc electrodeposition from deep eutectic solvents," *Electrochim. Acta*, vol. 56, no. 14, pp. 5272–5279, 2011.

[7] C. Muller, M. Sarret, and M. Benballa, "Complexing agents for a Zn – Ni alkaline bath," *J. Electroanal. Chem.*, vol. 519, pp. 85–92, 2002.

[8] H. . Nakano, S. . Shibata, S. . Arakawa, S. . Oue, and S. . Kobayashi, "Electrodeposition behavior of Zn-Co alloys from an alkaline zincate solution containing triethanolamine," *ISIJ Int.*, vol. 53, no. 10, pp. 1858–1863, 2013.

[9] M. G. Hosseini, H. Ashassi-Sorkhabi, and H. A. Y. Ghiasvand, "Electrochemical studies of Zn-Ni alloy coatings from non-cyanide alkaline bath containing tartrate as

complexing agent," *Surf. Coatings Technol.*, vol. 202, no. 13, pp. 2897–2904, 2008.

[10] L. M. Muresa, J. Eymard, D. Blejan, and E. Indrea, "Zn-Ni alloy coatings from alkaline bath containing triethanolamine. influence of additives," *Stud. Univ. BABEŞ-BOLYAI, Chem.*, vol. 1, pp. 7–44, 2010.

[11] Z. Feng, Q. Li, J. Zhang, P. Yang, and M. An, "Studies on the enhanced properties of nanocrystalline Zn–Ni coatings from a new alkaline bath due to electrolyte additives," *RSC Adv.*, vol. 5, no. 72, pp. 58199–58210, 2015.

[12] K. M. Zohdy, "Surface protection of carbon steel in acidic solution using ethylenediaminetetraacetic disodium salt," *Int. J. Electrochem. Sci.*, vol. 10, no. 1, pp. 414–431, 2015.

[13] J. B. Bajat, A. B. Petrović, and M. D. Maksimović, "Electrochemical deposition and characterization of zinc-nickel alloys deposited by direct and reverse current," *J. Serbian Chem. Soc.*, vol. 70, no. 12, pp. 1427–1439, 2005.

[14] S. Shivakumara, U. Manohar, Y. Arthoba Naik, and T. V. Venkatesha, "Influence of additives on electrodeposition of bright Zn-Ni alloy on mild steel from acid sulphate bath," *Bull. Mater. Sci.*, vol. 30, no. 5, pp. 455–462, 2007.

[15] V. Soare *et al.*, "Synthesis and performance of Zn-Ni-P thin films," *Chinese Phys. B*, vol. 24, no. 3, 2015.

[16] S. Fashu, C. D. Gu, J. L. Zhang, M. L. Huang, X. L. Wang, and J. P. Tu, "Effect of EDTA and NH_4Cl additives on electrodeposition of Zn-Ni films from choline chloride-based ionic liquid," *Trans. Nonferrous Met. Soc. China (English Ed.*, vol. 25, no. 6, pp. 2054–2064, 2015.

[17] A. Conde, M. A. Arenas, and J. J. de Damborenea, "Electrodeposition of Zn-Ni coatings as Cd replacement for corrosion protection of high strength steel," *Corros. Sci.*, vol. 53, no. 4, pp. 1489–1497, 2011.

[18] G. N. L. R. Bapu, J. Ayyapparaju, and G. Devaraj, “Electrodeposition of Zinc-Nickel Alloy from Fluoroborate Baths- As a Substitiute for Electrogalvanising,” *B. Electrochem.*, vol. 3 (2), pp. 139–141, 1987.

[19] C. wei Su, F. jiao He, H. Ju, Y. bin Zhang, and E. li Wang, “Electrodeposition of Ni, Fe and Ni-Fe alloys on a 316 stainless steel surface in a fluorborate bath,” *Electrochim. Acta*, vol. 54, no. 26, pp. 6257–6263, 2009.

[20] H. Faid, L. Mentar, M. R. Khelladi, and A. Azizi, “Deposition potential effect on surface properties of Zn–Ni coatings,” *Surf. Eng.*, vol. 33, no. 7, pp. 529–535, 2017.

[21] M. V. Tomić, M. M. Bučko, M. G. Pavlović, and J. B. Bajat, “Corrosion stability of electrochemially deposited Zn-Mn alloy coatings,” *Contemp. Mater.*, vol. 1, no. 1, pp. 87–93, 2010.

[22] Y. F. Jiang, L. F. Liu, C. Q. Zhai, Y. P. Zhu, and W. J. Ding, “Corrosion behavior of pulse-plated Zn-Ni alloy coatings on AZ91 magnesium alloy in alkaline solutions,” *Thin Solid Films*, vol. 484, no. 1–2, pp. 232–237, 2005.

[23] J. R. Garcia, D. C. B. do Lago, and L. F. de Senna, “Electrodeposition of Cobalt Rich Zn-Co alloy Coatings from Citrate Bath,” *Mater. Res.*, vol. 17, no. 4, pp. 947–957, 2014.

[24] Y. Zhang and D. G. Ivey, “Electroplating of Nanocrystalline CoFeNi Soft Magnetic Thin Films from a Stable Citrate-Based Bath,” *Chem. Mater.*, vol. 16, no. 7, pp. 1189–1194, 2004.

[25] M. Pushpavanam and K. Balakrishnan, “Zinc-nickel alloy deposition in the presence of citrate ions,” *J. Appl. Electrochem.*, vol. 26, no. 10, pp. 1065–1069, 1996.

[26] Z. Feng, L. Ren, J. Zhang, P. Yang, and M. An, “Effect of additives on the corrosion mechanism of nanocrystalline zinc-nickel alloys in an alkaline bath,” *RSC Adv.*, vol. 6, no. 91, pp. 88469–88485, 2016.

[27] G. M. de Oliveira and I. A. Carlos, “Silver-zinc electrodeposition from a thiourea

solution with added EDTA or HEDTA," *Electrochim. Acta*, vol. 54, no. 8, pp. 2155–2163, 2009.

[28] M. R. H. de Almeida, E. P. Barbano, M. F. de Carvalho, I. A. Carlos, J. L. P. Siqueira, and L. L. Barbosa, "Electrodeposition of copper-zinc from an alkaline bath based on EDTA," *Surf. Coatings Technol.*, vol. 206, no. 1, pp. 95–102, 2011.

[29] B. G, G. E, S. M, M. C, and P. J., "Characterization of zinc– nickel alloys obtained from an industrial chloride bath," *J. Appl. Electrochem.*, vol. 28, pp. 1113-1120., 1998.

[30] B. C, B. JP, and R. A., "Structure and thermal stability of zinc–nickel electrodeposits.," *J. Appl. Electrochem.*, vol. 29, no. 1045–1051, 1999.

[31] B. H, B. H, B. JP, R. A, and et al. Marolleau, Marolleau, "Structure of zinc–nickel alloyelectrodeposits," *J. Mater. Sci.*, vol. 34, pp. 881–886, 1999.

[32] F. L, F. R, Q. E, and R. G., "Electrodeposition of zinc-nickel alloys from chloride solution," *J. Appl. Electrochem.*, vol. 17, pp. 574–582, 1987.

[33] A. Gomes, I. Almeida, T. Frade, and A. C. Tavares, "Stability of Zn–Ni–TiO_2 and Zn–TiO_2 nanocomposite coatings in near-neutral sulphate solutions," *J. Nanoparticle Res.*, vol. 14, no. 2, p. 692, 2012.

[34] A. Vlasa, S. Varvara, A. Pop, C. Bulea, and L. M. Muresan, "Electrodeposited Zn–TiO2 nanocomposite coatings and their corrosion behavior," *J. Appl. Electrochem.*, vol. 40, no. 8, pp. 1519–1527, 2010.

[35] J. . Friel, "Atmospheric corrosion products on aluminium, zinc, and aluminium-zinc metallic coatings," *Corrosion*, vol. 42, pp. 422–426, 1986.

[36] K. R. Sriraman, S. Brahimi, J. A. Szpunar, J. H. Osborne, and S. Yue, "Characterization of corrosion resistance of electrodeposited Zn-Ni Zn and Cd coatings," *Electrochim. Acta*, vol. 105, pp. 314–323, 2013.

[37] M. Bučko, J. Rogan, S. I. Stevanović, A. Perić-Grujić, and J. B. Bajat, "Initial corrosion

protection of Zn-Mn alloys electrodeposited from alkaline solution," *Corros. Sci.*, vol. 53, no. 9, pp. 2861–2871, 2011.

[38] J. yin FEI, G. zheng LIANG, W. li XIN, and W. kang WANG, "Surface Modification With Zinc and Zn-Ni Alloy Compositionally Modulated Multilayer Coatings," *J. Iron Steel Res. Int.*, vol. 13, no. 4, pp. 61–67, 2006.

[39] D. Blejan and L. M. Muresan, "Corrosion behavior of Zn-Ni-Al_2O_3 nanocomposite coatings obtained by electrodeposition from alkaline electrolytes," *Mater. Corros.*, vol. 64, no. 5, pp. 433–438, 2013.

[40] M. Gavrila, J. P. Millet, H. Mazille, D. Marchandise, and J. M. Cuntz, "Corrosion behaviour of zinc-nickel coatings, electrodeposited on steel," *Surf. Coatings Technol.*, vol. 123, no. 2–3, pp. 164–172, 2000.

[41] G. Barceló, M. Sarret, C. Müller, and J. Pregonas, "Corrosion resistance and mechanical properties of zinc electrocoatings," *Electrochim. Acta*, vol. 43, no. 1–2, pp. 13–20, 1998.

[42] T. V. Byk, T. V. Gaevskaya, and L. S. Tsybulskaya, "Effect of electrodeposition conditions on the composition, microstructure, and corrosion resistance of Zn-Ni alloy coatings," *Surf. Coatings Technol.*, vol. 202, no. 24, pp. 5817–5823, 2008.

[43] M. M. Abou-Krisha, "Electrochemical studies of zinc-nickel codeposition in sulphate bath," *Appl. Surf. Sci.*, vol. 252, no. 4, pp. 1035–1048, 2005.

[44] S. Fashu, C. D. Gu, X. L. Wang, and J. P. Tu, "Influence of electrodeposition conditions on the microstructure and corrosion resistance of Zn-Ni alloy coatings from a deep eutectic solvent," *Surf. Coatings Technol.*, vol. 242, pp. 34–41, 2014.

[45] F. H. Assaf, A. M. A. El-Seidy, M. M. A.-K. And, and A. A. Eissa, "Electrodeposition and Characterization of Zn-Ni-Mn Alloy from Sulfate Bath: Influence of Current Density 100727," vol. 10, pp. 1–14, 2015.

[46] Y. Guan and X. Peng, "A novel electrodeposited Cu-Zn-Bi film with increased corrosion

resistance in a 0.05 M K2SO4solution," *Appl. Surf. Sci.*, vol. 258, no. 2, pp. 822–826, 2011.

[47] M. M. Abou-Krisha, A. G. Alshammari, F. H. Assaf, and F. A. El-Sheref, "Electrochemical behavior of Zn-Co-Fe alloy electrodeposited from a sulfate bath on various substrate materials," *Arab. J. Chem.*, pp. 0–7, 2014.

[48] B. M. Praveen and T. V. Venkatesha, "Electrodeposition and properties of Zn-nanosized TiO_2 composite coatings," *Appl. Surf. Sci.*, vol. 254, no. 8, pp. 2418–2424, 2008.

[49] B. M. Praveen and T. V. Venkatesha, "Electrodeposition and Corrosion Resistance Properties of Zn-Ni/TiO_2 Nano composite Coatings," *Int. J. Electrochem.*, vol. 2011, pp. 1–4, 2011.

[50] C. Zhao, Y. Yao, and L. He, "Electrodeposition and characterization of Ni-W/ZrO2 nanocomposite coatings," *Bull. Mater. Sci.*, vol. 37, no. 5, pp. 1053–1058, 2014.

[51] D. Blejan, D. Bogdan, M. Pop, A. V. Pop, and L. M. Muresan, "Structure, morphology and corrosion resistance of Zn-Ni-TiO_2 composite coatings," *Optoelectron. Adv. Mater. Commun.*, vol. 5, no. 1, pp. 25–29, 2011.

[52] Q. Zhao, Y. Liu, and C. Wang, "Development and evaluation of electroless Ag-PTFE composite coatings with anti-microbial and anti-corrosion properties," *Appl. Surf. Sci.*, vol. 252, no. 5, pp. 1620–1627, 2005.

[53] H. Y. Zheng and M. Z. An, "Electrodeposition of Zn-Ni-Al_2O_3 nanocomposite coatings under ultrasound conditions," *J. Alloys Compd.*, vol. 459, no. 1–2, pp. 548–552, 2008.

[54] S. Ghaziof and W. Gao, "Electrodeposition of single gamma phased Zn-Ni alloy coatings from additive-free acidic bath," *Appl. Surf. Sci.*, vol. 311, pp. 635–642, 2014.

[55] A. Vlasa, S. Varvara, A. Pop, C. Bulea, and L. M. Muresan, "Electrodeposited Zn-TiO2 nanocomposite coatings and their corrosion behavior," *J. Appl. Electrochem.*, vol. 40, no. 8, pp. 1519–1527, 2010.

[56] M. K. Punith Kumar, T. V. Venkatesha, M. K. Pavithra, and A. N. Shetty, "A Study on Corrosion Behavior of Electrodeposited Zn-Rutile TiO_2 Composite Coatings," *Synth. React. Inorganic, Met. Nano-Metal Chem.*, vol. 42, no. 10, pp. 1426–1434, 2012.

[57] C. M. Kumar, P. Kumar, T. V. Venkatesha, K. Vathsala, and K. O. Nayana, "Electrodeposition and corrosion behavior of Zn-Ni and Zn-Ni-Fe_2O_3 coatings," *J. Coatings Technol. Res.*, vol. 9, no. 1, pp. 71–77, 2012.

[58] T. Jin, F. mei Kong, R. qin Bai, and R. liang Zhang, "Anti-corrosion mechanism of epoxy-resin and different content Fe_2O_3 coatings on magnesium alloy," *Front. Mater. Sci.*, vol. 10, no. 4, pp. 367–374, 2016.

[59] O. Hammami, L. Dhouibi, P. Berçot, E. M. Rezrazi, and E. Triki, "Study of Zn-Ni alloy coatings modified by Nano-SiOparticles incorporation," *Int. J. Corros.*, vol. 2012, 2012.

[60] V. G. Roev, R. A. Kaidrikov, and A. B. Khakimullin, "Zinc – Nickel Electroplating from Alkaline Electrolytes Containing Amino Compounds," vol. 37, no. 7, pp. 756–759, 2001.

[61] R. Fratesi, G. Roventi, G. Giuliani, and C. R. Tomachuk, "Zinc-cobalt alloy electrodeposition from chloride baths," *J. Appl. Electrochem.*, vol. 27, no. 9, pp. 1088–1094, 1997.

[62] I. H. Karahan and H. S. Güder, "Electrodeposition and properties of Zn, Zn–Ni, Zn–Fe and Zn–Fe–Ni alloys from acidic chloride–sulphate electrolytes," *Trans. IMF*, vol. 87, no. 3, pp. 155–158, 2009.

[63] O. S. I. Fayomi and A. P. I. Popoola, "An Investigation of the Properties of Zn Coated Mild Steel," *Int. J. Electrochem. Sci*, vol. 7, pp. 6555–6570, 2012.

[64] A. P. I. Popoola and O. S. Fayomi, "Performance evaluation of zinc deposited mild steel in chloride medium," *Int. J. Electrochem. Sci.*, vol. 6, no. 8, pp. 3254–3263, 2011.

[65] S. Basavanna and Y. Arthoba Naik, "Electrochemical studies of Zn-Ni alloy coatings

from acid chloride bath," *J. Appl. Electrochem.*, vol. 39, no. 10, pp. 1975–1982, 2009.

[66] B. M. Durodola, J. A. O. Olugbuyiro, S. A. Moshood, O. S. Fayomi, and A. P. I. Popoola, "Study of influence of zinc plated mild steel deterioration in seawater environment," *Int. J. Electrochem. Sci.*, vol. 6, no. 11, pp. 5605–5616, 2011.

[67] Q. Li, H. Lu, J. Cui, M. An, and D. Li, "Electrodeposition of nanocrystalline zinc on steel for enhanced resistance to corrosive wear," *Surf. Coatings Technol.*, vol. 304, pp. 567–573, 2016.

[68] G. S. Frankel, "Pitting Corrosion of Metals," *J. Electrochem. Soc.*, vol. 145, no. 6, p. 2186, 1998.

[69] R. C. Newman and W. R. Whitney, "understanding the corrosion of stainless steel," *Corrosion*, vol. 57, pp. 1030–1041, 2001.

[70] H. B. Li, J. Z.H., C. Y., and Z. R. Zhang, "Fabrication of high nitrogen austenitic stainless steels with excellent mechanical and pitting corrosion properties," *J. Met. Mater.*, vol. 16, pp. 517–524, 2009.

[71] Y. Kim and R. G. Buchheit, "A characterization of the inhibiting effect of Cu on metastable pitting in dilute Al-Cu solid solution alloys," *Electrochim. Acta*, vol. 52, no. 7, pp. 2437–2446, 2007.

[72] T. Jin, W. Zhang, N. Li, X. Liu, L. Han, and W. Dai, "Surface characterization and corrosion behavior of 90/10 copper-nickel alloy in marine environment," *Materials (Basel).*, vol. 12, no. 11, 2019.

[73] W. Miao, I. S. Cole, A. K. Neufeld, and S. Furman, "Pitting Corrosion of Zn and Zn-Al Coated Steels in pH 2 to 12 NaCl Solutions," 2007.

3.0 Optimization of Zinc-Nickel Film Electrodeposition for Better Corrosion Resistant Characteristics

Preface

In this chapter, the most important deposition factors influencing the corrosion resistant activity of Zn-Ni deposits are explored by using an experimental design method. The complete experimental design is divided into four parts (1) a two-level fractional factorial design (FFD), (2) a response surface design the steepest ascent analysis, (3) a central composite design (CCD), and (4) corrosion behaviour test to achieve the optimized factors for Zn-Ni deposition. To analyse the optimized samples in step 4 the following analytical techniques were used (a) Electrochemical Impedance Spectroscopy (EIS) was employed to study the corrosion resistant property of the optimized Zn-Ni alloy coatings, (b) XRD was to analyze the phase compositions in deposit Zn-Ni films and found the relationship between film phase compositions and corrosion resistant properties, (c) SEM was used to analyze the microstructure of the Zn-Ni deposits and its effect on the corrosion resistant properties of the deposits. Moreover, energy dispersive spectroscopy (EDS) is used to measure the corrosion product chemical compositions of the optimized samples. This chapter brings a new study to explored the numerous factors and levels to affect the Zn-Ni alloy electroplating, to enhance the corrosion resistant properties of the coated samples. The content of this chapter has been published as a manuscript in the Canadian Journal of Chemical Engineering, 1–14, 2019.

Abstract

Corrosion is one of the main causes of structural deterioration in offshore and marine structures. One way to mitigate the effect of corrosion is with Zn-Ni electroplated coatings. An experimental design and optimization procedures for Zn-Ni alloy electroplating was an explored. This study analyzed a five-variable experimental plan comprised of four steps: (1) a two-level fractional factorial design (FFD), (2) a response surface design the steepest ascent analysis, (3) a central composite design (CCD), and (4) corrosion behaviour test to optimize the factors in Zn-Ni deposition. The critical plating variables in step 1 were zinc/nickel molar concentration ratio, current density, citrate concentrations, plating temperature and plating time, to determine their influence the polarization resistance and corrosion resistance. In steps 2 and 3 the significant variables were studied using the steepest ascent method and the central composite design (CCD) to find the most optimal conditions for zinc-nickel electroplating. These conditions were found to be a Zn/Ni molar concentration ratio 0.66, a plating temperature of 28^0C, an electroplating current density of 60mA/cm^2, an electroplating time of 13 minutes, and a citrate concentration of 0.062 mol/l. From the corrosion behaviour test of step-4 was found that the films with higher intensity of γ-$NiZn_3$, γ-Ni_2Zn_{11}, and γ-Ni_3Zn_{22} phases exhibited better corrosion resistance.

Keywords: Experimental statistics, Corrosion current, Zn-Ni alloy, Electroplating, Impedance spectroscopy.

3.1 Introduction

The most of the marine and offshore structures are constructed from steel and have the highest probability for the incidents due to corrosion degradation[1]. Corrosion is the process to deteriorate the metals by the electrochemical reactions[2][3][4][5][6]. One way to mitigate the effect of corrosion is to create a barrier between the metal and corrosive environments by apply metal electroplated coatings. The sacrificial metallic coating such as zinc (Zn) and cadmium (Cd) are used to protect steel structures/components from corrosion. However, the Cd coating in any form such as cyanide-based and Cd compounds are carcinogenic and growing with the environmental and health issue the used of Cd coating is restricted[7]. Zinc is the most important metal to galvanically protect steel structures from corrosion in industrial applications[8]. Zinc is available in many forms including sheet and strips which makes it easier to use. However, the primary use of zinc in galvanic protection is to form a layer on steel to protect the steel from corrosion[9]. Zn (E_0 = -0.76 V)[10] has a more negative reduction potential than Fe (E_0 = -0.44 V)[10] and dissolves rapidly in the higher corrosive environment. A thin zinc layer is deposited to form the corrosion resistant barrier on the surface of metal/steel structures. Zn-coated steels exhibit higher corrosion resistance in the harsh environment, but their service lives are mitigated significantly due to the growth of corrosion products layers on the coated surface, commonly called white rust[11][12][13][14]. The lifespan of a zinc coating is decreased due to dissolution in corrosive solution providing a significant motive power between Zn and steel substrates. When Zn is alloyed with the Ni the mechanical properties of the coating are strengthened and the corrosion resistant properties increased. To enhance the corrosion resistant property of the Zn coating is to make alloying with Fe, Co and Ni. According to the literature[15][16], zinc alloy coatings such as Zn-Ni, Zn-Co and Zn-Fe can result in higher corrosion resistance compared to pure zinc coating. Due to the excellent corrosion resistant property of nickel, Zn-Ni alloy coatings are used extensively to protect steel substrates

[17]. This is especially true in the automobile industry[18][19]. Zn-Ni alloys possess better mechanical and thermal properties compared to pure Zn and other Zn alloys[13][20]. The electrodeposition of Zn-Ni alloy provides significantly better corrosion resistance to coated steel structures in an aggressive environment[21] [22][23]. Currently, Zn-Ni alloy coating offers a crucial eco-friendly substitute for toxic cadmium coating[24][25]. However, Zn-Ni coatings had higher polarization resistance after wear testing as compared to zinc and cadmium coatings.

Research has been completed on Zn-Ni electrodeposition at different conditions. Gavrila et al. [19] studied the Zn-Ni electrodeposited on steel from a neutral saline solution under different preparation conditions (e.g., the composition of the bath, the current density of Zn-Ni deposition, degassing and chromate passivation). Fashu et al. [26] studied the vital electrodeposition parameters, such as the temperature of the bath, plating voltage and electrolyte composition. Both Gavrila et al.[19] and Fashu et al.[26] examined the behaviour of the parameters on Zn-Ni films deposited from chlorine-chloride-urea baths. The electrochemical analysis indicated that Zn-Ni coatings deposited from the 0.45 mol/l of Zn and 0.05 mol/l of Ni bath at 55 ^{0}C and 0.8V exhibited compact, flatten and void-free texture with ideal Zn content, showed highest corrosion resistance compared with Zn-Ni coatings obtained from other baths with different Zn-Ni compositions.

The electroplating potential of Zn-Ni deposited at different condition is discussed by Abou-Krisha and they observed the potential for Zn, Ni, and Zn-Ni alloy deposition from a sulfate bath at different conditions. Zinc deposition was found to start at -1.14V, Zn-Ni alloy coating began at -1.12V, and Ni deposition started at -0.85V. In all cases this was followed by a rapid move to more negative potential. They found, Ni deposits at a lower potential, Zn deposits at a higher potential, and Zn-Ni alloy deposits at medium potential because Ni deposition is strongly inhibited in the presence of Zn^{+2}, whereas, Zn deposition is induced with the presence

of Ni^{+2}. They concluded that plated Zn-Ni alloys exhibited better corrosion resistance than pure zinc coating[27].

Faid et al. [28] studied the electrodeposition of Zn-Ni coating on a mild steel substrate from a sulfate bath under different deposition potentials. The researchers observed that the content of nickel in the deposit was increased by applying a more negative deposition potential. The electrochemical analysis revealed that the Zn-Ni coating obtained at the most negative deposition potential exhibited the best corrosion resistance.

There is literature available that addresses Zn alloy deposited from citrate baths. Garcia et al.[29] plated Zn-Co alloy films on carbon steel at 25^0C from citrate-added baths. The investigators found that current density and a sodium citrate complexing agent influenced the deposition process of the Zn-Co alloy. Uniform coating, small grain size, and better corrosion resistant were obtained at high current density, which led to increased cobalt content in the coating. Zhang and Ivey[30] reported on the application of potassium citrate to stabilize a Co-Fe-Ni plating bath and prevent metal hydroxide precipitation at higher pH.

The optimum conditions for the Zn-Ni electroplating were reported by Assaf et al. [31]. They examined the effects of electroplating parameters including bath composition, temperature and current density on the deposition of copper, zinc and brass on a steel substrate. This work revealed that zinc deposited at a low current density ($<3mA/cm^2$) and low zinc content ($<15g/dm^3$) in the bath affected the formation of fine grains and left some bare areas. The authors indicate that this behaviour may be due to the low cathodic current efficiency of zinc deposition and strong evolution of hydrogen gas. There is a limited study focusing on the Zn-Ni deposited from citrate bath. Therefore, the authors have focused on the factors of Zn-Ni electrodeposition from citrate bath.

As seen from the literature, several experimental studies have been completed on Zn-Ni deposited from non-citrate and citrate baths at various operating conditions. No systematic

design of experiment study was found for Zn-Ni alloy deposited from a citrate bath, that includes optimum parameter conditions and hydrogen evolution reaction (HER) suppression to improve corrosion resistant properties of the coating. To study the design of experiments of Zn-Ni alloy deposited from citrate bath lead to finding the optimum conditions for Zn-Ni electroplating to enhance the corrosion resistant properties of the coating. During the electrodeposition of metals, hydrogen is evolved due to electrolysis. The evolved hydrogen may diffuse outward and become trapped in the substrate/coating interface or migrate inward into the steel lattice causing delayed embrittlement when the component is subjected to stress. To suppress hydrogen deposition and stabilize the plating baths alkalis and complexing agents (e.g., acetate and citrate) were added into the baths for ideal Zn, Zn-Ni and Zn-Ni composite electroplating. According to the above results, the corrosion resistant property, uniformity, thickness, and mechanical hardness of the plated films were also improved [28][32][33][34][29][35]. To fill this gap, a research study was conducted to study Zn-Ni alloy deposition at different levels of operating conditions.

3.2 Methodology

To find the critical electroplating variables affecting the corrosion current density (I_{corr}) of Zn-Ni-deposits (specimen), a four step experimental plan was developed. The results from each step informed the next step in the process to determine the optimum conditions for Zn-Ni electroplating and their corrosion tests.

Step 1: Two-level factorial fraction design (FFD): FFD was used to design the experiments to determine the important variables that affect I_{corr} and R_p. The analysis of variance (ANOVA) was conducted to achieve a mathematical evaluation of each outcome, containing the main factor and two-factor interaction. The main factors such as current density of the deposition (R), plating time (S) and citrate concentration (T) are considered as a main variable and it was

used as an initial variable for step 2, to obtain the vicinity toward the optimized experimental settings.

Step 2: Steepest ascent analysis (SAA): SAA was used to consider the main variables for the zinc-nickel plating with the lowest possible activity of I_{corr} to encourage higher corrosion resistant properties. However, the experimental conditions at run 8 are chosen as the central point for the central composite design (CCD). The significant variables and their values were used as an initial point for step 3.

Step 3: The central composite design (CCD): CCD was used to explain the corrosion current activity of Zn-Ni samples in contrast to the plating variables in the vicinity to the optimal conditions.

Step 4: Corrosion behaviour test: The corrosion resistant behaviour of the optimized coated samples from step 3 is studied in a short period lab scale experiment using Atlantic Ocean seawater. The effect of the optimum operating conditions on Zn-Ni plating quality and corrosion behaviour was observed and discussed. To analyse the optimized samples in step 4 the following analytical techniques were used:

- Electrochemical Impedance Spectroscopy (EIS) was employed to analyze the corrosion resistant property of the optimized Zn-Ni alloy coatings.
- XRD was to analyze the phase compositions in deposit Zn-Ni films and found the relationship between film phase compositions and corrosion resistant properties.
- SEM was used to analyze the microstructure of the Zn-Ni deposits and its effect on the corrosion resistant properties of the deposits. Moreover, energy dispersive spectroscopy (EDS) is used to measure the corrosion product chemical compositions of the optimized samples.

The complete experimental design block diagram of the factors, responses and the four steps of statistical analysis is shown in Figure 3.1.

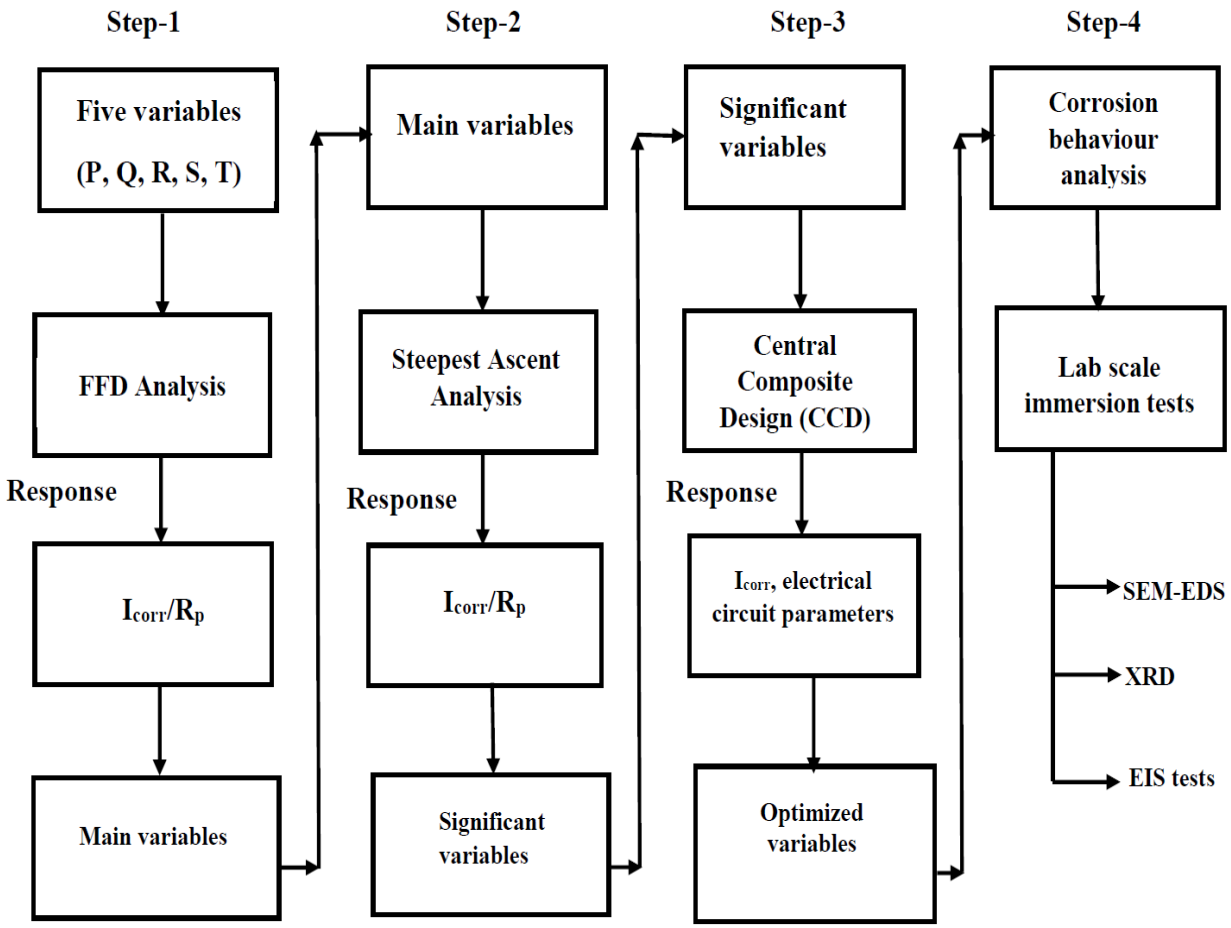

Figure 3.1 Methodology for the experimental design in block diagrams.

3.3 Experimental Conditions

A Zn-Ni electrodeposition was conducted in a 200 ml bath solution. A rectangular steel plate with a 10 cm^2 was used as the working electrode (cathode). A graphite plate was used as a counter electrode (anode). The anode and cathode were connected to a DC power supply via a multi-meter. Before electrodeposition the working electrode was prepared with the emery paper of 400, 800 and 1200 grit paper and polished with diamond paste. The electrode was washed with the acetone/ethyl alcohol and dried in air. The Zn-Ni electroplated sample at different conditions were tests by the electrochemical techniques. All electrochemical tests were carried out in a three-electrode cell at room temperature. The reference electrode used was Ag/AgCl/KClsat. The potentiodynamic polarization tests (Tafel plot) were identified in

the potential range of -1.5V to 0.5V at a scan rate of 10mV/s, respectively. The electrochemical impedance spectroscopy (EIS) was measured at equivalent to the respective samples open circuit potential (OCP's) values. The Bode/Nyquist plots were measured at the amplitude of 10mV in the frequency range of 10^{-2} Hz to 10^{5} Hz. Zahner Thales software was used to fit the measured curves. To study the corrosion behaviour of a Zn-Ni optimized specimens, the sample was submerged in Atlantic Ocean seawater at pH of 7.93 at 20.2 ^{0}C for 3hours , 12hours , 24 hours, 48 hours and 72 hours respectively, and measurements were conducted. Two equivalent coated samples were measured for the same Zn-Ni deposits. This setup is illustrated in Figure 3.2.

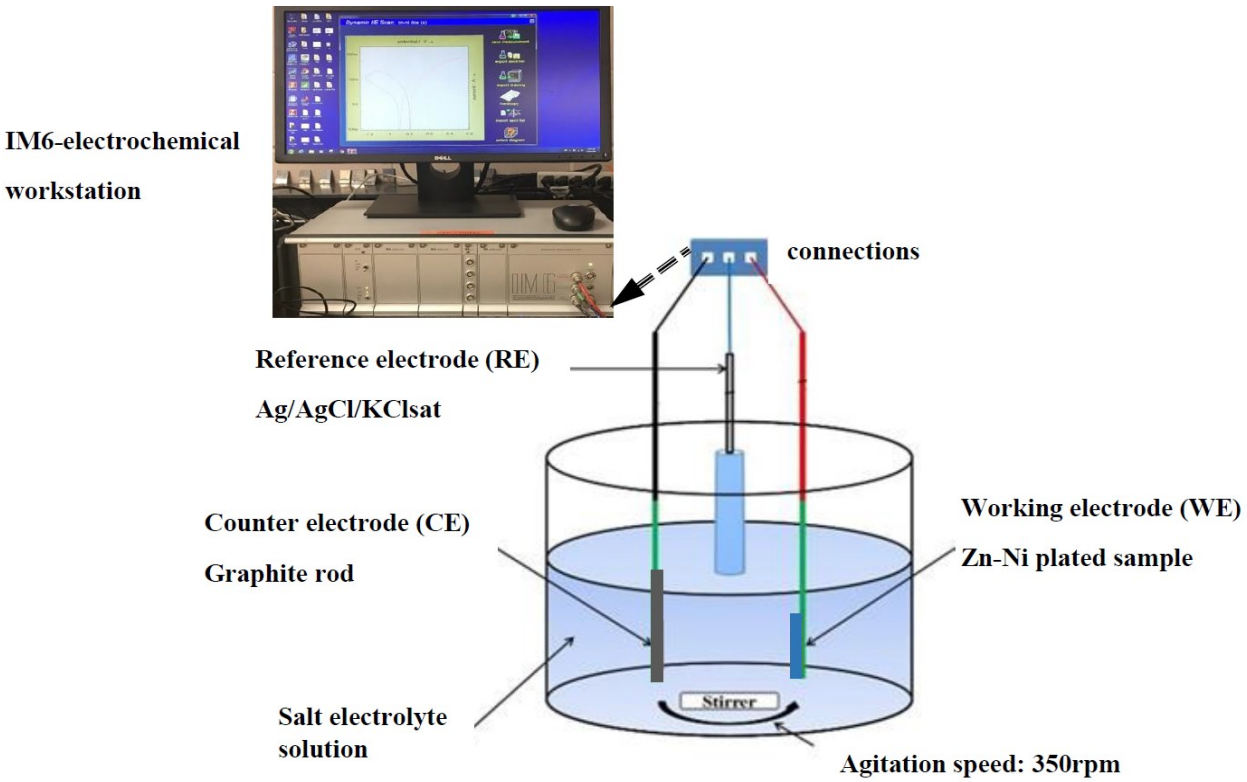

Figure 3.2 The convention three electrode cell configuration for electrochemical analysis.

Five variables were chosen for this experimental plan:

1. Zinc-nickel molar concentration ratio (P)
2. Temperature of the electrolyte solution (Q)
3. Current density of the electroplating (R)

4. Plating time (S)
5. Complexing agent ($N_3(C_6H_{17}O_7)$) (T)

The two level of chloride bath containing zinc chloride ($ZnCl_2$), nickel hydroxide hexahydrate ($NiCl_2.6H_2O$), sodium dodecyl sulphate (SDS), boric acid (H_3BO_3), sodium chloride (NaCl), and ammonium citrate ($N_3(C_6H_{17}O_7)$) are shown in Table 3.1. The pH of the bath was adjusted to acidic by adding hydrochloric acid; the cathodic current densities were in the range of 20 to 60 mA/cm^2. The cathodic substrates were steel. The area of the steel plate for electroplating was 10 cm^2.

Table 3.1. Bath compositions for the electrodeposition of Zn-Ni alloy coatings

	Molar Concentrations (mol/l)	
Bath Compositions	**Level-1**	**Level-2**
$ZnCl_2$	0.36	0.55
$NiCl_2.6H_2O$	0.31	0.21
H_3BO_3	0.16	0.16
SDS	0.00017	0.00017
NaCl	0.17	0.17
NH_4Cl	0.46	0.46
$(N_3(C_6H_{17}O_7))$	0.04	0.20

Data generation and analysis:

- The EIS and the polarization data were tabulated from the IM6-electrochemical workstation (ZAHNER-Elektrik GmbH & Co.KG, Germany).
- The morphological images were investigated by scanning electron microscope
- The chemical compositions of the corroded samples were analysed by the energy dispersive spectroscopy (FEI MLA 650F).

- The crystal phase structure of the coating and the corroded compounds deposited on the coated surface was measured by the Rigaku Ultima IV X-ray diffractometer with a copper x-ray source and a scintillation counter detector (λ=1.5418A^0). Minitab software was used to design the complete statistical experiments.

3.4 Result and Discussions

3.4.1 Step-1: Two-level fractional factorial design (FFD) analysis

A two-level FFD was used to determine the significance of each plating variables affecting the electrochemical behaviour of the zinc-nickel coating. Corrosion current (I_{corr}) and polarization resistance (R_p) are the best indicators of electrochemical behaviour. An increase in corrosion protection is indicated when I_{corr} values of the coated sample decreases and R_p values increase. A two-level FFD technique applied to the five plating variables to determine the effect on zinc-I_{corr} values of the Zn-Ni coated samples. Table 2 shows the levels for each variable. The complete bath composition of the Zn-Ni electroplating was presented in Table 3.1. The fixed levels of these five variables are given in Table 3.2.

Table 3.2. Factors and levels for the 2^{5-1} two-level FFD design

Factors		**Levels**	
		-1	1
P	Zn/Ni molar concentration ratio	0.66	1.50
Q	Temperature of bath (^{0}C)	20 (RT)	50
R	Current density (mA/cm^2)	20	60
S	Plating Time (min)	10	20
T	Citrate concentration (mol/l)	0.04	0.20

To understand the influence of individual parameters along with the relations among these factors on the corrosion resistant properties and polarization resistance of the zinc-nickel

deposits is studied by the four steps of experimental design[36][37]. The controlled and fixed variables with their responses and the analysis methods of each steps are shown in the Figure 3.3.

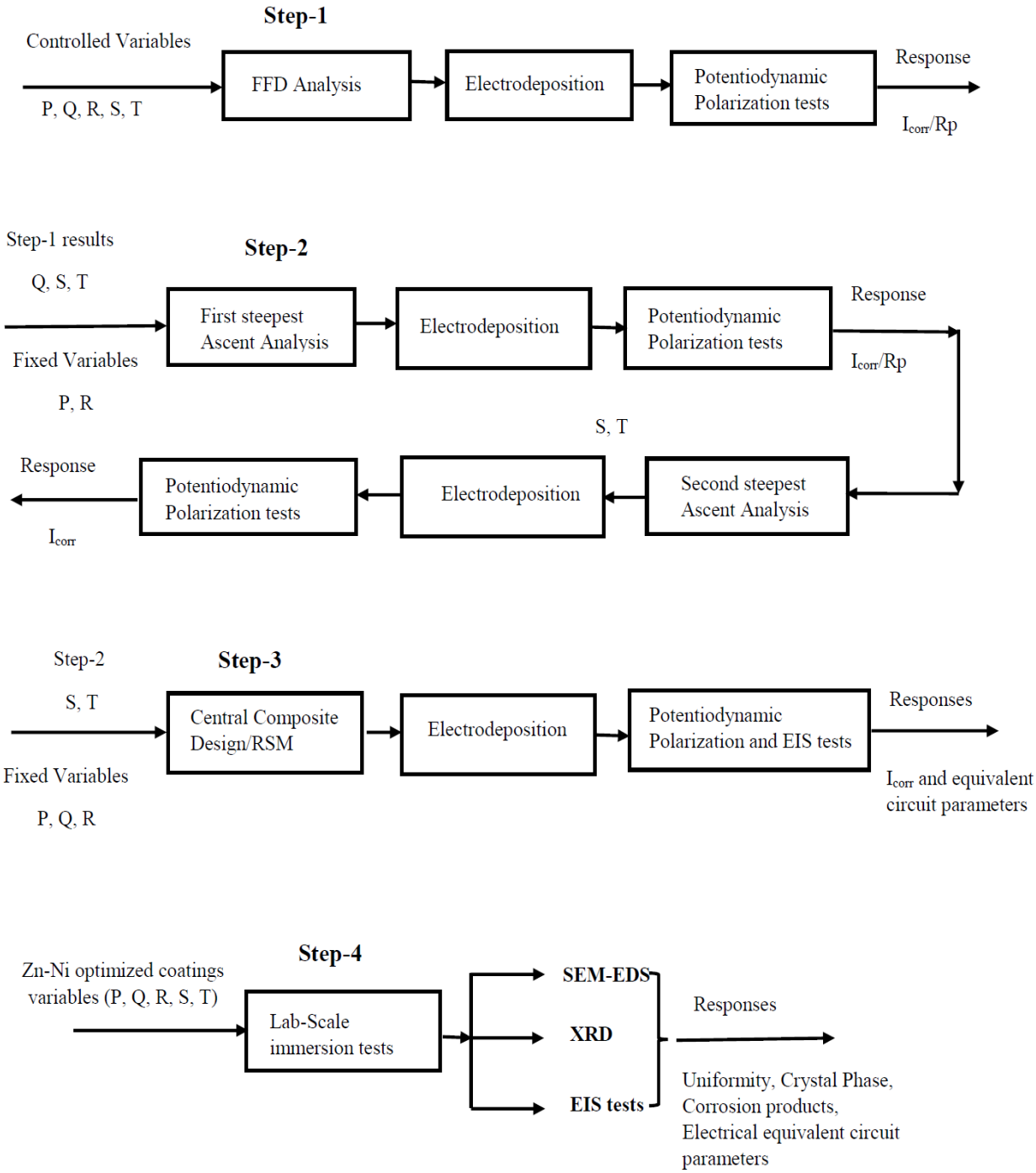

Figure 3.3 The controlled and fixed variables with their responses and analysis methods.

In the FFD statistical study (step-1), the corrosion resistant activity (represented as I_{corr} and R_p) of the zinc-nickel plating is considered the response variable. I_{corr} is inversely related to corrosion resistant property of the coated sample and proportionally related to the hydrogen evolution reaction that occurs on the zinc-nickel cathode[38]. The two-level FFD statistical modelling and the resulting I_{corr} and R_p values is presented in Table 3.3.

Table 3.3. The two-level FFD statistical modelling and the measured I_{corr} and R_p values with the important equivalence I = PQRST

Run order	**P**	**Q**	**R**	**S**	**T**	**Corrosion current I_{corr} ($\mu A/cm^2$)**	**Polarization Resistance, R_p (Ωcm^2)**
1	-1	1	-1	-1	-1	1930	51.7
2	1	1	-1	1	-1	1540	53.0
3	1	-1	-1	1	1	2800	36.8
4	-1	-1	1	-1	-1	964	83.0
5	1	-1	-1	-1	-1	2800	34.8
6	-1	-1	1	1	1	2390	38.0
7	1	1	1	-1	-1	1780	52.9
8	-1	-1	-1	1	1	2580	37.3
9	-1	1	1	1	1	2350	40.1
10	1	-1	1	-1	-1	987	84.4
11	1	1	1	1	1	3170	34.7
12	-1	-1	-1	-1	-1	803	97.4
13	1	1	-1	1	1	2390	40.1
14	1	-1	1	1	1	1770	52.4
15	-1	1	-1	1	1	2680	36.2
16	-1	1	1	-1	-1	1910	47.9

The corrosion current density (I_{corr}) varies from 987 to 3170 μA/cm^2, and polarization resistance (R_p) varies from 34.7 to 97.4 Ωcm^2, indicating that the corrosion resistance is dependent on the deposition conditions.

Analysis of Variance (ANOVA) is a statistical method to mathematically evaluate each outcome, containing the main factor and two-factor interaction based on the resultant value is listed in Table 3.3. ANOVA was carried out to justify the efficacy of the statistical models. The ANOVA regression study is shown in Table 3.4.

Table 3.4. Analysis of Variance (ANOVA) for 2^{5-1} FFD

Source	**Dfi**	**SSi**	**MSi**	***F-value**	**P-value**
P	1	31257	31257	0.78	0.417
Q	1	634434	634434	1.59	0.263
R	1	478080	478080	1.20	0.324
S	1	60639	60639	0.15	0.713
T	1	773316	773316	1.93	0.223
PQ	1	36433	36433	0.09	0.775
PS	1	248864	248864	0.62	0.266
QR	1	407101	407101	1.02	0.664
QS	1	96384	96384	0.24	0.644
RT	1	112220	112220	0.28	0.619
Error	5	199320	399864		
Total	15	7688053			

*R^2 (adj.) = 0.97

Where,

Dfi = Degree of freedom for factor i

SSi = Sum of square of factor i

MS = Mean of Square; = SSi/Dfi

F-values = the ratio of model sum of square and model sum of error (MSF/MSE)

P-Values = Probability of factor i

Corresponding to the significant relation I= PQRST initiated by Box et al.[39]. The estimation of main factor result (e.g. factor (T) citrate concentration) is identical to that of its other factors such as four-factor interaction effect of P (the Zn/Ni molar concentration ratio) x Q (Temperature of the electrolyte solution) x R (Current density of the deposition) x S (Plating time of the electroplating). Therefore, the main factor effect (T) and the interaction effect of P x Q x R x S are said to be limited [36][39][40]. Subsequently, the effect of high order such as three or higher order interactions is supposed to be negligible. Therefore, the effect of P x Q x R x S interaction can be unnoticed, and the main effect factor such as "T" can be separated from the confined effect of this FFD study. The analogous condition is also suitable for the factors P to Q.

It is demonstrated from the Table 3.4 that the ANOVA is acquired from the separation of the total variability (SST) into its constituents such as the sum of the square model (SS_{model}) and the sum of the square error (SS_{error})[36]. If only P x R, Q x T, R x S and S x T interfaces are consolidated into the error then the factors P, Q, R, S and T interactions P x Q, P x S, P x T, Q x R, Q x S and R x T have statistically significant effect on the corrosion resistant action of zinc-nickel plating (shown in column 5 in Table 3.4). The quality of the model developed was determined based on the coefficient of determination (R_2) value. Data given in Table 4 demonstrate that all the model were significant, given that P-values are less than one. The closer the R_2 value to unity, the more accurate the response predicted by a model. The value of the coefficient of determination R_2 is 0.97. Moreover, The F values are larger for a temperature of the electrolyte solution (Q), current density (R) citrate concentration (T), this means that these factors have a significant effect of decreasing the Icorr values. Whereas, the level of parameter Q is close to the vicinity for the best conditions. Therefore, Q is excluded from the steepest ascent analysis (Step 2) instead parameter S is involved due to its large level of vicinity toward

the optimized conditions. Factors R, S and T are considered in the step-2 to lead to the optimized experimental settings.

The combination of the experimental variables effects and ANOVA data, a fitted polynomial model with statistical significance can be generated as follows:

$$I_{corr} = 2102 - 151y_P - 215y_Q + 187y_R + 17y_S - 589y_T - 52y_Py_Q - 135y_Py_S + 172y_Qy_R - 84y_Qy_D + 90y_Ry_T \quad (1)$$

Where, y_i is the coded variables of the different factors (i.e. P, Q, R, S and T) which affect the corrosion current. The coded variable, y_i are characterized in the standard form as following [40].

$$Y_{i\,(high)} = (Y_{i\,(high)} - Y_{i\,(mean)})/Z_i \; (=+1)$$

$$Y_{i\,(low)} = (Y_{i\,(low)} - Y_{i\,(mean)})/Z_i \; (=-1)$$

$$Y_{i\,(mean)} = (Y_{i\,(low)} + Y_{i\,(high)})/2$$

$$Z_i = (Y_{i\,(high)} - Y_{i\,(low)})/2$$

Where, $Y_{i\,(high)\,and}$ $Y_{i\,(low)}$ represents the high and low level of factors "i" in regular units such as ^0C, mA/cm^2, molarity and minutes.

The polynomial equation with the significant effects of the three important factors R, S and T are presented in the resulting equations:

$$I_{corr} = 2102 + 187y_R + 174y_S - 589y_T \quad (2)$$

The effect of factors from P to T on the corrosion current density of Zn-Ni deposits are shown in Figure 3.4. The most significant change in I_{corr} noted in Figure 4 was for plating time (S) and citrate concentration (T). As seen from Figure 3.4 that the variable P, Q, S and T has lower I_{corr} values at their low level (-1). Whereas, for the variable R, the least I_{corr} values at high level (seen from Figure 3.4). The sharpest change from 1900 to 2200 $\mu A/cm^2$, 1550 to 2300 $\mu A/cm^2$ and 1550 to 2500 $\mu A/cm^2$ with decreasing temperature of the electrolyte solution (Q), increasing electroplating time (S) and citrate concentration (T) (Table 3.3). Therefore, these

three parameters are significant to decrease the corrosion current density of the zinc-nickel plating leading to an increase of the corrosion resistant properties of the plated samples.

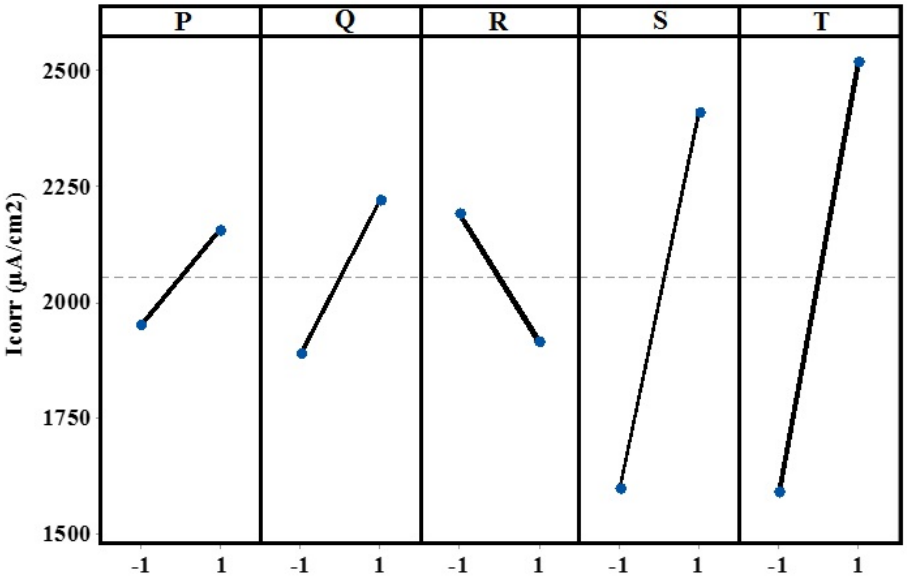

Figure 3.4 The research design for the main plating variables i.e. Zn/Ni molar concentration ratio (P), Temperature of the electrolyte solution (^{0}C) (Q), the electroplating current density (mA/cm^2) (R), Plating Time (min) (S), the complexing agent (Citrate (molarity)) (T). (+) and (-) indicate the high and low levels of these factors, respectively.

As seen from the Figure 3.4 that the most important factor to study after the step-1 is the Q, R, S, and T. However, the current density (Q) of the plated sample is close to the optimum values (tested from the experimental exploration test), after the 60mA/cm^2 of plating current density, the coated samples are burned and the black coated sample are exhibited lead to exhibit higher I_{corr} values. Therefore, Q, S, and T are further studied by the first and second steepest ascent analysis. The first approach of the steepest ascent analysis is explained as a result of equation 2 and Figure 3.4.

3.4.2 Step-2: Steepest ascent analysis (SAA)

The variables identified in Step 1, plating time (S), citrate concentration (T) and temperature (Q) were further explored through additional experiments. To approach the most favourable condition for Zn-Ni electroplating and to increase corrosion resistance of the resulting coating

the steepest ascent analysis was conducted. The path of the steepest ascent analysis is statistically employed to approach the closest range for the optimal parameters for the zinc-nickel plating to improve the corrosion resistant properties of the electroplated sample. The variables identified as less significant in step-1 (P, R) were fixed at 0.66 and 60mA/cm^2, respectively. As seen from the Figure 4, at low level of P and high level of R values, I_{corr} is lower and this leads to higher corrosion resistant property. While, it is stated by the steepest ascent approach[39][36][40], the variables under study were concurrently moved to the $+187Z_R$ and $+174Z_S$ in y_R and y_S directions, correspondingly for each $-589Z_T$ in the y_T direction such as the ratio of the step size is 1:1:2.

The standard positions on the first approach of the steepest ascent analysis are listed in Table 3.5. The minimum corrosion current density (I_{corr}) = 704 µA/cm^2 of the electroplated samples was found at the experimental setting of run 6.

Table 3.5. positions on the first approach of the steepest ascent analysis

Run order	**Temperature (Q)**	**Plating Time (S)**	**Citrate (T)**	**Corrosion current, I_{corr} (µA/cm^2)**
1	48	18	0.185	1770
2	44	17	0.164	1940
3	40	16	0.143	1560
4	36	15	0.123	1310
5	32	14	0.102	1070
6	28	13	0.082	704
7	24	12	0.061	835
8	20	10	0.041	834

It is shown in Table 5 that the I_{corr} values gradually decreased from run 1 to 5. It is shown that the corrosion resistant of Zn-Ni deposits is not considered to be a determined function of the factor Q, S and T.

Table 5 shows that from runs 6-8, the activity of corrosion current (I_{corr}) increases from 704 to 834 μA/cm^2 However, when the deposition setting was changed from run 6 to 10 (Table 6 from run order 6 to 10), the I_{corr} value is least at run 8. Afterwards, the I_{corr} value increase (Table 3.6 of run 9 and 10).

It is concluded from Table 5 that the temperature (Q) (below 28^{0}C) in the electrolyte solution is an unusual variable which influences the I_{corr} activity of the specimen.

Equation 2 represents the most uncomplicated correlation among the I_{corr} values and the Q, S and T plating variables, a second steepest ascent analysis was performed when the temperature of the electrolyte solution is kept constant (temperature 28^{0}C). The result of the second steepest ascent analysis is listed in Table 6. It is observed that the minimum I_{corr} value is found at run 8, demonstrating that the experimental setting of run 8 should be near the optimum conditions. Therefore, the second steepest ascent study shows that the Zn/Ni molar concentration ratio (P) equal to 0.66, current density (R) is 60mA/cm^2 and the temperature of plating bath (Q) is 28^{0}C, plating time (S) is 13 minutes and citrate concentration (T) is 0.061 exhibit lower I_{corr} values lead to improving the corrosion resistant properties of the Zn-Ni samples. The variables P, Q, R, S, T were optimized from the first and second steepest ascent analysis. To determine more precise values of the variables, the central composite design (CCD) study is demonstrated in step-3.

Table 3.6. positions on the second approach of the steepest ascent analysis

Run order	**S**	**T**	**Corrosion current, I_{corr} (μA/cm^2)**
1	20	0.205	1450
2	19	0.185	1030
3	18	0.164	1500
4	17	0.143	966
5	16	0.123	994

6	15	0.102	793
7	14	0.082	886
8	13	0.061	676
9	12	0.041	866
10	10	0.020	932

3.4.3 Step-3: Central composite design (CCD)

From the Step-2, the most influential variables are plating time (S) and citrate concentration (T). Whereas the uncontrolled variables are Zn/Ni molar concentration ratio (P), current density (R) and the temperature of plating bath (Q). The experimental conditions found from Step 2 at run 8 are chosen as the central point for the central composite design (CCD). The data of the corrosion current density (I_{corr}) and the electrochemical analysis of the coated sample determined by equivalent electrical circuit of the fitted Nyquist plots for the zinc-nickel plating in the CCD statistical modelling are listed in Table 3.7. The response for this analysis was I_{corr} and equivalent electrical circuit parameters.

Table 3.7. Corrosion current density (I_{corr}) and the electrochemical analysis determined by equivalent electrical circuit for the Zn-Ni deposits in the central composite design (CCD)

Run order	**S**	**T**	**Corrosion current, I_{corr} ($\mu A/cm^2$)**	**R_{sol} (Ωcm^2)**	**R_{ox} (Ωcm^2)**	**R_{coat} (Ωcm^2)**	**R_{ct} (Ωcm^2)**	**C_{ox} (μFcm^{-2})**	**C_{coat} (μFcm^{-2})**	**C_{dl} ($nFcm^{-2}$)**
1	-1	1	753	2.18	4.23	592.5	282.2	800.8	6.40	664.7
2	1	1	812	17.74	31.23	465.6	332.4	939.8	5.23	13.99
3	$\sqrt{2}$	0	821	14.38	34.21	453.3	215.5	89.98	3.42	12.14
4	-1	-1	1320	35.69	19.97	900.0	1.11K	59.19	7.15	96.9
5	$-\sqrt{2}$	0	1270	13.92	41.01	94.84	751.1	7.48	4.06	65.4
6	0	$-\sqrt{2}$	1370	30.67	24.46	154.6	105.9	264.2	7.89	9.53

7	1	-1	1130	26.20	23.44	150.6	31.12	43.35	6.10	17.95
8	0	$\sqrt{2}$	857	18.46	36.00	654.3	454.4	20.59	6.29	17.55
9	0	0	596	20.96	42.36	2.96K	1.47K	700.8	9.49	190.1
10	0	0	610	20.50	40.36	2.78K	1.45K	705.1	10.00	190.8
11	0	0	600	19.01	39.33	2.88K	1.52K	709.8	8.93	180.9

Potentiodynamic polarization (Tafel) plots are used to demonstrate the electrocatalytic behaviour of zinc-nickel deposits concerning the I_{corr} values. The Tafel curves in logarithmic scale for the specimen of runs (2); (4) and (9) are shown in Figure 3.5. The polarization curves were measured at their respective open circuit potentials (OCP's) of various coated samples. The I_{corr} values are computed from the intercepts on the cathodic and anodic slopes of the Tafel curve by the extrapolation, obtained by silver/silver chloride with saturated potassium chloride as a salt bridge (Ag/AgCl/KClsat) as a reference electrode and are tabulated in Table 3.7. It is seen in Table 3.7, and Figure 3.5 that the I_{corr} value of run 9 is the minimum (596 µA/cm^2) than the other coated sample. In order to attain the high accuracy, there are three equivalent samples repeated at centre point at same parameter such as run 9, 10 and 11. These samples exhibit lower corrosion current density leads to exhibits higher corrosion resistant property.

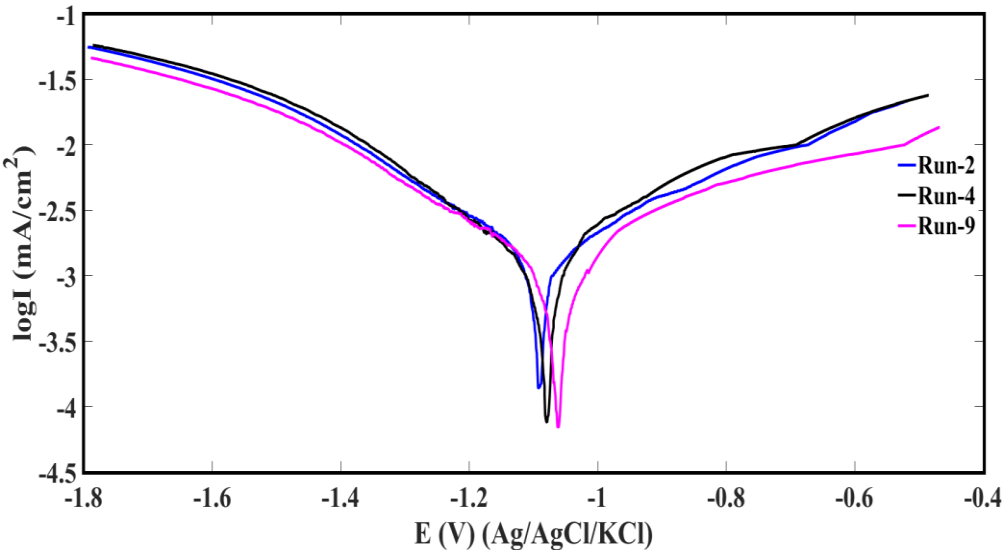

Figure 3.5 Polarization curve in logarithmic scale for Zn-Ni deposits of runs (2), (4), and (9) in Table 7.

The electrochemical impedance spectroscopy (EIS) is carried out to identify the electrocatalytic influences on the zinc-nickel plating. The experimental data were measured and listed in Table 3.7 more specific. The Nyquist plot for Zn-Ni deposits of runs (2); (4) and (9) is as shown in Figure 3.6. In this study, the values measured by the Nyquist plots are fitted by the three parallel arrangement of the resistance and capacitance in the electrical equivalent circuit model (EECM) as shown in Figure 3.7. The shape of the Nyquist plot resembles a semicircle and under the passivation contexts are presented as the uncompleted semi-circle[9][41][42]. The diameters of the semicircle of the run 9 sample are larger than those of the run 2 and 4, indicating that the run 9 sample acquire better corrosion resistance in comparison to the run 2 and 4. The Nyquist and Bode plot of Zn-Ni deposits consists of three well-defined capacitive arcs. However, electrochemical behaviour and the geometric factor of the coated samples is influenced by the shape of the spectroscopy [43][44]. Where R_{sol} represents the solution/electrolyte resistance. R_{ox} and C_{ox} correspond to the resistance and capacitance of the formation of the thin oxide film that is reinforced by the ionic conduction through its pores. R_{coat} and C_{coat} correspond to the resistance and capacitance of the corrosion resistant films (i.e. Zn-Ni coated samples). R_{ct} represents the charge transfer resistance. C_{dl} corresponds to the electric double layer capacitance. The electrical circuit modelling demonstrated the best fit to the experimental data. Furthermore, the R_{ct} values of these curves are extremely high (>1.5 $K\Omega cm^2$). As a result, all the zinc-nickel plated samples showed passive behaviour and attributed to the formation of inert compact oxide films on the surface of the deposits. It is observed from Figure 3.5 that the solid lines signify the best-fit curves. Zn-Ni coating resistance (R_{coat}) of run 9, 10 and 11 exhibits higher resistance of around 2.8 $K\Omega cm^2$.

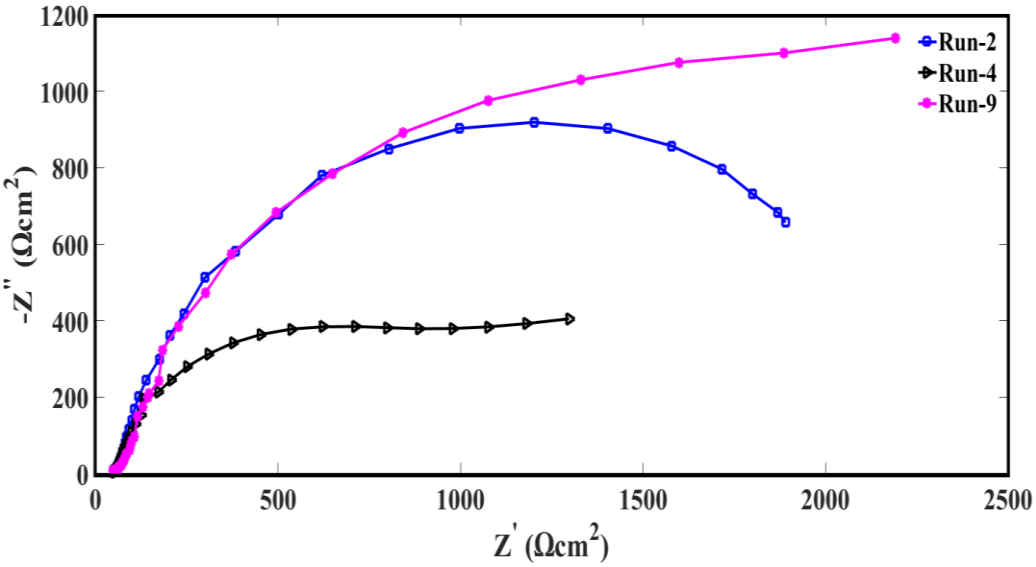

Figure 3.6 Nyquist plot for Zn-Ni deposits of runs (2), (4), and (9) in Table 7.

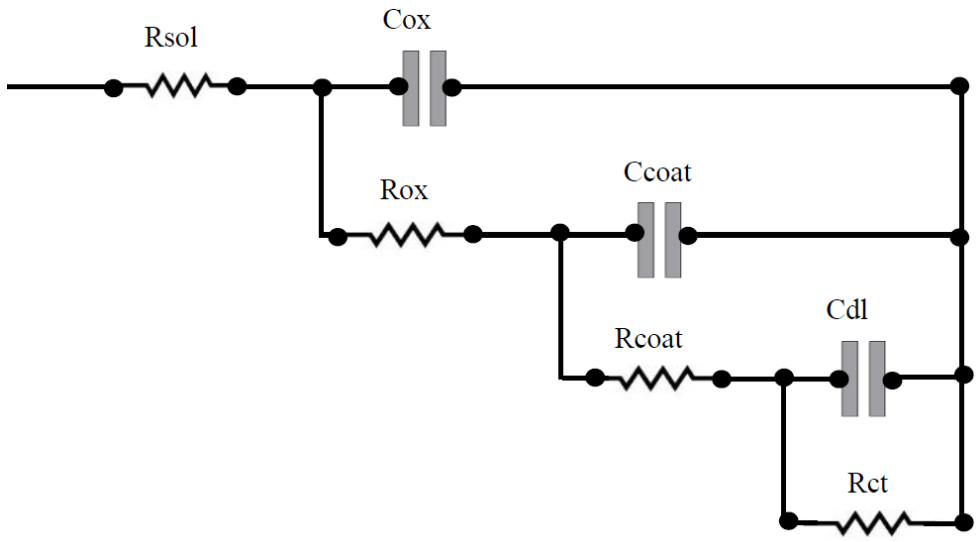

Figure 3.7 The equivalent electrical circuit model for the Zn-Ni coated and immersed samples.

The Bode plots for the specimen of runs (2); (4) and (9) is presented in Figure 3.8 (a) and (b). In the bode plots, the resistive behaviour is achieved at a higher frequency in which the values of impedance modulus (|Z|) is kept constant, and the phase angle (θ) is approaching zero. Furthermore, the capacitive behaviour is achieved at low and medium frequencies in which the value of impedance modulus (|Z|) is inclined and phase angle (θ) approach to the maximum value[45][9]. It is noticed from the Figure 3.7 that the impedance modulus of run 9 is higher

in comparison to run 2 and 4. Moreover, Figure 3.8 shown the higher phase angle for run 9 in comparison to the other samples lead to exhibits higher corrosion resistant properties to the coated sample.

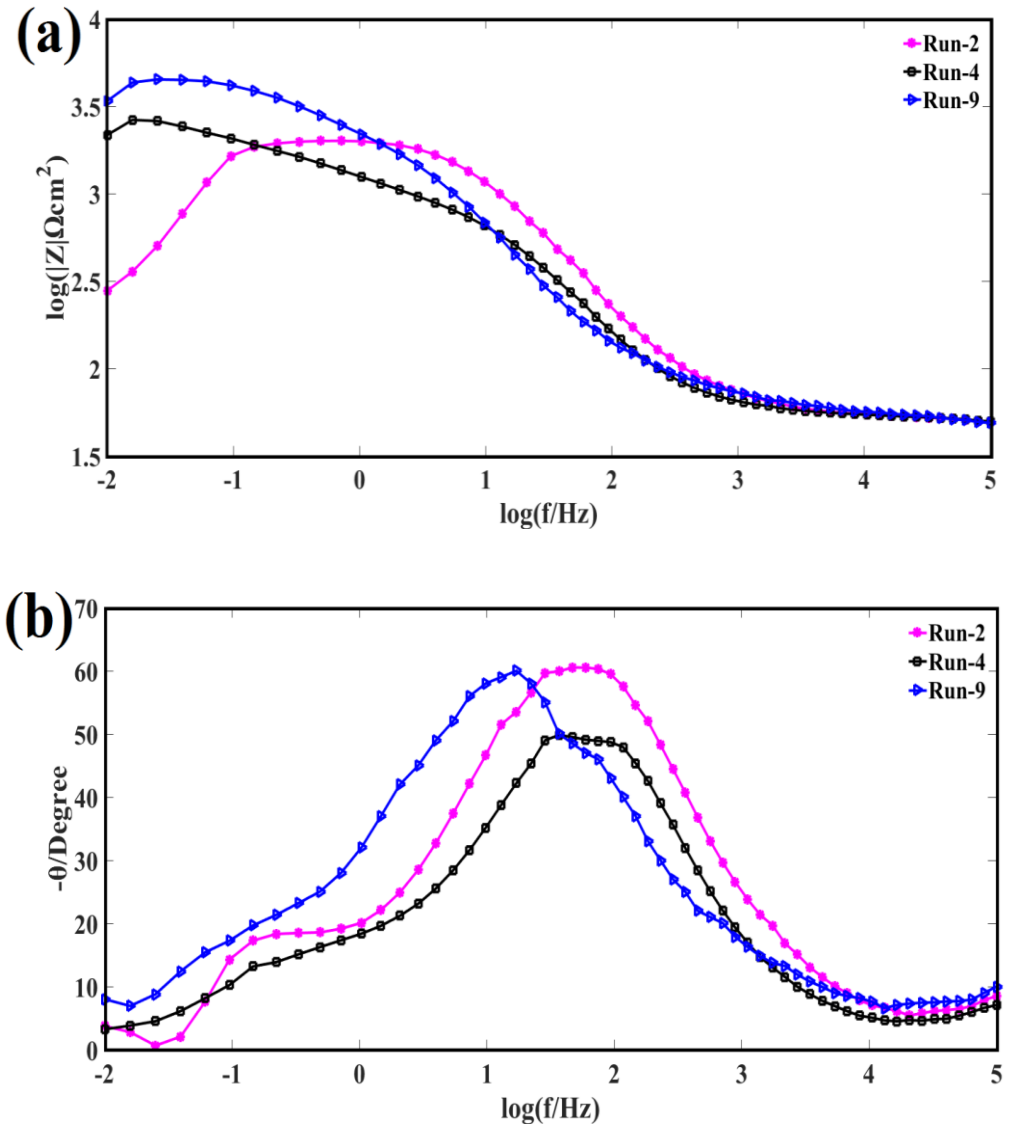

Figure 3.8 Bode plots for the Zn-Ni deposits of runs (2), (4), and (9) in Table 7; (a) log |Z| vs. log f; (b) phase angle vs. log f.

The regression analysis is subjected to the I_{corr}, resistance (R_{coat}) and capacitance (C_{coat}) data (Table 3.7) of the corrosion resistant films (i.e. Zn-Ni coated samples). The ANOVA/FFD study of every single regression equation, the statistical significant relationships were

eliminated from the extensive second-order model. The second order polynomial equations for these three responses I_{corr}, R_{coat} , and C_{coat} are generated by the Minitab software:

$$I_{corr}\ (\mu A/cm^2) = 602.2 - 95.7y_S - 201.3y_T + 202.7y_S^2 + 236.7y_T^2 + 62.2y_Sy_T \quad (3)$$

$$R_{coat}\ (\Omega cm^2) = 2851 - 46.2y_S + 89.3y_T - 1241.6y_S^2 - 1176.4y_T^2 + 156y_Sy_T \quad (4)$$

$$C_{coat}\ (\mu Fcm^{-2}) = 9.270 - 0.391y_S - 0.485y_T - 2.564y_S^2 - 0.889y_T^2 - 0.030y_Sy_T \quad (5)$$

Equations (3), (4) and (5) demonstrated the relative significant effects of the linear, quadratic and correlation of the plating time (y_S) and complexing agent (y_T) of the response variables. The ANOVA/FFD study for the values of I_{corr}, resistance (R_{coat}) and capacitance (C_{coat}) of the Zn-Ni deposits were conducted in this study. ANOVA generated values (Table 3.7) show the regression equations 3 to 5 are statistically significant. This indicates that the equation 3 to 5 represents the dependence of corrosion current density for the Zn-Ni plating on factor S and T. In this study, the response surface methodology (RSM) method is used to examine the relation between plating time (y_S) and complexing agent (citrate) (y_T) with the responses such as I_{corr}, resistance (R_{coat}) and capacitance (C_{coat}), the response variable is assumed to be efficient of their available variables[39][36][40][37]. Hence, the temperature of the plating electrolyte has to be maintained constant at the temperature equal to 28^0C in Step-3 (CCD).

The 3D surface graph of all the response variables against the plating time (y_S) and citrate concentration (y_T) is generated by employing consequent regression models (equation 3 to 5). It simplifies the straight-forward consideration for the dependency of these responses on the coating variables. The conventional 3D diagrams of corrosion current density (I_{corr}), corrosion resistant coating (R_{coat}) and capacitance (C_{coat}) in the CCD study are shown in Figures 3.9-3.11, respectively.

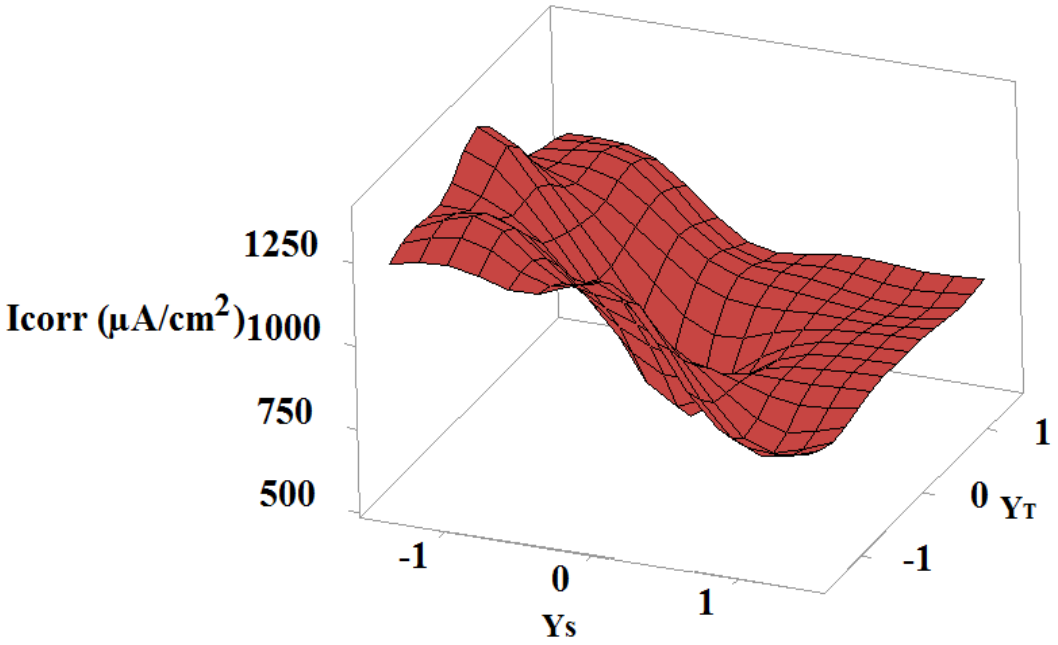

Figure 3.9 3D surface graph of corrosion current densities on the Zn-Ni deposits in the CCD against plating time (y_S) and complexing agent (citrate) (y_T).

Figure 3.9 shows that the corrosion current density (I_{corr}) is an efficient function of plating time (y_S) and the citrate concentration (y_T). The trend shows that I_{corr} values gradually decreases with decreasing plating time of the electroplating (y_S) and after 13 minutes of the electroplating time, again increase. Note that an extreme region with the minimum I_{corr} (596 µA/cm^2) occurs at the 13 minutes of the plating time and the citrate concentration (y_T) close to 0.06 mol/l. However, the I_{corr} values reach maximum (1370 µA/cm^2) at 13 minutes with 0.062 mol/l of citrate concentration (y_T). As seen from the above analysis that the specimen with the minimum I_{corr} values were electroplated from the electrolyte bath containing Zn/Ni molar concentration ratio 0.66, plating temperature 28^{0}C, electroplating current density 20 mA/cm^2, electroplating time 13 minutes and citrate concentration 0.062 mol/l. This result was confirmed and it is shown in Table 3.8.

Table 3.8. The optimum I_{corr} values at the final process for the design of experiments

Run order	Zn/Ni ratio	Ionic	Temperature (^{0}C)	Current density (mA/cm^2)	Plating Time (min)	Citrate (mol/l)	Corrosion current, (μA/cm^2)	I_{corr}
1	0.66		28	60	10	0.06	779	
2	0.66		28	60	11	0.06	843	
3	0.66		28	60	12	0.06	841	
4	0.66		28	60	13	0.06	520	
5	0.66		28	60	14	0.06	1030	
6	0.66		28	60	15	0.06	1060	
7	0.66		28	60	16	0.06	1120	

In Figure 3.10, the 3D surface graph of the corrosion resistant coating (R_{coat}) on the Zn-Ni deposits in the CCD against plating time (y_S) and the citrate concentration (y_T) shows the similar effect as displayed in Figure 3.8.

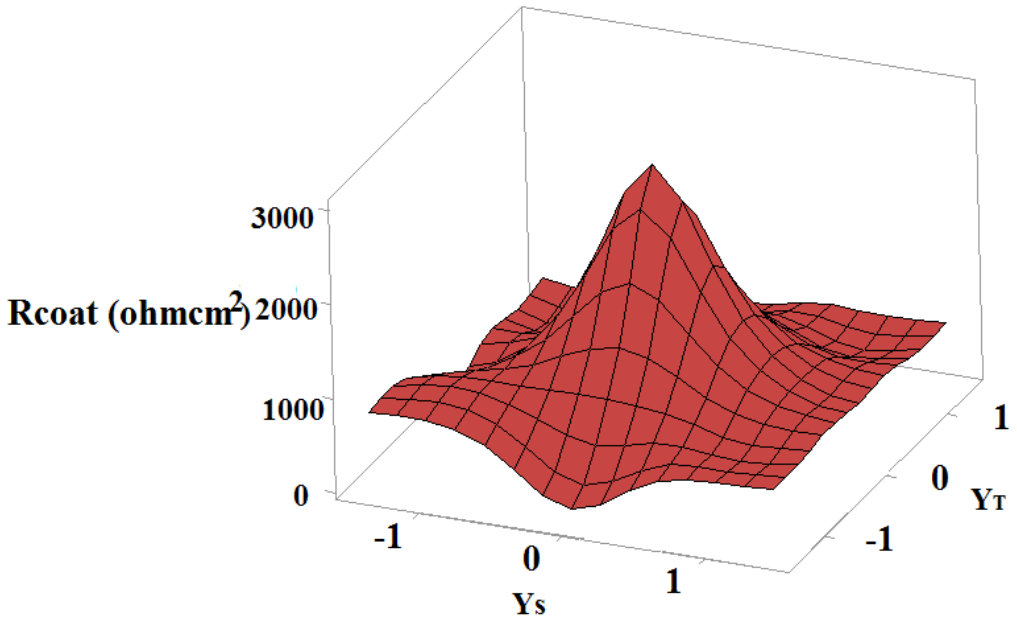

Figure 3.10 3D surface graph coating resistance on the Zn-Ni deposits in the CCD against plating time (y_S) and the complexing agent (citrate) (y_T).

As the plating time and citrate concentration decreases, the R_{coat} values keep increasing indicating higher corrosion resistant protection the coating. The extreme region with the maximum R_{coat} value (2.96 KΩcm^2) occurs at 13 minutes of the plating time and citrate concentration (x_T) close to 0.062 mol/l. However, the R_{coat} values reach a minimum (94.84 Ωcm^2) values at 13 minutes with 0.062 mol/l of citrate concentration (y_T).

The dependence of corrosion resistant capacitance (C_{coat}) on the plating time (y_S) and citrate concentration (y_T) is shown in Figure 3.9.

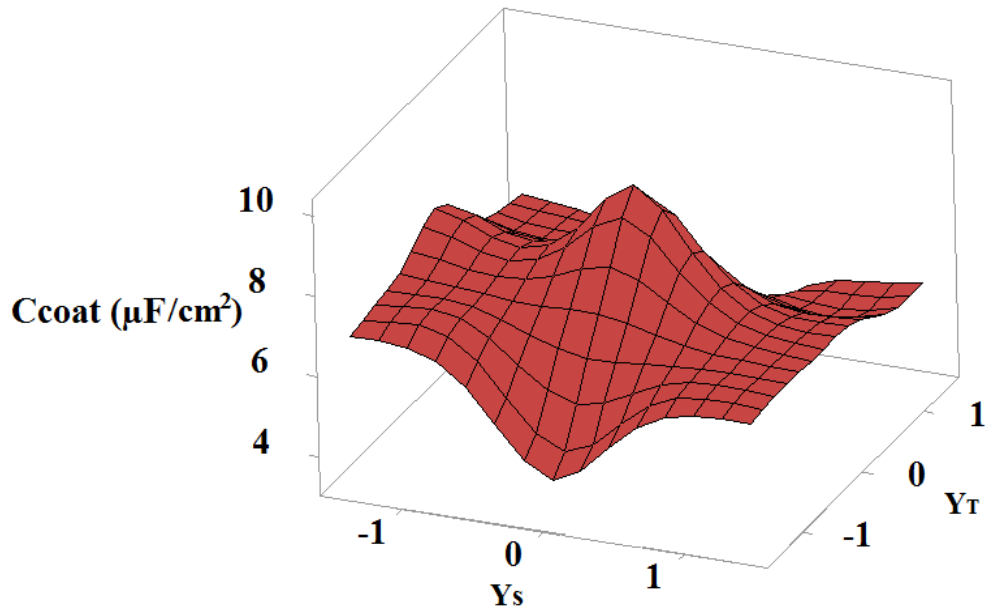

Figure 3.11 3D surface graph of the double layer capacitance of the Zn-Ni deposits in the CCD against plating time (y_S) and the complexing agent (citrate) (y_T).

Figure 3.11 shows that C_{coat} gradually decreases with decreasing plating time (y_S) and after 13 minutes of the electroplating time, again increase. Note that an extreme region with the minimum C_{coat} values (3.42 µFcm^{-2}) occurs at 20 minutes of the plating time and citrate concentration (y_T) close to 0.06 mol/l. However, the C_{coat} values reaches a maximum (10 µFcm^{-2}) at a 13 minute with 0.06 mol/l of citrate concentration (y_T) (run 10). As seen from the above analysis, the deposits with the maximum double layer capacitance (C_{coat}) should be electroplated from the electrolyte bath containing Zn/Ni molar concentration ratio 0.66, plating

temperature 28^0C, electroplating current density 60mA/cm^2, electroplating time 13 minutes, and citrate concentration 0.062 mol/l.

The CCD result shows the dependence of I_{corr}, resistance (R_{coat}) and capacitance (C_{coat}) of the corrosion resistant films on the Zn-Ni deposits.

Step-4: Corrosion behaviour tests: The Zn-Ni optimized coated samples such as Zn/Ni molar concentration ratio (P) = 0.66, plating temperature (Q) = 28^0C, electroplating current density (R) = 60 mA/cm^2, electroplating time (S) = 13 minutes, citrate concentration (T) = 0.062 mol/l are immersed in the the short period lab scale Atlantic Ocean seawater at pH of 7.93 at 20.2 ^{0}C for 3hours, 12 hours, 24 hours, 48 hours, and 72 hours respectively. To achieve the better corrosion tests on the optimized electroplated samples, the SEM, XRD and EIS analytical techniques were analyzed and discussed.

3.4.4 Surface morphological and corrosion products analysis

The surface morphologies of Zn-Ni alloy deposits form citrate bath at different immersion time is shown in Figure 3.12. The coated sample is immersed in lab-scale Atlantic Ocean seawater after 0 hour, 3 hours, 12 hours, 24 hours, 48 hours, and 72 hours, respectively.

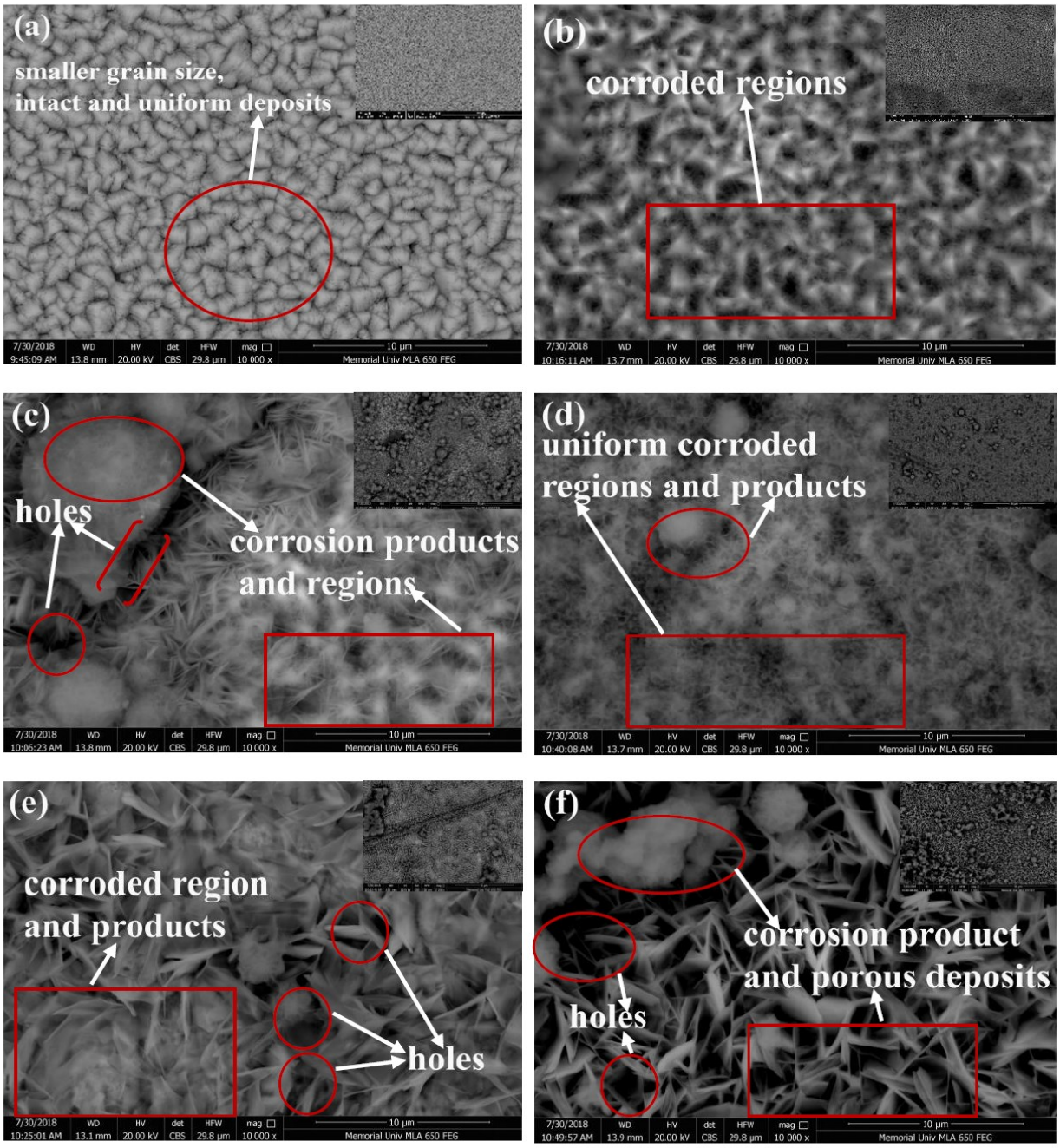

Figure 3.12 The SEM images of corroded Zn-Ni alloy coating from citrate baths immersed at (a) 0 hour, (b) 3 hours, (c) 24 hours, (d) 12 hours, (e) 48 hours, and (f) 72 hours.

All the images are taken at the same magnification and respective bath conditions. The image shown in the inset is at lower magnifications. The Zn-Ni deposits at optimum conditions (Run-4 in Table 3.8) from citrate baths exhibited uniform, compact and dense deposits which is favourable for corrosion resistance (Figure 3.12 (a)). The Zn-Ni coated surface after 3 hours immersion exhibits similar morphology with the uniform dissolution of zinc and corroded

regions is appeared (Figure 3.12 (b)). After increasing the immersion time to 12 hours, some flakes like particles and the white corroded island is observed on the surface of the deposits (Figure 3.12 (c)). At 24 hours of immersion time, the uniform corrosive products dispersed on the coated surface and some white island-like structure are seemed (Figure 3.12 (d)). Furthermore, some small holes and cracks are also observed on that surface. Similar results have been reported by Feng et al.[46]. The EDS results explained that these corrosion products look like the white island is embellished with the C, O and Cl which is considered as the accumulation and conglomeration of the corrosion products. As the immersion time increases to the 48 hours the large white flakes, corrosion products with regular small holes are exhibited on the surface (Figure 3.12 (e)). At 72 hours of immersion time reveals loose and porous corrosion products appeared on the surface. However, large magnitude of a white island and numerous holes are also observed on the surface (Figure 3.12 (f)). Similar result has been reported by Feng et al. [46][47] and Gomes et al.[48]. This can also be explained by the high dissolution of zinc occurs at large exposure lead to reduce the corrosion resistant properties of the Zn-Ni coated samples.

The EDS analysis is used to calculate the corrosion products composition including C, O, Cl, Ni on the Zn-Ni coated samples. The corrosion products formed on the coated surface at different immersion time as shown in Table 3.9. The Zn-Ni deposits without the immersion test exhibit 94% of Zn and 6% of Ni content, demonstrating that the presence of Ni leads to increase the corrosion resistant and hardness of the coating. At 3 hours of immersion the corrosion product shows the presence of C, O and Cl contents on the coated surface. It is shown that the homogeneous corrosion products film covered the coated surface after 3 hours of immersion time. Also, it was observed that the thickness of the layer is increased, as the immersion time increased. This is demonstrated by the increasing O and Cl contents and reducing the Zn and Ni contents in the deposits. However, at 24 hours of the immersion reveals

more Zn and Ni contents in comparison to the 12 hours lead to provide more protective passive layer. The amount of chlorine significantly increases, as the immersion time increased. However, highest chlorine content is observed at 72 hours of the immersion leads to exhibit porous, non-uniform and loose coating and provide least corrosion resistant deposits.

Table 3.9. The EDS analysis of the corrosion products composition of Zn-Ni alloy coating from citrate baths immersed at 0 hour, 3 hours, 24 hours, 12 hours, 48 hours, and 72 hours

Sample	**Composition (at%)**					
	Immersion time (hours)	**Zn**	**C**	**O**	**Cl**	**Ni**
Zn-Ni optimized coatings	0	94.0	-	-	-	6.0
	3	41.95	21.26	28.62	5.53	2.63
	12	33.40	24.00	34.52	6.70	1.30
	24	33.92	22.80	34.58	7.10	1.62
	48	17.50	28.54	43.92	8.53	1.51
	72	16.44	26.04	39.16	17.19	1.15

3.4.5 X-Ray Diffraction (XRD) analysis

The typical XRD pattern for the optimized Zn-Ni electroplating setting is presented in Figure 3.13. The crystal phase structures and peaks were examined by XRD and the database used to match the peaks was pdf# 03-065-5310 and 00-004-0831 RDB minerals[49], international centre for diffraction database (ICDD). It is noticeable from the figure that the Zn-Ni electroplating contains three dominant peaks from γ-$NiZn_3$, γ-Ni_2Zn_{11} and Ni_3Zn_{22} at 38°, 42° and 68°, respectively. The γ-Ni_2Zn_{11} phase with (330) plane orientation exhibit higher intensity than those of other γ-phases, i.e., γ-$NiZn_3$ and Ni_3Zn_{22}, demonstrating that γ-Ni_2Zn_{11} phase with (330) plane orientation plays an assertive role in the Zn-Ni alloy corrosion resistant coatings[50][51][52]. The Zn-Ni γ-phases are the key components for improving the corrosion resistant property of the Zn-Ni electrodeposits.

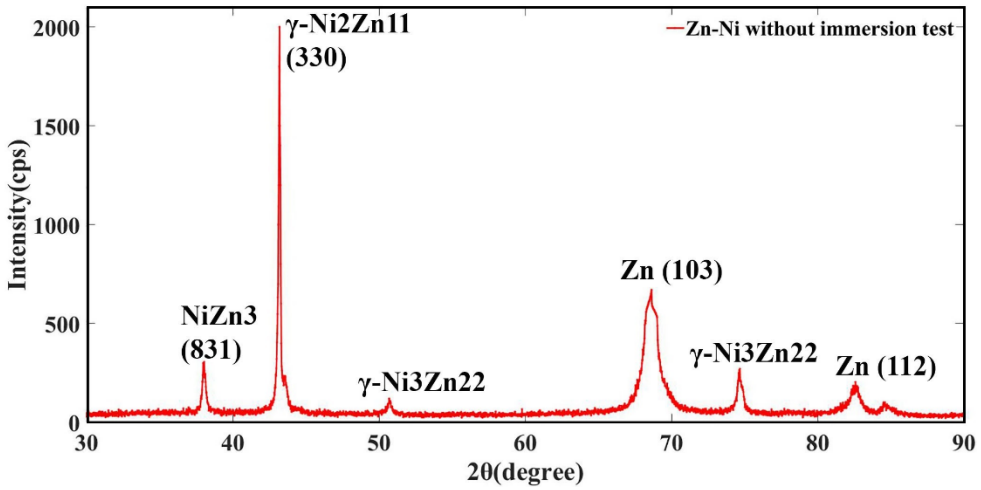

Figure 3.13 XRD patterns for optimized Zn-Ni alloy electroplating deposited from citrate baths.

The corrosion products such as simonkolleite ($Zn_5(OH)_8Cl_2.H_2O$), hydrozincite ($Zn_5(CO_3)_2(OH)_6$), zinc oxide (ZnO), smithsonite ($ZnCO_3$) and zinc hydroxide ($Zn(OH)_2$) is found in Zn alloys [53][24][54][55][56][46]. Hydrozincite and simonkolleite have appeared to be a perfect-crystallized form and many intense reflections demonstrated from the peaks. It is notified that the intensity of the hydrozincite, smithsonite and zinc oxide peaks is often enlarged reflection and most of them are overlapped with simonkolleite exhibited a weak crystallized form of these phases. The corresponding results have been demonstrated by Feng et al.[52].

3.4.6 Impedance spectroscopy analysis

The corrosion mechanisms of Zn-Ni samples at room temperature is examined by the electrochemical impedance spectroscopy (EIS) analysis such as Nyquist plots as shown in Figure 3.14.

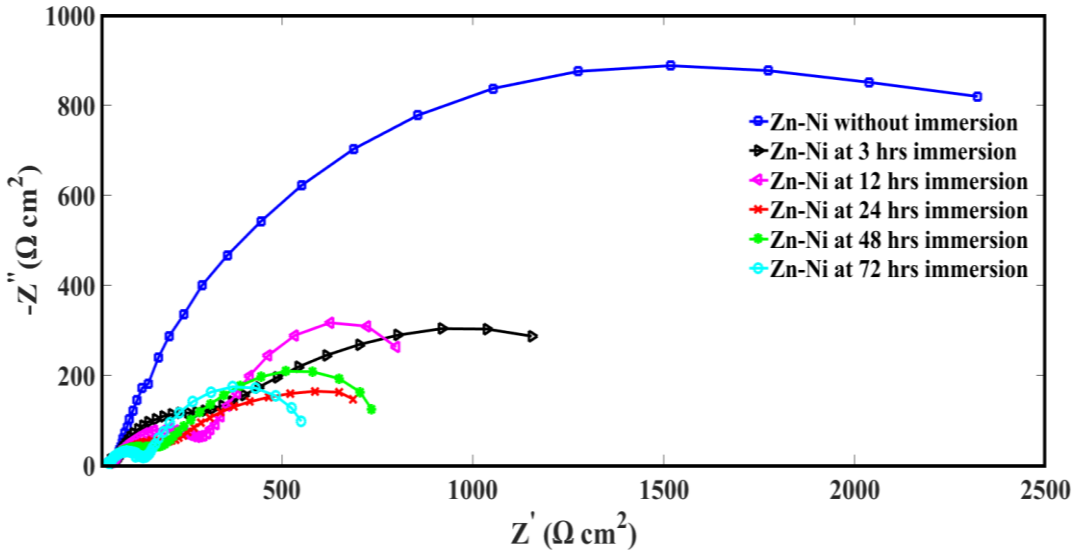

Figure 3.14 Nyquist plots for Zn-Ni coating from citrate bath immersed at 0 hour, 3 hours, 24 hours, 12 hours, 48 hours, and 72 hours.

The Zn-Ni samples are immersed in lab-scale Atlantic Ocean seawater at pH after 0 hour, 3 hours, 12 hours, 24 hours, 48 hours, and 72 hours, respectively. The open circuit potential range of frequency is 10mHz to 100kHz, and the amplitude is 10mV. The measured EIS data are displayed as the Nyquist plot is as shown in Table 3.10.

Table 3.10. Electrochemical parameters determined by equivalent circuit modelling

Zn-Ni sample	**Immersion time (hours)**	**R_{sol} (Ωcm^2)**	**R_{ox} (Ωcm^2)**	**R_{coat} (Ωcm^2)**	**R_{ct} (Ωcm^2)**	**C_{ox} ($\mu F cm^{-2}$)**	**C_{coat} ($\mu F cm^{-2}$)**	**C_{dl} ($nF cm^{-2}$)**
	0	44.04	17.47	2.58K	712.8	100.4	6.17	47.22
	3	15.69	43.91	409.0	637.5	185.4	6.98	18.74
Zn-Ni optimized	12	17.51	36.25	276.1	694.2	693.9	4.18	13.07
coatings	24	13.18	28.68	297.4	384.3	391.7	3.04	5.26
	48	13.57	31.25	154.7	705.7	124.7	4.09	4.76
	72	13.71	33.09	98.32	504.0	502.3	3.98	4.18

The Nyquist plots (Figure 3.15) of Zn-Ni alloy samples consist of well-defined three capacitive arcs in which the solution resistance (R_{sol}) is in electrical series with the three parallel arrangement of the resistance and capacitance is fitted in the electrical equivalent circuit model

(EECM). A small arc at high frequency is correlated to the oxide film developed in the air[57][46]. The arcs can be premediated for the corrosion products layer, and the double electric layer behaviour of the specimen is determined at the middle and low frequencies[58][46], consecutively. It is noticed from the Figure 3.15 that the Zn-Ni coating (Zn-Ni without immersion) at the optimum conditions (Run-4 in Table 3.8) reveal a higher impedance modulus and coating resistance (R_{coat}) as tabulated in Table 3.7. Moreover, the immersion time increases, the width of the plots decreases, demonstrating the decrease in the corrosion resistance of the coated samples.

The values of R_{coat} have drastic change from the resistance 409.0 Ωcm^2 at 3hours immersion to 98.32 Ωcm^2 at 72 hours of the immersion test and capacitance 6.98 μFcm^{-2} to 3.98 μFcm^{-2}, due to the increase of the porosity, non-uniformity and the formation of hydrogen bubbles of the Zn-Ni alloy film immersed at 72 hours, which is the evidence by the decrease of the value of R_{coat}. It is also observed form the R_{coat} values of 12 hours and 24 hours are approximately the same lead to increase the corrosion product layer on the coated surface at 24 hours of immersion. The similar EECM has been reported by Feng et al. (2016) prepared Zn-Ni alloy coating from a novel DMH-based electrolyte bath as a replacement of zinc and cadmium coatings[47][46]. However, Zn-Ni alloy at 72 hours of immersion indicates the easier access of the corrosive solution on the coating surface exhibit lower corrosion resistance and capacitance in comparisons to the Zn-Ni alloy without immersion. The charge transfers resistance (R_{ct}) of the coating immersed at 3 hours is 637.5 Ωcm^2 and the Zn-Ni alloy immersed at 72 hours is 504 Ωcm^2. The value of R_{ct} (384.3 Ωcm^2) decreases in the initial 24 hours of the immersion time, which indicates that the dissolution of zinc and non-uniformity on the surface to reduce the corrosion resistant properties of the coating. After 24 hours of immersion time, the corrosion resistant of the plated sample is continuous decreases as shown in Figure 3.15. Feng et al.[46][47], Gomes et al. [48] and Vlasa et al.[59] has reported the similar results.

3.5. Conclusions

The most important deposition factors influencing the corrosion resistant activity of the Zn-Ni deposits are citrate concentration, bath temperature and plating time from the FFD Study. Through the path of the steepest ascent study, the vicinity of the optimal electroplating settings for electroplating the Zn-Ni samples with the minimum activity of corrosion current density (I_{corr}) leads to exhibit better corrosion resistant properties. The optimal settings are Zn/Ni molar concentration ratio = 0.66, electroplating time = 13 minutes, electroplating current density = 60 mA/cm^2 and bath temperature = 28^{0}C and citrate concentration 0.062 mol/l, for the Zn-Ni samples with the with the highest activity of corrosion surrent density (I_{corr}) obtained by the regression model through CCD coupled with the surface response method. The morphological structure the Zn-Ni deposits at optimum conditions from citrate baths exhibited uniform, compact and dense deposits which is favourable for corrosion resistance. The γ-Ni_2Zn_{11} phase with (330) plane orientation exhibit higher intensity than those of other γ-phases, i.e., γ-$NiZn_3$ and Ni_3Zn_{22}, demonstrating that γ-Ni_2Zn_{11} phase with (330) plane orientation plays an assertive role in the Zn-Ni alloy corrosion resistant coatings. This demonstrates that the co-deposition of different zinc and zinc-nickel phases will help to form a uniform and dense deposit. According to the XRD results, simonkolleite ($Zn_5(OH)_8Cl_2.H_2O$), hydrozincite ($Zn_5(CO_3)_2(OH)_6$), zinc oxide (ZnO), and zinc hydroxide ($Zn(OH)_2$) is the main corrosion products for Zn-Ni alloy coatings. As the immersion time increases, the dominant corrosion products are simonkolleite and zinc oxide.

Acknowledgments

The authors thankfully acknowledge the financial support provided by the Natural Science and Engineering Council of Canada (NSERC) and the Canada Research Chair (CRC) Tier I Program.

References

[1] M. H. Wood, A. L. Vetere Arellano, and L. Van Wijk, Corrosion - Related Accidents in Petroleum Refineries. 2013.

[2] B. M. Durodola, J. A. O. Olugbuyiro, S. A. Moshood, O. S. Fayomi, and A. P. I. Popoola, "Study of influence of zinc plated mild steel deterioration in seawater environment," Int. J. Electrochem. Sci., vol. 6, no. 11, pp. 5605–5616, 2011.

[3] R. E. Melchers, "Pitting Corrosion of Mild Steel in Marine Immersion Environment—Part 1: Maximum Pit Depth," Corrosion, vol. 60, no. 9, pp. 824–836, 2004.

[4] R. E. Melchers, "Mathematical modelling of the diffusion controlled phase in marine immersion corrosion of mild steel," Corros. Sci., vol. 45, pp. 923–940, 2003.

[5] R. E. Melchers, "The effect of corrosion on the structural reliability of steel offshore structures," Corros. Sci., vol. 47, no. 10, pp. 2391–2410, 2005.

[6] R. Melchers and R. Jeffrey, "The critical involvement of anaerobic bacterial activity in modelling the corrosion behaviour of mild steel in marine environments," Electrochim. Acta, vol. 54, no. 1, pp. 80–85, 2008.

[7] Sriraman Kankoduthavanitham Rajagopalan, "Characterization of Electrodeposited Zn-Ni Alloy Coatings as a replacement for Electrodeposited Zn and and Cd Coatings," McGill University, Montreal, Quebec, Canada, 2012.

[8] E. Del Angel, R. Vera, and F. Corvo, "Atmospheric corrosion of galvanised steel in different environments in Chile and Mexico," Int. J. Electrochem. Sci., vol. 10, no. 10, pp. 7985–8004, 2015.

[9] L. Veleva, M. Acosta, and E. Meraz, "Atmospheric corrosion of zinc induced by runoff," Corros. Sci., vol. 51, no. 9, pp. 2055–2062, 2009.

[10] V. K. Tables, S. Electrode, M. Dekker, and N. York, "Electrochemical series CRC," pp.

20–29.

[11] A. Kalendová, “Comparison of the anticorrosion efficiencies of pigments based on condensed phosphates and polyphosphosilicates,” Anti-Corrosion Methods Mater., vol. 50, no. 2, pp. 82–90, 2003.

[12] A. Y. Hosny, M. E. El-Rafei, T. A. Ramadan, B. A. El-Gafari, and S. M. Morsy, “Corrosion resistance of zinc coatings produced from a sulfate bath,” Met. Finish., vol. 93, no. 11, pp. 55–59, 1995.

[13] G. Barceló, M. Sarret, C. Müller, and J. Pregonas, “Corrosion resistance and mechanical properties of zinc electrocoatings,” Electrochim. Acta, vol. 43, no. 1–2, pp. 13–20, 1998.

[14] K. Lin, C. Yang, and J. Lee, “Correlation of Microstructure with Corrosion and Electrochemical-behavior of the batch-type hot-dip al-zn coatings .1. zn and 5-% al-zn coatings,” Corros. J. Sci. Technol., 1991.

[15] R. Fratesi, G. Roventi, G. Giuliani, and C. R. Tomachuk, “Zinc-cobalt alloy electrodeposition from chloride baths,” J. Appl. Electrochem., vol. 27, no. 9, pp. 1088–1094, 1997.

[16] I. H. Karahan and H. S. Güder, “Electrodeposition and properties of Zn, Zn–Ni, Zn–Fe and Zn–Fe–Ni alloys from acidic chloride–sulphate electrolytes,” Trans. IMF, vol. 87, no. 3, pp. 155–158, 2009.

[17] J. yin FEI, G. zheng LIANG, W. li XIN, and W. kang WANG, “Surface Modification With Zinc and Zn-Ni Alloy Compositionally Modulated Multilayer Coatings,” J. Iron Steel Res. Int., vol. 13, no. 4, pp. 61–67, 2006.

[18] D. Blejan and L. M. Muresan, “Corrosion behavior of Zn-Ni-Al2O3 nanocomposite coatings obtained by electrodeposition from alkaline electrolytes,” Mater. Corros., vol. 64, no. 5, pp. 433–438, 2013.

[19] M. Gavrila, J. P. Millet, H. Mazille, D. Marchandise, and J. M. Cuntz, “Corrosion

behaviour of zinc-nickel coatings, electrodeposited on steel," Surf. Coatings Technol., vol. 123, no. 2–3, pp. 164–172, 2000.

[20] M. G. Hosseini, H. Ashassi-Sorkhabi, and H. A. Y. Ghiasvand, "Electrochemical studies of Zn-Ni alloy coatings from non-cyanide alkaline bath containing tartrate as complexing agent," Surf. Coatings Technol., vol. 202, no. 13, pp. 2897–2904, 2008.

[21] R. Gnanamuthu, S. Mohan, G. Saravanan, and C. W. Lee, "Comparative study on structure, corrosion and hardness of Zn-Ni alloy deposition on AISI 347 steel aircraft material," J. Alloys Compd., vol. 513, pp. 449–454, 2012.

[22] R. Ramanauskas, L. Muleshkova, L. Maldonado, and P. Dobrovolskis, "Characterization of the corrosion behaviour of Zn and Zn alloy electrodeposits: Atmospheric and accelerated tests," Corros. Sci., vol. 40, pp. 401 – 410, 1998.

[23] R. Fratesi and G. Roventi, "Corrosion resistance of Zn-Ni alloy coatings in industrial production," Surf. Coat. Technol., vol. 82, pp. 158 – 164, 1996.

[24] K. R. Sriraman, S. Brahimi, J. A. Szpunar, J. H. Osborne, and S. Yue, "Characterization of corrosion resistance of electrodeposited Zn-Ni Zn and Cd coatings," Electrochim. Acta, vol. 105, pp. 314–323, 2013.

[25] M. K. P. Kumar et al., "Electroplating of Nanocrystalline CoFeNi Soft Magnetic Thin Films from a Stable Citrate-Based Bath," Surf. Eng. Appl. Electrochem., vol. 16, no. 2, pp. 1189–1194, 2015.

[26] S. Fashu, C. D. Gu, X. L. Wang, and J. P. Tu, "Influence of electrodeposition conditions on the microstructure and corrosion resistance of Zn-Ni alloy coatings from a deep eutectic solvent," Surf. Coatings Technol., vol. 242, pp. 34–41, 2014.

[27] M. M. Abou-Krisha, "Electrochemical studies of zinc-nickel codeposition in sulphate bath," Appl. Surf. Sci., vol. 252, no. 4, pp. 1035–1048, 2005.

[28] H. Faid, L. Mentar, M. R. Khelladi, and A. Azizi, "Deposition potential effect on surface

properties of Zn–Ni coatings," Surf. Eng., vol. 33, no. 7, pp. 529–535, 2017.

[29] J. R. Garcia, D. C. B. do Lago, and L. F. de Senna, "Electrodeposition of Cobalt Rich Zn-Co alloy Coatings from Citrate Bath," Mater. Res., vol. 17, no. 4, pp. 947–957, 2014.

[30] Y. Zhang and D. G. Ivey, "Electroplating of Nanocrystalline CoFeNi Soft Magnetic Thin Films from a Stable Citrate-Based Bath," Chem. Mater., vol. 16, no. 7, pp. 1189–1194, 2004.

[31] F. H. Assaf, S. S. Abd El Rehim, A. S. Mohamed, and A. M. Zaky, "Electroplating of brass from citrate-based alloy baths," Indian J. Chem. Technol., vol. 2, no. 3, pp. 147–152, 1995.

[32] M. V. Tomić, M. M. Bučko, M. G. Pavlović, and J. B. Bajat, " Corrosion stability of electrochemically deposited Zn-Mn alloy coatings," Contemp. Mater., vol. 1, no. 1, pp. 87–93, 2010.

[33] Y. F. Jiang, L. F. Liu, C. Q. Zhai, Y. P. Zhu, and W. J. Ding, "Corrosion behavior of pulse-plated Zn-Ni alloy coatings on AZ91 magnesium alloy in alkaline solutions," Thin Solid Films, vol. 484, no. 1–2, pp. 232–237, 2005.

[34] F. L. G. Silva, D. C. B. Do Lago, E. D'Elia, and L. F. Senna, "Electrodeposition of Cu-Zn alloy coatings from citrate baths containing benzotriazole and cysteine as additives," J. Appl. Electrochem., vol. 40, no. 11, pp. 2013–2022, 2010.

[35] A. Conde, M. A. Arenas, and J. J. de Damborenea, "Electrodeposition of Zn-Ni coatings as Cd replacement for corrosion protection of high strength steel," Corros. Sci., vol. 53, no. 4, pp. 1489–1497, 2011.

[36] H. Rushing, A. Karl, and J. Wisnowski, "Design and Analysis of Experiments," Des. Anal. Exp. by Douglas Montgomery A Suppl. Using JMP, pp. 101–128, 2013.

[37] C. C. Hu, C. H. Tsay, and A. Bai, "Optimization of the hydrogen evolution activity on zinc-nickel deposits using experimental strategies," Electrochim. Acta, vol. 48, no. 7,

pp. 907–918, 2003.

[38] P. Ganesan, S. P. Kumaraguru, and B. N. Popov, “Development of compositionally modulated multilayer Zn-Ni deposits as replacement for cadmium,” Surf. Coatings Technol., vol. 201, no. 18, pp. 7896–7904, 2007.

[39] G. E. P. . Box, J. S. Hunter, and W. G. Hunter, Statistics for experimenters : an introduction to design, data analysis, and model building. Wiley, New York, 1978.

[40] J. A. Cornell, How to Apply Response Surface Methodology, vol. 8. ASQC, Wisconsin., 1990.

[41] F. Mansfeld, H. Shih, C.H.Tsai, and H. Greene, “Analysis of EIS Data for Common Corrosion Processes,” Am. Soc. Test. Mater., vol. 1188, pp. 37–53, 1993.

[42] A. Tozar and I. H. Karahan, “Structural and corrosion protection properties of electrochemically deposited nano-sized Zn-Ni alloy coatings,” Appl. Surf. Sci., vol. 318, pp. 15–23, 2014.

[43] M. K. Punith Kumar, T. V. Venkatesha, M. K. Pavithra, and A. N. Shetty, “A Study on Corrosion Behavior of Electrodeposited Zn-Rutile TiO_2 Composite Coatings,” Synth. React. Inorganic, Met. Nano-Metal Chem., vol. 42, no. 10, pp. 1426–1434, 2012.

[44] F. La Mantia, J. Vetter, and P. Novák, “Impedance spectroscopy on porous materials: A general model and application to graphite electrodes of lithium-ion batteries,” Electrochim. Acta, vol. 53, no. 12, pp. 4109–4121, 2008.

[45] S. Fajardo, D. M. Bastidas, M. Criado, and J. M. Bastidas, “Electrochemical study on the corrosion behaviour of a new low-nickel stainless steel in carbonated alkaline solution in the presence of chlorides,” Electrochim. Acta, vol. 129, pp. 160–170, 2014.

[46] Z. Feng, L. Ren, J. Zhang, P. Yang, and M. An, “Effect of additives on the corrosion mechanism of nanocrystalline zinc–nickel alloys in an alkaline bath,” RSC Adv., vol. 6, no. 91, pp. 88469–88485, 2016.

[47] Z. Feng, M. An, L. Ren, J. Zhang, P. Yang, and Z. Chen, “Corrosion mechanism of nanocrystalline Zn-Ni alloys obtained from a new DMH-based bath as a replacement for Zn and Cd coatings,” RSC Adv., vol. 6, no. 69, pp. 64726–64740, 2016.

[48] A. Gomes, I. Almeida, T. Frade, and A. C. Tavares, “Stability of Zn–Ni–TiO2 and Zn–TiO2 nanocomposite coatings in near-neutral sulphate solutions,” J. Nanoparticle Res., vol. 14, no. 2, p. 692, 2012.

[49] C. J.K. and D. S., “Crystal structure of delta-NiZn,” J. Inst. Met., vol. 99, pp. 26–27, 1971.

[50] Y. Boonyongmaneerat and K. Saenapitak, S Saengkiettiyut, “Reverse pulse electrodeposition of Zn-Ni alloys from a chloride bath,” J. Alloy. Compd., vol. 487, pp. 479–482, 2009.

[51] Z. Feng, Q. Li, J. Zhang, P. Yang, and M. An, “Studies on the enhanced properties of nanocrystalline Zn–Ni coatings from a new alkaline bath due to electrolyte additives,” RSC Adv., vol. 5, no. 72, pp. 58199–58210, 2015.

[52] Z. Feng, Q. Li, J. Zhang, P. Yang, and M. An, “Electrochemical Behaviors and Properties of Zn-Ni Alloys Obtained from Alkaline Non-Cyanide Bath Using 5,5’-Dimethylhydantoin as Complexing Agent,” J. Electrochem. Soc., vol. 162, no. 9, pp. D412–D422, 2015.

[53] J. Friel, “Atmospheric corrosion products on aluminium, zinc, and aluminium-zinc metallic coatings,” Corrosion, vol. 42, pp. 422–426, 1986.

[54] M. Bučko, J. Rogan, S. I. Stevanović, A. Perić-Grujić, and J. B. Bajat, “Initial corrosion protection of Zn-Mn alloys electrodeposited from alkaline solution,” Corros. Sci., vol. 53, no. 9, pp. 2861–2871, 2011.

[55] M. Mouanga and P. Berçot, “Comparison of corrosion behaviour of zinc in NaCl and in NaOH solutions; Part II: Electrochemical analyses,” Corros. Sci., vol. 52, no. 12, pp.

3993–4000, 2010.

[56] Z. I. Ortiz, P. Díaz-Arista, Y. Meas, R. Ortega-Borges, and G. Trejo, “Characterization of the corrosion products of electrodeposited Zn, Zn-Co and Zn-Mn alloys coatings,” Corros. Sci., vol. 51, no. 11, pp. 2703–2715, 2009.

[57] J. Winiarski, W. Tylus, M. S. Krawczyk, and B. Szczygieł, “The influence of molybdenum on the electrodeposition and properties of ternary Zn-Fe-Mo alloy coatings,” Electrochim. Acta, vol. 196, pp. 708–726, 2016.

[58] J. Chen, Y. Song, D. Shan, and E. H. Han, “Study of the corrosion mechanism of the in situ grown Mg-Al-CO32-hydrotalcite film on AZ31 alloy,” Corros. Sci., vol. 65, pp. 268–277, 2012.

[59] A. Vlasa, S. Varvara, A. Pop, C. Bulea, and L. M. Muresan, “Electrodeposited Zn-TiO_2 nanocomposite coatings and their corrosion behavior,” J. Appl. Electrochem., vol. 40, no. 8, pp. 1519–1527, 2010.

4.0 Electrochemical Behaviour and Analysis of Zn and Zn-Ni Alloy Anti-Corrosive Coating Deposited from Citrate Baths

Preface

In this chapter, the development of pure Zn and Zn-Ni alloy coating on steel substrates by using potassium citrate as a complexing agent. The stability of the electroplating bath studied through a stability diagram or Pourbaix diagram. The effects of plating variables such as bath composition and current density on coating composition, morphology and corrosion property were investigated. Electrochemical behavior of the deposition bath on steel plates was studied by cyclic voltammetry (CV). Potentiodynamic polarization measurement (Tafel) and EIS were carried out to evaluate the corrosion protection performance of the Zn-Ni alloy coatings. The equivalent electrical circuits obtained from the experimental fitted data of Nyquist and Bode plot also demonstrated the Zn-Ni deposited from citrate in comparison to the pure Zn and Zn-Ni from the non-citrate bath. XRD technique is used for structural phase analysis and to calculate average crystal size of the coating. SEM was used for morphological analysis, and AFM was used for topographical analysis. This chapter brings a new study to explored the effect of potassium citrate on Zn-Ni electroplating bath, to enhance the corrosion resistant and mechanical properties of the coated samples. The content of this chapter has been published as a manuscript in the Royal Society of Chemistry-Advances, 28861-28873, 2018.

Abstract

The anticorrosive coating is an effective approach for protecting the steel structures/machinery against corrosion in process industries. Electrodepositions of zinc and zinc-nickel alloy films

on steel substrate under the various level of deposition conditions from baths containing potassium citrate were studied. The effects of plating variables such as bath composition and current density on the coating composition, morphology, corrosion and mechanical property were systematically investigated. The electrochemical and mechanical behaviour of Zn-Ni deposit obtained at 60mA/cm^2 from citrate bath exhibited lower corrosion current (I_{corr}), and less negative corrosion potential (E_{corr}) compared to pure Zn and Zn-Ni alloy coatings from the non-citrate bath. Crystallite size of Zn-Ni coating deposited from citrate bath is 35.40 nm, and Ni content of the coating is 8.3 wt%. The morphological properties and crystalline phase structure of the alloy coating were examined by scanning electron microscopy (SEM) and X-ray diffraction (XRD). The topographical structure of the coatings was analyzed by atomic force microscopy (AFM). The dominant γ-$NiZn_3$ (815) and γ-Ni_2Zn_{11} (330) (631) plane orientation in zinc-nickel alloy films improved corrosion resistance. Zn-Ni films with smaller grain size with uniform coating had increased impedance modulus and improved corrosion resistance.

Keywords: Electrodeposition, Pure Zn coatings, Zn-Ni coatings, Citrate bath, Crystallite size, Impedance Spectroscopy, Microhardness.

4.1. Introduction

Corrosion is one of the significant sources of equipment failure and safety problems in offshore and marine operations[1][2]. The anti-corrosive coating is a useful approach for protecting the steel structures/machinery against corrosion [2]. Pure zinc coating was widely used as the sacrificial coating to protect the steel structure from the corrosion. To improve the corrosion resistance property of steels in a harsh environment, significant efforts were made to strengthen their anti-corrosive properties [3][4]. One of the ways to improve the corrosion resistant properties of zinc coating is to make alloying with Fe, Cu and Ni. According to the

literature[5][6], zinc alloy coatings such as Zn-Ni[7][8][9], Zn-Cu[10] and Zn-Fe [11]alloy films are often used to provide excellent corrosion resistance and maintain strong mechanical properties for steel equipment. They have better corrosion resistance compared to pure zinc coating[5][6]. Electrodeposition is one of the most economical and frequent technologies for producing metallic coatings[12]. The Zn alloy coatings deposited from citrate bath have been studied by Silva et al. (2010) They deposited Cu-Zn alloy coating on mild steel substrate from a bath containing sodium citrate as a complexing agent and benzotriazole and cysteine as additives. The results demonstrated that the coatings obtained with additives were brighter with small grain size. Cystine in an electrodeposition bath increases the potential for hydrogen evolution reaction (HER) and also prevents direct zinc deposition, and the deposited film exhibits high corrosion resistance[10]. It is found that citrate significantly increases the stability of the baths and denser coatings are deposited due to higher bath pH [9].

Assaf et al. (1995) studied the effects of electroplating parameters such as bath composition, temperature and current density on the deposition of copper, zinc, and brass on a steel substrate. However, they found that the zinc deposited at a low current density (<3mA/cm^2) and low zinc content (<15g/dm^3) in the bath affect the formation of fine grains and leave some bare areas. This behaviour may be due to the low cathodic current efficiency of zinc deposition and strong evolution of hydrogen gas[13].

Rastogi and Pandey (2009) studied the electrodeposition of Zn-Mn-Mo alloy from citrate baths, by investigating various parameters such as current density, temperature, pH, deposition time and the concentration of chemical compounds. They found the optimum conditions were $ZnSO_4.H_2O$ 30g/l, $MnSO_4.H_2O$ 60g/l, $(NH_4)_2MoO_3$ 4g/l, $C_6H_8O_7.H_2O$ 5g/l, pH 2.05, temperature of 25^0C, deposition time of 30 minutes, and current density of 4.0 A/dm^2; and semi-bright, light grey and adherent deposits were obtained[14].

Nowadays, Zn-Ni alloy coatings are a foremost eco-friendly substitute for toxic cadmium coating[7] and have attracted significant attention due to providing better corrosion resistance and mechanical properties at higher temperatures and severe environmental conditions, compared to pure zinc and other zinc alloy coating[9]. Several analyses have been undertaken to understand the characteristics of the electrodeposition process of Zn-Ni alloys. It is found that the features of the deposited coating depend on the current density, pH, bath composition, applied voltage, additives and temperature[6]. The phases and crystal structure of the surface of the deposited Zn-Ni alloy are significant characteristics which control corrosion resistance and other mechanical properties[7, 8].

As seen from the above literature, there are several experimental studies have been implemented on the Zn-Ni deposited from citrate bath at various operating conditions. To the best of the author's knowledge, there is no systematic study specifically for comparing pure Zn and Zn-Ni alloy deposited from citrate and non-citrate, optimum parameter conditions and challenge to suppress the hydrogen evolution reaction (HER) to improve corrosion resistant properties of the coating. Therefore, in order to fulfil this gap, the present research is to utilize the incremental study on the pure Zn and Zn-Ni alloy deposited at various level of operating conditions is investigated and analyzed.

The present paper studies pure Zn and Zn-Ni alloy coating on steel substrates to improve corrosion resistance using potassium citrate as a complexing agent. The effects of plating variables such as bath composition and current density on coating composition, morphology and corrosion property were investigated. XRD technique is used for structural phase analysis and to calculate average crystal size of the coating. SEM was used for morphological analysis, and AFM was used for topographical analysis. Electrochemical behaviour of the deposition bath on steel plates was studied by cyclic voltammetry (CV). Potentiodynamic polarization measurement (Tafel) and EIS were carried out to evaluate the corrosion protection performance

of the Zn-Ni alloy coatings. The equivalent electrical circuits obtained from the experimental fitted data of Nyquist and Bode plot also demonstrated the Zn-Ni deposited from citrate in comparison to the pure Zn and Zn-Ni from the non-citrate bath. The effect of an optimum operating parameter on deposit character and their corrosion behaviour was observed and discussed

4.2. Challenge - Establishment of stable baths for Zn and Zn-Ni containing coatings

Due to the negative reduction potential of Zn/Zn^{2+} electrode. Zn is more challenging to be electroplated than hydrogen gas[16]

$$Zn^{2+}(aq) + 2e^- \longrightarrow Zn(s) \qquad E_{Zn/Zn^{2+}} = -0.762\ V$$

$$2H^+(aq) + 2e^- \longrightarrow H_2(g) \qquad E_{2H/H2} = 0.000\ V$$

The hydrogen ions in the electrolyte solution will be deposited before zinc, as H^+ ions have a more positive reduction potential under the standard state. To overcome and modify this problem the higher pH bath electroplating is preferable. Generally, high pH bath (alkaline) is not stable. Therefore, most of the electroplating is developed as an acidic bath. The major problem, to use of acidic bath is the hydrogen evolution reaction is occurring in the electrolyte and to exhibiting non-uniform less corrosion resistant coatings. Although, in this work, the citrate bath has relative low pH, the addition of citrate is still helpful to stabilize the plating bath during electrodeposition because the reduction of hydrogen will increase the pH around the cathode. Thus, the existence of citrate in the bath can prevent the precipitation of metal hydroxides around the cathode.

To electrodeposit Zn coatings with suitable composition and microstructure, which lead to ideal corrosion resistant and mechanical properties, the development of a stable plating bath with relatively high pH is vital. To suppress hydrogen deposition and stabilize the plating baths, alkalis and complexing agents (e.g., acetate and citrate) were added into the baths for ideal Zn, Zn-Ni and Zn-Ni composite electroplating. According to the above results, the corrosion

resistant property, uniformity, thickness, and mechanical hardness of the plated films were also improved. [16] [17] [18] [10] [19] [20]

4.2.1 The effect of the Complexing agent on the stability of a plating bath

The stability of the electroplating bath studied through a stability diagram or Pourbaix diagram. Complexing agents such as potassium citrate were employed to stabilize the metal and alloy plating baths.

Figure 4.1 (a) and (b) are the pourbaix diagram calculated for the Zn-Ni alloy deposited form non-citrate, 0.0816 mol/l and 0.163 mol/l citrate baths. The dashed lines 'a' and 'b' refer to the equilibrium lines for H^+/H_2 and $(O_2+H_2O)/OH^-$ respectively [21].

It can be seen from the figure that, thermodynamically, the stability of a Zn-Ni alloy plating bath is dominated by the precipitation of $Zn(OH)_2$ and $Ni(OH)_2$ at pH 6.2 and 6.8 (Figure 4.1(a)). The pH is shown by arrow line, in which red colour line shows the indication of $Zn(OH)_2$ whereas, green line shows the indication of $Ni(OH)_2$. Afterwards, the addition of 0.0326 mol/l of potassium citrate, the Zn-Ni alloy plating bath is thermodynamically stable until pH 7.2 for $Zn(OH)_2$ and pH 7.8 for $Ni(OH)_2$ are reached with the given concentration of metal ions (Figure 1(b)), and the formation of the stable complexing species such as $Zn[C_6H_5O_7]^-$ and $Ni[C_6H_5O_7]^-$ Therefore, it is observed form these two pourbaix diagram that $Zn(OH)_2$ and $Ni(OH)_2$ precipitation is extended to one pH on the pH scale and it forms stability in the electrolyte bath.

From Figure 4.1(b), it is apparent that citrate has the strongest complexing power for Zn ions, followed by Ni ions. Therefore, $Zn[C_6H_5O_7]$ (aq) and $Ni[C_6H_5O_7]$ (aq) contribute to stabilizing the Zn-Ni elements in the bath solution.

The calculated stability diagrams demonstrate that, thermodynamically, citrate can effectively stabilize Zn-Ni alloy plating baths, preventing the precipitation of metal hydroxides at a higher

pH. Bath stability tests on baths with and without the addition of potassium citrate have been conducted.

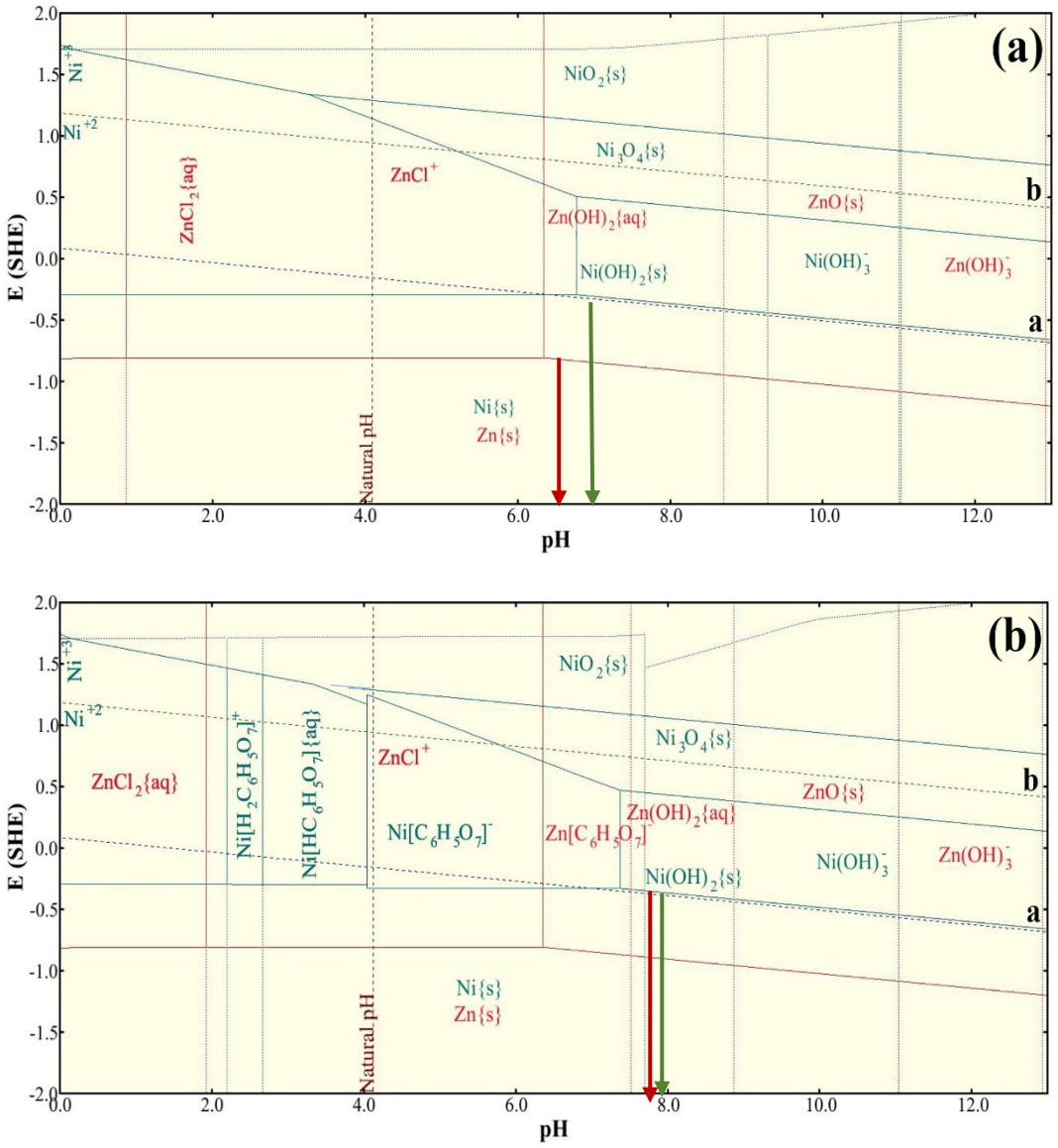

Figure 4.1 Pourbaix diagram for Zn-Ni alloy plating from non-citrate bath; (b) Zn-Ni alloy plating from 0.0326 mol/l of citrate bath

4.3. Experimental details

The electrodeposition experiments were carried out in a bath with a 200 ml solution at room temperature. A rectangular steel plate of 10 cm^2 was used as the working electrode (WE), and a graphite rod was used as the counter electrode (CE). The reference area of the coated sample is 1 cm^2 for the electrochemical analysis. The CE and WE were connected to the DC power

supply via a multi-meter. There were three types of baths prepared: bath-1 (chloride bath without potassium citrate containing $ZnCl_2$, SDS and NaCl); bath-2 (chloride bath without potassium citrate containing $ZnCl_2$, $NiCl_2.6H_2O$, SDS and NaCl); and bath-3 (chloride bath with potassium citrate containing $ZnCl_2$, $NiCl_2.6H_2O$, SDS, NaCl, $K_3(C_6H_5O_7)$ and H_3BO_3), as shown in Table 4.1. They were degreased with 10wt% sodium hydroxide solution for 5 min, then rinsed with 10% hydrochloric acid and alcohol or acetone for a few seconds. The operating conditions for electrodeposition are listed in Table 4.2. After deposition, the Zn and Zn–Ni alloy coatings were washed with distilled water and dried in air.

Table 4.1. Bath compositions for the electrodeposition of pure Zn and Zn-Ni alloy coatings

Bath Composition	**Concentrations**		
	Bath-1	**Bath-2**	**Bath-3**
Zinc Chloride ($ZnCl_2$)	60 (g/l)	60 (g/l)	60 (g/l)
Nickel (II) chloride hexahydrate ($NiCl_2.6H_2O$)	-	20 (g/l)	20 (g/l)
Boric Acid (H_3BO_3)	-	-	8 (g/l)
Sodium dodecyl sulfate (SDS)	$1.7.10^{-5}$ mol/l	$1.7.10^{-5}$ mol/l	$1.7.10^{-5}$ mol/l
Potassium Citrate ($K_3(C_6H_5O_7)$)		-	8 (g/l)
Sodium chloride (NaCl)	8 (g/l)	8 (g/l)	8 (g/l)
	Bath pH=2.0	Bath pH =2.0-2.5	Bath pH =2.5 -3.0

Table 4.2. Operating conditions for depositing the pure Zn and Zn-Ni alloy coatings

Operating conditions	**Samples**
Anode	Graphite rod
Cathode	Steel plates
Current density	20, 40, 60 mA/cm^2
Plating Time	10 minutes
Stirred Speed	350 rpm
Temperature	Room

Electrochemical analyses were performed using a ZAHNER IM6 electrochemical workstation produced by ZAHNER-Elektrik GmbH & Co.KG, Germany. The electrochemical analysis experiments were carried out in a conventional three-electrode cell with a 200ml solution. A 10 cm^2 rectangular steel plate was used as the cathode. A graphite rod was used as the anode. Silver/silver chloride with saturated potassium chloride as a salt bridge (Ag/AgCl/KClsat) was used as the reference electrode. The schematic stability diagrams were plotted from OLI Analyzer Studio software. The morphology of the deposited samples was investigated by scanning electron microscopy equipped with energy dispersive spectroscopy (FEI MLA 650F). A Rigaku Ultima IV X-ray diffractometer with a copper x-ray source and a scintillation counter detector (λ=1.5418A^0)was used to study the crystal phase structures of deposits, and the databases used to identify the peaks were pdf# 03-065-5310 and 00-004-0831 RDB Minerals, International Centre for Diffraction Database (ICDD).

The Debye-Scherrer equation is used to calculate the average crystallite size of the samples from the peak width at the half maximum of the crystal peaks (β)[22];

$$t = \frac{0.94\lambda}{\beta Cos\theta}$$

Where t is the crystallite size, λ is the wavelength of the X-ray radiation, θ is the Bragg's angle of the peak and β is the angular width of the peak at full width at half maximum (FWHM).

The topographical structure of the coatings was analyzed by atomic force microscopy (Asylum research MFP 3D). The hardness of the coating is measured by Vickers Microhardness Testing machine.

4.4. Results and Discussion

4.4.1 Chemical compositions and Surface morphology

The surface morphology of the electrodeposited pure Zn and Zn-Ni coating deposited from citrate bath, and non-citrate bath was investigated using SEM, as shown in Figure 4.2. The

deposited Zn-Ni alloy coating is developed regarding its uniformity, porosity and grain size by varying bath compositions and current density. As the current density increase, the over-potential increases lead to increase the nucleation rate and reduce the grain size of the coating. This result is investigated and reported by El-sherik et al. [23] and Feng et al. [24]. The sample (a) pure Zn coating deposited from non-citrate at same current density exhibits bigger grain size, rough structures with some cracks and holes, as also shown in Figure 4.3 using AFM analysis. Whereas sample (b) deposited from citrate bath showed a uniform surface with smaller grain sizes and sample (c) deposited from the non-citrate bath at same conditions reveals non-uniformity, swelling with larger and coarser grain sizes are found due to the HER, and the bath is not stable. Therefore, sample (b) shows uniformity with adherent and dense Zn-Ni coating surface (Figure 4.2 (b)). The incorporation of Ni into the Zn matrices slightly modifies the morphology of the Zn-Ni coatings. The Zn coating is composed of hemispherical structures; however, after incorporation, the structure is changed[25] [24]. Similar result has been demonstrated by Feng et al. (2015), with adding the complexing agents, significantly decrease of the grain size can be observed and the deposits are smooth, homogeneous, uniform, compact and fine-grained without any pores or pinholes at the surface[26] as shown in Figure 4.2 (b). The optimum value of the plating current density is 60mA/cm^2, exhibited lower grain size and denser coating. The coating is shown in Figure 4.2 and 4.3 is plated at 60mA/cm^2. Rahman et al. (2009) reported that from 40-60mA/cm^2 plating current density grain of the deposit is smaller, uniform and no porosity is found whereas, with increasing plating, current density after 60mA/cm^2 have to produce non-uniform crystals and coarse-grained coatings[15].

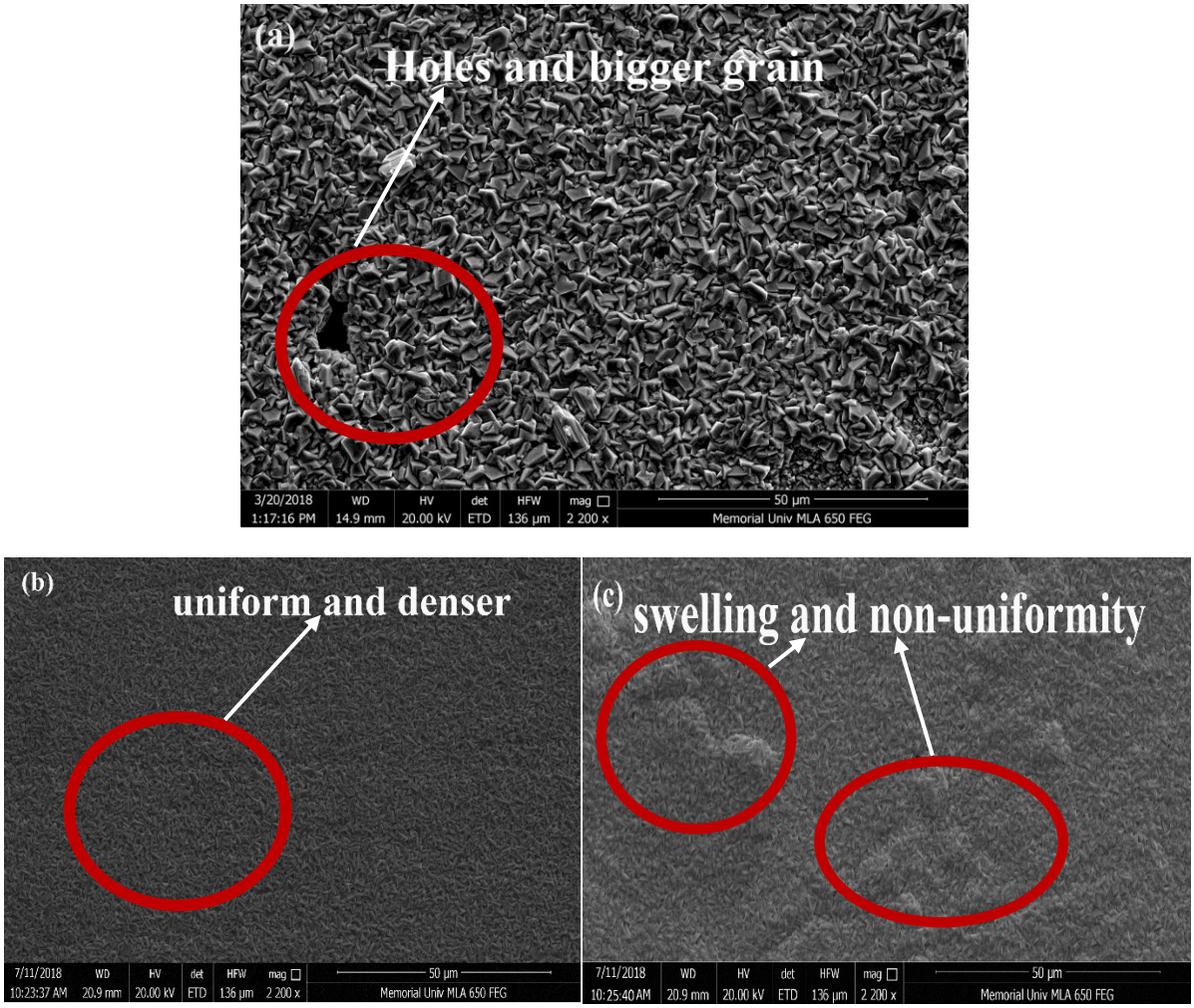

Figure 4.2 The SEM images of pure Zn and Zn-Ni alloy coatings, (a) pure Zn deposited from the non-citrate bath, (b) Zn-Ni deposited from citrate bath, (c) Zn-Ni deposited from non-citrate

The surface morphology of the corroded pure Zn and Zn-Ni alloy coating immersed in sodium chloride solution as shown in Figure 4.3. All the images are at the same magnification whereas, the image shown in the inset, is at higher magnifications. It can be clearly seen that the corrosion products formed on Zn and Zn-Ni alloy coatings. The sample (a) pure Zn coating and sample (c) Zn-Ni deposited from non-citrate demonstrated that the formation of uniformly distributed voids and porous structures on the surface of the coating. When the tensile and compressive stress applied to the porous corroded samples then the samples cracks after a long exposure of time[27]. Whereas sample (b) deposited from citrate bath has less such effect formed on the surface of the coating. Moreover, after the immersion test, the uniform and compact corrosion products are appeared on the sample (b) and attain higher corrosion resistant

properties. As per the above results, after the immersion in 3.5% NaCl solution; the corrosion product is formed on the coated surface. Therefore; the wettability of the coated surface has a significant effect on the corrosion prevention on the Zn and Zn-Ni deposits[28].

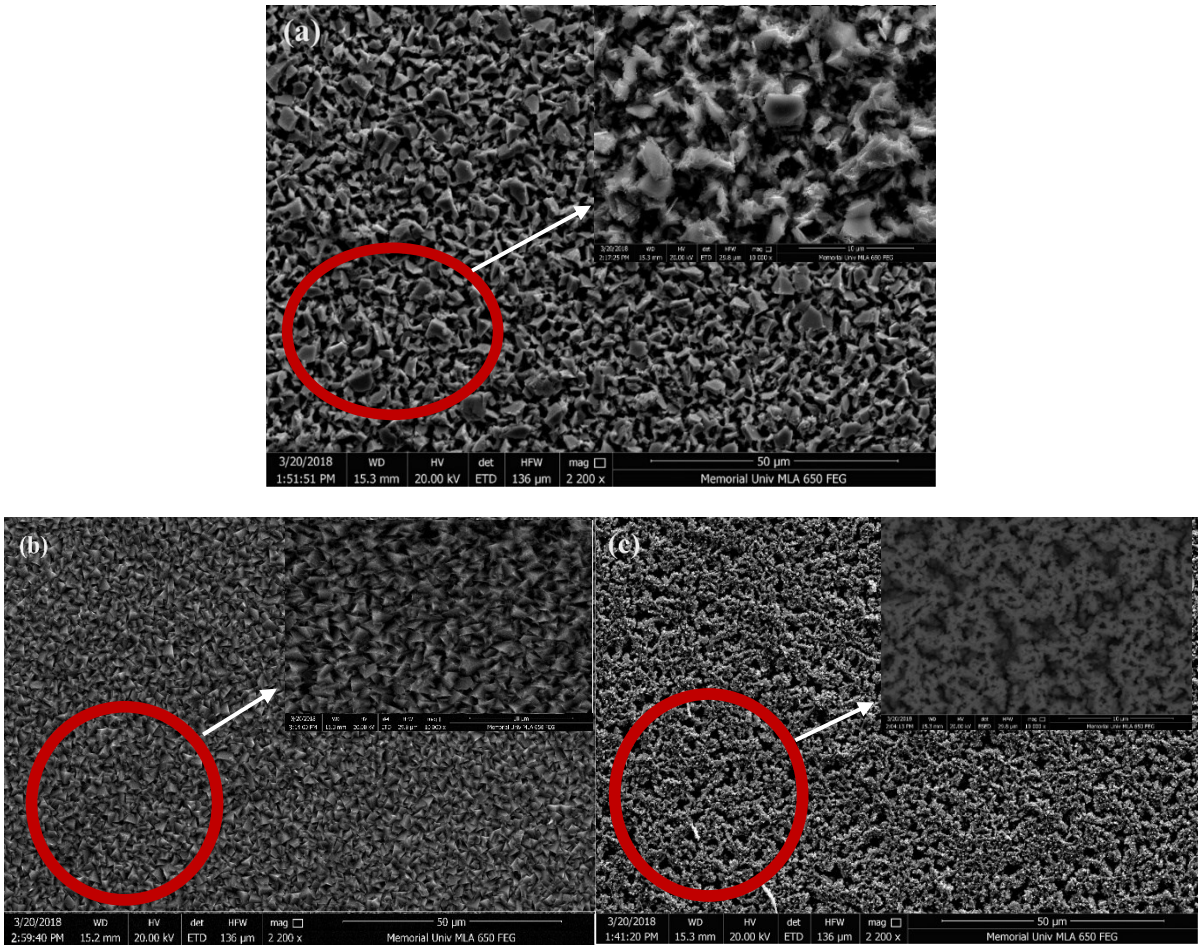

Figure 4.3 The SEM images of the corroded pure Zn and Zn-Ni alloy coatings, (a) pure Zn deposited from the non-citrate bath, (b) Zn-Ni deposited from citrate bath, (c) Zn-Ni deposited from non-citrate

4.4.2 Atomic Force Microscopy (AFM) analysis

The topographical 2D and 3D images of pure Zn and Zn-Ni alloy coated samples (a), (b) and (c) surface obtained by AFM measurement deposited from citrate bath and non-citrate bath at are shown in Figure 4.4. In the case of sample (a), the cathodic deposition is non-uniform, heterogeneous and have a large peak with bigger grains are formed in comparison to another sample. Sample (b) and (c) are less coarse and uniform in texture. Whereas, sample (b) showed uniform, homogeneous, compact and small peaks with regular grain size led to exhibit higher mechanical and corrosion resistant properties. The additives or complexing agents are adsorbed

on the Zn-Ni matrix preferentially and inhibits Zn-Ni alloy depositions, resulting in the smaller reduction of Zn^{+2} and Ni^{+2} on these matrices, therefore smooth and homogeneous deposits can be observed [29]. The roughness factor illustrates the initial surface irregularities, non-uniformity and heterogeneity. Therefore irregular surface demonstrates higher dissolution rate, especially in the presence of corrosive environment [30]. This surface factor suggests the non-linear dependence of the coated uniformity [26][31]; deposited from citrate or non-citrate bath.

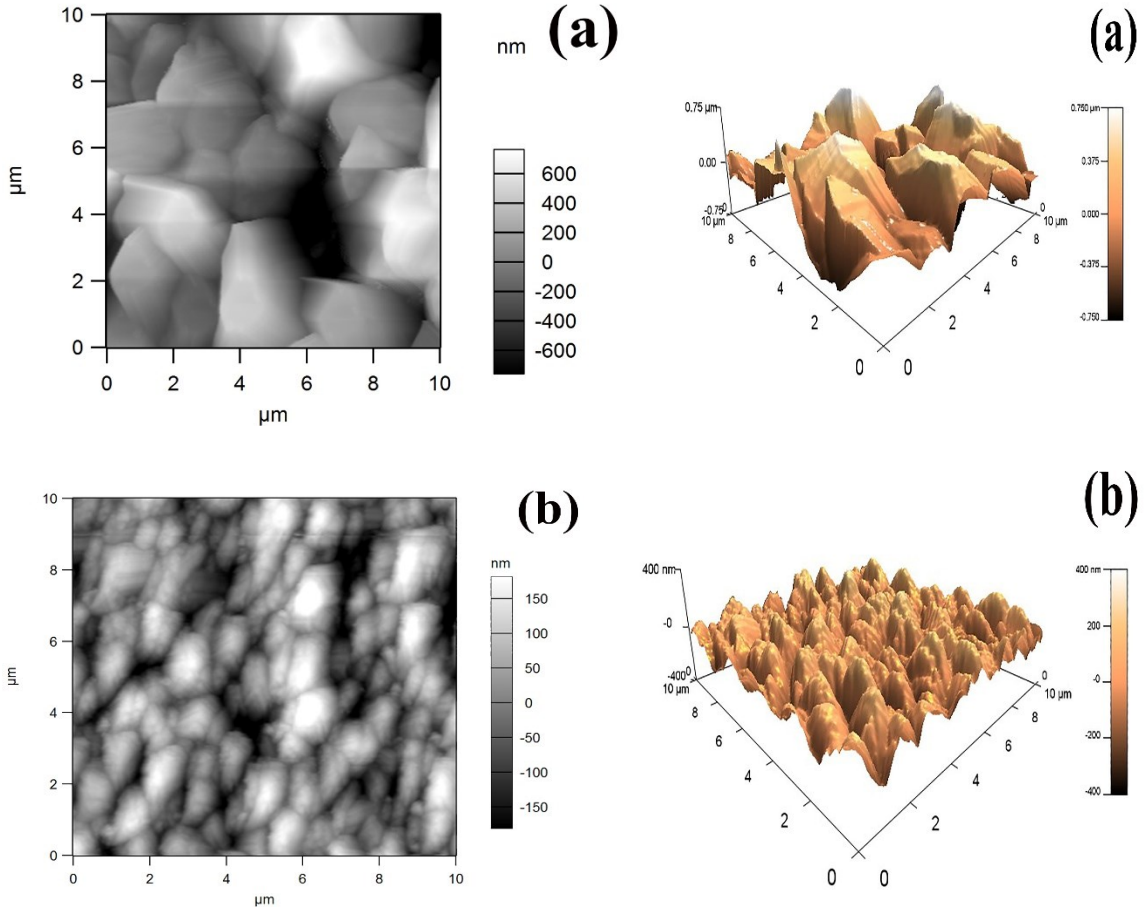

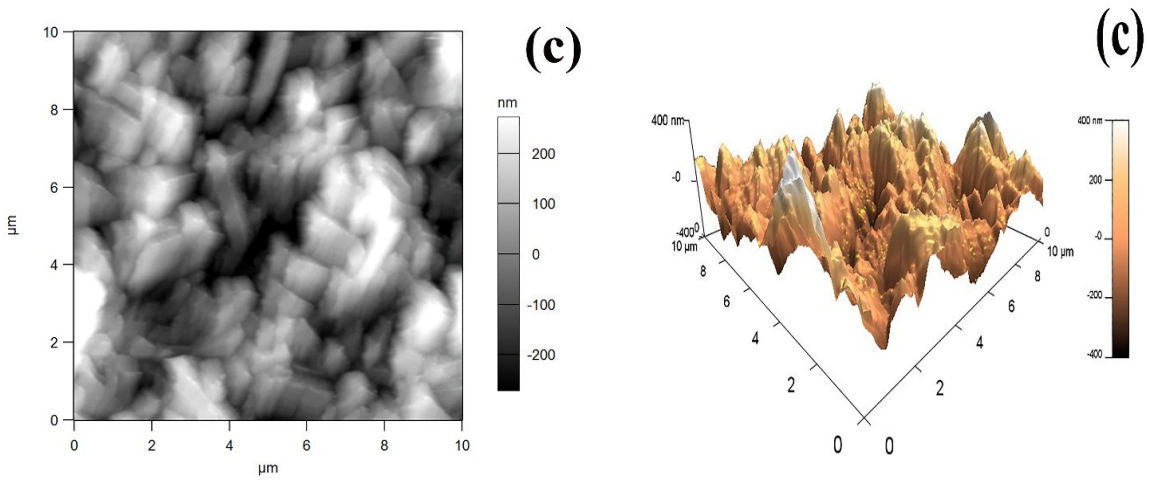

Figure 4.4 2D and 3D images of Zn and Zn-Ni alloy coating electrodeposited (a) Pure Zn coating from non-citrate (b) Zn-Ni coating deposited from citrate (c) Zn-Ni coating deposited from non-citrate

4.4.3 Cyclic Voltammetry studies

Cyclic voltammetry (CV) is used to characterize the electrochemical behaviour and kinetics of electrochemical reactions [32]. Figure 4.5 shows the CVs behaviour recorded for the deposition and dissolution of pure Zn and Zn-Ni from citrate and non-citrate bath has been plated on steel plates from a chloride bath at room temperature. The CV of given conditions was characterized by the presence of two peaks in an anodic scan and one peak in a cathodic scan. The anodic peaks seen in the anodic scan during the electrochemical oxidation of alloy can be attributed to the dissolution of the coating in the alloy from different intermetallic phases [33]. The two anodic peaks start from 293mV for Zn-Ni alloy deposited from citrate and non-citrate corresponds to the dissolution of constituents γ-$NiZn_3$ and γ-Ni_2Zn_{11} and dissolution of Ni from their phases [34][35][8]. Therefore, the voltammetric behaviour of Zn-Ni alloy states the properties of its structure and components of the deposited phase. The anodic current density of pure Zn coating is high in comparison to the Zn-Ni coating leads to increase the dissolution rate of pure Zn

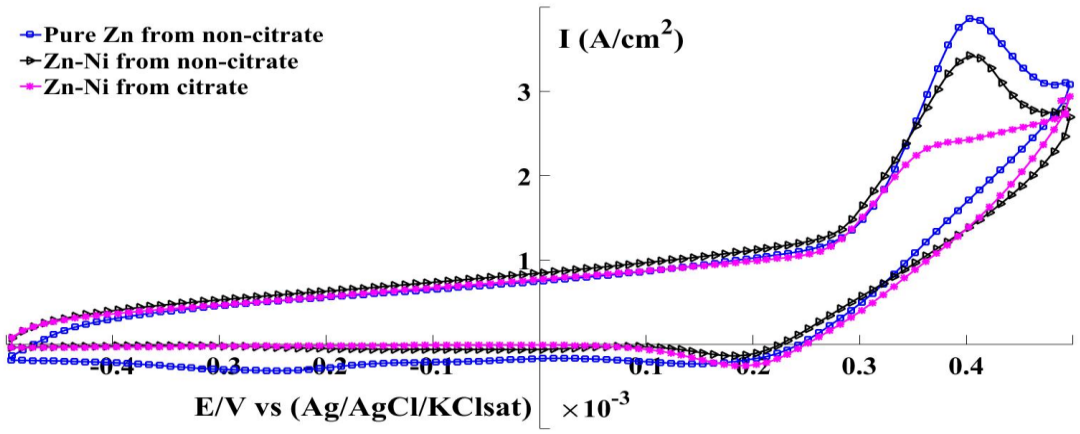

Figure 4.5 Cyclic Voltammogram for pure Zn and Zn-Ni coating from electrolytic baths at scan rate of 5mV/s.

4.4.4 X-Ray Diffraction (XRD) analysis

The distinguished crystalline phase and orientations of the pure Zn and Zn-Ni coated samples at different conditions are shown by XRD patterns. It is observed from Figure 4.6 that coatings contain three dominant diffraction peaks such as Zn (101), γ-$NiZn_3$ (831) and γ-Ni_2Zn_{11} (330). The important peaks of pure Zn coating comprise at 36^0, 43^0 and 54^0 matches to the Zn (002), Zn (101) and Zn (102). The peaks at about 38^0, 43^0 and 73^0 corresponds to γ-$NiZn_3$ (831) and γ-Ni_2Zn_{11} (330) (631) phases of the Zn-Ni alloy. The other peaks are at 51^0, 69^0 and 82^0 matching the Zn-Ni (111) and Zn (110) (200) phases. The Zn-Ni coating deposited from citrate bath has the highest intensity of the γ-phase (γ-Ni_2Zn_{11}) with (330) plane orientation whereas, for pure Zn coating is Zn (101) as shown in Figure 4.6 (a) and (b). Moreover, the peak value of γ-phase with (330) plane orientation is higher than that of other γ-phase orientations such as γ-$NiZn_3$, demonstrating that γ-phase with (330) plane orientation plays an assertive role in the Zn-Ni alloy coatings[36] [31] [28]. The intensity of the γ-phase (γ-Ni_2Zn_{11}) of sample (b) is high in comparison to the sample (c). The crystal peaks intensities illustrated the information about the number of phases and also the relative amount of Zn-Ni in the deposits[37]. Therefore, the coating with high-intensity γ-phase with (330) (831) plane orientation exhibits better corrosion resistance.

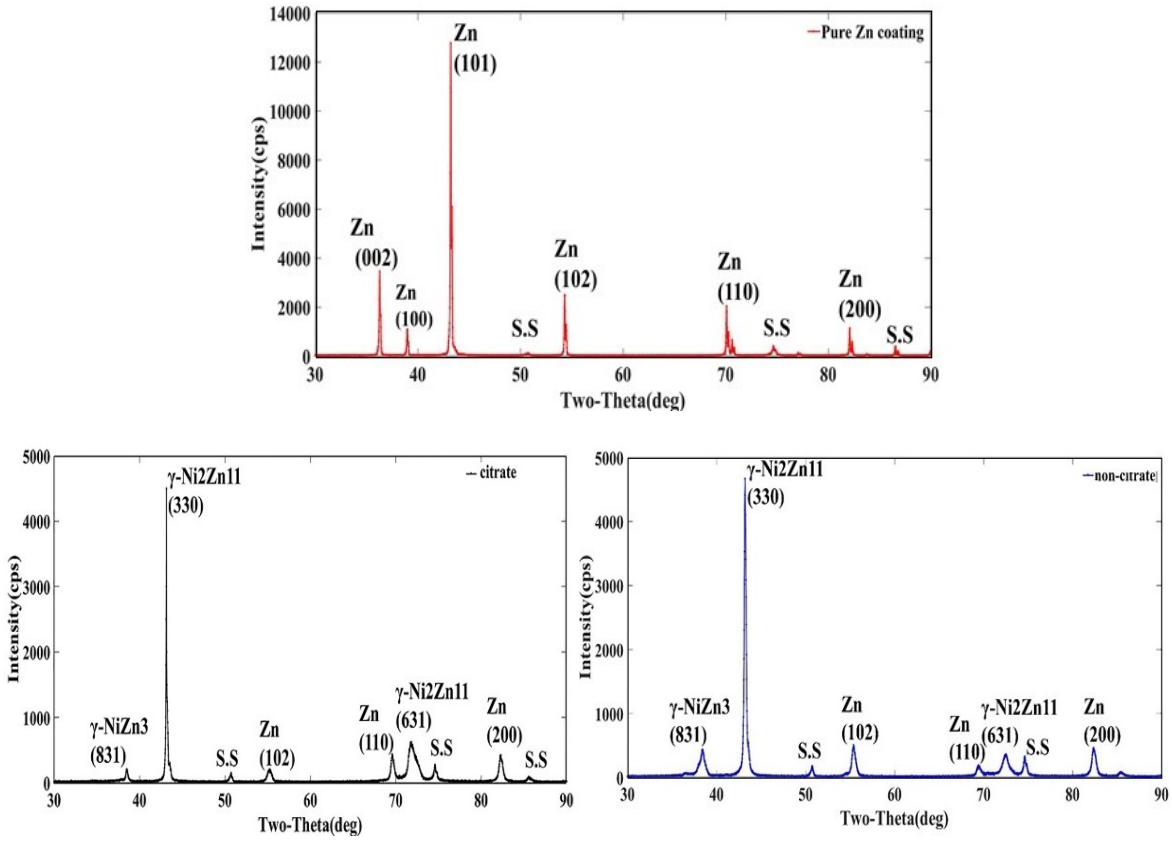

Figure 4.6 XRD patterns for the pure Zn and Zn-Ni alloy coatings using different baths (a) pure Zn coating deposited from non-citrate (b) deposited with citrate, (c) deposited from non-citrate

4.4.5 Potentiodynamic Polarization analysis

The Potentiodynamic polarization curves of the pure Zn and Zn-Ni alloy films deposited from citrate and non-citrate baths at three different plating current densities ranging from 20-60mA/cm^2 were studied. The polarization analysis was performed in an aerated 3.5% NaCl solution at room temperature, and the scan rate was 10mV/s as tabulated in Table 4.3. The polarization curves of different coatings were measured at their open circuit potential (OCP), and corrosion current densities (I_{corr}) and corrosion potentials (E_{corr}) were calculated from the intercepts on the Tafel slopes by extrapolation, obtained with reference to the silver and silver chloride electrode with saturated potassium chloride as salt bridge (Ag/AgCl/KCl_{sat}). The corrosive activity of the Zn-Ni alloy coating in corrosive media is directly related to corrosion potentials. The corrosion resistance of the coating is mainly related to their structural morphologies, chemical compositions and phase compositions[37].

It has been studied that the main cathodic reduction of pure Zn and Zn alloy is oxygen reduction, which is the rate controlling step for the corrosion[38]. However, the superior corrosion resistance of the deposits corresponds to the more positive corrosion potential (E_{corr}) values or lower corrosion current (I_{corr}) [39]. It is observed from Table 4.3 that the E_{corr} of pure Zn coating at 40mA/cm^2 deposited from the non-citrate bath is less negative in comparison to the Zn plated at 20 and 60 mA/cm^2. However, I_{corr} for the pure Zn coating plated at 60mA/cm^2 exhibits lower value (4.76mA/cm^2). Therefore, the increase of plating current density leads to produce less corrosion resistance properties of the Zn coating. Moreover, Zn-Ni alloy coatings deposited from citrate and non-citrate baths exhibited, as the plating current density increases, the I_{corr} decreases, and less negative E_{corr} was recorded. The similar result has been found by Assaf et al.[40] and Abou Krisha[41] that increasing the plating current density improves Ni content in the coating and shifts the E_{corr} toward more positive potential, which leads to provide higher corrosion resistance property.

The E_{corr} of Zn coating deposited from the non-citrate bath at 60 mA/cm^2 exhibits more negative potential (-0.810V), whereas, those of Zn-Ni alloy coatings deposited from the non-citrate bath and citrate bath are -0.790V and -0.760V, respectively. It is also noticeable from Table 4.3 that the E_{corr} shifts to more positive value as the plating current density increases, and the Zn-Ni alloy coating deposited from citrate bath improved the corrosion resistant properties of the steel.

The I_{corr} of the sample (b) at 60mA/cm^2 is 2.98 mA, whereas for the sample (a) is 4.76 mA and sample (c) is 5.9 3mA. The sample (b) coating possesses a lower I_{corr} value than the other coated samples. The least I_{corr} is due to the stable citrate bath Zn-Ni coated samples with decreased HER, which exhibited uniform and high anti-corrosive coating and is also shown on the sample (b) SEM images, which has small grain size, compact, bright and uniform Zn-Ni coating. Sample (c) coated film have swelling and non-uniformity on the surface due to hydrogen

evolution. Moreover, as the current density of Zn-Ni plated sample is increases led to decrease the corrosion rate of the coated sample whereas for pure Zn plating, it increases (Table 4.3).

Table 4.3. Polarization data for the Zn-Ni coatings from different plating baths and different current densities

Samples	**Deposition current density, (mA/cm^2)**	**Corrosion Potential, E_{corr} (mV)**	**Corrosion current, I_{corr} (mA/cm^2)**	**Corrosion rate (μmpy)**
(a) Pure Zn from non-citrate	20	-820	7.39	40.51
	40	-810	6.22	38.58
	60	-814	4.76	41.54
(b) Zn-Ni from citrate	20	-798	7.15	29.8
	40	-780	5.91	36.13
	60	-760	2.98	27.28
(c) Zn-Ni from non-citrate	20	-800	8.51	35.27
	40	-812	8.90	38.29
	60	-790	5.93	32.64

The optimal result of the Zn and Zn-Ni coated sample deposited from citrate and non-citrate baths at 60 mA/cm^2 current density is shown in Figure 4.7, illustrated that Zn-Ni alloy coating from citrate bath exhibited less Icorr and more positive Ecorr in comparison to the pure Zn and Zn-Ni alloy coating deposited from non-citrate bath led to enhance the corrosion resistant properties of the coating. The author has deposited Zn-Ni alloy at lower and higher concentration of citrate. However, the coated sample is non-uniform and exhibited minimum corrosion resistance properties to the bare steel. Therefore, after the exploration test these concentrations are selected and used in this paper.

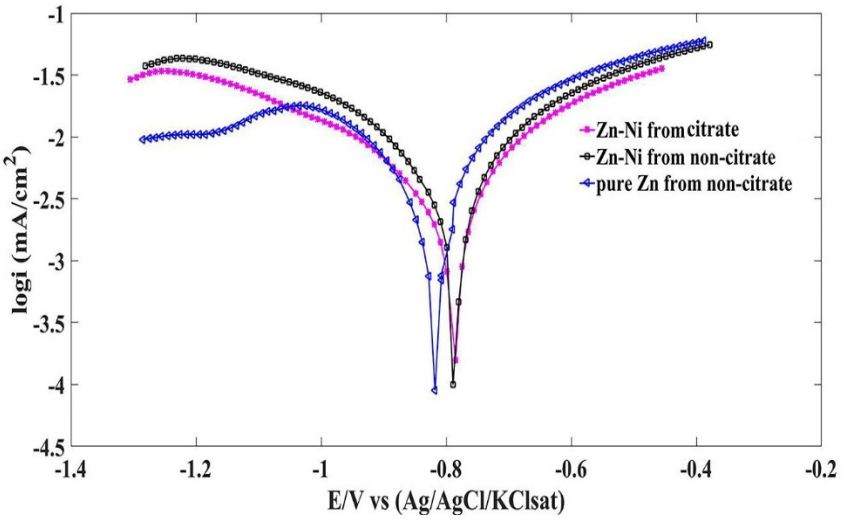

Figure 4.7 Polarization curve for the pure Zn and Zn-Ni alloy coatings deposited from citrate and non-citrate baths

As observed from Table 4.4, that the corrosion potential of the pure Zn coated samples are more negative than the Zn-Ni alloy coating. This implies that all of the electrodeposited Zn-Ni sample offers more corrosion protection to the bare steel substrate. The corrosion rate of Zn-Ni deposited from citrate and non-citrate is 27.28 μmpy and 41.54 μmpy whereas, for pure Zn is 32.64 μmpy, this implies that Zn-Ni deposited from citrate exhibited higher corrosion resistant properties in comparison to Zn-Ni from non-citrate and pure Zn coatings. On the other hand, Table 4.4, it is also observed that the Ni content in the Zn-Ni coating deposited from citrate bath is 8.3wt% whereas, Zn-Ni without citrate is 4.3 wt%. This can be attributed to the higher surface activity of Zn ions in comparison with nickel ions. The average crystal size of pure Zn coating is 80.92 nm whereas Zn-Ni coating deposited from citrate bath is 35.40 nm (Table 4.4).

Table 4.4. The optimized results for the pure Zn and Zn-Ni alloy coating deposited from citrate and non-citrate

Bath condition	**Composition of Coating (wt%)**		**Average Crystallite Size (nm)**	**Ecorr (mV vs Ag/AgCl)**	**Icorr (mA/cm^2)**	**Corrosion rate (μmpy)**
	Zn	**Ni**				
(a) Pure Zn from non-citrate	100	-	80.92	-814	4.76	41.54

(b) Zn-Ni from citrate	91.7	8.3	35.40	-760	2.98	27.28
(c) Zn-Ni from non-citrate	95.7	4.3	40.78	-790	5.93	32.64

4.4.6. Electrochemical Impedance Spectroscopy (EIS) analysis

The Electrochemical Impedance Spectroscopy (EIS) measurement is used as a corrosion resistance technique to evaluate the characteristics and kinetics of the electrochemical process prevailing at the electrode/solution interface in corrosive solutions [42][43]. The EIS measurements are carried out by the deposition of citrate and non-citrate baths in a 3.5% NaCl solution to calculate the corrosion resistance behaviour of Zn-Ni coatings. The OCP's range of frequency is 100kHz to 100mHz, the amplitude is 10mV, and scan rate is 10mV/s. The measured EIS data are displayed as Nyquist, and typically Bode plot is as shown in Figures 4.8, 4.9 and 4.10. In the Nyquist plots, the polarization resistance resembles the shape of a semicircle [37][8]. The result from deposition all the impedance deposited at different current densities are shown in Figure 4.8. The EIS measurement of the pure Zn coating deposited from non-citrate bath exhibited less impedance modulus. However, Zn-Ni alloy coating deposited from citrate bath shown higher impedance modulus than the Zn-Ni alloy deposited from the non-citrate bath at 20 mA/cm^2. The best coating with the maximum impedance modulus is found at 60mA/cm^2 for the sample (b) as shown in Figure 4.2 (b). The worst coating with the least impedance modulus is found at 20 mA/cm^2 of pure Zn coating as shown in Figure 4.8 (a), and it is related to a very small arc at high frequencies, formed the oxide film in the air [44].

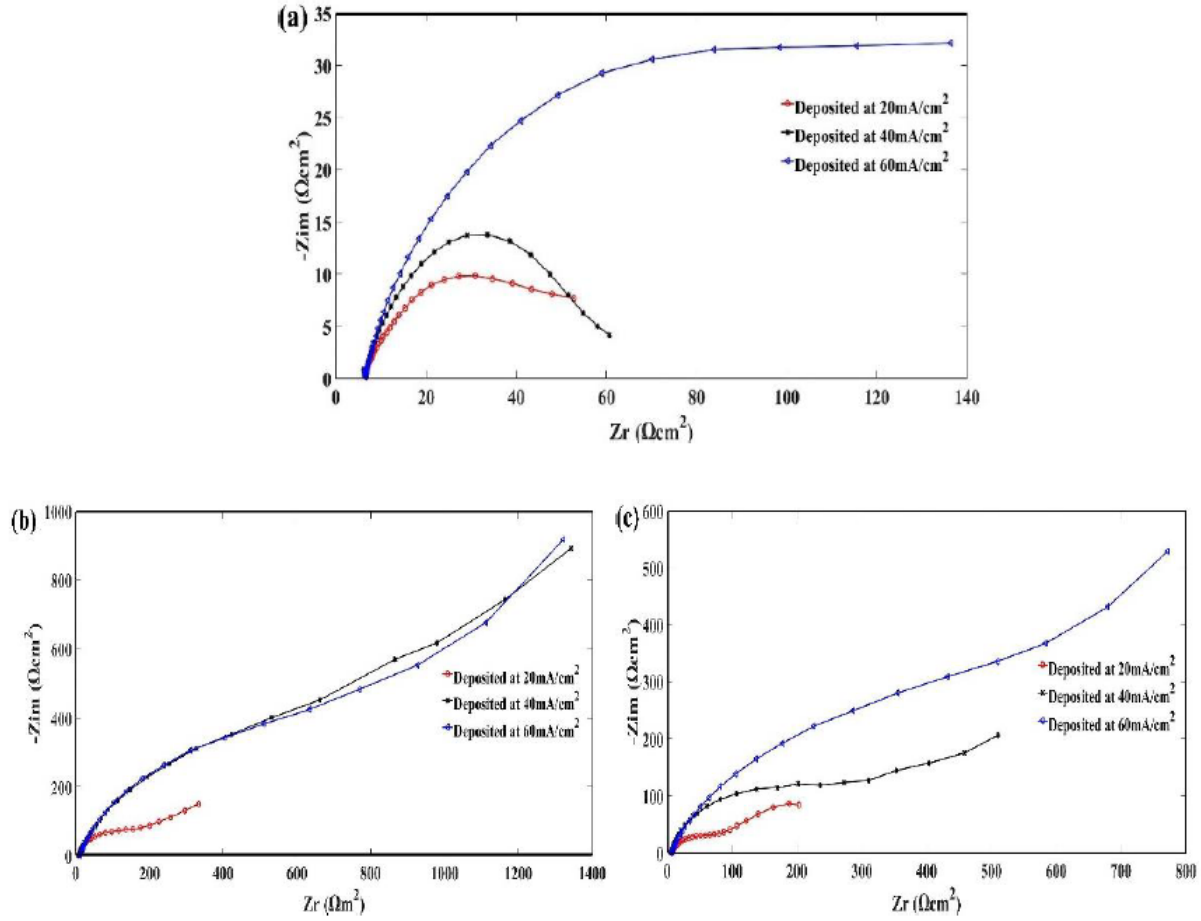

Figure 4.8 Nyquist plot for the Zn-Ni alloy coatings at different current densities, (a) pure Zn deposited from the non-citrate bath, (b) Zn-Ni deposited from citrate bath, (c) Zn-Ni deposited from non-citrate

The optimal results of the Nyquist plot at 60mA/cm^2 current density are shown in Figure 4.9. The corrosion resistance of the present Zn-Ni alloy coating can be explicated by the equivalent electrical circuit. The electrical circuits are shown in Figure 4.10, where R_{sol} represents the solution/electrolyte resistance between the reference and the working electrode (i.e., Zn-Ni coated specimen). R_3 and CPE_3 correspond to the resistance and capacitance of the formation of the thin oxide film that is reinforced by the ionic conduction through its pores. R_2 and CPE_2 correspond to the resistance and capacitance of the pure Zn and Zn-Ni alloy films. R_1 represents the charge transfer resistance associated with the reaction of zinc oxide and reduction of oxygen. CPE_1 corresponds the electric double layer capacitance at the interface of coating/electrolyte solution [28].

The Mathematical equation for the impedance of constant phase element (CPE) is given below[45]

$$Z(Q) = y_0^{-1}(jw)^{-\alpha}$$

Where y_0 is coefficient of constant phase element, j^2 =-1 imaginary constant, w is the frequency and α is the exponential of CPE. For α=0 represents the full resistor, for α =-1 represents inductor, for α=1 represents ideal capacitor, for α = 0.5 represents Warbug impedance [45].

All the measured impedance values were fitted using Zahner Thales software. The calculated fit data of the electrical equivalent circuit deposited from citrate and non-citrate bath for the pure Zn and Zn-Ni alloy coating are shown in Table 4.5. The charge transfers resistance (R_1) of the pure Zn coating is 55.6 Ωcm^2.Whereas, for Zn-Ni coating deposited from citrate bath is 3.6 $K\Omega cm^2$ and for the non-citrate Zn-Ni alloy sample value is 688.6 Ωcm^2 illustrates that the higher oxide reduction and zinc oxide reaction occurring on the Zn-Ni coated surface deposited from citrate bath, and less R_1 value is due to the increase of the active surface, which is related to the discontinuity and porosity of the coated film. It is well known that higher polarization resistance (R_1) values indicate better corrosion resistance. The coating resistance (R_2) of Zn-Ni from citrate bath is 879 Ωcm^2, from the non-citrate bath is 264.7 Ωcm^2, and pure Zn coating from the non-citrate bath is 67.65 Ωcm^2. The decrease of R_1 from Zn-Ni to pure Zn from citrate to non-citrate bath indicates that the easier access of the electrolyte on pure Zn coated surface deposited from non-citrate baths. Moreover, pure Zn coating deposited from non-citrate bath had least R_1 and R_2 which means that electrolyte molecules diffused into the coating surface exhibit less corrosion resistance. In the initial measurement, the low-frequency capacitive magnitude is less because there is less effect of corrosive media on the working electrode and thus the obtained impedance response is pure due to the coated surface. As a result, Zn-Ni alloy from citrate bath had maximum coating resistance (R_2) with minimum capacitance (CPE_2) of 879 Ωcm^2 and 28.2 μFcm^2. Similar electrical equivalent circuit has been reported by Feng et

al. [24] prepared Zn-Ni alloy coating from a new DMH-based bath as a replacement of Zn and Cd coatings. This behaviour indicates that the addition of the complexing agent ($K_3(C_6H_5O_7)$) in a bath is a simple and effective process to improve the corrosion resistance of Zn-Ni alloy coating.

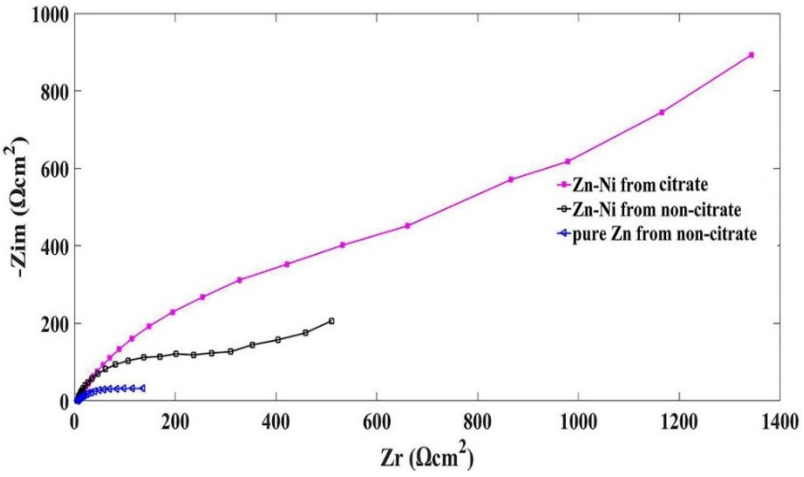

Figure 4.9 Nyquist plot for the pure Zn and Zn-Ni alloy coatings deposited from citrate and non-citrate baths

As seen in the Bode plot, that in the view of impedance vs frequency, impedance value increases by adding the potassium citrate. As for bode plots of frequency vs phase angle, phase angle also increases from citrate bath, as shown in Figure 4.10 (a) and (b).

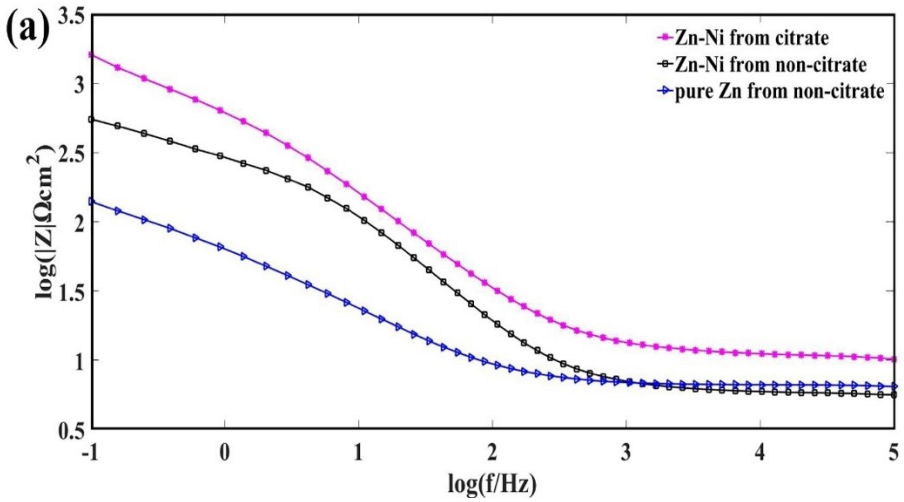

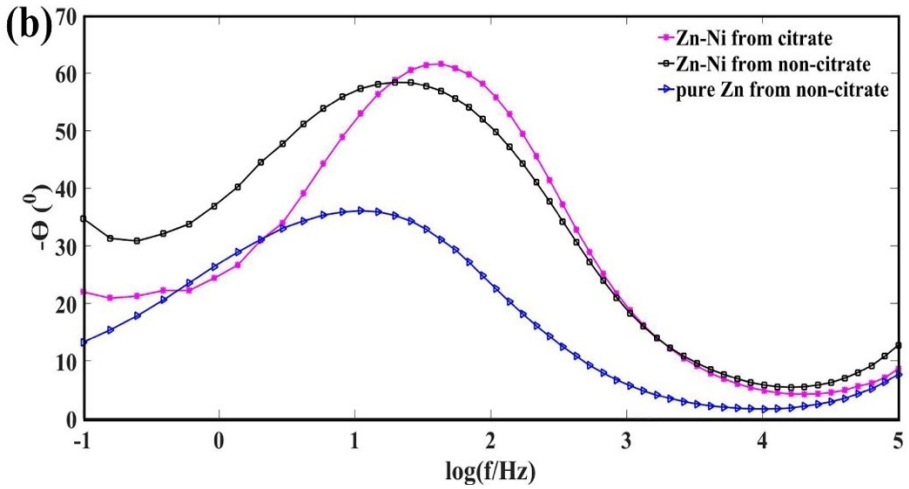

Figure 4.10 Bode plot for the pure Zn and Zn-Ni alloy coatings deposited from citrate and non-citrate baths, (a) Log modulus Z vs. log f, (b) Phase angle vs. log f

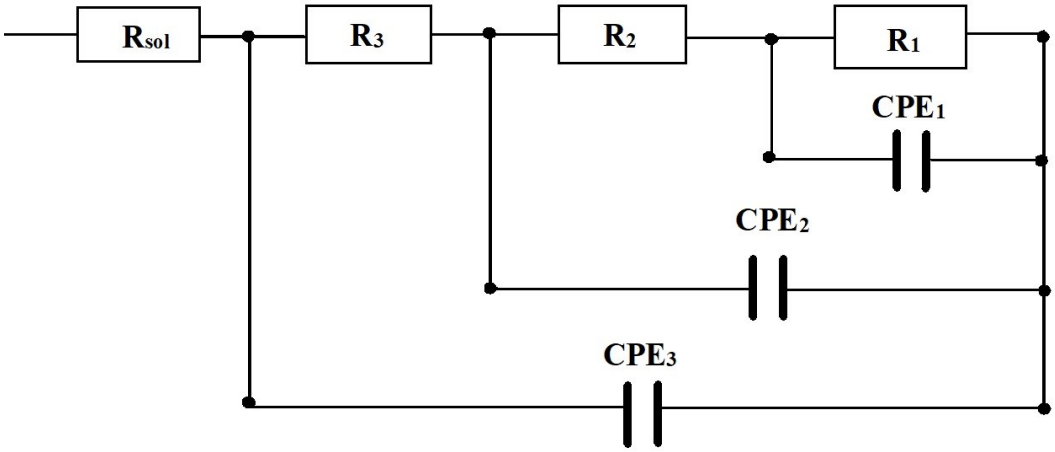

Figure 4.11 Electrical equivalent circuit modelling used for the simulation of EIS data of pure Zn and Zn-Ni alloy coating deposited from citrate and non-citrate baths

Table 4.5. Electrochemical parameters determined by equivalent circuit modelling

Bath condition	**R_{sol}** (Ωcm^2)	**R_1** (Ωcm^2)	**R_2** (Ωcm^2)	**R_3** (Ωcm^2)	**CPE_1** ($\mu F^{\alpha} cm^2$)	**CPE_2** ($\mu F^{\alpha} cm^2$)	**CPE_3** ($nF^{\alpha} cm^2$)
Pure Zn from non-citrate	3.06	55.6	67.65	3.5	893.3 $\alpha = 0.761$	173.5 $\alpha = 0.712$	61.3 $\alpha = 1.0$
Zn-Ni from non-citrate	2.62	688.6	264.7	3.3	105.5 $\alpha = 0.599$	63.7 $\alpha = 0.858$	104.0 $\alpha = 1.0$
Zn-Ni from citrate	3.08	3.6K	879	4.2	39.8 $\alpha = 0.626$	28.2 $\alpha = 0.766$	98.3 $\alpha = 1.0$

4.4.7 Vickers Microhardness test

The Vickers microhardness values obtained from different bath conditions of pure Zn and Zn-Ni alloy coatings electrodeposited on steel are shown in Figure 4.12. The development of film microhardness showed an increase from 154 HV for Pure coating from non-citrate (sample (a) to 223 HV (sample(b)) prepared from citrate bath. It is concluded that the microhardness was affected by the deposition of Zn-Ni from citrate bath. Thus, the crystallite size is a significant variable which affects the hardness value[46] [47]. The smaller grain size suggests that there is a more substantial amount of grain boundaries that obstruct dislocation motion and then create harder materials.

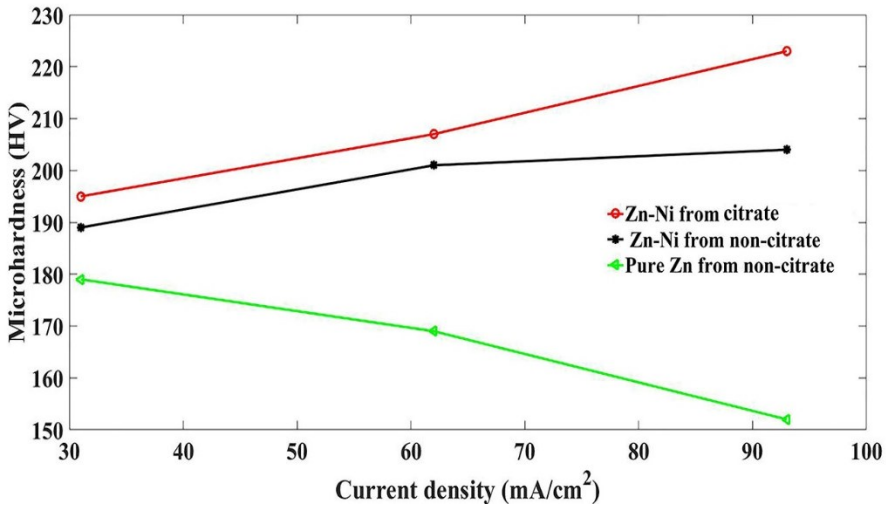

Figure 4.12 Vickers microhardness value of pure Zn and Zn-Ni alloy electrodeposit on steel from different baths

4.5 Conclusions and discussions

The electrochemical behaviour of pure Zn and Zn-Ni alloy coating from citrate and non-citrate bath and the stability of the electrolyte bath has been studied in this work. According to the above analysis, the following conclusions can be made as follows:

- Stabilized plating baths and complexing agents such as potassium citrate are employed for Zn-Ni alloy electrodeposition. This extends the precipitation of nickel hydroxide

($Ni(OH)_2$), and zinc monoxide ($Zn(OH)_2$) to a higher pH and the hydrogen evolution reaction is suppressed.

- The potentiodynamic polarization results reveal that the sample (b) coating possesses a lower I_{corr} value and more positive corrosion potential than the other two coated samples. The least I_{corr} is due to the stable citrate bath Zn-Ni coated samples with decreased HER, which exhibited uniform and higher corrosion resistance and the SEM images showed the formation of denser and more uniform coating. The phase structure of the Zn-Ni deposits from citrate bath has the highest intensity of γ-phase (γ-$NiZn_3$) (815), and γ-Ni_2Zn_{11} (330) (631) plane orientation exhibits better corrosion resistance.
- The EIS measurement of the sample (b) deposited from citrate bath shown higher impedance modulus than the other coated samples. Further EIS measurements carried out for the sample (a) and sample (c) deposited from the non-citrate bath showed less impedance modulus in comparison to samples (b). The best coating with the maximum impedance modulus is found at 60mA/cm^2 for sample (b). The electrical equivalent circuit modelling data best fit the generated Nyquist plot demonstrated that the Zn-Ni alloy coating on steel substrate deposited from citrate bath had maximum coating resistance (R_2) with minimum capacitance (CPE_2). This behaviour indicates that the addition of the complexing agent ($K_3(C_6H_5O_7)$) in a bath is a simple and effective process to improve the corrosion resistance of Zn-Ni alloy coating.
- The higher current density also leads to the reduced grain size and provides less coarse stronger and more uniform coating. The development of film microhardness shows an increase in the hardness from 154 HV for pure Zn (sample (a)) and 223 HV for Zn-Ni coating deposited from non-citrate (sample (c)) to (sample (b)) prepared from citrate bath.

References

[1] T. V. Venkatesha, S. K. Rajappa, and B. M. Praveen, "Chemical treatment of zinc surface and its corrosion inhibition studies," Bull. Mater. Sci., vol. 31, no. 1, pp. 37–41, 2008.

[2] C. C. Lin and C. M. Huang, "Zinc-nickel alloy coatings electrodeposited by pulse current and their corrosion behavior," J. Coatings Technol. Res., vol. 3, no. 2, pp. 99–104, 2006.

[3] V. G. Roev, R. A. Kaidrikov, and A. B. Khakimullin, "Zinc – Nickel Electroplating from Alkaline Electrolytes Containing Amino Compounds," Russian Journal of Electrochemistry, vol. 37, no. 7, pp. 756–759, 2001.

[4] D. Blejan, D. Bogdan, M. Pop, A. V. Pop, and L. M. Muresan, "Structure, morphology and corrosion resistance of Zn-Ni-TiO_2 composite coatings," Optoelectron. Adv. Mater. Commun., vol. 5, no. 1, pp. 25–29, 2011.

[5] R. Fratesi, G. Roventi, G. Giuliani, and C. R. Tomachuk, "Zinc-cobalt alloy electrodeposition from chloride baths," J. Appl. Electrochem., vol. 27, no. 9, pp. 1088–1094, 1997.

[6] I. H. Karahan and H. S. Güder, "Electrodeposition and properties of Zn, Zn–Ni, Zn–Fe and Zn–Fe–Ni alloys from acidic chloride–sulphate electrolytes," Trans. IMF, vol. 87, no. 3, pp. 155–158, 2009.

[7] K. R. Sriraman, S. Brahimi, J. A. Szpunar, J. H. Osborne, and S. Yue, "Characterization of corrosion resistance of electrodeposited Zn-Ni Zn and Cd coatings," Electrochim. Acta, vol. 105, pp. 314–323, 2013.

[8] A. Tozar and I. H. Karahan, "Structural and corrosion protection properties of electrochemically deposited nano-sized Zn-Ni alloy coatings," Appl. Surf. Sci., vol. 318, pp. 15–23, 2014.

[9] R. Gnanamuthu, S. Mohan, G. Saravanan, and C. W. Lee, “Comparative study on structure, corrosion and hardness of Zn-Ni alloy deposition on AISI 347 steel aircraft material,” J. Alloys Compd., vol. 513, pp. 449–454, 2012.

[10] F. L. G. Silva, D. C. B. Do Lago, E. D’Elia, and L. F. Senna, “Electrodeposition of Cu-Zn alloy coatings from citrate baths containing benzotriazole and cysteine as additives,” J. Appl. Electrochem., vol. 40, no. 11, pp. 2013–2022, 2010.

[11] F. Ebrahimi and H. . Li, “Structure and properties of electrodeposited nanocrystalline FCC Ni-Fe alloys,” Mater. Sci. Eng., vol. A, 347, p. 93, 2003.

[12] W. Schwarzacher, “Electrodeposition: A Technology for the Future,” Electrochem. Soc. Interface, vol. 15, no. 1, pp. 32–35, 2006.

[13] F. H. Assaf, S. S. Abd El Rehim, A. S. Mohamed, and A. M. Zaky, “Electroplating of brass from citrate-based alloy baths,” Indian J. Chem. Technol., vol. 2, no. 3, pp. 147–152, 1995.

[14] R. Rastogi and A. Pandey, “Electrolytic deposition of Zn-Mn-Mo alloys from a citrate bath,” Indian J. Chem. Technol., vol. 17, no. 5, pp. 381–385, 2010.

[15] M. J. Rahman, S. R. Sen, M. Moniruzzaman, and K. M. Shorowordi, “Morphology and Properties of Electrodeposited Zn-Ni Alloy Coatings on Mild Steel,” J. Mech. Eng. Mech. Eng. Div, vol. 40, no. 1, 9-14, 2009.

[16] H. Faid, L. Mentar, M. R. Khelladi, and A. Azizi, “Deposition potential effect on surface properties of Zn–Ni coatings,” Surf. Eng., vol. 33, no. 7, pp. 529–535, 2017.

[17] M. V Tomić, M. M. Bučko, M. G. Pavlović, and J. B. Bajat, “Corrosion Stability of Electrochemically Deposited Zn-Mn Alloy Coatings,” Surface and Interface Analysis, vol. 1, pp. 87–93, 2010.

[18] Y. F. Jiang, L. F. Liu, C. Q. Zhai, Y. P. Zhu, and W. J. Ding, “Corrosion behavior of pulse-plated Zn-Ni alloy coatings on AZ91 magnesium alloy in alkaline solutions,” Thin

Solid Films, vol. 484, no. 1–2, pp. 232–237, 2005.

[19] J. R. Garcia, D. C. B. do Lago, and L. F. de Senna, “Electrodeposition of Cobalt Rich Zn-Co alloy Coatings from Citrate Bath,” Mater. Res., vol. 17, no. 4, pp. 947–957, 2014.

[20] A. Conde, M. A. Arenas, and J. J. de Damborenea, “Electrodeposition of Zn-Ni coatings as Cd replacement for corrosion protection of high strength steel,” Corros. Sci., vol. 53, no. 4, pp. 1489–1497, 2011.

[21] H.-H. Huang, “The Eh-pH Diagram and Its Advances,” Metals (Basel)., vol. 6, no. 3, p. 23, 2016.

[22] A. Patterson, “The Scherrer formula for X-ray particle size determination,” Phys. Rev., vol. 56, pp. 978–982, 1939.

[23] A. M. El-Sherik, U. Erb, and J. Page, “Microstructural evolution in pulse plated nickel electrodeposits,” Surf. Coatings Technol., vol. 88, no. 1–3, pp. 70–78, 1997.

[24] Z. Feng, M. An, L. Ren, J. Zhang, P. Yang, and Z. Chen, “Corrosion mechanism of nanocrystalline Zn–Ni alloys obtained from a new DMH-based bath as a replacement for Zn and Cd coatings,” RSC Adv., vol. 6, no. 69, pp. 64726–64740, 2016.

[25] L. E. Moron et al., “Electrodeposition and corrosion behavior of Zn coatings formed using as brighteners arene additives of different structure,” Surf. Coat. Technol., vol. 205, pp. 4985 – 4992, 2011.

[26] Z. Feng, Q. Li, J. Zhang, P. Yang, H. Song, and M. An, “Electrodeposition of nanocrystalline Zn-Ni coatings with single gamma phase from an alkaline bath,” Surf. Coatings Technol., vol. 270, pp. 47–56, 2015.

[27] H. Jie, Q. Xu, L. and Wei, and Y. Min, “Etching and heating treatment combined approach for superhydrophobic surface on brass substrates and the consequent corrosion resistance,” Corros. Sci., vol. 102, pp. 251–258, 2016.

[28] Z. Feng, Q. Li, J. Zhang, P. Yang, and M. An, “Electrochemical Behaviors and

Properties of Zn-Ni Alloys Obtained from Alkaline Non-Cyanide Bath Using 5,5'-Dimethylhydantoin as Complexing Agent," J. Electrochem. Soc., vol. 162, no. 9, pp. D412–D422, 2015.

[29] M. G. Hosseini, H. Ashassi-Sorkhabi, and H. A. Y. Ghiasvand, "Electrochemical studies of Zn-Ni alloy coatings from non-cyanide alkaline bath containing tartrate as complexing agent," Surf. Coatings Technol., vol. 202, no. 13, pp. 2897–2904, 2008.

[30] Y. Lin and J. Selman, "Electrodeposition of corrosion- resistant Ni-Zn alloy: I. Cyclic voltammetric study.," J Electrochem Soc., vol. 140, pp. 1299–1303, 1993.

[31] Z. Feng, Q. Li, J. Zhang, P. Yang, and M. An, "Studies on the enhanced properties of nanocrystalline Zn–Ni coatings from a new alkaline bath due to electrolyte additives," RSC Adv., vol. 5, no. 72, pp. 58199–58210, 2015.

[32] C. C. Hu and C. Y. Chang, "Anodic stripping of zinc deposits for aqueous batteries: Effects of anions, additives, current densities, and plating modes," Mater. Chem. Phys., vol. 86, no. 1, pp. 195–203, 2004.

[33] A. C. . Cheung, O. Bretschger, F. Mansfeld, and K. . Nealson, "FUEL127-performance of different strains of the genus Shewanella in a microbial fuel cell," Abstr. Pap. Am. Chem. Soc., vol. 234, 2007.

[34] S. Basavanna and Y. . Naik, "Electrochemical studies of Zn–Ni alloy coatings from acid chloride bath," J. Appl. Electrochem., vol. 39, no. 1975–1982, 2009.

[35] E. Kus, K. Nealson, and F. Mansfeld, "The effect of different exposure conditions on the biofilm/copper interface," Corros. Sci., vol. 49, pp. 3421–3427, 2007.

[36] Y. Boonyongmaneerat and K. Saenapitak, S Saengkiettiyut, "Reverse pulse electrodeposition of Zn-Ni alloys from a chloride bath," J. Alloy. Compd., vol. 487, pp. 479–482, 2009.

[37] F. Mansfeld, H. Shih, C.H.Tsai, and H. Greene, "Analysis of EIS Data for Common

Corrosion Processes," Am. Soc. Test. Mater., vol. 1188, pp. 37–53, 1993.

[38] E. McCafferty, "Validation of corrosion rates measured by the Tafel extrapolation method 3215.," Corros. Sci., vol. 47, pp. 3202–3215, 2005.

[39] D. Gelman, D. Starosvetsky, and Y. Ein-Eli, "Copper corrosion mitigation by binary inhibitor compositions of potassium sorbate and benzotriazole," Corros. Sci., vol. 82, pp. 271–279, 2014.

[40] F. H. Assaf, A. M. A. El-Seidy, M. M. Abou-Krisha, and A. A. Eissa, "Electrodeposition and Characterization of Zn-Ni-Mn Alloy from Sulfate Bath: Influence of Current Density, International Journal of Electrochemical Science, 100727," vol. 10, pp. 1–14, 2015.

[41] M. M. Abou-Krisha, "Effect of pH and current density on the electrodeposition of Zn-Ni-Fe alloys from a sulfate bath," J. Coatings Technol. Res., vol. 9, no. 6, pp. 775–783, 2012.

[42] M. K. Punith Kumar, T. V. Venkatesha, M. K. Pavithra, and A. N. Shetty, "A Study on Corrosion Behavior of Electrodeposited Zn-Rutile TiO_2 Composite Coatings," Synth. React. Inorganic, Met. Nano-Metal Chem., vol. 42, no. 10, pp. 1426–1434, 2012.

[43] S. Fashu, C. D. Gu, J. L. Zhang, M. L. Huang, X. L. Wang, and J. P. Tu, "Effect of EDTA and NH_4Cl additives on electrodeposition of Zn-Ni films from choline chloride-based ionic liquid," Trans. Nonferrous Met. Soc. China (English Ed., vol. 25, no. 6, pp. 2054–2064, 2015.

[44] J. Winiarsiki, W. Tylus, K. Winiarska, and B. Szczygiel, "Understanding corrosion via corrosion products characterizatio: I. Case study of the role of Mg alloying in Zn-Mn coating on steel," Corros. Sci., vol. 51, pp. 1251–1262, 2009.

[45] F. Mansfeld, "Recording and analysis of Ac impedance data for corrosion stud- ies.1. Background and methods of analysis," Corrosion, vol. 37, pp. 301–307, 1981.

[46] A. Portinha, V. Teixeira, J. O. Carneiro, S. N. Dub, R. Shmegera, and C. J. Tavares, “Hard ZrO_2/Al_2O_3 nanolaminated PVD coatings evaluated by nanoindentation,” Surf. Coatings Technol., vol. 200, no. 1–4 SPEC. ISS., pp. 765–768, 2005.

[47] O. Hammami, L. Dhouibi, P. Berçot, E. M. Rezrazi, and E. Triki, “Study of Zn-Ni alloy coatings modified by Nano-SiO particles incorporation,” Int. J. Corros., vol. 2012, 1-8, , 2012.

5.0 EDTA stabilized bath for electrodeposition of Zn-Ni alloy coatings and corrosion resistant analysis in 3.5 wt.% NaCl solutions

Preface

In this chapter, Zn-Ni alloy coating electrodeposited on steel substrates by using ethylene-diamine-tetra-acetic acid (EDTA) as a complexing agent. XRD technique was used for phase analysis and to calculate the average crystal size of the coating. SEM was used for morphological analysis equipped with energy dispersive spectroscopy (EDS), AFM was used for topographical analysis. Potentiodynamic polarization measurement (Tafel) and electrochemical impedance spectroscopy (EIS) were carried out to evaluate the corrosion resistance behavior of Zn-Ni alloy coatings. The electrical equivalent circuit obtained from the Nyquist plot was experimentally fitted for Zn-Ni deposited from non-EDTA baths in comparison to EDTA bath. The effect of the optimum operating conditions on electroplating character and their corrosion resistance behavior was observed and discussed. This chapter brings a new study to explored the effect of ethylene-diamine-tetra-acetic acid (EDTA) on Zn-Ni electroplating bath, to enhance the corrosion resistant properties and uniform morphology of the coated samples. The content of this chapter has been published as a manuscript in the Materials Proceedings, 2019.

Abstract

The electrodeposition of Zn-Ni alloy film on steel substrate from a chloride bath containing ethylene-diamine-tetra-acetic acid (EDTA) was investigated in this study. Polarization tests demonstrated that the Zn-Ni alloy deposited from 0.119 mol/l of EDTA bath at 20 mA/cm^2 current density exhibited lower corrosion current (I_{corr}) and more positive corrosion potential (E_{corr}). The impedance modulus and corrosion resistance were improved with a fine and robust

uniform coating. At 24 hours of immersion time, the samples exhibit higher corrosion resistance leads to the formation of strong corrosion product layers. The morphological properties, crystalline phases, and topographical structures of Zn-Ni coatings were characterized by scanning electron microscopy (SEM), X-ray diffraction (XRD) and atomic force microscopy (AFM). The chemical composition analysis revealed that the Zn-Ni coatings deposited from EDTA baths have higher Zn content and intensity of Ni_2Zn_{11} γ-phase, which exhibited better corrosion resistance properties.

Keywords: Electrodeposition, Zn-Ni alloy, EDTA bath, Polarization test, Impedance Spectroscopy.

5.1 Introduction

Zinc and zinc alloy coatings are extensively used to prevent corrosion under different working surroundings. The electrodeposition of zinc and zinc alloy has been widely used to reduce corrosion attack on steels. The pure zinc coating is unsatisfactory due to low corrosion protection to steels, which is unacceptable under severe atmospheric corrosion conditions [1]. On the other hand, Zn-Ni alloy coating has gained increased interest compared with pure Zn coating [2][3]. Various complexing agents have been studied by researchers such as amines [4][5], tartrate [4], tri-ethanolamine [5], sodium acetate, citrate [6], and ethylenediaminetetraacetic acid (EDTA) [7]. The challenge in Zn-Ni electroplating is to develop a stable electrolyte for depositing uniform Zn-Ni coating on steel. To suppress hydrogen evolution, a bath with a relatively high pH is favorable. Complexing agents (EDTA) are often added into electroplating baths to improve bath stability (prevent precipitation), control the plating rate, crystallization mechanism, film uniformity, and luster as they can form complexes with metal ions as shown in the below reaction[8][9]. EDTA is used extensively in

industrial applications because it has a strong ability to bind the metal cations in water solution[10].

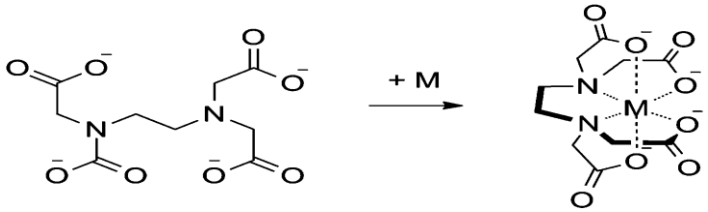

Fashu et al. [11] observed that increasing the concentration of EDTA led to an increase of Zn content in the deposited film while a decrease of Zn content was obtained when NH_4Cl instead of EDTA was added. They also noted that Zn-Ni films deposited from EDTA containing bath provide less anti-corrosion property in comparison to those plated from NH_4Cl comprising bath, which is not consistent with the study of Zohdy [10]. As seen from the literature, studies have been conducted on Zn-Ni plating from EDTA bath at various operating conditions, there was no systematic study found to determine the optimal concentration of EDTA, plating current density, and bath composition. To fulfill the knowledge gap, research was needed to find the operating conditions at a various level.

5.2 Methodology

The negative reduction potential of Zn/Zn^{2+} electrode. Zn is more challenging to be electrodeposited than hydrogen gas [12]. The reduction potential of zinc is ($E_{Zn/Zn}^{2+}$ = -0.762V) and hydrogen ($E_{2H/H2}$ = 0.000V). Hydrogen ions in the solution will be deposited before zinc as H^+ ions have a more positive reduction potential under the standard state. To suppress hydrogen deposition and stabilize the plating baths, alkalis, and complexing agents (e.g., EDTA) were added into the baths for Zn, Zn-Ni and Zn-Ni/solid composite electrodeposition, which result in improved corrosion resistance property, uniformity, thickness, and enhanced hardness of the plated films [12]. The images for Zn-Ni from non-EDTA and Zn-Ni from EDTA baths are shown in Figure 5.1. The electroplating bath prepared from non-EDTA shown

precipitation and un-stability after 8 hours. Adding EDTA will also suppress hydrogen evolution reaction (HER) and improve Zn-Ni corrosion resistance behavior. The Zn-Ni electroplating bath without EDTA has pH = 2.0. However, the Zn-Ni bath with EDTA has pH = 3.5. Increasing pH from 2.0 to 3.5 will decrease the hydrogen concentration in plating bath up to a hundred times, and they can form complexes with metal ions such as $Ni[C_{10}H_{12}N_2O_8]$.

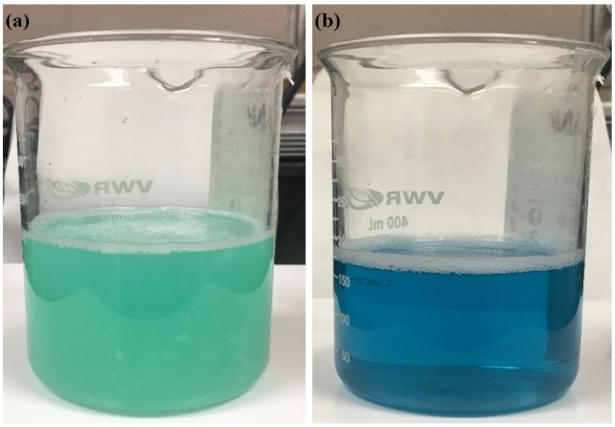

Figure 5.1 Electroplating bath images for (a) Zn-Ni from non-EDTA, and (b) Zn-Ni from EDTA

The resistant of Zn-Ni deposited from EDTA, and non-EDTA bath samples are observed by the short-time lab-scale 3.5 % NaCl solution immersion tests. XRD technique was used for phase analysis and to calculate the average crystal size of the coating. SEM was used for morphological analysis equipped with energy dispersive spectroscopy (EDS), AFM was used for topographical analysis. Potentiodynamic polarization measurement (Tafel) and electrochemical impedance spectroscopy (EIS) were carried out to evaluate the corrosion resistance behavior of Zn-Ni alloy coatings. The electrical equivalent circuit obtained from the Nyquist plot was experimentally fitted for Zn-Ni deposited from non-EDTA baths in comparison to EDTA bath. The effect of the optimum operating conditions on electroplating character and their corrosion resistance behavior was observed and discussed.

5.3 Experimental details

The electroplating was carried out in a 200 ml electrolyte solution at room temperature. A rectangular steel plate with a 10 cm^2 was used as the working electrode (cathode). A graphite rod was used as a counter electrode (anode). The anode and cathode were connected to the DC power supply via a multi-meter. The electroplating current density is 20, 40, and 60 mA/cm^2 at room temperature for 15 minutes.

A rectangular steel plate with a 10 cm^2 area was used as the working electrode (cathode). A graphite rod was used as a counter electrode (anode). The Ag/AgCl/KClsat was used as a reference electrode. The reference area of the coated sample is 1 cm^2 for the electrochemical testing.

The different bath compositions for the electrodeposition of Zn-Ni alloy coating are shown in Table 5.1. The cathodic substrates were steel, which was degreased with 10 wt.% NaOH solution for 2 min and then activated with alcohol or acetone for a few seconds. After electrodeposition, Zn–Ni alloy coatings were washed with distilled water and dried with air.

Table 5.1. Bath compositions for the electrodeposition of Zn-Ni alloy coatings

Bath Compositions	**Molar Concentrations (mol/l)**		
	Bath-1	**Bath-2**	**Bath-3**
$ZnCl_2$	0.366	0.366	0.366
$NiCl_2.6H_2O$	0.105	0.105	0.105
H_3BO_3	-	0.161	0.161
SDS	0.00017	0.00017	0.00017
EDTA	-	0.085	0.119
NaCl	-	0.171	0.171

In this study, the electrochemical analysis was conducted by IM6-electrochemical workstation manufactured by ZAHNER-Elektrik GmbH & Co.KG, Germany. The structural images were investigated by SEM provided with the EDS (FEI MLA 650F). The crystal phase structures of

Zn-Ni deposits were studied by the X-ray diffractometer (XRD) manufactured by Rigaku Ultima. The topographical structure of the coatings was analyzed by atomic force microscopy (Asylum research MFP 3D).

5.4 Experimental Results and Discussions

5.4.1 Morphological and Chemical compositions analysis

Scanning electron microscopy (SEM) images for Zn-Ni alloy coatings deposited from EDTA and non-EDTA baths at room temperature are shown in Figure 5.2. The deposited film is based on the porosity, uniformity and grain size of the coating produced by varying bath composition, plating current density, and EDTA concentrations. The morphological images of all the samples are at the same magnification, equal plating current densities with respective bath conditions. Zn-Ni coating from the non-EDTA bath (sample (a)) causing cracks, holes, and non-uniformity on the coating due to the formation and release of hydrogen bubbles. Zn-Ni coating from EDTA baths (sample (b) and (c)) exhibit smaller, more uniform grain sizes, small cracks found on the coatings due to the stability of the bath solution and suppress hydrogen evolution reactions [10]. The incorporation of nickel into the zinc matrices marginally modifies the morphologies of the Zn-Ni coatings. Zinc coating is composed of semi-circular shape, after inclusion with EDTA, the structure was changed [13][14]. Similar result has been demonstrated by Feng et al. [6], adding EDTA led to decrease the grain size significantly can be observed and the deposits are smooth, homogeneous, dense, and fine-grained without any holes on the surface [15] are shown in Figure 5.2 (b) and (c).

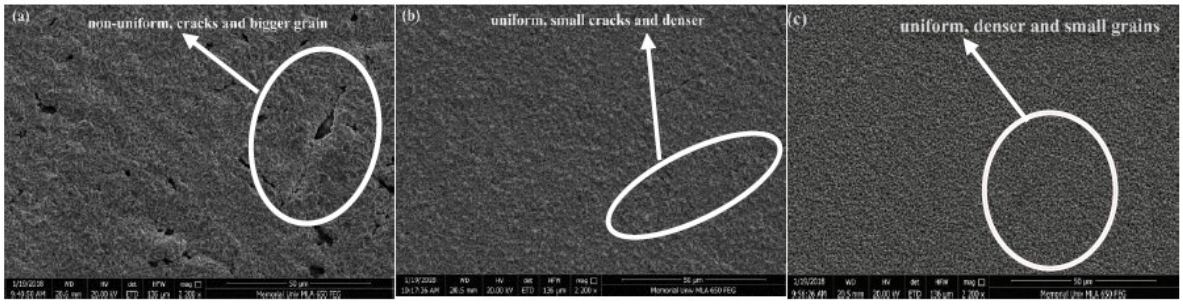

Figure 5.2 SEM micrographics of Zn-Ni alloy coating electrodeposited at (a) Zn-Ni deposited from a non-EDTA bath, (b) Zn-Ni deposited from 0.085 mol/l of EDTA bath, (c) Zn-Ni deposited from 0.119 mol/l of EDTA bath

Zinc-Nickel coating deposited from EDTA bath proves that the zinc content in the coating increases with the increase in EDTA concentrations is shown in Table 5.2, which leads to appearing hard, compact, uniform, and less coarse with small grain size Zn-Ni coating. Zn-Ni coating was containing an amino-complexing agent, which is the firm understanding reported by Fashu et al.[11] compared EDTA and ammonium chloride (NH_4Cl) as a definitive result for the complexing agents. Therefore, most preferable surface morphology, uniformity, adherence, hardness, and compactness is with the addition of a complexing agent and increasing plating current density [16].

Table 5.2. The EDS analysis for surface chemical composition of Zn-Ni coating electrodeposited (a) Zn-Ni deposited from a non-EDTA bath, (b) Zn-Ni deposited from 0.085 mol/l of EDTA bath, (c) Zn-Ni deposited from 0.119 mol/l of EDTA bath

Samples	Element	Wt.%	At. %
(a)	Zinc	96.80	96.45
	Nickel	3.20	3.55
(c)	Zinc	96.79	96.44
	Nickel	3.21	3.56
(b)	Zinc	97.55	97.17
	Nickel	2.45	2.83

5.4.2 Atomic Force Microscopy (AFM) analysis

The topographical 3D images of Zn-Ni coated samples (a), (b), and (c) obtained using AFM analysis are shown in Figure 5.3. Zn-Ni coating deposited from non-EDTA forms holes on the

deposit surface due to the release of the hydrogen bubbles, thereby inhibiting the deposition rate of the Zn-Ni alloy on the substrate sites. The hydrogen is absorbed on the surface of a substrate by the following reactions:

$$H^+ + e^- \longrightarrow H \qquad [17]$$

$$H + H \longrightarrow H_2 \qquad [18],[12]$$

The complexing agent (EDTA) is adsorbed on the Zn-Ni matrix preferentially and inhibits Zn-Ni alloy depositions, resulting in the smaller reduction of Zn^{+2} and Ni^{+2} on these matrices. Therefore, smooth and homogeneous deposits can be observed [4]. The roughness factor illustrates the initial surface irregularities, non-uniformity, and heterogeneity. Thus, the irregular surface demonstrates a higher dissolution rate, especially in the presence of a corrosive environment [19]. It can be seen from the images that the surface roughness of the Zn-Ni deposits decreases with the addition of EDTA. As a result, the molar concentration of EDTA increases leads to form the uniform, dense, and adherent coating on the substrate.

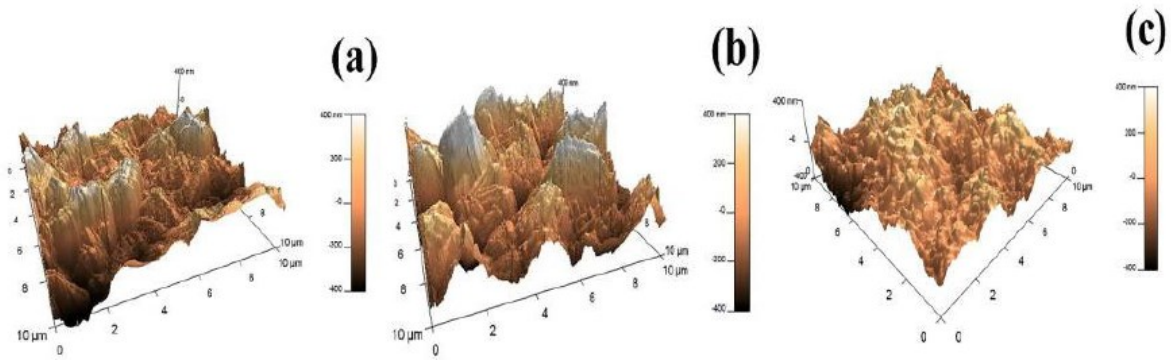

Figure 5.3 Topographical 3D images of Zn-Ni alloy coating electrodeposited at (a) Zn-Ni deposited from a non-EDTA bath, (b) Zn-Ni deposited from 0.085 mol/l of EDTA bath, (c) Zn-Ni deposited from 0.119 mol/l of EDTA bath

5.4.3 X-Ray Diffraction (XRD) analysis

The crystalline phase and orientation of Zn-Ni alloy coated sample deposited from EDTA, and non-EDTA baths are presented using XRD patterns are shown in Figure 5.4, and the crystalline structure of Zn-Ni deposits are observed. Zn-Ni deposited from non-EDTA bath shows two

prominent diffraction peaks of the γ-phase (γ-Ni_2Zn_{11}) and (γ-$NiZn_3$) with (330) and (831) plane orientations. The γ-phase with (330) plane orientation is detected in all coatings with varying intensity, demonstrated that γ-phase with (330) plane plays a significant role in the Zn-Ni alloy coatings [20][6][21]. The intensities of the crystal peaks illustrate the information about the number of phases and the relative amount of Zn-Ni in the deposits [22]. Zn-Ni deposited from EDTA bath; the grain size decreases, another γ-phase (γ-Ni_2Zn_{11}) with (321) phase orientation appears. Moreover, increasing the molar concentration of EDTA, increase the intensity of γ-Ni_2Zn_{11} with (321) plane orientation. Conversely, as the height of the peaks corresponding to γ-Ni_2Zn_{11} phase increases, resulting to enhance the relative zinc content in the deposits. Therefore, the Zn-Ni deposition with γ-phase (γ-Ni_2Zn_{11}) with (321) and (330) plane orientation exhibited better corrosion resistance properties.

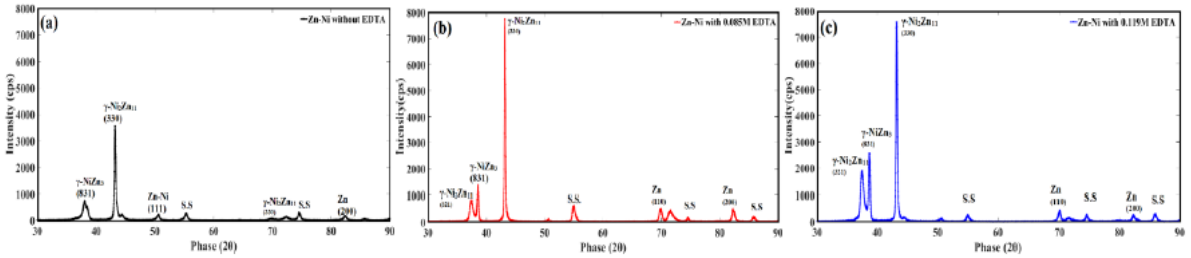

Figure 5.4 XRD patterns for the Zn-Ni alloy coatings obtained at different baths, (a) Zn-Ni deposited from a non-EDTA bath, (b) Zn-Ni deposited from 0.085 mol/l of EDTA bath, (c) Zn-Ni deposited from 0.119 mol/l of EDTA bath

5.4.4 Potentiodynamic polarization measurements

The potentiodynamic polarization curve obtained from Zn-Ni alloy coating deposited from EDTA and non-EDTA baths at three different plating current densities ranging from 20-60mA/cm^2 performed at room temperature, and the scan rate was 5mV/s. The corrosion current density (I_{corr}), corrosion potential (E_{corr}) and anodic, and cathodic Tafel slopes (βa and βc) were calculated from the intercept on Tafel slope by the extrapolation process and obtained with reference to Ag/AgCl/KCl_{sat} electrode and are tabulated in Table 5.3. It is observed from Table 5.3 for the samples (a) and (b), as the plating current density increased, the corrosion potential

(E_{corr}) increases and corrosion current (I_{corr}) decreases. The similar result was obtained by Abou Krisha [23], Tozar et al. [22], and Assaf et al. [16]. However, increasing the plating current density shifts the E_{corr} value positively leading to lower I_{corr} , which indicates improved corrosion resistance property in the coating [23][22][16]. The I_{corr} of the sample (a) at 60 mA/cm^2 is 1380 μA, whereas sample (b) and (c) is 1490 μA and 2430 μA. Thus, sample (a) at 60 mA/cm^2 possess higher corrosion resistance properties in comparison to another sample at different plating densities. Rahman et al. [24] reported that from 40-60 mA/cm^2 plating current density, the grain of the deposit is smaller, uniform, and no porosity is found, whereas with increasing plating current density after 60 mA/cm^2, produce non-uniform crystals and coarser-grained deposits [24]. As seen from Table 5.3, the more positive corrosion potential (-0.75V) and least corrosion current (560μA) is noticeable for Zn-Ni deposited from 0.119 mol/l of EDTA bath sample at 20 mA/cm^2. The lowest I_{corr} is due to the stable EDTA bath Zn-Ni coated samples with decreased HER, which exhibited uniform and high corrosion resistance coating and is observed on the sample (c), which has small grain size, compact, bright, and uniform Zn-Ni coating. Sample (a) coated film has holes, cracks, and non-uniformity on the plated surface due to the formation of hydrogen bubbles.

Table 5.3. Polarization data for the Zn-Ni coatings from different plating baths and with respective current densities

Samples	**Deposition current density, (mA/cm^2)**	**Corrosion Potential, E_{corr} (mV)**	**Corrosion current density, I_{corr} (μA/cm^2)**	**βa (V/dec)**	**βc (V/dec)**	**Corrosion rate (μmpy)**
	20	-850	1580	0.250	-0.265	3938
(a)	40	-827	1530	0.196	-0.223	783.4
	60	-792	1380	0.120	-0.169	1034
	20	-806	1480	0.195	-0.261	2927
(b)	40	-879	4180	0.200	-0.241	4082
	60	-797	1490	0.135	-0.179	3015

	20	-753	560	0.082	-0.133	768.7
(c)	40	-791	4080	0.380	-0.425	2769
	60	-762	2430	0.216	-0.284	808.3

Zn-Ni alloy coating deposited from 0.119 mol/l of EDTA exhibited the lowest corrosion current (I_{corr}), and positive corrosion potential led to enhance the corrosion resistance properties of the coating. It is described by Zohdy [10] that increasing the concentration of EDTA in bath decrease the I_{corr} values, to improving the corrosion resistance properties of the coating [10]. Tafel plot for Zn-Ni alloy deposited from EDTA and non-EDTA at 20 mA/cm^2 are shown in Figure 5.5. The corrosion potential of the coated samples without EDTA is more negative than the Zn-Ni deposited from EDTA bath. This implies that electrodeposited Zn-Ni alloy deposited from EDTA bath coatings offers sacrificial protection on a bare steel substrate. Table 4 shows that the corrosion potential of Zn-Ni deposited from 0.119M EDTA is -753 mV and the corrosion rate is 768.7 µmpy, whereas Zn-Ni deposited from non-EDTA is -889 mV and corrosion rate 3938 µmpy.

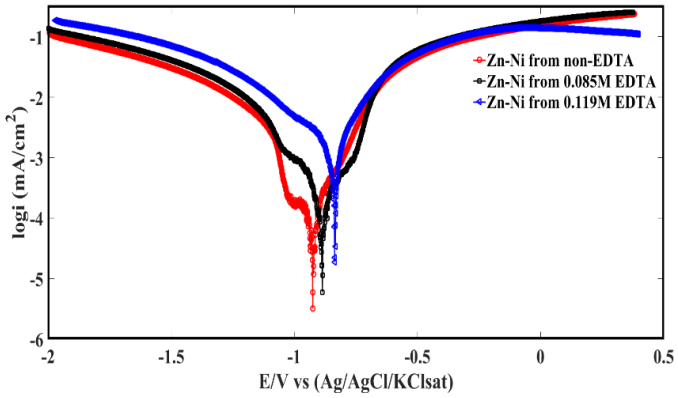

Figure 5.5 Tafel plots for Zn-Ni deposited from EDTA and non-EDTA baths

Table 5.4. The optimized results for the Zn-Ni alloy coating deposited from EDTA and non-EDTA

Bath condition	E_{corr} (mV vs Ag/AgCl)	I_{corr} (μA/cm^2)	Corrosion rate (μmpy)
Zn-Ni deposited from non-EDTA	-850	1580	3938
Zn-Ni deposited from 0.085M EDTA	-806	1780	2927
Zn-Ni deposited from 0.119M EDTA	-753	560	768.7

5.5.5 Electrochemical Impedance Spectroscopy (EIS) analysis

The electrochemical impedance spectroscopy (EIS) measurement is suitable to evaluate the kinetics and characteristics of an electrochemical process at the electrode/electrolyte interfaces [25][11]. The open current potential in the range of the frequency is 100 kHz to 100 mHz, the signal amplitude is 10 mV, and scan rate is 10 mV/s. In the Nyquist plot, the polarization resistance has resembled the shape of a semicircle [26][22]. The Nyquist plot for Zn-Ni alloy deposited from EDTA and non-EDTA at without immersion test are shown in Figure 5.6. Zn-Ni deposited from non-EDTA has less impedance modulus in comparison to deposited from EDTA bath due to the unstabilized bath (formation of hydrogen evolution reaction) lead to exhibit lower corrosion resistance. However, Zn-Ni deposited from 0.119 mol/l of EDTA exhibit higher impedance modulus in comparison to Zn-Ni deposited from 0.085 mol/l of EDTA. It is suggested that the Zn-Ni deposited from 0.119 mol/l of EDTA show higher corrosion resistance and confirmed the excellent bath composition at 20 mA/cm^2 of plating current density with the formation of a stabilized bath.

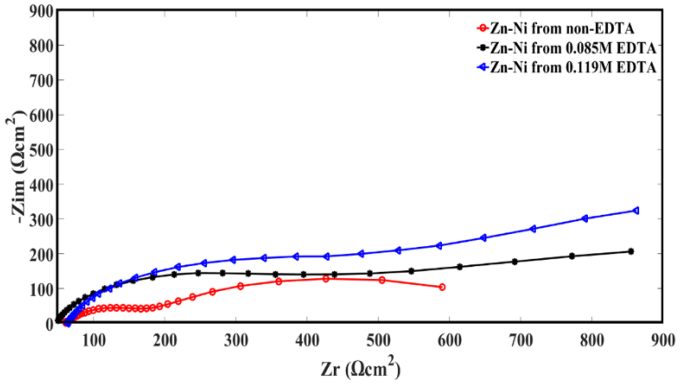

Figure 5.6 Nyquist plot for Zn-Ni deposited from EDTA and non-EDTA baths

EIS measured data for Zn-Ni alloy deposited from EDTA and non-EDTA with the immersion test at 12 hours, and 24 ourss immersion test are displayed as the Nyquist plot are shown in Figure 5.7. The electrical circuit are shown in Figure 5.8, where R_{sol} represents the resistance from the corrosive media. R_1 and C_1 correspond to the resistance and capacitance of the corrosion product layers' interface at the underneath of the pores connected with the charge transfer resistance. R_{ct} and C_{dl} represent the resistance and capacitance associated with the charge transfer resistance and electric double-layer capacitance. In this study, the capacitance is referred to as the constant phase element (CPE)[27], to obtain an optimum fitting result. The calculated fit data of the electrical equivalent are shown in Table 5.5.

The diameter of the capacitive loop increases with increase in EDTA molar concentration for 12 and 24 hours' immersion tests. R_1 values exhibit changes at 12 hours of immersion in which Zn-Ni deposited from non-EDTA bath attains high values (486.6 Ωcm^2) in comparison with the Zn-Ni deposited from 0.085 mol/l of EDTA (354 Ωcm^2), whereas Zn-Ni deposited at 0.119 mol/l of EDTA exhibits higher resistance (520 Ωcm^2). This is evident by the increase of C_1 values. The charge transfers resistance (R_{ct}), and double-layer capacitance (C_{dl}) for 12 hours of immersion tests exhibit the same behavior. Zn-Ni-0.119 mol/l of EDTA at 12 hours' immersion formed stabilized, uniform and compact deposits, increase the strength of corrosion product layer lead to exhibit higher corrosion resistance. At 24 hours of immersion tests, Zn-Ni deposited from EDTA baths exhibit higher R_1 and C_1 values. The R_1 value for Zn-Ni-0.119

mol/l of EDTA at 24 hours is 643.6 Ωcm^2, whereas Zn-Ni-non-EDTA is 340.9 Ωcm^2. Zn-Ni deposited from EDTA bath exhibit higher corrosion resistance in the immersion tests due to stabilization of bath. The charge transfers resistance (R_{ct}) and double-layer capacitance (C_{dl}) for 24 hours of immersion tests exhibit similar behavior, Zn-Ni-0.119 mol/l of EDTA at 24 hours' immersion formed strong corrosion product layer lead to exhibit higher corrosion resistance. At 12 hours of immersion test, all samples have lower R_1, C_1, R_{ct}, and C_{dl} values. In contrast, at 24 hours of immersion time, the samples exhibit higher corrosion resistance leads to the formation of strong corrosion product layers.

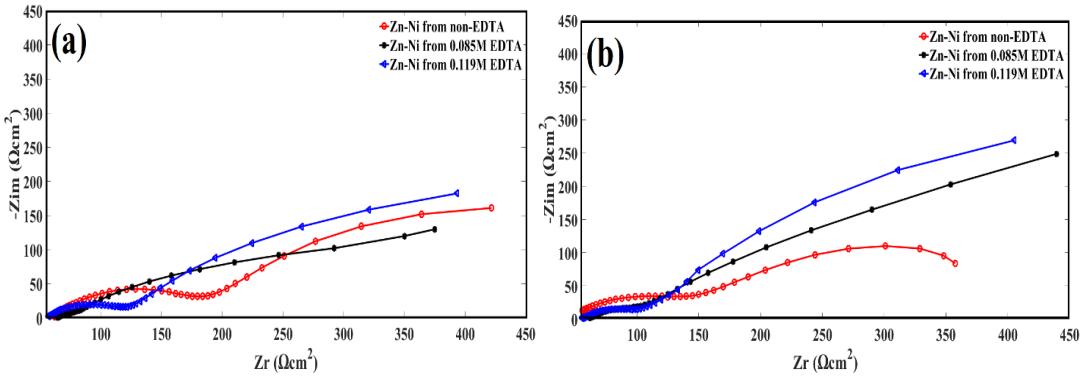

Figure 5.7 Nyquist plot for Zn-Ni from EDTA and non-EDTA baths electrodeposited at (a) Immersed at 12 hours (b) Immersed at 24 hours

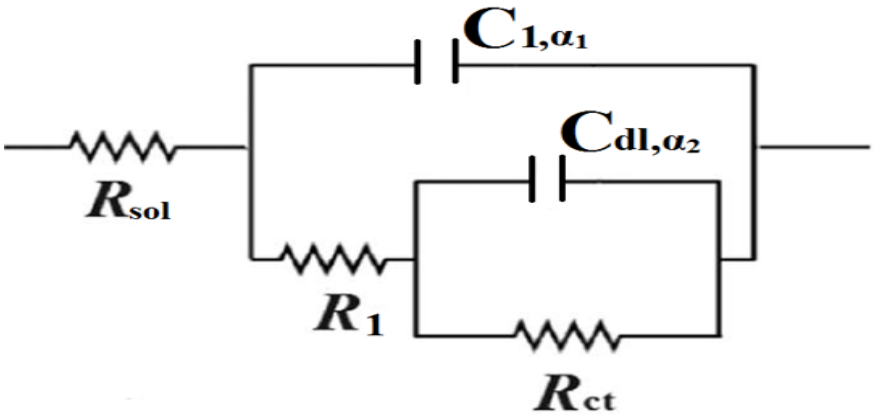

Figure 5.8 Electrical equivalent circuit modelling used for the simulation of EIS data of Zn-Ni alloy coating from EDTA and non-EDTA baths

Table 5.5. Electrochemical parameters determined by equivalent circuit modelling

Samples	Immersion time (hours)	R_{sol} (Ωcm^2)	R_1 (Ωcm^2)	R_{ct} (Ωcm^2)	C_1 ($s^{\alpha 1}\Omega^{-1}cm^2$)	α_1	C_{dl} ($s^{\alpha 1}\Omega^{-1}cm^2$)	α_2
(a)	12	60.3	486.6	136.9	61.0	0.8	3.3	0.7
(b)		63.9	354.0	100.5	56.3	0.9	5.6	0.5
(c)		64.6	520.0	177.2	96.1	0.7	8.3	0.6
(a)	24	43.5	340.9	124.7	94.9	0.7	4.5	0.6
(b)		59.9	621.1	144.7	113.8	0.7	9.2	0.5
(c)		56.5	643.6	150.7	204.6	0.7	9.9	0.7

5.6 Conclusions

Potentiodynamic polarization result revealed that the Zn-Ni deposited from 0.119 mol/l of EDTA bath exhibited lowest I_{corr} and more positive E_{corr} values. The least I_{corr} was due to the Zn-Ni coating deposited from a stable EDTA bath with decreased HER, which showed a uniform and better corrosion resistance coating. At 12 hours of immersion test, all samples have lower R_1, C_1, R_{ct}, and C_{dl} values. In contrast, at 24 hours of immersion time, the samples exhibit higher corrosion resistance leads to the formation of strong corrosion product layers. SEM and AFM images showed that the sample (a), Zn-Ni coating from non-EDTA bath had cracks, holes, and non-uniformity on the coating due to the formation and release of hydrogen bubbles. However, Zn-Ni coating from EDTA bath (sample (b) and (c)) increase microhardness and exhibit more uniform grain sizes with γ-Ni_2Zn_{11} plane orientation and no holes are found on the coatings due to the stability of the bath solution and the occurrence of less hydrogen evolution reactions.

Acknowledgments

The authors thankfully acknowledge the financial support provided by the Natural Science and Engineering Council of Canada (NSERC), the Canada Research Chair (CRC) Tier I Program and use of atomic force microscopy (AFM) from Dr. Erika Merschrod lab at Department of Chemistry, Memorial University of Newfoundland, NL, Canada.

References

[1] T. Tsuru, S. Kobayashi, T. Akiyama, H. Fukushima, S. K. Gogia, and R. Kammel, "Electrodeposition behaviour of zinc-iron group metal alloys from a methanol bath," *J. Appl. Electrochem.*, vol. 27, no. 2, pp. 209–214, 1997.

[2] R. Fratesi and G. Roventi, "Corrosion resistance of Zn-Ni alloy coatings in industrial production," *Surf. Coat. Technol.*, vol. 82, pp. 158 – 164, 1996.

[3] I. H. Karahan and H. S. Güder, "Electrodeposition and properties of Zn, Zn–Ni, Zn–Fe and Zn–Fe–Ni alloys from acidic chloride–sulphate electrolytes," *Trans. IMF*, vol. 87, no. 3, pp. 155–158, 2009.

[4] M. G. Hosseini, H. Ashassi-Sorkhabi, and H. A. Y. Ghiasvand, "Electrochemical studies of Zn-Ni alloy coatings from non-cyanide alkaline bath containing tartrate as complexing agent," *Surf. Coatings Technol.*, vol. 202, no. 13, pp. 2897–2904, 2008.

[5] L. M. Muresa, J. Eymard, D. Blejan, and E. Indrea, "Zn-Ni alloy coatings from alkaline bath containing triethanolamine. influence of additives," *Stud. Univ. BABEŞ-BOLYAI, Chem.*, vol. 1, pp. 7–44, 2010.

[6] Z. Feng, Q. Li, J. Zhang, P. Yang, and M. An, "Studies on the enhanced properties of

nanocrystalline Zn–Ni coatings from a new alkaline bath due to electrolyte additives," *RSC Adv.*, vol. 5, no. 72, pp. 58199–58210, 2015.

[7] J. B. Bajat, A. B. Petrović, and M. D. Maksimović, "Electrochemical deposition and characterization of zinc-nickel alloys deposited by direct and reverse current," *J. Serbian Chem. Soc.*, vol. 70, no. 12, pp. 1427–1439, 2005.

[8] A. P. Abbott, J. C. Barron, G. Frisch, K. S. Ryder, and A. F. Silva, "The effect of additives on zinc electrodeposition from deep eutectic solvents," *Electrochim. Acta*, vol. 56, no. 14, pp. 5272–5279, 2011.

[9] E. Bakker, "Complexometric titrations : new reagents and concepts to overcome old limitations," pp. 4252–4261, 2016.

[10] K. M. Zohdy, "Surface protection of carbon steel in acidic solution using ethylenediaminetetraacetic disodium salt," *Int. J. Electrochem. Sci.*, vol. 10, no. 1, pp. 414–431, 2015.

[11] S. Fashu, C. D. Gu, J. L. Zhang, M. L. Huang, X. L. Wang, and J. P. Tu, "Effect of EDTA and NH_4Cl additives on electrodeposition of Zn-Ni films from choline chloride-based ionic liquid," *Trans. Nonferrous Met. Soc. China (English Ed.*, vol. 25, no. 6, pp. 2054–2064, 2015.

[12] H. Faid, L. Mentar, M. R. Khelladi, and A. Azizi, "Deposition potential effect on surface properties of Zn–Ni coatings," *Surf. Eng.*, vol. 33, no. 7, pp. 529–535, 2017.

[13] L. E. Moron *et al.*, "Electrodeposition and corrosion behavior of Zn coatings formed using as brighteners arene additives of different structure," *Surf. Coat. Technol.*, vol. 205, pp. 4985 – 4992, 2011.

[14] Z. Feng, M. An, L. Ren, J. Zhang, P. Yang, and Z. Chen, "Corrosion mechanism of

nanocrystalline Zn-Ni alloys obtained from a new DMH-based bath as a replacement for Zn and Cd coatings," *RSC Adv.*, vol. 6, no. 69, pp. 64726–64740, 2016.

[15] Z. Feng, Q. Li, J. Zhang, P. Yang, H. Song, and M. An, "Electrodeposition of nanocrystalline Zn-Ni coatings with single gamma phase from an alkaline bath," *Surf. Coatings Technol.*, vol. 270, pp. 47–56, 2015.

[16] F. H. Assaf, A. M. A. El-Seidy, M. M. A.-K. And, and A. A. Eissa, "Electrodeposition and Characterization of Zn-Ni-Mn Alloy from Sulfate Bath: Influence of Current Density 100727," vol. 10, pp. 1–14, 2015.

[17] R. Fratesi and G. Roventi, "Electrodeposition of zinc-nickel alloy coatings from a chloride bath containing NH4Cl," *J. Appl. Electrochem.*, vol. 22, no. 7, pp. 657–662, 1992.

[18] W. Kantek, M. Sahre, and W. Paatsch, "Transition metal effects in the corrosion protection of electroplated zinc alloy coatings," *Electrochim Acta.*, vol. 39, pp. 1151–1157, 1994.

[19] Y. Lin and J. Selman, "Electrodeposition of corrosion- resistant Ni-Zn alloy: I. Cyclic voltammetric study.," *J Electrochem Soc.*, vol. 140, pp. 1299–1303, 1993.

[20] Y. Boonyongmaneerat and K. Saenapitak, S Saengkiettiyut, "Reverse pulse electrodeposition of Zn-Ni alloys from a chloride bath," *J. Alloy. Compd.*, vol. 487, pp. 479–482, 2009.

[21] Z. Feng, Q. Li, J. Zhang, P. Yang, and M. An, "Electrochemical Behaviors and Properties of Zn-Ni Alloys Obtained from Alkaline Non-Cyanide Bath Using 5,5'-Dimethylhydantoin as Complexing Agent," *J. Electrochem. Soc.*, vol. 162, no. 9, pp. D412–D422, 2015.

[22] A. Tozar and I. H. Karahan, “Structural and corrosion protection properties of electrochemically deposited nano-sized Zn-Ni alloy coatings,” *Appl. Surf. Sci.*, vol. 318, pp. 15–23, 2014.

[23] M. M. Abou-Krisha, “Effect of pH and current density on the electrodeposition of Zn-Ni-Fe alloys from a sulfate bath,” *J. Coatings Technol. Res.*, vol. 9, no. 6, pp. 775–783, 2012.

[24] M. J. Rahman, S. R. Sen, M. Moniruzzaman, and K. M. Shorowordi, “Morphology and Properties of Electrodeposited Zn-Ni Alloy Coatings on Mild Steel,” *J. Mech. Eng. Mech. Eng. Div*, vol. 40, no. 1, 2009.

[25] M. K. Punith Kumar, T. V. Venkatesha, M. K. Pavithra, and A. N. Shetty, “A Study on Corrosion Behavior of Electrodeposited Zn-Rutile TiO_2 Composite Coatings,” *Synth. React. Inorganic, Met. Nano-Metal Chem.*, vol. 42, no. 10, pp. 1426–1434, 2012.

[26] F. Mansfeld, H. Shih, C.H.Tsai, and H. Greene, “Analysis of EIS Data for Common Corrosion Processes,” *Am. Soc. Test. Mater.*, vol. 1188, pp. 37–53, 1993.

[27] G. . Brug, A. L. . Van Deen Adeen, M. Sluyters-Rehbach, and J. . Sluyters, “The Analysis of the Electrode Impedance Complicated by the presence of a Constant Phase Element,” *J Electroanal Chem*, vol. 176, pp. 275–295, 1984.

6.0 Corrosion Behavior of Zn-Ni alloy and Zn-Ni-nano-TiO_2 composite coatings electrodeposited from ammonium citrate baths

Preface

In this chapter, electrochemical analysis of Zn-Ni alloy and Zn-Ni-nanoTiO_2 composite coatings deposited on steel from ammonium citrate containing bath was studied. The impact of Titania (TiO_2) nanoparticles on the Zn-Ni alloy has been studied to find the noble corrosion potential and least corrosion current of the coated samples. The surface characterization and crystalline phase texture of the coatings were investigated by scanning electron microscopy (SEM) integrated with energy dispersive spectroscopy (EDS) and X-ray diffraction (XRD). The topographical structure of the coating was analyzed by atomic force microscopy (AFM). The electrical equivalent circuit obtained from the Nyquist plot was experimentally fitted for Zn-Ni alloy and Zn-Ni-nanoTiO_2 composite coatings. The most significant corrosion products for Zn-Ni alloy electroplating is also analyzed and studied. This chapter brings a new study to explored the effect of Titania (TiO_2) nanoparticles on the Zn-Ni alloy deposited on steel from ammonium citrate containing bath, to enhance the corrosion resistant properties and corrosion products behaviour on the coated samples. This article is submitted to the professors for review and comments.

Abstract

Electrochemical and corrosion behaviour analysis of Zn-Ni alloy and Zn-Ni-nanoTiO_2 composite coatings electrodeposited on steel from ammonium citrate containing bath was studied. The complexation of zinc and nickel ions by citrate stabilized the electroplating bath. The electrochemical behaviour of samples showed that Zn-Ni alloy with the incorporation of

0.003 mol/l of Titania (TiO_2) nanoparticles exhibited noble corrosion potential (E_{corr}) and decreasing corrosion current (I_{corr}) leading to increasing impedance modulus with a less coarse, compact and stronger uniform coating of 25.84 nm grain size. The surface characterization and crystalline phase texture of the coatings were investigated by scanning electron microscopy (SEM) integrated with energy dispersive spectroscopy (EDS) and X-ray diffraction (XRD). The topographical structure of the coating was analysed by atomic force microscopy (AFM). The chemical composition result showed that the Zn-Ni-0.003TiO_2 coating electrodeposited from citrate bath at various immersion tests reduced dezincification in the coating; the higher intensity of γ-phase (γ-$NiZn_3$) (815) and γ-Ni_2Zn_{11} (330) (631) plane orientation and appearance of β-Ti improved corrosion resistance performance of the coating. The most significant corrosion products for Zn-Ni alloy electroplating are simonkolleite, hydrozincite, zincite, and wulfingite.

Keywords: Electrodeposition, Zn-Ni-nanoTiO_2, surface morphology, citrate bath, impedance spectroscopy.

6.1 Introduction

Zinc coatings are broadly use for the protection of steel structures and process equipment from corrosion. Significant efforts have been achieve to increase the corrosion resistant properties of steel in harsh environment[1][2]. Zinc coatings usually form alloys with metals such as iron (Fe), cobalt (Co), and nickel (Ni). According to the research[3][4], Zn-Co, Zn-Ni, and Zn-Fe can improve the corrosion resistant properties in comparison to pure zinc coating. Currently, Zn-Ni alloy coatings have become an important and eco-friendly alternative for toxic cadmium coatings[5]. A further alternative approach to increase corrosion resistant and mechanical properties of the coatings is to introduce Zn-Ni composite coatings. The inclusion of reinforcing particles can improve various properties of the alloy coatings such as dispersal

toughening, oxidation resistance at elevated temperature, self-lubricity, wear, and anti-corrosion performance[6]. Co-deposition of TiO_2, Al_2O_3, ZrO_2, SiO_2, Fe_2O_3 and SiC explored on Zn-Ni alloy to further enhance the corrosion resistant and mechanical properties of the coating[6][7][2][8]. The incorporation of particulates on the Zn-Ni surface refine the crystal size and shape, which increase the corrosion resistance, microhardness, and wear resistance properties. Among the nanomaterials considered titanium dioxide (TiO_2) has attained more attention in the recent years. Successful results has been reported on the co-deposition of TiO_2 with Ni, Cu, Zn and Ag metals[9].

Significant advancement has been made in various aspects of the nanoscale materials because of the abundant availability of nanoparticles, and they are mostly used in composite coatings for achieving better corrosion and mechanical resistant properties. There are different types of titanium dioxide incorporated in the Zn-Ni matrix that have been studied by several authors, Vlasa et al.[10] reported two different types of TiO_2 such as Anatase and Degussa incorporated with pure Zn. The anti-corrosion corrosion behaviour of Zn-nanoTiO_2 coating electropdeosited on steel surface was analysed. It was specified that the pure zinc coating exhibited lower corrosion resistant properties in comparison to the porous nanocomposite coatings and this was significantly influenced by the TiO_2 texture and concentration. Kumar et al.[11] prepared the composite coating with rutile (a mineral composed primarily of TiO_2) TiO_2 nanoparticles (size $\leq$ 100nm). The impedance spectroscopy measurements have found that the coatings obtained from 6 g/l of rutile TiO_2 nanoparticles (D_2) showed a higher impedance modulus relative to other coatings. It was concluded that the Kumar et al.[11] successfully deposited Zn-TiO_2 composite coatings on mild steel from bath solution containing 2, 6, and 10 g/l of rutile TiO_2 nanoparticles. The percentage of TiO_2 content in D_2 provides condensed and uniform surface to the D_2 deposition. The decrease of the size was anticipated to increase their catalytic activity

and total surface area[12]. However, the authors found that the study of Titania TiO_2 incorporated with the Zn-Ni alloy matrix has not been explored.

The phase crystalline structure and morphology of the Zn-Ni-TiO_2 have been studied by Praveen et al.[6] and they analyzed the effects and behaviour of TiO_2 as composites coating deposited on mild steel. The potential cathodic line lessened the hydrogen reduction process and the corrosion rate. This was inferred that Zn-Ni-TiO_2 composite coating has a superior corrosion inhibition property than the pure Zn-Ni alloy, while the steel surface always possesses cracks, gaps, crevices, and micro holes. Therefore, those gaps were filled by TiO_2 and composite coating dispersed on the metal.

Anwar et al.[13] studied the constancy of pure Zn and Zn-Ni alloy electroplating bath and they found that the addition of potassium citrate in the plating bath extends the precipitation of metal oxide to an elevated pH (from 2 to 5) and supress the formation of hydrogen evolution reaction (HER). Zhang and Ivey[14] prepared the Co-Fe-Ni plating bath by the addition of potassium citrate to stabilize the plating bath and deposit uniform coating, inhibiting the precipitation of $M(OH)_2$ at high pH. On the basis of those studies on citrate bath, it was found that citrate significantly increases the stability of the bath and denser platings are deposited due to higher bath pH. This was examined from the above literatures that there is limited information available on the Zn-Ni alloy and Zn-Ni-nanoTiO_2 composite coating deposited from ammonium citrate baths. This helps to stabilize the bath and exhibit uniform and corrosion resistant coatings.

Pure zinc and zinc-nickel alloy exposed to the corrosive environment, it transformed the alloy into the dealloying and dezincification[15] [5]. Dealloying are the selective corrosion of one and more than one component of material in the alloy, and dezincification is the selectively removal of zinc from the alloy. One of the main reasons to increase the anti-corrosion performance of the coated sample while immersing in the corrosive solvents are the formation

of corrosion products. This was evidence that the corrosion products act as a barrier against diffusion leading to decrease the corrosion rate of the coated sample. The composition of the corrosion products layer has a significant impact on the corrosion resistant properties of the Zn-Ni alloys. The principal corrosion products in moisture environments are zinc oxide (ZnO) and zinc hydroxide ($Zn(OH)_2$)[16]. Moreover, due to the standard components of carbon dioxide in the air, the appearance of smithsonite ($ZnCO_3$) and hydrozincite ($Zn_5(CO_3)_2(OH)_6$) was feasible. Simonkolleite ($Zn_5(OH)_8Cl_2.H_2O$) was the most favorable component formed in the hydrophilic solution, and it contains high chloride (Cl^-) contents. However, simonkolleite was contemplated as an active-passive layer[5][17]. It was affirmed that the corrosion resistant properties of Zn-Ni alloy electroplating were dependent on the formation of corrosion products. Hence, it was required to do the analysis and observe the corrosion product process and the constrained effect of their film during the corrosion mechanism.

As seen from the literature, a number of experimental analyses have been carried out on Zn-Ni alloy and Zn-Ni-TiO_2 under different operating settings, there was less study found to compare Zn-Ni alloy and composite coatings deposited from ammonium citrate bath at optimum TiO_2 concentration. Additionally, the challenge to suppress HER led to enhance the corrosion resistant performance of the coating has not been explored. This study also considers the formation of corrosion products on the coated samples. Therefore, to fulfil this knowledge gap, the research was needed to find the optimum conditions for the Zn-Ni alloy and Zn-Ni nanosized Titania TiO_2 electrodeposited from ammonium citrate bath.

6.2 Experimental Details

Zn-Ni alloy and Zn-Ni-nanoTiO_2 electroplated samples were prepared at (20^{o}C) room temperature in 200 ml electrolyte bath. A steel plate with dimension of 2.5 cm x 4.0 cm were used as working electrode. Before electrodeposition, the substrate was grinding with the emery

paper and polished with the diamond paste. The steel plates before electroplating were degreased by 10% hydrochloric acid and 10% sodium hydroxide for 5 minutes and then rinsed with alcohol/acetone for a few seconds. The electroplating current density ranges from 30-50 mA/cm^2 at room temperature for 15 minutes and agitation speed is from 350-700 rpm. The auxiliary electrode was graphite plate and saturated calomel electrode (SCE) (Hg/Hg_2Cl_2) was used as a reference electrode. After the electrodeposition, the samples were rinsed with with tab water and dehydrated with dry ambient air. The electrochemical and corrosion behaviour measurements were carried out in the three-electrode cell setup in a glass cell by employing ASTM G5-94 standards.[18]

There was three types of bath prepared (a) Chloride bath deposited from non-citrate containing: $ZnCl_2$ (Acros organics - 98% extra pure), $NiCl_2.6H_2O$ (Acros organics - 97% extra pure), SDS (Fisher Bioreagents), NH_4Cl (Sigma Aldrich - 99.5%) and NaCl (Acros organics - 99.5% for analysis). (b) Chloride bath deposited with citrate containing: $ZnCl_2$, $NiCl_2.6H_2O$, SDS, NH_4Cl, NaCl, $N_3(C_6H_{17}O_7)$) (Alfa Aesar – 97%) and H_3BO_3 (Alfa Aesar – 99.99% metal basis). (c) Chloride bath deposited with citrate containing: $ZnCl_2$, $NiCl_2.6H_2O$, SDS, NH_4Cl, NaCl, $N_3(C_6H_{17}O_7)$), H_3BO_3 and Titania TiO_2 (Sigma Aldrich – nano powder, 21 nm primary particle size (TEM), 99.5% trace metals basis) are shown in Table 6.1. The nano-TiO_2 partcile size can suspended stably in an aqueous Zn-Ni salt electrolyte due to nano particle, if particle size is larger than it tends to settle down and not easy to deposit uniform composite films.

Table 6.1. Bath compositions of citrate-based baths for the electrodeposition of Zn-Ni alloy and Zn-Ni-nanoTiO_2 composite coatings

Bath Compositions	**Molar Concentrations (mol/l or M)**		
	Bath-1	Bath-2	Bath-3
Zinc Chloride ($ZnCl_2$)	0.550	0.550	0.550

Nickel (II) Chloride hexahydrate ($NiCl_2.6H_2O$)	0.105	0.105	0.105
Boric Acid (H_3BO_3)	-	0.161	0.161
Ammonium Chloride (NH_4Cl)	0.46	0.46	0.46
Sodium dodecyl sulfate (SDS)	0.00017	0.00017	0.00017
Ammonium Citrate tribasic ($N_3(C_6H_{17}O_7)$)	-	0.0816	0.163
Sodium chloride (NaCl)	0.171	0.171	0.171
Titanium dioxide (TiO_2)	-		0.0033, 0.0066, 0.0125
	Bath pH = 2.0	Bath pH = 3.5	Bath pH = 4.0-4.5

The exploration tests have been done for achieving the vicinity of the factors and levels of the electroplating condition. There were four samples plated on same conditions on which two samples used for morphology and two for electrochemical analysis for attaining the redundancy and accuracy of the results. The electrochemical and corrosion measurements were accomplished using an IM6 electrochemical workstation, Zahner, Germany. The surface morphological structure of the coating were studied by SEM integrated with EDS (FEI MLA 650F). The topographical structure of the coatings was inspected by AFM (Asylum research MFP 3D). The crystal phase texture and peaks were investigated by XRD (Rigaku Ultima IV X-ray diffractometer with a copper x-ray source) and material database used to matches the generated peaks by using pdf# 03-065-5310 [19] and 00-004-0831[20] RDB Minerals and ICDD.

The Debye-Scherrer equation is used to calculate the average crystallite size of the coated samples from the peak width at the half maximum of the crystal peaks (β) [21]

$$t = \frac{0.94\lambda}{\beta.\mathrm{Cos}\theta}$$

Where, t = crystallite size,

λ = wavelength of the XRD (λ=1.5418A^0),

θ = Bragg's angle of the peak and,

β = angular width of the peak at full width at half maximum (FWHM).

6.2.1 Establishment of stable baths for Zn and Zn-Ni containing coatings

The negative reduction potential of Zn/Zn^{2+} electrode is challenge for zinc to be electroplated than hydrogen gas [22]. The reduction potential of zinc is ($E_{Zn/Zn}^{2+}$ = -0.762V) and hydrogen ($E_{2H/H2}$ = 0.000V). The H^+ ions in the electrolyte solution will be deposited before zinc, as H^+ ions have a more positive reduction potential under the standard state. To overcome and modify this problem the higher pH bath electroplating is preferable. Generally, high pH bath (alkaline) is not stable. Therefore, most of the electroplating is developed as an acidic bath. The major problem to use of acidic bath is the hydrogen evolution reaction is occurring in the electrolyte and to exhibiting non-uniform less corrosion resistant coatings. To electrodeposit Zn coatings with suitable composition and microstructure lead to ideal corrosion resistant and mechanical properties, the development of a stable plating bath with relatively high pH is vital. Alkalis and a complexing agent such as acetate, EDTA, and citrate were used to stabilize the electroplating bath and suppress the hydrogen deposition on the cathode. These complexing agents were added into the baths for pure Zn, Zn-Ni alloy and Zn-Ni composite coating to improve the anti-corrosion property, homogeneity, thickness, compactness, and mechanical property of the electroplated films [22][23][24][25][26][27]. The images for Zn-Ni from non-citrate and Zn-Ni from citrate baths are shown in Figure 6.1. The electroplating bath prepared from non-citrate shown precipitation and un-stability, the bath made from citrate shown non-precipitation and uniform stability throughout the electroplating. It will increase the homogeneity, grain size, and form denser deposition. Adding citrate will also suppress hydrogen evolution reaction and improve Zn-Ni corrosion resistance behaviour. The Zn-Ni electroplating bath without citrate have pH = 2.0, whereas the Zn-Ni bath with citrate have pH

= 4.5. Increasing pH from 2.0 to 4.5 will decrease the hydrogen concentration in plating bath up to hundred times. Thus, increasing pH of the electroplating baths will lead to supress the hydrogen evolution reaction on the working electrodes (Zn-Ni alloy and Zn-Ni-nanoTiO_2 composite).

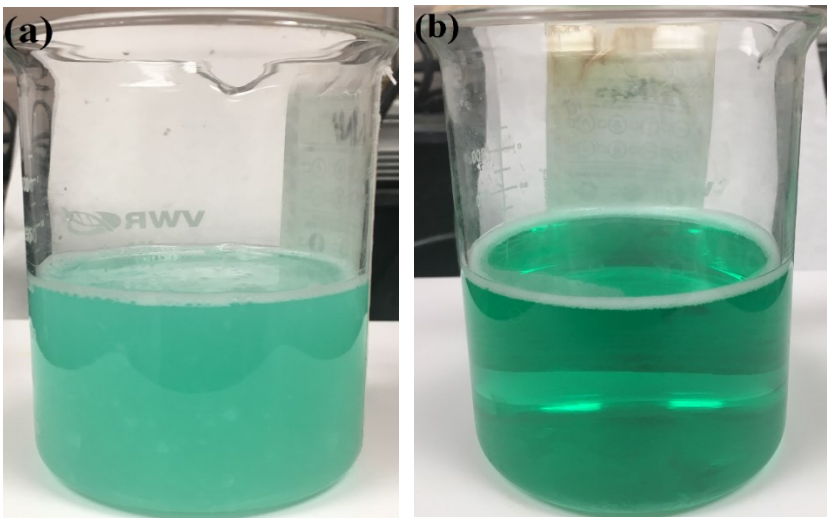

Figure 6.1. Electroplating bath images for (a) Zn-Ni from non-citrate and (b) Zn-Ni from citrate.

6.2.2 Electrochemical and corrosion behaviour analysis

The electrochemical measurements and corrosion behaviour analysis of the coated samples were conducted in the three-electrode glass cell. The electroplated sample was a working electrode, graphite plate was an auxiliary electrode and saturated calomel electrode (SCE) was a reference electrode. At the beginning of the analysis, the open circuit potential (OCP) was measured. The polarization curves were measured in the range of -1.5V to 0.5V at a scan rate of 10 mV/s after 12 hours, 24 hours and 48 hours immersion, respectively. An EIS was measured at the frequency range of 10^5 Hz to 10^{-2} Hz with the amplitude of 10mV. The coated samples were immersed in lab scale seawater at pH of 7.93 at 20 ^{0}C for 12 hours, 24 hours and 48 hours, respectively, and then electrochemical impedance spectroscopy (EIS) was carried out. The impedan ce data was fitted by using Thales simulation software and there are similar two electroplated samples were measured for each level of the films. The corrosion mechanism and the process of the zinc-nickel alloy corrosion products compositions was discussed.

6.4 Result and Discussion

6.4.1 Cyclic Voltammetry (CV) analysis

The electrochemical behaviour of Zn-Ni alloy and Zn-Ni-nanoTiO_2 composite coatings was studied using cyclic voltammetry technique (shown in Figure 6.2). The CV of the Zn-Ni deposits was characterized by the presence of three peaks (a_1, a_2 and a_3) in an anodic scan and two peaks (c_1 and c_2) in a cathodic scan. At positive scale of the potential is corresponds to the anodic dissolution of the electroplated samples (electrochemical oxidation) in which the anodic peaks are seen whereas, negative scale of the potential is represented the cathodic reduction of the electroplated samples in which the cathodic peaks are seen[28]. A γ-phase with the BCC textures are the most needed Zn-Ni alloy phase for increasing the anti-corrosion properties of the coating in high percentage of chlorine contains saline seawater[29]. There are three anodic peaks for Zn-Ni alloy and Zn-Ni-nanoTiO_2 deposits corresponds to the constituents of two-phase at δ-phase (Ni_3Zn_{22}) and γ-phase (Ni_2Zn_{11}). The first and second anodic peaks consist with the dissolution of zinc start from δ and γ-phase, respectively. The third peak match to the dissolution of Ni from their phases[30][31][32]. Therefore, the voltammetry behaviour of the coatings affirms the characteristics of the components and the texture of the deposited phase[32]. The anodic current density of Zn-Ni alloy coating is 4 mA/cm^2 whereas Zn-Ni-nanoTiO_2 composite coating is 2 mA/cm^2. Therefore, Zn-Ni alloy coating increases the dissolution rate in comparison to Zn-Ni-TiO_2 deposits.

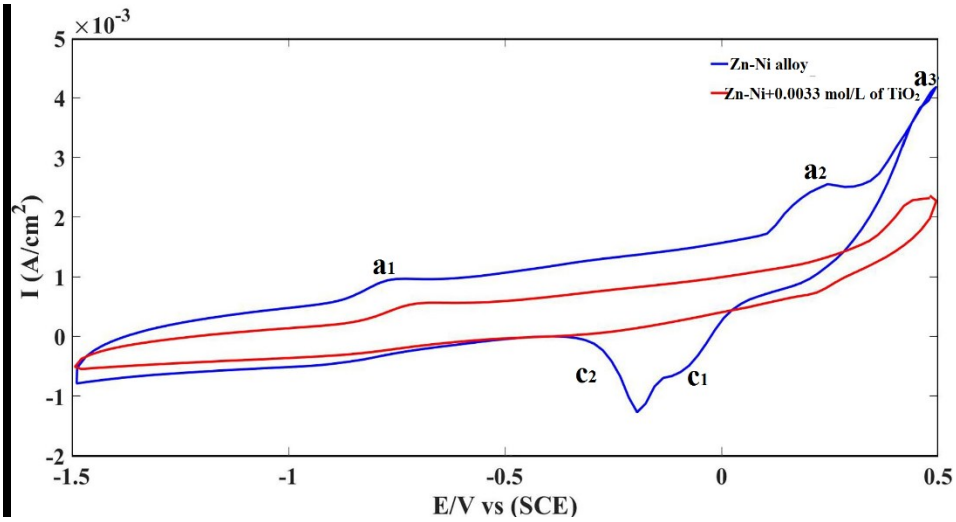

Figure 6.2 Cyclic voltammogram of Zn-Ni and Zn-Ni-nanoTiO_2 composite coating deposited at a scan rate of 10 mV/s

6.4.2 Atomic Force Microscopy (AFM) images

The topographical 3D images of the alloy and composites electroplated samples (a), (b), (c), (d) and (e) surface obtained by AFM measurements are shown in Figure 6.3. The cathodic deposition of the sample (a) is non-uniform, heterogeneous, rough surface and had a broad peak with large crystal grain size equal to 54.40 nm are formed. In contrast, Zn-Ni alloy deposited from citrate bath exhibits uniform and more homogeneous surface with smaller grain size equal to 45.09 nm. Furthermore, the surface roughness of the Zn-Ni-nanoTiO_2 composite coatings are much lower than that of the Zn-Ni alloy coatings. It can also be seen that the Zn-Ni-TiO_2 coating deposited from citrate bath contains regular surface, less coarse, compact and stronger nanosized uniform coating of 25.84 nm grain size in comparison to non-composite Zn-Ni alloy coating, demonstrating that the Zn-Ni alloy with citrate bath shown levelling capability with the addition of TiO_2 composite additives. The additives are adsorbed on the surface of zinc-nickel matrix and inhibit the depositions. Therefore, uniform and smooth deposits can be observed[33]. The surface of the deposits shift from rough to smooth surface is due to the addition of composites additives and the inhibition effects during electroplating.

In contrast, the surface roughness of Zn-Ni alloy coating deposited from the non-citrate bath is greater than that of the Zn-Ni alloy and Zn-Ni-nanoTiO_2 composite coating from citrate baths.

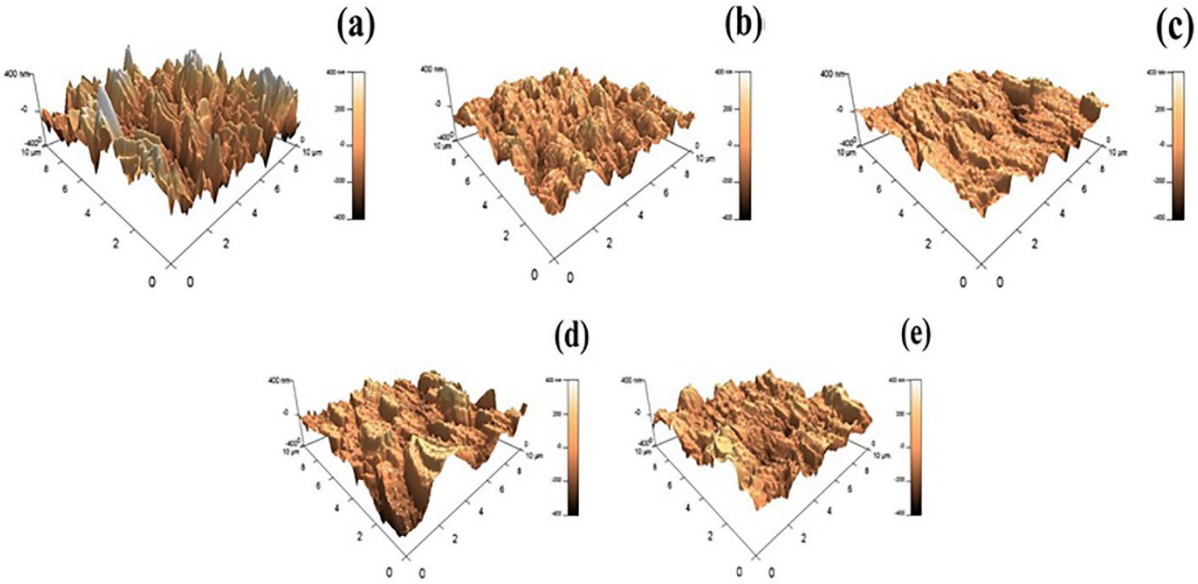

Figure 6.3 3D images of Zn-Ni and Zn-Ni-nanoTiO_2 composite coating electrodeposited at (a) Zn-Ni from non-citrate, (b) Zn-Ni from citrate, (c) Zn-Ni+0.0033 mol/l of TiO_2 from citrate, (d) Zn-Ni+0.0066 mol/l of TiO_2 from citrate, (e) Zn-Ni+0.0125 mol/l of TiO_2 from citrate

6.4.3 X-Ray diffraction (XRD) analysis

XRD pattern of the Zn-Ni films prepared from three different baths are shown in Figure 6.4. It is noticed from graphs that mostly Zn-Ni coatings contains three dominant peaks such as γ-$NiZn_3$, Ni_3Zn_{22} and γ-Ni_2Zn_{11}. The prominent peaks of the pure Zn-Ni coating with and without citrate bath comprises of 38, 43, 52 and 75 degree matches to the γ-$NiZn_3$, γ-Ni_2Zn_{11} and Ni_3Zn_{22}. The Zn-Ni-0.0033TiO_2 and Zn-Ni-0.0066TiO_2 have the highest intensity of the γ-phase (γ-Ni_2Zn_{11}) with (330) plane orientation. Moreover, the peak value of γ-phase with (330) plane orientation is superior to that of other γ-phases e.g. γ-$NiZn_3$ however phase texture of an alloy and composite coatings possess γ-phase with (330) plane orientation plays a determined role in the corrosion resistance performance[34][35][36]. Peak intensity of the γ-Ni_2Zn_{11} of sample (c) and (d) is high in comparison to the sample (a) and (b). The crystal peak intensities illustrated the evidence concerning to the number of phases. Furthermore, the relative amount

of zinc-nickel in the deposits[37]. Therefore, coating with higher-intensity of γ-phase with (330) plane positioning decrease corrosion rate. Similar results were found by Anwar et al.[38] The TiO_2 peaks on the x-ray diffraction patterns are usually very wide, flat and difficult to identified due to the nanosized of the particle however in this XRD pattern did not show any TiO_2 peaks.

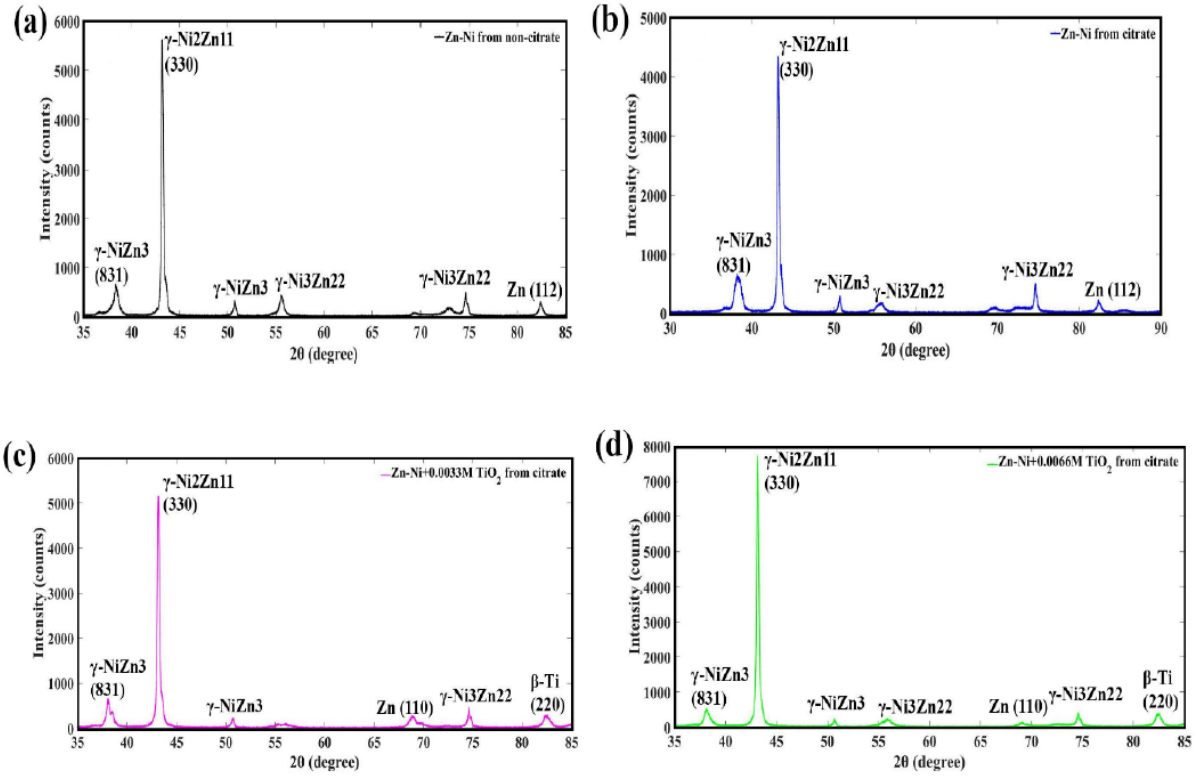

Figure 6.4 XRD patterns for Zn-Ni and Zn-Ni-TiO_2 composite coating electrodeposited at (a) Zn-Ni from non-citrate, (b) Zn-Ni from citrate, (c) Zn-Ni+0.0033 mol/l of TiO_2 from citrate, (d) Zn-Ni+0.0066 mol/l of TiO_2 from citrate

6.4.4 Surface morphology and chemical compositions of corrosion products

The scanning electron microscopy (SEM) was used for the surface characterization and texture of the alloy and composite film electrodeposited at a different molar concentration of TiO_2 nanoparticles. The deposited Zn-Ni alloy coating is developed regarding its homogeneity, permeance and crystal grain size by changing TiO_2 concentration deposited from citrate and non-citrate baths. Zn-Ni from non-citrate bath (Figure 6.5 (a)) shows discontinuity,

heterogeneity and protuberance with larger grain sizes are found due to the HER and the bath is not stable. However, Zn-Ni coating from citrate bath (Figure 6.5 (b)) exhibit more uniform and smaller grain sizes with fewer holes and cracks on the coatings due to the stability of the bath solution and the occurrence of less hydrogen evolution reactions. As it can be observed from Zn-Ni coating with embedded TiO_2 nanoparticles (Figure 6.5 (c) (d) and (e)) change the crystalline structure of the metal deposits which decrease the grain size and shape because the nanoparticle stipulates more nucleation sites and hinder the crystal growth. It is mentioned that by increasing the molar concentration of TiO_2 in the electrolyte, the nanoparticle showed a specific susceptibility to forming conglomerates on the coated surface. The large amount of TiO_2 enhance the surface energy and escalates the interactions between the particles [39][10]. These conglomerates are incorporated and disperse all over the plating surface (Figure 5 (d) and (e)) and their dimensions' increases, as the TiO_2 content increased.

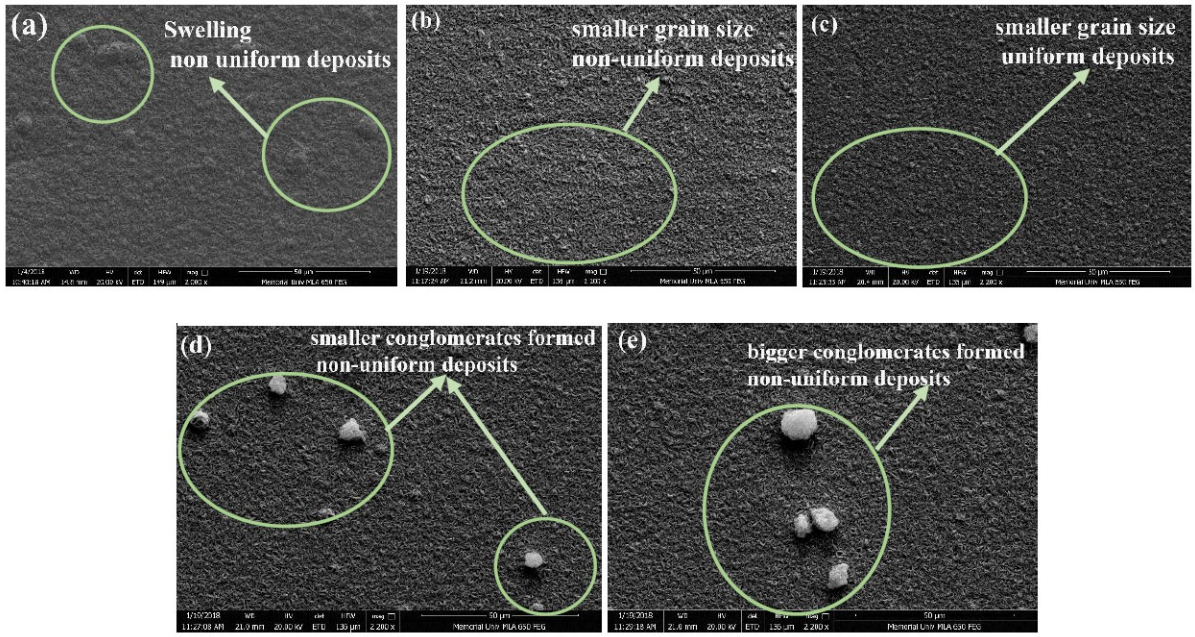

Figure 6.5 The SEM images of Zn-Ni and Zn-Ni-nanoTiO_2 composite coating electrodeposited at (a) Zn-Ni from non-citrate, (b) Zn-Ni from citrate, (c) Zn-Ni+0.0033 mol/l of TiO_2 from citrate, (d) Zn-Ni+0.0066 mol/l of TiO_2 from citrate, (e) Zn-Ni+0.0125 mol/l of TiO_2 from citrate

Figure 6.6, 6.7, and 6.8 demonstrates the surface morphologies of Zn-Ni alloy and Zn-Ni-nanoTiO_2 composite coatings immersed in lab scale seawater after 12 hours, 24 hours and 48 hours respectively. The images are taken at identical magnification; smaller images are at 2,200 and bigger images are at 10,000 magnifications. The Zn-Ni alloy with and without citrate after 12 hours of immersion has corrosion products, and it is covered with white island, observed at low magnification images (Figure 6.6 (a)). Zn-Ni-0.003TiO_2 immersed after 12 hours exhibits similar morphology as deposited (Figure 6.6 (c)). Some white clouds like structure are observed at some part of the surface due to the active properties of the coating. The EDS results revealed that these island and clouds are enriched with C, O and Cl and it is related with the aggregation of corrosion products. The similar result has been examined and reported by Feng et al.[40] Although TiO_2 concentration increases, the surface shows the cracks and solid corrosion products have appeared at large magnification image (Figure 6.6 (d) and 6.6 (e)).

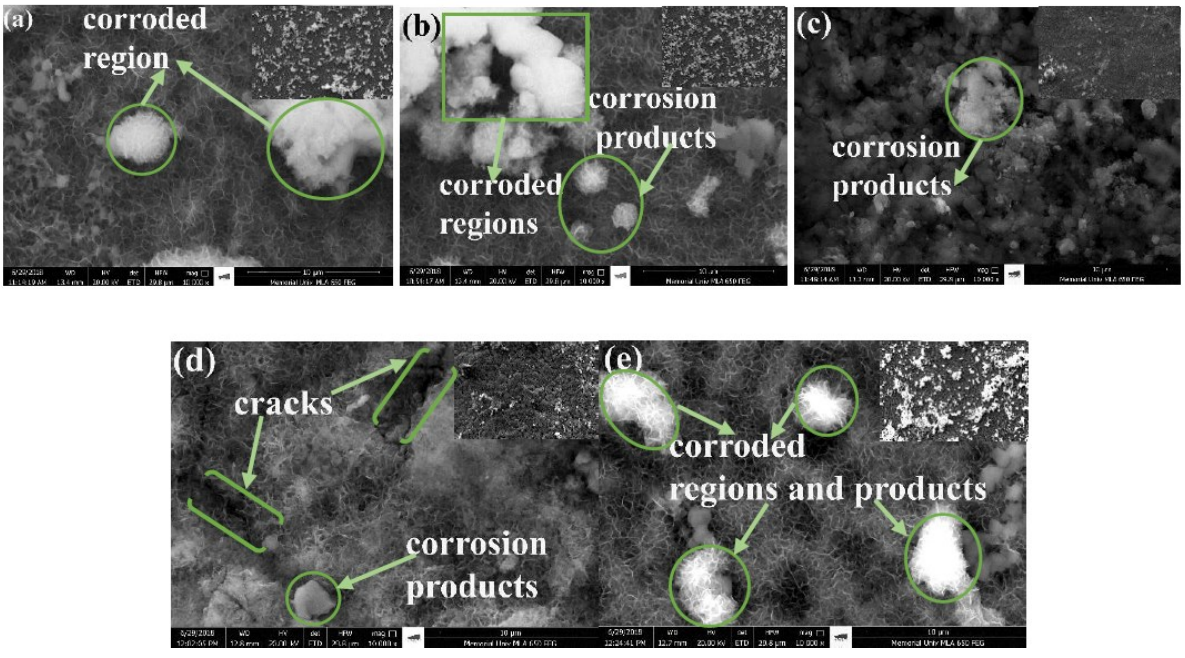

Figure 6.6 The SEM images of corroded Zn-Ni and Zn-Ni-nanoTiO_2 composite coating electrodeposited at (a) Zn-Ni from non-citrate, (b) Zn-Ni from citrate, (c) Zn-Ni+0.0033 mol/l of TiO_2 from citrate, (d) Zn-Ni+0.0066 mol/l of TiO_2 from citrate, (e) Zn-Ni+0.0125 mol/l of TiO_2 from citrate after 12 hours of immersion time.

Zn-Ni alloy with and without citrate after 24 hours of immersion has corrosion products, porosity, cracks, holes and it is also covered with white island, observed at larger magnification images. Zn-Ni-0.003TiO_2 immersed after 24 hours exhibits smaller and intact corrosion products with some white clouds (Figure 6.7 (c)). White clouds like structure are observed at some parts of the surface due to the active properties of the coating. As the TiO_2 concentration increases, the surface appeared more cracks, pits and solid corrosion products have appeared at large magnification image (Figure 6.7 (d) and 6.7 (e)).

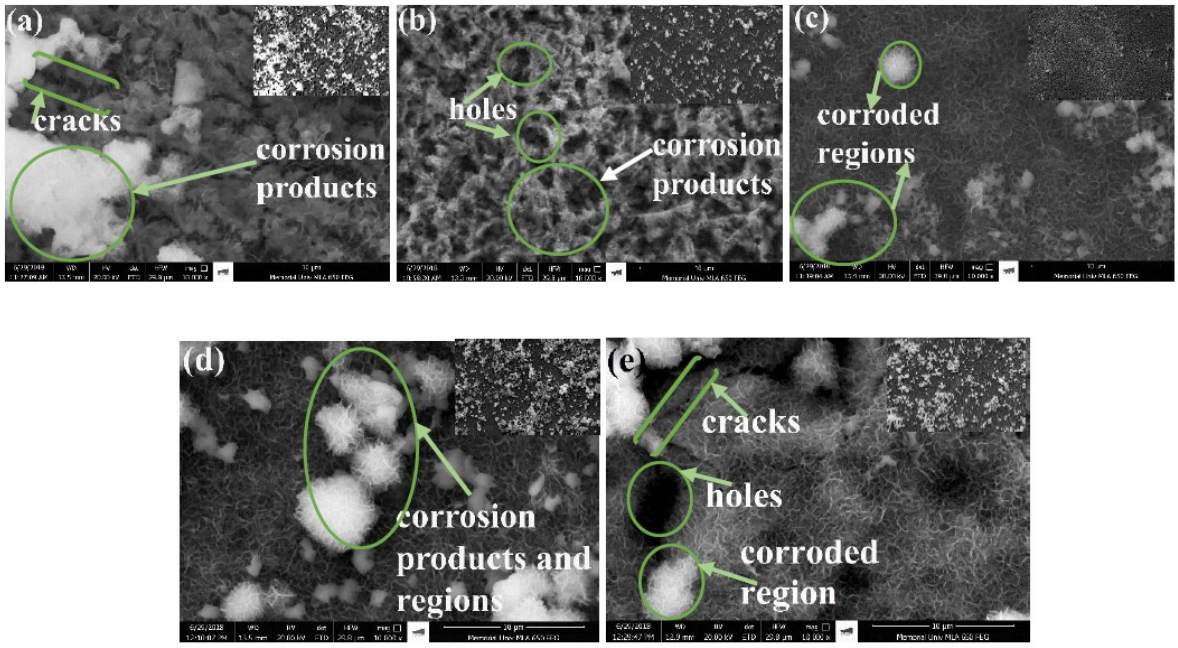

Figure 6.7 The SEM images of corroded Zn-Ni and Zn-Ni-nanoTiO_2 composite coating electrodeposited at (a) Zn-Ni from non-citrate, (b) Zn-Ni from citrate, (c) Zn-Ni+0.0033 mol/l of TiO_2 from citrate, (d) Zn-Ni+0.0066 mol/l of TiO_2 from citrate, (e) Zn-Ni+0.0125 mol/l of TiO_2 from citrate after 24 hours of immersion time

The plating surface thoroughly covers the corrosion products, and mostly layer becomes loosened and permeable as the immersion time increases, especially after long time exposure such as 48 h as shown in Figure 6.8. This may be signifying that the reduction in the corrosion resistance properties of the electroplated samples. Larger island and big clouds are seen at the low magnification. The similar results have been reported by Feng et al. [40][41] and Gomes et al.[42]. Sample (a) has covered with flake and lamellae structure corrosion products (Figure

6.8 (a)). Moreover, sample (d) is completely covered with cloudy corrosion products with holes is appeared in the image (Figure 6.8 (d)). Nonetheless, the corrosion products layer formed on Zn-Ni-0.0033TiO_2 sample (c) (Figure 6.8 (c)) revealed less cloudy and compact structures had been seen in comparison to other samples.

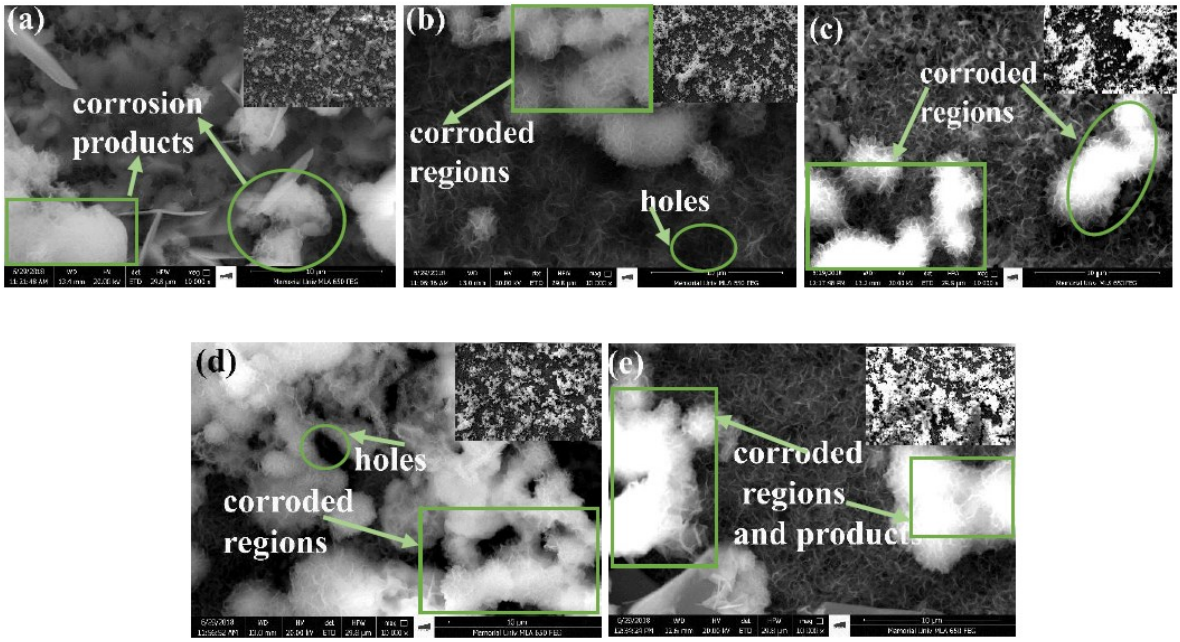

Figure 6.8 The SEM images of corroded Zn-Ni and Zn-Ni-nanoTiO_2 composite coating electrodeposited at (a) Zn-Ni from non-citrate, (b) Zn-Ni from citrate, (c) Zn-Ni+0.0033 mol/l of TiO_2 from citrate, (d) Zn-Ni+0.0066 mol/l of TiO_2 from citrate, (e) Zn-Ni+0.0125 mol/l of TiO_2 from citrate after 48 hours of immersion time

The EDS analysis also determined the presence of TiO_2 on thecomposite coatings. The deposits obtained from Zn-Ni with TiO_2 in the plating bath, EDS spectroscopy revealed the presence of Titanium (Ti), indicating the occurrence of TiO_2 nanoparticle in the Zn-Ni coating (Figure 6.9 (b)).

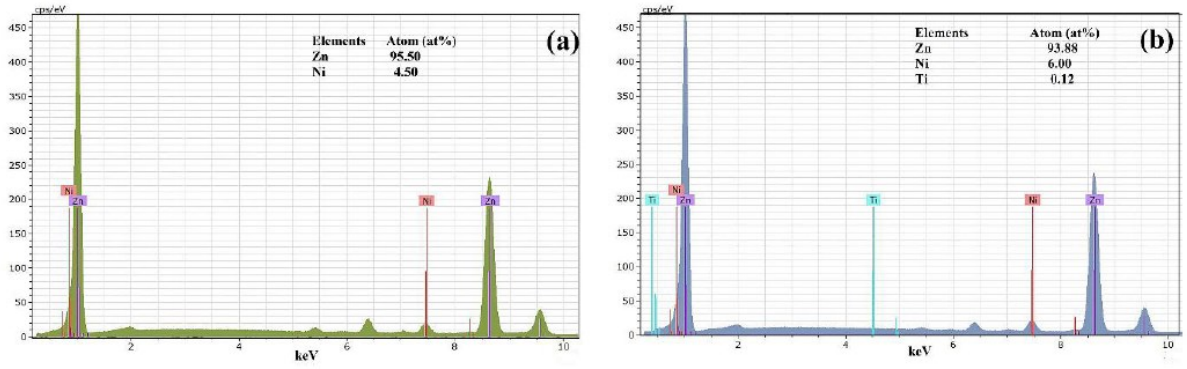

Figure 6.9 EDS peaks of Zn-Ni alloy and Zn-Ni-nanoTiO_2 composite coating electrodeposited (a) Zn-Ni without TiO_2, (b) Zn-Ni with TiO_2

The EDS investigation of the corrosion products composition (Zn, C, O Cl and Ni) of Zn-Ni alloy and Zn-Ni-nanoTiO_2 samples at after 12 hours, 24 hours and 48 oursh of immersion time are shown in Table 6.2. It is observed from the EDS data, as the immersion time increase, the corrosion product layer is also increasing. This is demonstrated by the enhancement of the oxygen and chlorine on the coated surface and by the dissolution of Zn and Ni contents. Though, for all the samples, the amount of Cl content is high at 12 hours of immersion time except sample (a). The Zn content in the coating is decreased for all samples as the immersion time increase showed the dezincification. However, for sample (a), the Zn content decreased at 24 hours (21.55%) and then increase at 48 hours (25.14%). It is observed from Table 6.2 that the Zn-Ni+0.003TiO_2 sample exhibits higher Zn and lowers Cl contents after the immersion test.

Table 6.2. Corrosion products composition of Zn-Ni and Zn-Ni-nanoTiO_2 composite coatings

Samples		**Compositions (at%)**				
	Immersion time (hours)	**Zn**	**C**	**O**	**Cl**	**Ni**
(a) Zn-Ni from non-citrate	12	33.94	24.57	32.88	7.55	1.03
	24	21.55	28.55	39.52	9.79	0.52
	48	25.14	27.22	37.88	9.34	0.37

(b) Zn-Ni from citrate	12	33.48	17.75	33.33	14.70	0.71
	24	27.46	27.64	37.88	9.42	0.38
	48	25.20	27.77	37.64	8.92	0.63
(c) Zn-Ni+0.0033TiO_2 from	12	34.80	21.75	31.16	11.00	1.20
citrate	24	29.65	26.39	36.30	6.74	0.90
	48	29.30	23.64	36.63	9.60	0.75
(d) Zn-Ni+0.0066TiO_2 from	12	27.00	29.20	31.80	11.10	1.26
citrate	24	25.69	27.14	35.26	11.00	0.90
	48	24.53	28.40	30.11	16.08	0.63
(e) Zn-Ni+0.0125TiO_2 from	12	32.00	25.33	35.74	7.13	0.75
citrate	24	29.70	22.84	34.10	12.20	1.07
	48	26.08	23.00	35.19	14.96	0.71

6.4.5 Development of corrosion mechanism

In the exposure to the air, there is a formation of natural oxide layers on the surface of electroplated samples [35]. However, the oxide layers are loose and porous, and it cannot control the penetration of Cl^- ions, therefore, Zn-Ni exposed surface is corroded. Accordingly, through the anodic oxidation of zinc (equation (1)), the anions and cations discharged into the electrolyte, and the reduction reaction occurs at the working electrode (Zn-Ni alloy samples) (equation (2)), respectively.

$$Zn \longrightarrow Zn^{2+} + 2e^- \qquad (1)$$

$$O_2 + 2H_2O + 4e^- \longrightarrow 4OH^- \qquad (2)$$

The corrosion mechanism and the electrochemical process of the Zn-Ni coated alloy constitutes the dissolution of zinc which is equalized by the reduction of O_2 at the working electrode (cathode); afterwards, zinc hydroxide ($Zn(OH)_2$) is formed, and it can desiccate to form zinc oxide (ZnO) (equation (3)). In the presence of saline solution, Na^+ moves toward the cathode

while Cl^- migrates toward the anodic sites saturated with dissolved zinc, therefore, simonkolleite form according to the equation (4).

$$Zn^{2+} + O_2 + H_2O \longrightarrow Zn(OH)_2 \longrightarrow ZnO + H_2O \quad (3)$$

$$5Zn^{2+} + 8OH^- + 2Cl^- \longrightarrow Zn_5(OH)_8Cl_2 \quad (4)$$

The carbonate ions formed through the dissolution of carbon dioxide (equation (5) - (7)). Subsequently, The OH^- ions and Zn^{2+} ions are produced by equation (1) and (2) combines with CO_3^{-2} ions to generate hydrozincite precipitation (equation (9)). The occurrence of hydrozincite signifies the formation of active sites on Zn-Ni alloy[43]

$$CO_2 + H_2O \longrightarrow H_2CO_3 \quad (5)$$

$$H_2CO_3 + H_2O \longrightarrow H_2CO_3^- + H_3O^+ \quad (6)$$

$$H_2CO_3^- + H_2O \longrightarrow CO_3^{-2} + H_3O^+ \quad (7)$$

$$5Zn^{2+} + 2CO_3^{-2} + 6OH^- \longrightarrow Zn_5(CO_3)_2(OH)_6 \quad (8)$$

$$5ZnO_{(s)} + 5CO_{2(g)} + 3H_2O \longrightarrow Zn_5(CO_3)_2(OH)_{6(s)} \quad (9)$$

The formation of simonkolleite is before the precipitation of hydrozincite revealed that the sufficient Cl^- is present in Zn-Ni alloy during immersion. However, the formed hydrozincite may be unstable in the strong solution of Cl^- ions and can be disintegrated into simonkolleite corresponds to equation (10). Conferring the researchers observed and reported by Odnevall et al.[44], in an appropriate condition the hydrozincite, simonkolleite and zinc oxide layered structure convert from one phase to another. As the immersion time increases lead to increase the active anodic species on the coating surface and produce significant amount of zinc oxide. As a consequence, the presence of ZnO increase the pH of the electrolyte. The abundance of zinc oxide can also be related with the possibility of hydrozincite (equation (11)). This is due to the fact that ZnO is more consistent and stable corrosion products[45].

$$Zn_5(CO_3)_2(OH)_6 + 2Cl^- + 2OH^- \longrightarrow Zn_5(OH)_8Cl_2 + CO_3^{-2} \quad (10)$$

$$Zn_5(CO_3)_2(OH)_6 + 2OH^- \longrightarrow 5ZnO + 5HCO_3^- + 3H_2O \quad (11)$$

As seen from the surface morphological images and corroded composition tests that the formation of corrosion products on the Zn-Ni-0.0033TiO_2 samples are fully dispersed, compact and strong. It will lead to form the protection layer on the surface of sample from the corrosive environment.

6.4.6 Characteristics of corrosion products

The characterisation of the Zn-Ni alloy corrosion products was measured by the X-ray diffraction are shown in Figure 6.10. As seen from the Figure 4, XRD graphs at without immersion tests, single γ-phase is observed at 43 degree, whereas after 24 hours of immersion, the peaks at 43 degree indicates the appearance of both γ-$NiZn_3$ and γ-Ni_2Zn_{11}. The sharp intensity of $NiZn_3$ and Ni_2Zn_{11} indicates that Zn-Ni alloy cannot completely dissolve after 24 hours of immersion in lab scale 3.5% NaCl solution. The corrosion products such as simonkolleite ($Zn_5(OH)_8Cl_2.H_2O$), hydrozincite ($Zn_5(CO_3)_2(OH)_6$), zinc oxide/zincite (ZnO), smithsonite ($ZnCO_3$) and zinc hydroxide wulfingite ($Zn(OH)_2$) is found in Zn and Zn alloys and it is visible in the immersion test[16][5][17][46][47][40].Simonkolleite and hydrozincite have well-crystallized form and appeared many intense reflections of the peaks. Moreover, majority of the hydrozincite has overlap on the peaks of simonkolleite. Away from these peaks, there are also an appearance and indication of $Zn(OH)_2$, ZnO and $Zn(CO)_3$. It is notified that the intensity of hydrozincite, smithsonite, and zinc oxide peaks is often broadened reflection, and some are superimposed with simonkolleite formed a weak crystallized form of these phases.

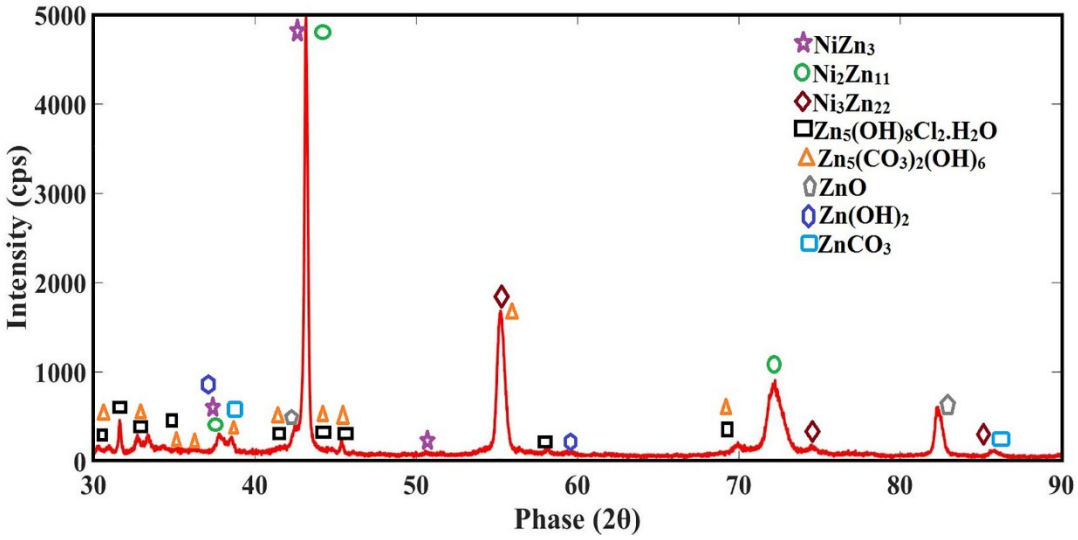

Figure 6.10 XRD patterns of Zn-Ni sample after 24 hours of immersion

6.4.7 Electrochemical measurement analysis

The potentiodynamic polarization curves are used to examine the electrochemical measurement of Zn-Ni and Zn-Ni-nanoTiO_2 composite film at room temperature are shown in Figure 6.11. The polarization values were evaluated at their OCP's readings of different electroplating samples and corrosion current densities (I_{corr}) and corrosion potentials (E_{corr}) were computed from the intercepts on the Tafel slopes by extrapolation, are tabulated in Table 6.3. It is stated that the E_{corr} values are more negative correspond to the steel (E_{corr} = -0.66V)[40] over the entire immersion time for Zn-Ni and Zn-Ni-nanoTiO_2 sample, suggesting the sacrificial property on the steel specimen. The corrosion activity of the Zn-Ni alloy coating in corrosion media is directly related to corrosion potentials. The corrosion resistance performance of the electroplated sample is mainly related to their structural morphologies, chemical compositions and phase compositions[37].

It is observed from Figure 6.11 and Table 6.3 that the corrosion current (I_{corr}) of Zn-Ni coating deposited from citrate bath (0.08 mol/l of ammonium citrate) at without immersion is minimum (494 µA/cm^2) than non-citrate bath Zn-Ni coating (732 µA/cm^2). It is also noticeable that the Zn-Ni alloy coating deposited from citrate bath exhibited less negative corrosion potential

(E_{corr}) than the coating deposited from non-citrate bath. Moreover, Zn-Ni specimen from non-citrate bath shifts more negative corrosion potential and maximum corrosion current led to form holes, cracks and non-uniformity on the coated surface due to the hydrogen reduction on the cathode forming the hydrogen bubbles on the coated sample during electroplating.

The anodic and cathodic polarization behaviour of Zn-Ni-nanoTiO_2 deposited from of citrate bath (0.16 mol/l of ammonium citrate) at a different molar concentration of TiO_2 nanoparticle without immersion, embedded in Zn-Ni matrix is also presented and analyzed in Figure 6.11 and Table 6.3. As it can be seen from the Table 6.3, except for the case of Zn-Ni+0.0033 mol/l of TiO_2, the corrosion potential (E_{corr}) values of the composite coating are more negative than the other Zn-Ni alloy, indicating that Zn-Ni+0.0033 mol/l of TiO_2 composite coatings are more active than pure Zn-Ni and other Zn-Ni-nanoTiO_2 composite coatings. The presence of TiO_2 particles in the Zn-Ni alloy matrix have emerged as a uniform passive layer lead to increase the corrosion resistance performance of the coating.[10] Similar results were obtained by Vlasa et al.[10], Praveen et al.[6], Kumar et al.[11] and Gomes et al.[9].

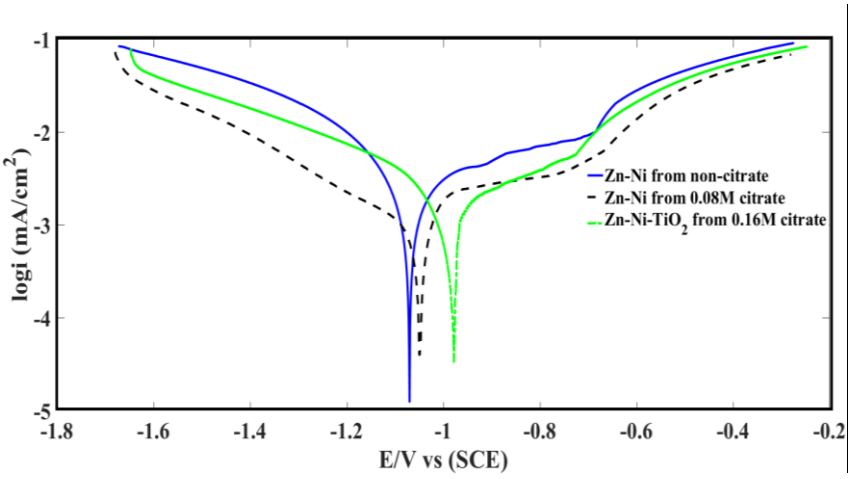

Figure 6.11 Polarization curve in logarithmic scale for Zn-Ni and Zn-Ni-nanoTiO_2 composite coating

Table 6.3. Polarization data for the Zn-Ni and Zn-Ni-nanoTiO_2 composite coating

Samples	E_{corr} (V vs SCE)	I_{corr} (µA/cm^2)
(a) Zn-Ni from non-citrate	-1.08	732

(b) Zn-Ni from citrate	-1.02	494
(c) Zn-Ni+0.0033 mol/l of TiO_2	-0.90	176

6.4.8 Electrochemical impedance spectroscopy (EIS) analysis

The electrochemical kinetics and corrosion mechanism of the Zn-Ni alloy and Zn-Ni-nanoTiO_2 samples can potentially measure by EIS method. Moreover, it can estimate the characteristics and kinetics of the electrochemical process happening at the interface of coating and corrosive media[11][48]. The impedance measurement of Zn-Ni alloy and Zn-Ni-nanoTiO_2 composite coatings are displayed in the form of Nyquist plots at room temperature and shown in Figure 6.12. The open circuit potential (OCP's) range of frequency is 10 mHz to100 kHz. The shape of impedance modulus is look like a semicircle[37][32].The Nyquist plots of the coated samples consist of clearly-defined capacitive arcs and at the high frequency of the plot is contemplated as the corrosion products. In contrast, at the low-level frequency, it is considered as the electric double layer [49][40], respectively. The EIS measurement of Zn-Ni-nanoTiO_2 sample shown maximum impedance values in comparison to other coated samples. Further impedance measurement carried out for Zn-Ni deposited from citrate bath showed more impedance modulus in comparison to Zn-Ni from non-citrate coating. It means that after the incorporation of 0.0033 mol/l of TiO_2 with citrate bath exhibit better corrosion resistance performance of the coating. Gomes et al.[42] and Vlasa et al.[10] have observed the analogous result. Therefore, it indicates the significant influence of TiO_2 nanoparticles inclusion on the kinetics of both cathodic and anodic reaction of Zn-Ni coating. It is also noticed from the Nyquist plot that the Zn-Ni alloy coating without TiO_2 and deposited from non-citrate bath showed least impedance modulus, is due to the un-stabilized and without the incorporation of

TiO_2 nanoparticles on the Zn-Ni matrix and it also increases the active surface area on Zn-Ni coated specimen. Thus, the worst coating with the minimum impedance modulus is found for Zn-Ni from non-citrate bath and without the incorporation of TiO_2 nanoparticles are shown in Figure 6.12 and it is related to a minimal arc at high frequencies, formed the oxide film in the air.[50]

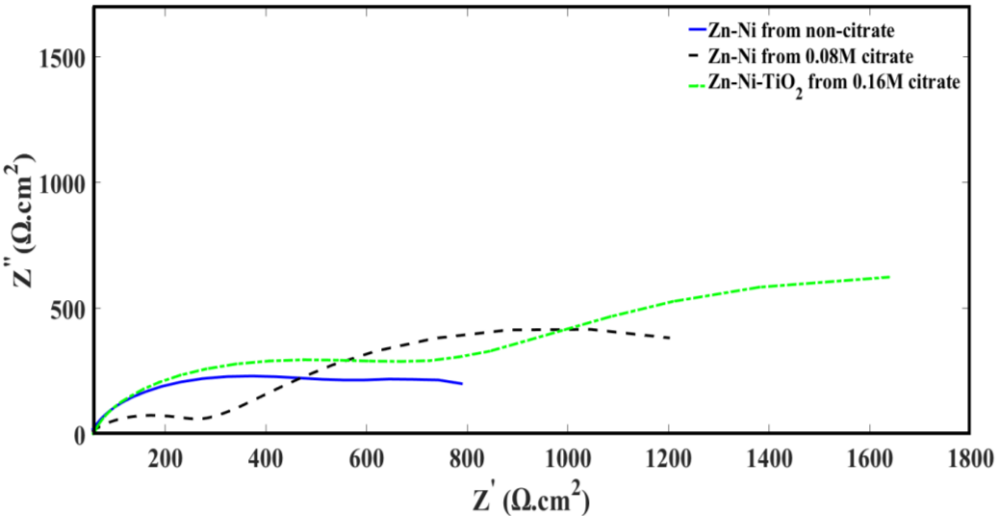

Figure 6.12 Nyquist plot for Zn-Ni and Zn-Ni-nanoTiO_2 composite coating

The analysis of the shape of the impedance spectroscopy with the fitted electrical alternative circuit data assists in identifying the complete electrochemical activity exist on the coated surface when it contacts with the corrosive environment. However, the shape of the spectroscopy is significantly persuaded by the electrochemical process at the surface and by the geometric components of working electrode [11][51]. The authors have fit the experimental impedance spectroscopy data (Nyquist plots) to the various arrangements of resistors (R) and the constant phase element (C). The electrical circuits are shown in Figure 6.14, where R_s represents the solution resistance. R_1 and C_1 is the resistance and capacitance of the corrosion product layers' interface at the underneath of the pores connected with the charge transfer resistance. R_2 and C_2 represent the resistance and capacitance associated with the charge transfer resistance and electric double layer capacitance.

The Mathematical equation for the impedance of constant phase element (CPE) is given below[52][53]

$$Z(Q) = y_0^{-1}(jw)^{-\alpha}$$

Where y_0 is coefficient of the constant phase element, j^2 =-1 imaginary constant, w is the frequency, and α is the exponential of CPE. For α=0 represents the full resistor, for α =-1 represents inductor, for α=1 represents ideal capacitor, for α = 0.5 represents Warbug impedance[52] [53].

Zahner Thales software integrated with IM6 electrochemical workstation was used to measure the impedance values. The calculated fitted data of the electrical equivalent circuit of Zn-Ni alloy and Zn-Ni-nanoTiO_2 composite coating are shown in Table 6.4. The impedance measurement data of the simulated electrical circuit shows the best fit with the Nyquist and Bode experimental values. The relative error of each parameter is less than 8%. As seen from Figure 6.13 (a), (b), and (c), the Zn-Ni-nanoTiO_2 deposited from citrate bath at different immersion time have maximum impedance modulus values in comparison to the other coated samples. It is also observed that the immersion time increases lead to increase the impedance modulus values due to the deposition of dense and strong corrosion product components on the surface of the coated samples.

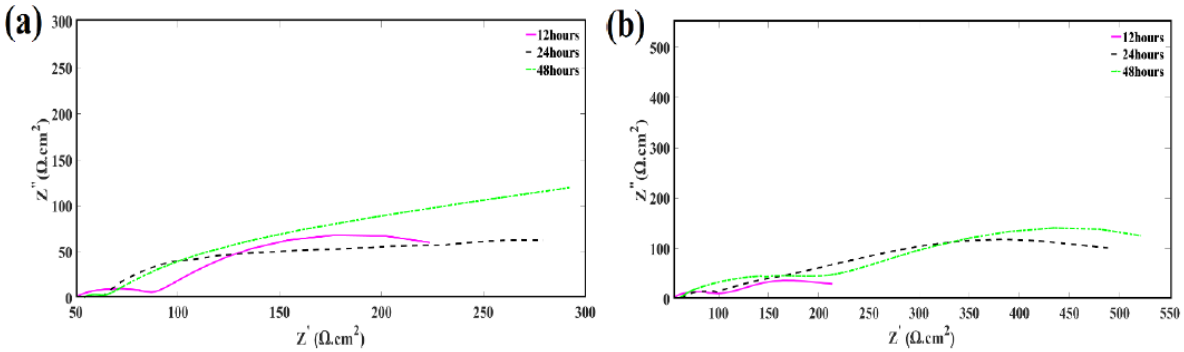

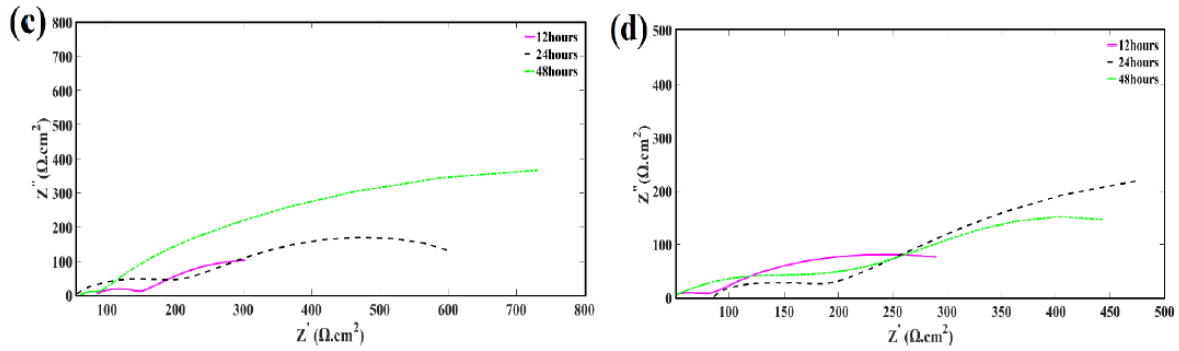

Figure 6.13 Nyquist plot for Zn-Ni and Zn-Ni-nanoTiO_2 composite coating electrodeposited at (a) Zn-Ni from non-citrate, (b) Zn-Ni from citrate, (c) Zn-Ni+0.0033 mol/l of TiO_2 from citrate, and (c) Zn-Ni+0.0125 mol/l of TiO_2 from citrate.

The C_1 and R_1 values changes over the complete immersion time. R_1 values increases significantly after 12 hours of immersion time for the Zn-Ni alloy and Zn-Ni-nanoTiO_2 composite coatings, indicating that the corrosion resistance properties of the deposited sample increases. This behaviour is due to the strong corrosion product layer formed on the coated surface and inhibit the corrosive solution to penetrate on the corrosion product layer during immersion tests. This is evidence from the increase in C_1 values. The value of R_1 at 48 hours is high for all the samples. However, the maximum value is 700.1 Ωcm^2 for Zn-Ni-0.003TiO_2 coating lead to provide anti-corrosion performance to the coated sample. Zn-Ni coating from the non-citrate bath at 12 hours of immersion test has least charge transfer resistance (R_{ct}) in comparison to other coated samples with and without incorporation of TiO_2 nanoparticles due to the un-stabilized bath plated coating and defects are formed due to the absence of TiO_2 incorporation. The Zn-Ni-nanoTiO_2 composite coating deposited from 0.033 mol/l of TiO_2 at 12 hours exhibited higher R_{ct} value than other coatings. Therefore, incorporation of 0.033 mol/l of TiO_2 in Zn-Ni coatings is improved their corrosion resistance behaviour than Zn-Ni alloy coatings. For Zn-Ni-0.003TiO_2 samples, the C_2 values slightly decrease at 24 hours immersion time and then increase at 48 hours. This is evident that there is the possibility of non-uniformity and sponginess of the corrosion product layer.

The least values of R_1 at 12 hours of immersion indicates that the corrosive solution easily reaches on the surface of Zn-Ni alloy and Zn-Ni composite. At 24 hours of immersion test, the R_1 value increases for all samples indicates the formation of a compact corrosion product layer leads to protect from corrosion. The values of R_1 and R_{ct} at 48 hours of immersion test is higher than the 24 hours for all samples. This behaviour is related to decrease of the corrosion rate on the coated surface, it can also be associated with the formation of uniform, denser and compact corrosion product layers. The similar behaviour has been seen for all the coated samples such as pure Zn-Ni, Zn-Ni and Zn-Ni-TiO_2 samples exhibits the similar behaviour in which the values of R_1 is increases after 12 hours of immersion test. Feng et al. [40][41], Gomes et al.[42] and Vlasa et al.[10] also reported the analogous result and revealed that the addition of complexing agent and incorporation of titanium dioxide lead to increase the corrosion resistance performance of the Zn-Ni alloy coated samples.

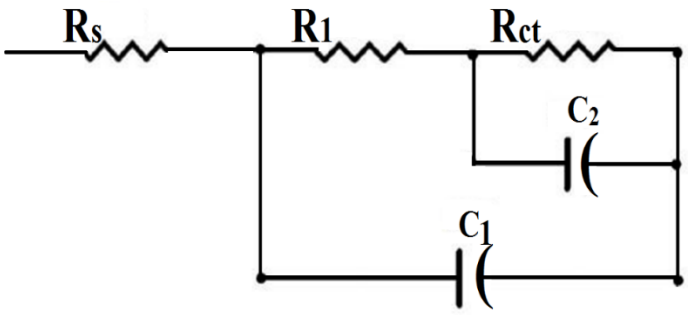

Figure 6.14 Electrical equivalent circuit modelling used for the simulation of EIS data of Zn-Ni alloy and Zn-Ni-nanoTiO$_2$ composite coating

Table 6.4. Optimum EIS fitting parameters of Zn-Ni alloy and Zn-Ni-nanoTiO$_2$ deposits with various immersion time

Samples	**Immersion time (hours)**	**Rs (Ωcm^2)**	**R_1 (Ωcm^2)**	**R_{ct} (Ωcm^2)**	**C_1 ($s^{-\alpha}\Omega cm^2$)**	**α**	**C_2 ($s^{-\alpha}\Omega cm^2$)**	**α**
Zn-Ni deposited	12	47.8	194.9	45.4	40.8	0.80	5.0	0.80
from	24	62.3	318.5	81.4	57.4	0.84	17.8	0.78
non-citrate bath	48	54.0	453.0	90.6	303.9	0.89	39.9	0.56

Zn-Ni from citrate	12	51.2	139.3	59.9	70.0	0.70	5.9	0.52
bath	24	59.8	374.9	148.6	127.4	0.65	8.4	0.66
	48	59.9	434.4	180.1	216.2	0.64	6.5	0.67
Zn-Ni+0.0033	12	52.7	530.9	180.1	97.5	0.71	3.4	0.65
mol/l of TiO_2	24	79.4	359.9	77.5	366.4	0.70	2.7	0.54
from citrate bath	48	62.1	700.1	80.8	149.6	0.80	11.3	0.55
Zn-Ni+0.0125	12	42.5	209.9	50.0	57.5	0.69	5.4	0.64
mol/l of TiO_2	24	59.4	448.1	124.4	242.8	0.69	4.0	0.57
from citrate bath	48	46.9	390.6	185.8	395.3	0.81	5.7	0.53

6.5 Conclusion and Discussion

This study focuses on the deposition of Zn-Ni alloy and Zn-Ni-nanoTiO_2 films to enhance an anti-corrosion performance and mechanical properties of the coated samples. The polarization result revealed that stable citrate bath helped to deposit uniform coating with decreased hydrogen evolution reaction (HER). The least I_{corr} values and small grain or crystal size, compactness and homogeneous texture exhibited better anti-corrosion properties. The electrochemical and corrosion behaviour of coatings are concluded as follows:

- The potentiodynamic polarization results reveal that the Zn-Ni-0.0033 mol/l of TiO_2 coating deposited from citrate bath possesses a lower I_{corr} value and more positive corrosion potential than the other coated samples. The least I_{corr} is due to the stable citrate bath Zn-Ni coated samples with decreased HER which exhibited uniform and higher corrosion resistance and the SEM images showed the formation of denser and more uniform coating.

- The crystalline phase texture of the Zn-Ni alloy deposits from citrate bath has the maximum intensity of γ-phase (γ-$NiZn_3$) (815), γ-Ni_2Zn_{11} (330) (631) and Ni_3Zn_{22} plane orientation lead to increase the performance of corrosion resistance of the coating.
- The impedance measurement of the Zn-Ni-0.0033 mol/l of TiO_2 coating deposited from citrate bath increase impedance modulus than the other coated samples. The excellent coating with the maximum impedance modulus is Zn-Ni-0.0033 mol/l of TiO_2, and it exhibited compact and robust corrosion products at after 48 hours' immersion test.
- The electrical circuit data showed that the Zn-Ni-nanoTiO_2 composite coating deposited from 0.033 mol/l of TiO_2 at 12 hr exhibit higher R_1 and R_{ct} value than other coatings. The incorporation of TiO_2 and complexing agent in a bath is an effective process to corrosion resistance and mechanical properties of the coating.
- Increasing the immersion time lead to increase the composition of simonkolleite and zinc oxide (ZnO). The corrosion resistance performance decreased at 12 hours of immersion time due to the formation of the maximum amount of ZnO. This is also accompanied by the growth of the porous corrosion products. Furthermore, the corrosion resistance increases at 24 hours and 48 hours, due to the disposition of robust and compact corrosion product layers.

Acknowledgement

The authors express gratitude to the financial commitment provided by Natural Science and Engineering Council of Canada (NSERC), the Canada Research Chair (CRC) Tier I Program and use of atomic force microscopy (AFM) from Dr. Erika Merschrod lab at Department of Chemistry, Memorial University of Newfoundland, NL, Canada.

References

[1] V. G. Roev, R. A. Kaidrikov, and A. B. Khakimullin, “Zinc – Nickel Electroplating from Alkaline Electrolytes Containing Amino Compounds,” vol. 37, no. 7, pp. 756–759, 2001.

[2] D. Blejan, D. Bogdan, M. Pop, A. V. Pop, and L. M. Muresan, “Structure, morphology and corrosion resistance of Zn-Ni-TiO2 composite coatings,” Optoelectron. Adv. Mater. Commun., vol. 5, no. 1, pp. 25–29, 2011.

[3] R. Fratesi, G. Roventi, G. Giuliani, and C. R. Tomachuk, “Zinc-cobalt alloy electrodeposition from chloride baths,” J. Appl. Electrochem., vol. 27, no. 9, pp. 1088–1094, 1997.

[4] I. H. Karahan and H. S. Güder, “Electrodeposition and properties of Zn, Zn–Ni, Zn–Fe and Zn–Fe–Ni alloys from acidic chloride–sulphate electrolytes,” Trans. IMF, vol. 87, no. 3, pp. 155–158, 2009.

[5] K. R. Sriraman, S. Brahimi, J. A. Szpunar, J. H. Osborne, and S. Yue, “Characterization of corrosion resistance of electrodeposited Zn-Ni Zn and Cd coatings,” Electrochim. Acta, vol. 105, pp. 314–323, 2013.

[6] B. M. Praveen and T. V. Venkatesha, “Electrodeposition and Corrosion Resistance Properties of Zn-Ni/TiO_2 Nano composite Coatings,” Int. J. Electrochem., vol. 2011, pp. 1–4, 2011.

[7] C. Zhao, Y. Yao, and L. He, “Electrodeposition and characterization of Ni-W/ZrO2 nanocomposite coatings,” Bull. Mater. Sci., vol. 37, no. 5, pp. 1053–1058, 2014.

[8] Q. Zhao, Y. Liu, and C. Wang, “Development and evaluation of electroless Ag-PTFE composite coatings with anti-microbial and anti-corrosion properties,” Appl. Surf. Sci.,

vol. 252, no. 5, pp. 1620–1627, 2005.

[9] J. Fustes, A. Gomes, and M. I. Da Silva Pereira, “Electrodeposition of Zn-TiO_2 nanocomposite films-effect of bath composition,” J. Solid State Electrochem., vol. 12, no. 11, pp. 1435–1443, 2008.

[10] A. Vlasa, S. Varvara, A. Pop, C. Bulea, and L. M. Muresan, “Electrodeposited Zn-TiO2 nanocomposite coatings and their corrosion behavior,” J. Appl. Electrochem., vol. 40, no. 8, pp. 1519–1527, 2010.

[11] M. K. Punith Kumar, T. V. Venkatesha, M. K. Pavithra, and A. N. Shetty, “A Study on Corrosion Behavior of Electrodeposited Zn-Rutile TiO_2 Composite Coatings,” Synth. React. Inorganic, Met. Nano-Metal Chem., vol. 42, no. 10, pp. 1426–1434, 2012.

[12] S. Myagmarjav et al., “Characterization of the Ni-Zn/TiO_2 Nanocomposite Synthesized by the Liquid-Phase Selective-Deposition Method,” Mater. Trans., vol. 45, no. 7, pp. 2035–2038, 2004.

[13] S. Anwar, Y. Zhang, and F. Khan, “Electrochemical behaviour and analysis of Zn and Zn–Ni alloy anti-corrosive coatings deposited from citrate baths,” RSC Adv., vol. 8, no. 51, pp. 28861–28873, 2018.

[14] Y. Zhang and D. G. Ivey, “Electroplating of Nanocrystalline CoFeNi Soft Magnetic Thin Films from a Stable Citrate-Based Bath,” Chem. Mater., vol. 16, no. 7, pp. 1189–1194, 2004.

[15] M. Stein, S. Owens, H.W, Pickering and K. Weil, “Dealloying studies with electrodeposited zinc-nickel alloy films,” Electrochim Acta., vol. 43, pp. 223–226, 1998.

[16] J. Friel, “Atmospheric corrosion products on aluminium, zinc, and aluminium-zinc metallic coatings,” Corrosion, vol. 42, pp. 422–426, 1986.

[17] M. Bučko, J. Rogan, S. I. Stevanović, A. Perić-Grujić, and J. B. Bajat, “Initial corrosion protection of Zn-Mn alloys electrodeposited from alkaline solution,” Corros. Sci., vol.

53, no. 9, pp. 2861–2871, 2011.

[18] A. S. T. M. Designation, “Standard Reference Test Method for Making Potentiostatic and Potentiodynamic Anodic,” Annu. B. ASTM Stand., pp. 79–85, 1999.

[19] A. Johansson, H. Ljung, and S. Westman, “X-Ray and Neutron Diffraction on Ni,Zn and Fe,Zn,” Acta Chem. Scand., vol. 22, pp. 2743–2753, 1968.

[20] G. Nover and K. Schubert, “The Crystal Structure of $NiZn_3$,” J. Less Common Met., vol. 75, pp. 51–63, 1980.

[21] A. Patterson, “TheScherrerformulaforX-ray particle size determination,” Phys. Rev., vol. 56, pp. 978–982, 1939.

[22] H. Faid, L. Mentar, M. R. Khelladi, and A. Azizi, “Deposition potential effect on surface properties of Zn–Ni coatings,” Surf. Eng., vol. 33, no. 7, pp. 529–535, 2017.

[23] M. V. Tomić, M. M. Bučko, M. G. Pavlović, and J. B. Bajat, “Corrosion staility of electrochemically deposited Zn-Mn alloy coatings,” Contemp. Mater., vol. 1, no. 1, pp. 87–93, 2010.

[24] Y. F. Jiang, L. F. Liu, C. Q. Zhai, Y. P. Zhu, and W. J. Ding, “Corrosion behavior of pulse-plated Zn-Ni alloy coatings on AZ91 magnesium alloy in alkaline solutions,” Thin Solid Films, vol. 484, no. 1–2, pp. 232–237, 2005.

[25] F. L. G. Silva, D. C. B. Do Lago, E. D’Elia, and L. F. Senna, “Electrodeposition of Cu-Zn alloy coatings from citrate baths containing benzotriazole and cysteine as additives,” J. Appl. Electrochem., vol. 40, no. 11, pp. 2013–2022, 2010.

[26] J. R. Garcia, D. C. B. do Lago, and L. F. de Senna, “Electrodeposition of Cobalt Rich Zn-Co alloy Coatings from Citrate Bath,” Mater. Res., vol. 17, no. 4, pp. 947–957, 2014.

[27] A. Conde, M. A. Arenas, and J. J. de Damborenea, “Electrodeposition of Zn-Ni coatings as Cd replacement for corrosion protection of high strength steel,” Corros. Sci., vol. 53, no. 4, pp. 1489–1497, 2011.

[28] A. C. . Cheung, O. Bretschger, F. Mansfeld, and K. . Nealson, “FUEL127-performance of different strains of the genus Shewanella in a microbial fuel cell,” Abstr. Pap. Am. Chem. Soc., vol. 234, 2007.

[29] Z. Feng, L. Ren, J. Zhang, P. Yang, and M. An, “Effect of additives on the corrosion mechanism of nanocrystalline zinc-nickel alloys in an alkaline bath,” RSC Adv., vol. 6, no. 91, pp. 88469–88485, 2016.

[30] S. Basavanna and Y. . Naik, “Electrochemical studies of Zn–Ni alloy coatings from acid chloride bath,” J. Appl. Electrochem., vol. 39, no. 1975–1982, 2009.

[31] E. Kus, K. Nealson, and F. Mansfeld, “The effect of different exposure conditions on the biofilm/copper interface,” Corros. Sci., vol. 49, pp. 3421–3427, 2007.

[32] A. Tozar and I. H. Karahan, “Structural and corrosion protection properties of electrochemically deposited nano-sized Zn-Ni alloy coatings,” Appl. Surf. Sci., vol. 318, pp. 15–23, 2014.

[33] M. G. Hosseini, H. Ashassi-Sorkhabi, and H. A. Y. Ghiasvand, “Electrochemical studies of Zn-Ni alloy coatings from non-cyanide alkaline bath containing tartrate as complexing agent,” Surf. Coatings Technol., vol. 202, no. 13, pp. 2897–2904, 2008.

[34] Y. Boonyongmaneerat and K. Saenapitak, S Saengkiettiyut, “Reverse pulse electrodeposition of Zn-Ni alloys from a chloride bath,” J. Alloy. Compd., vol. 487, pp. 479–482, 2009.

[35] Z. Feng, Q. Li, J. Zhang, P. Yang, and M. An, “Studies on the enhanced properties of nanocrystalline Zn–Ni coatings from a new alkaline bath due to electrolyte additives,” RSC Adv., vol. 5, no. 72, pp. 58199–58210, 2015.

[36] Z. Feng, Q. Li, J. Zhang, P. Yang, and M. An, “Electrochemical Behaviors and Properties of Zn-Ni Alloys Obtained from Alkaline Non-Cyanide Bath Using 5,5’-Dimethylhydantoin as Complexing Agent,” J. Electrochem. Soc., vol. 162, no. 9, pp.

D412–D422, 2015.

[37] F. Mansfeld, H. Shih, C.H.Tsai, and H. Greene, “Analysis of EIS Data for Common Corrosion Processes,” Am. Soc. Test. Mater., vol. 1188, pp. 37–53, 1993.

[38] S. Anwar, F. Khan, Y. Zhang, and S. Caines, “Optimization of Zinc-Nickel Film Electrodeposition for Better Corrosion Resistant Characteristics,” Can. J. Chem. Eng.

[39] B. M. Praveen and T. V. Venkatesha, “Electrodeposition and properties of Zn-nanosized TiO2 composite coatings,” Appl. Surf. Sci., vol. 254, no. 8, pp. 2418–2424, 2008.

[40] Z. Feng, L. Ren, J. Zhang, P. Yang, and M. An, “Effect of additives on the corrosion mechanism of nanocrystalline zinc–nickel alloys in an alkaline bath,” RSC Adv., vol. 6, no. 91, pp. 88469–88485, 2016.

[41] Z. Feng, M. An, L. Ren, J. Zhang, P. Yang, and Z. Chen, “Corrosion mechanism of nanocrystalline Zn-Ni alloys obtained from a new DMH-based bath as a replacement for Zn and Cd coatings,” RSC Adv., vol. 6, no. 69, pp. 64726–64740, 2016.

[42] A. Gomes, I. Almeida, T. Frade, and A. C. Tavares, “Stability of Zn–Ni–TiO2 and Zn–TiO2 nanocomposite coatings in near-neutral sulphate solutions,” J. Nanoparticle Res., vol. 14, no. 2, p. 692, 2012.

[43] W. Fürbeth and M. Stratmann, “The delamination of polymeric coatings from electrogalvanised steel – a mechanistic approach.,” Corros. Sci., vol. 43, pp. 207–227, 2001.

[44] I. Odnevall and C. Leygraf, “The formation of Zn4SO4(OH)6·4H2O in a rural atmosphere,” Corros. Sci., vol. 36, no. 6, pp. 1077–1087, 1994.

[45] K. Tano and S. Huguchi, “Development and Properties of zinc-aluminium alloy coated steel with high corrosion resistance (super zinc),” Nippon Steel Tech. Rep., vol. 25, pp. 29–37, 1985.

[46] M. Mouanga and P. Berçot, “Comparison of corrosion behaviour of zinc in NaCl and in

NaOH solutions; Part II: Electrochemical analyses," Corros. Sci., vol. 52, no. 12, pp. 3993–4000, 2010.

[47] Z. I. Ortiz, P. Díaz-Arista, Y. Meas, R. Ortega-Borges, and G. Trejo, "Characterization of the corrosion products of electrodeposited Zn, Zn-Co and Zn-Mn alloys coatings," Corros. Sci., vol. 51, no. 11, pp. 2703–2715, 2009.

[48] S. Fashu, C. D. Gu, J. L. Zhang, M. L. Huang, X. L. Wang, and J. P. Tu, "Effect of EDTA and NH_4Cl additives on electrodeposition of Zn-Ni films from choline chloride-based ionic liquid," Trans. Nonferrous Met. Soc. China (English Ed., vol. 25, no. 6, pp. 2054–2064, 2015.

[49] J. Winiarski, W. Tylus, M. S. Krawczyk, and B. Szczygieł, "The influence of molybdenum on the electrodeposition and properties of ternary Zn-Fe-Mo alloy coatings," Electrochim. Acta, vol. 196, pp. 708–726, 2016.

[50] J. Winiarsiki, W. Tylus, K. Winiarska, and B. Szczygiel, "Understanding corrosion via corrosion products characterizatio: I. Case study of the role of Mg alloying in Zn-Mn coating on steel," Corros. Sci., vol. 51, pp. 1251–1262, 2009.

[51] F. La Mantia, J. Vetter, and P. Novák, "Impedance spectroscopy on porous materials: A general model and application to graphite electrodes of lithium-ion batteries," Electrochim. Acta, vol. 53, no. 12, pp. 4109–4121, 2008.

[52] F. Mansfeld, "Recording and analysis of Ac impedance data for corrosion stud- ies.1. Background and methods of analysis," Corrosion, vol. 37, pp. 301–307, 1981.

[53] G. Brug, A. L. Van Deen Adeen, M. Sluyters-Rehbach, and J. Sluyters, "The Analysis of the Electrode Impedance Complicated by the presence of a Constant Phase Element," J Electroanal Chem, vol. 176, pp. 275–295, 1984.

7.0 Influence of Chloride and pH on the Pitting-Mechanism of Zn-Ni alloy Coating in Sodium Chloride Solutions

Preface

In this chapter, the pitting mechanism of Zn-Ni alloy coatings investigated in NaCl solution with different pH and chloride concentration. Three-level fractional factorial design (FFD) is implemented to find the optimized conditions for the pitting corrosion of the coated samples. XRD technique was used for phase analysis and to calculate the average crystal size of the coating. The pits growth and pits depth/diameter measurements were analyzed by using an Olympus Optical Microscope integrated with the stream essential image software. Pitting morphology and chemical compositions of the corrosion products were investigated using scanning electron microscopy equipped with energy dispersive spectroscopy (EDS). Potentiodynamic polarization measurement (Tafel) and EIS were employed to analyze the anti-corrosion performance of the Zn-Ni alloy coatings. This chapter brings a new study to explored the effect of pitting-corrosion on Zn-Ni alloy coatings in NaCl solutions with different pH and chloride concentration have been investigated and analyzed. This article is submitted to the Canadian Journal of Chemical Engineering.

Abstract

This paper presents the pitting corrosion behavior of Zn-Ni alloy coatings in NaCl solutions with different chloride concentrations and pH. The pitting behavior investigation is done using optical microscope, potentiodynamic polarization (Tafel slopes), electrochemical impedance spectroscopy (EIS) and scanning electron microscopy (SEM) integrated with energy dispersive spectroscopy (EDS). Design of the experiment with three-level fractional factorial design

(FFD) is used to analyze the behavior of pitting corrosion. The pitting behavior in acidic solution with low chloride concentration was found to be significantly different from that in the neutral solution with high chloride concentration. Electrochemical analysis indicates that the corrosion behavior of samples immersed at 0.35 mol/l of NaCl and pH = 3.0 at different exposure time have low impedance values compared to the 0.35 mol/l of NaCl and pH = 7.0 samples. SEM images show that the pH and chloride concentration in the electrolyte has a significant influence on the pitting morphology. Exclusive large pit morphology in acidic solution (pH = 3.0) with low chloride concentration (0.35 mol/l) was also observed. This provide new insight of pitting behavior on coated material. The study will serve an important tool to design or select metal coatings for marine environment.

Keywords: Fractional factorial design (FFD), Pitting corrosion, Zn-Ni alloy, Optical microscope, Pit depth/diameter, Electrochemical analysis.

7.1 Introduction

Mild steel is a well understood and studied iron alloy used in corrosive environment. It tends to form a passive layer at neutral and alkaline pH condition (pH = 6-12), which is determined by the presence of anions in the corrosive solutions[1]. Pitting is one of the most common and localized corrosion, which occurs at the sites of local failure of the passive layers[2][3]. It is an intensive and destructive surface attack and can cause the equipment failure by penetration. At the microscopic level, pits nucleate and are mostly obscured by the corrosion products. Therefore, pitting is one of the most detrimental and indiscernible forms of corrosion[4][5].

Various corrosion protection methods have been implemented to improve the life span of steel structures/machinery against corrosion and rusting[6]. Anti-corrosion coating is a common and useful approach for preventing the steel structures from corrosion. Electrodeposition is a widely applied technology for the fabrication of corrosion-resistant metallic coatings due to high

technological feasibility and economic viability. The thin layer of coating can provide a reasonable barrier between the steels and exposure environment. Due to its negative reduction potential, zinc is employed as a sacrificial anode in conventional corrosion-resistant methods [7]. It is well known that zinc coating is used in the automobile industry [8][9] and is extensively adapted for providing better corrosion resistance to mild steel in a corrosion environment. Zinc can be alloyed with the ferrous group metal such as Fe, Co, Ni, and Mg to enhance the anti-corrosion property of the coated specimens[7][10].

There are several study has been done on the pitting corrosion of the metal alloy on the steel surface, and one of the studies conducted an experiment on the Cu-Ni alloy pitting corrosion and has been reported by Jin et al .[11] at various exposure times in the marine environment (30^0C). It is revealed that the coated sample showed slight pits at one week in comparison to the months of the marine exposure. The pitting areas are small, and the Cu matrix is still apparent. Although some white and gray corrosion products gradually exhibited on the coated surface. Moreover, E_{corr} values shifted to the positive direction, and I_{corr} turned to the negative for the extension of the exposure time.

Electrochemical and morphological analyses of Zn and Zn alloy pitting corrosion have been studied by Miao et.al.[12] Pitting corrosion behavior of Zn and Zn alloy was examined using cyclic voltammetry and potential scan technique in the presence of 0.10 – 0.90 mol/l of NaCl over a pH range of 2 to 12. Zinc hydroxy chloride complexes were the principal element of a passive layer formed during the span of passivation which makes the passive layer considerably stable over a more extended period in the pH range of 2 to 12. However, increasing the concentration of chloride ions lead to break the passive layer and propagate the pit growth on the zinc surface.

Zn-Ni alloys provide superior anti-corrosion and mechanical property in comparison to the pure Zn coatings. Sriraman et al. [13] studied the corrosion behavior of Zn-Ni alloy coating to

replace pure Zn and Cd coatings. The researchers found that Zn-Ni coatings possess higher polarization resistance and lower corrosion current. Corrosion products formed on the coating surface lead to additional protection to the Zn-Ni coatings. It also increases the life span of the coating in comparison to the pure Zn and Cd coatings.

Several papers investigated the behavior of pitting corrosion on the steel surface in 0.35 mol/l NaCl solution. Wang et al. [14] studied the pitting corrosion mechanism of X-80 pipeline steel in sodium chloride solutions at various pH and NaCl concentrations. In neutral or acidic solutions containing 0.05 mol/l NaCl, a relatively thin and non-uniform corrosion product appeared on the pipeline surface. Moreover, pit propagated at horizontal and reasonable directions, and large pits were generated. In 1 mol/l NaCl solution, more intense pits are formed. However, the pits were smaller and initiated between the corrosion product and surface of the steel. In alkaline solutions, relatively thicker and dense corrosion products were formed on the steel surface leading to the prevention of oxygen penetration on the specimen surface, the latest work of Wang et al. [15] reported that the rate of pitting corrosion decreases with time and follows an exponential decay function. They found that increasing temperature of the solution led to increased pit growth, and mostly uniform corrosion was formed. However, the temperature does not influence on the pit shape.

Tian et al. [16] studied the behavior of metastable pits on 304-stainless steel by potentiostatic polarization analysis and 3D video microscope. The authors found that the average lifespan of the metastable pits was decreased by applied potential whereas the maximum lifespan of pits, the standard peak value of current transient and the pitting nucleation quantity were increased with the applied potential. It was also observed from this study that the pit shape changed during the pit grew.

As seen from the above literature, researches on electrochemical and morphological analyses of pitting corrosion have been implemented on Zn-Ni alloy coated samples. However, less

systematic studies have been conducted to investigate the pitting corrosion behavior of Zn-Ni alloy coating on mild steel. In this paper, the effects of chloride and pH on the pitting-mechanism of Zn-Ni alloy coatings in NaCl solutions have been investigated and analyzed. Optical microscope and scanning electron microscope (SEM) were used to measure the pits depth/diameter and visualization of pits behavior.

7.2 Experiment details

Zn-Ni electroplating was conducted in 200ml bath solution at room temperature. A rectangular mild steel plate with a surface area of 2.5 cm x 2.5 cm was used as the working electrode (cathode). A graphite plate was used as an auxiliary electrode (anode). The anode and cathode were connected to the DC power supply via a multi-meter. The bath compositions and conditions for the electrodeposition of Zn-Ni alloy coating are shown in Table 7.1. The chemical composition of the substrate (1080 mild steel) is listed in Table 7.2. Experimental setup for the variation of pits corresponding with immersion time are shown in Figure 7.1. After electrodeposition, the Zn-Ni coated sample was rinsed with distilled water and alcohol and dried with ambient air. The finished Zn-Ni specimen was then immersed in NaCl solution with different pH at various factors and levels. The standard guide ASTM G46-94 was used to examine and evaluate the pitting corrosion on samples. The pits growth and pits depth/diameter measurements were analyzed by using an Olympus Optical Microscope integrated with the stream essential image software. Pitting morphology and chemical compositions of the corrosion products were investigated using scanning electron microscopy (FEI MLA 650F) equipped with energy dispersive spectroscopy (EDS). Minitab 17 statistical software was used to design the complete statistical experiments. Potentiodynamic polarization measurement (Tafel) and EIS were employed to analyze the anti-corrosion performance of the Zn-Ni alloy

coatings. Electrochemical measurements were performed using an electrochemical workstation (IM6, ZAHNER-Elektrik GmbH & Co.KG, Germany).

Table 7.1. Bath compositions and operating conditions for the electrodeposition of Zn-Ni alloy coatings

Bath Compositions and Operating Conditions	**Molar Concentrations (mol/l)**
Zinc Chloride ($ZnCl_2$)	0.550
Nickel (II) Chloride hexahydrate ($NiCl_2.6H_2O$)	0.105
Boric Acid (H_3BO_3)	0.16
Ammonium Chloride (NH_4Cl)	0.46
Sodium dodecyl sulfate (SDS)	0.00017
Potassium Citrate ($K_3(C_6H_5O_7)$)	0.032
Sodium chloride (NaCl)	0.171
Anode	Graphite
Cathode	Mild steel
Current density	40 mA/cm^2
Plating Time	15 minutes
Temperature	Ambient

Table 7.2. Chemical compositions of AISI 1018 mild steel

Elements	**Mn**	**C**	**S**	**P**	**Fe**
Content (%)	0.60-0.90	0.15-0.20	0.05 (max)	0.05 (max)	98.90

7.3 Methodology

To find the key factor and levels of the pitting corrosion on Zn-Ni alloy coating (specimen), an experimental plan is developed. The result of first step in the experimental process is to determine the preparation of substrate and then Zn-Ni alloy electroplating on the basis of FFD

statistical analysis. Afterwards, the second step is to measure the pit diameter/depth and electrochemical analysis of designed samples to examine the critical conditions for the pitting corrosion on specimen. The complete methodology of the two steps of pitting corrosion testing process is shown in Figure 7.1. The design of experiment and the complete samples lists are as follows:

- Number of samples (Eighteen samples)
- Replication (Two samples prepared for one set of conditions; one for morphology and pit measurement; one for electrochemical analysis.

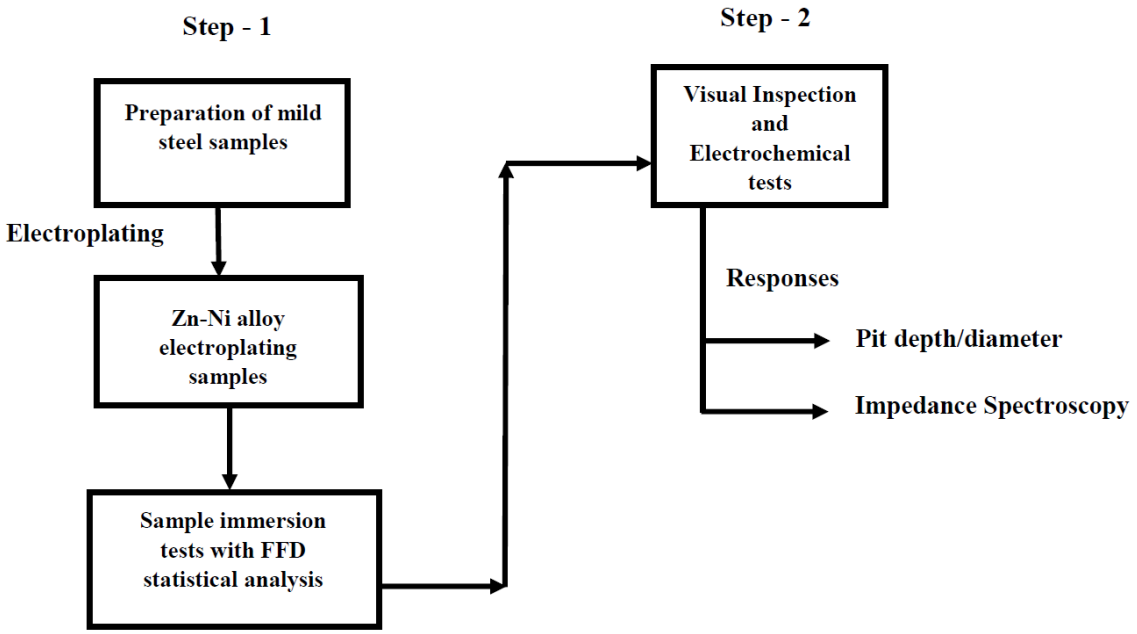

Figure 7.1 Methodology for the experimental process in block diagrams

The controlled and fixed factors with their responses and the levels of FFD design are shown in the Table 7.3 (a) and (b).

Table 7.3. Controlled and fixed factors with their responses

Factors	Levels	Measurement
NaCl concentration (mol/l)	0.30, 0.50 and 0.70 (controlled)	Pit diameter and depth
pH of electrolyte	4.0, 7.0 and 10.0 (controlled)	Poteniodynamic Polarization
Temperature (^{0}C)	RT (uncontrolled)	and Impedance Spectroscopy
Exposure time (hours)	2, 4, 6 and 8 (controlled)	
Material Type	Zn-Ni alloy	

Table 7.4. Factors and levels for the 2^{2-1} three levels of FFD design

Factors	Levels		
	1	2	3
NaCl concentration (A) (mol/l)	0.35	0.50	0.70
pH of the electrolyte (B)	4.0	7.0	10.0

A FFD method was applied to the two factors to determine their effects on pitting corrosion of Zn-Ni coated samples. Table 7.3 shows the levels for each factors. FFD statistical modelling is given in Table 7.4.

7.4 Experiment results and analysis

7.4.1Three-level fractional factorial design (FFD) analysis

A three-level fractional factorial design (FFD) was used to determine the significance of each factors affecting the pitting corrosion on the zinc-nickel coating. Pit depth/diameter are the best indicators of corrosion behaviour on the metal surface. An increase in pitting corrosion is indicated when pit diameter of the coated sample increases and until it converts into the uniform corrosion.

Similar design of experiment procedure has been adopted from Anwar et. al [17] The three-level FFD statistical modelling and the resulting pit diameter are presented in Table 7.4. As can be seen that the samples immersed at low pH (pH = 3.0) and higher NaCl concentration (0.5 mol/l and 0.70 mol/l) solution lead to increase the pitting diameter; however, except run 7 as the immersion time increases, the pit diameter had no remarkable growth. It may be due to the formation of the passive layer on the Zn-Ni alloy surface from corrosion and oxidation products [18][12]. Run 3 and run 10 at high NaCl concentration, low and neutral pH of solution has small pit diameter; however the corrosion rate is increases due to the more generalized form of corrosion (uniform corrosion) on entire surface of the coated samples. These samples have higher pit density (pits/mm^2) in comparison to other levels of NaCl solutions and similar results has been reported from Wint et al. [18].

Table 7.5. The fractional factorial design (FFD) statistical modelling

Run Order	**NaCl concentration (A)**	**pH of the electrolyte (B)**	**Pit diameter (µm) at 2 hours**	**Pit diameter (µm) at 4 hours**	**Pit diameter (µm) at 6 hours**	**Pit diameter (µm) at 8 hours**
1	1	1	48.00	70.00	78.00	83.60
2	2	1	35.81	36.80	68.00	90.40
3	3	2	23.00	31.00	37.00	42.54
4	3	1	43.00	49.00	51.00	60.13
5	2	3	36.00	42.00	58.00	87.00
6	1	3	39.00	42.00	49.00	52.00
7	1	1	49.40	82.00	94.00	108.00
8	1	2	31.00	77.00	85.42	85.98
9	2	2	42.14	78.64	84.65	85.04
10	3	2	29.70	36.12	35.81	37.48
11	2	1	31.38	38.29	75.43	89.20
12	2	2	37.44	78.18	82.64	85.19

13	3	3	46.23	50.22	53.74	71.22
14	1	2	55.97	70.95	78.45	82.74
15	1	3	44.64	53.60	53.94	55.15
16	3	1	20.00	30.61	36.36	45.80
17	2	3	37.44	42.44	58.10	82.93
18	3	3	48.00	33.97	49.58	69.41

7.4.2 General Factorial Regression: Pit diameter (µm) at 2 hours versus A, B

Analysis of variance (ANOVA) is a statistical method to mathematically evaluate each outcome, containing the main factors and two-factor interaction based on the resultant value is listed in Table 4. ANOVA was carried out to justify the efficacy of the statistical models [19]. The ANOVA regression study for pit diameter (µm) at 2 hours versus environmental factor such as NaCl concentration (A), pH of the electrolyte (B) is shown in Table 7.5 and for 4, 6 and 8 hours regression results are shown in Tables TA1 to TA3 in the appendix section. As seen from Table 5 that the F-value of factor B is higher in comparison to the other interactions which demonstrates factor B has more remarkable contribution to the formation of the pits at 2 hours of immersion tests; whereas from Table TA1, TA2 and TA3 in the appendix section has the higher F-value for factor A in comparison to the other interactions has significant contribution to the formation of the pits at 4, 6 and 8 hours of immersion tests. It means that the low level of NaCl concentration (0.35 mol/l) and low level of pH of the electrolyte (3.0) at initial period of immersion tests lead to exhibit more pits growth in comparison to the other levels of the factors. At a higher level of NaCl concentration and low-level pH of the electrolyte lead to form the uniform corrosion instead of pitting corrosion.

Table 7.6. Analysis of Variance (ANOVA) for 2^{2-1} fractional factorial design (FFD)

Source	**Dfi**	**SSi**	**MSi**	***F-value**	**P-value**
Model	8	6709.4	838.7	2.59	0.089
Linear	4	3612.3	903.1	2.79	0.092
A	2	802.8	401.4	1.24	0.048
B	2	2809.5	1404.7	4.34	0.229
AB	4	3097.1	774.3	2.39	0.127
Error	9	2910.6	323.4		
Total	17	9620.0			

*R^2 (adj.) = 0.75

Where,

Dfi = Degree of freedom for factor i.

SSi = Sum of square of factor i

MS = Mean of Square; = SSi/Dfi

F-values = the ratio of model sum of square and model sum of error (MSF/MSE)

P-Values = Probability of factor i

The combination of the experimental factors' effect and ANOVA data, a fitted polynomial model with statistical significance can be generated as follows:

Pit diameter (μm) at 2 hours = $35.34 + 7.99\ A_1 + 0.36\ A_2 - 8.53\ A_3 - 10.14\ B_1 + 17.60\ B_2 - 7.46\ B_3 - 22.69\ A_1{*}\ B_1 + 16.75\ A_1{*}B_2 + 5.94\ A_1{*}B_3 + 8.04\ A_2{*}B_1 + 1.49\ A_2{*}B_2 - 9.53\ A_2{*}B_3 + 14.65\ A_3{*}\ B_1 - 18.24\ A_3{*}B_2 + 3.58\ A_3{*}B_3$

Where,

A_1 = NaCl concentration at low level (1)

A_2 = NaCl concentration at medium level (2)

A_3 = NaCl concentration at high level (3)

B_1 = pH of the electrolyte at low level (1)

B_2 = pH of the electrolyte at medium level (2)

B_3 = pH of the electrolyte at high level (3)

7.5 Effect of pH and chloride concentration on the pitting morphology

All the images are taken at the same magnification by using a scanning electron microscopy (SEM) with respective bath conditions. The image shown in the inset is at higher magnifications. Particularly the composition of the Zn passive protective films is composed of $Zn(OH)_2$ and ZnO. Moreover, in the presence of Cl^- ions, the chloride ion react with Zn^{+2} to form various species such as $ZnCl_3^-$ and $ZnCl_2$ and surface-confined β-ZnOHCl that leads to forming the major corrosion product of zinc hydroxy chloride, $Zn_5(OH)_8Cl_2$ [12]. After the design of experiments, it was observed that the low level of NaCl concentration (0.35 mol/l), and low and medium level of pH (pH = 3.0 and 7.0) have the higher chances to form pits on the coated surface. At high level of Cl^- concentration and acidic pH lead to form the uniform corrosion and there is very rare detection of pitting corrosion. Therefore, authors have selected run 7, 8 and 9 for the further pitting corrosion investigation. The coated specimens immersed in 0.35 mol/l of NaCl and pH = 3.0 (run 7); 0.35 mol/l of NaCl and pH = 7.0 (run 8); and 0.50 mol/l of NaCl and pH = 7.0 (run 9) at 2 hours, respectively, and it is shown in Figure 7.2 (a), (b) and (c). SEM images of these coated samples are captured after the removal of the oxide layer in an ultrasonic bath. We can see from Figure 7.2 (a) that the pits formed in the acidic solution with 0.35 mol/l of NaCl solution have more immense pit growth in comparison to the pits formed from neutral solution with 0.35 mol/l of NaCl solution (Figure 7.2 (b)). In neutral solutions with 0.35 mol/l of NaCl solution does not appear to have any significance on the pit size. The pitting corrosion in neutral solution as confirmed through SEM images is persistence with the high impedance in the Nyquist plots with low Cl^- concentrations (Figure 7.10 (b)).

The electrochemical results and SEM images show that the passivity of Zn-Ni alloy from 0.35 mol/l of NaCl and pH = 3.0 and 0.50 mol/l of NaCl and pH = 7.0 are easily damaged and pitting corrosion is initiated in the presence of acidic solution with higher Cl^- ion.

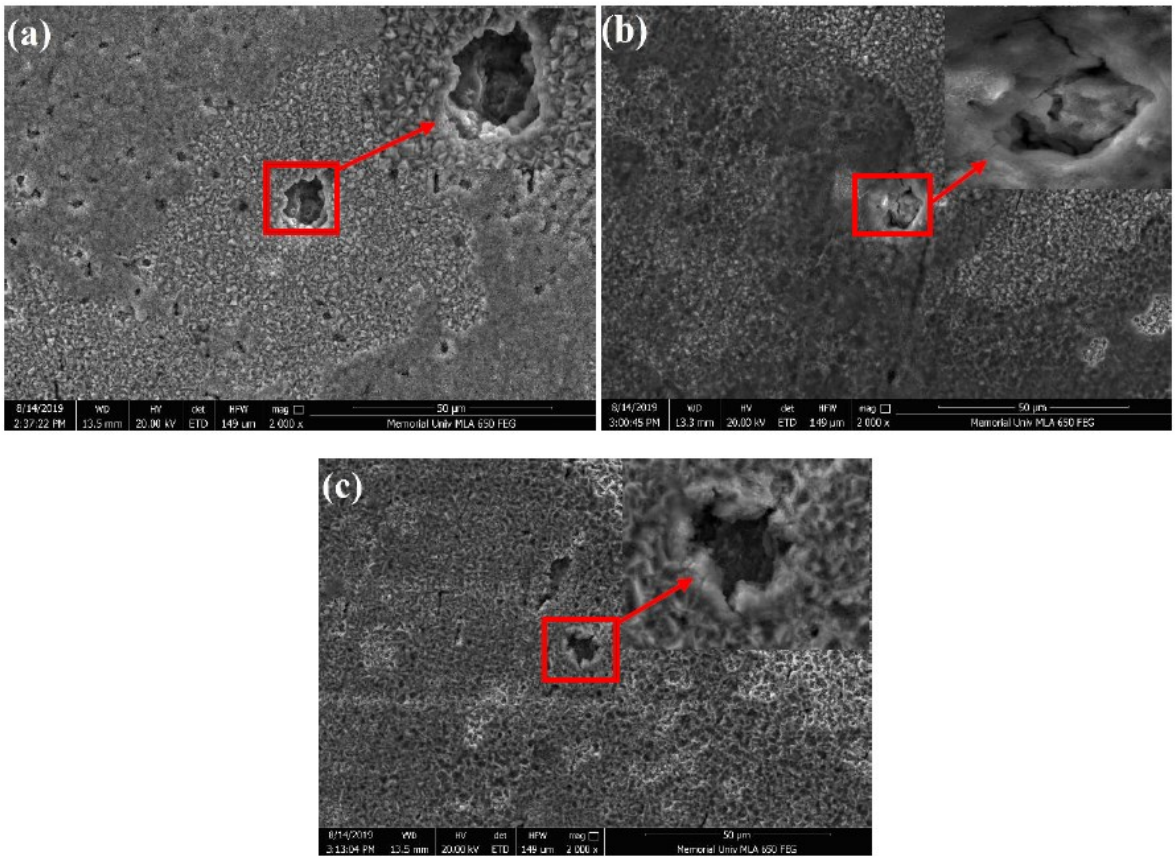

Figure 7.2 Pitting morphology of the corroded surface of (a) 0.35 mol/l of NaCl and pH = 3.0, (b) 0.35 mol/l of NaCl and pH = 7.0 and (c) 0.50 mol/l of NaCl and pH = 7.0 immersed at 2 hours (oxide layer removed in an ultrasonic bath)

As it can be seen from Figure 7.3 (d), (e) and (f) samples immersed at 4 hours respectively that the pits formed in the acidic solution with 0.35 mol/l of NaCl solution and neutral solution with 0.5 mol/l of NaCl concentration have many more massive pits with the diameter in the range of 60 – 80 μm are observed in comparison to the pits formed from neutral solution with 0.35 mol/l of NaCl solution. In a solution with higher Cl^- concentration (0.5 mol/l) have more intense pitting corrosion with larger pit growth. The pitting corrosion in neutral solution as confirmed

through SEM images is persistence with the high impedance in the Nyquist plots with low Cl^- concentrations (Figure 7.10 (b)). Similarly, the electrochemical results and SEM images show that the passivity of Zn-Ni alloy at immersed in 0.35 mol/l of NaCl and pH = 3.0; and 0.50 mol/l of NaCl and pH = 7.0 are easily damaged due to the higher Cl^- concentration, low pH and pitting corrosion is initiated.

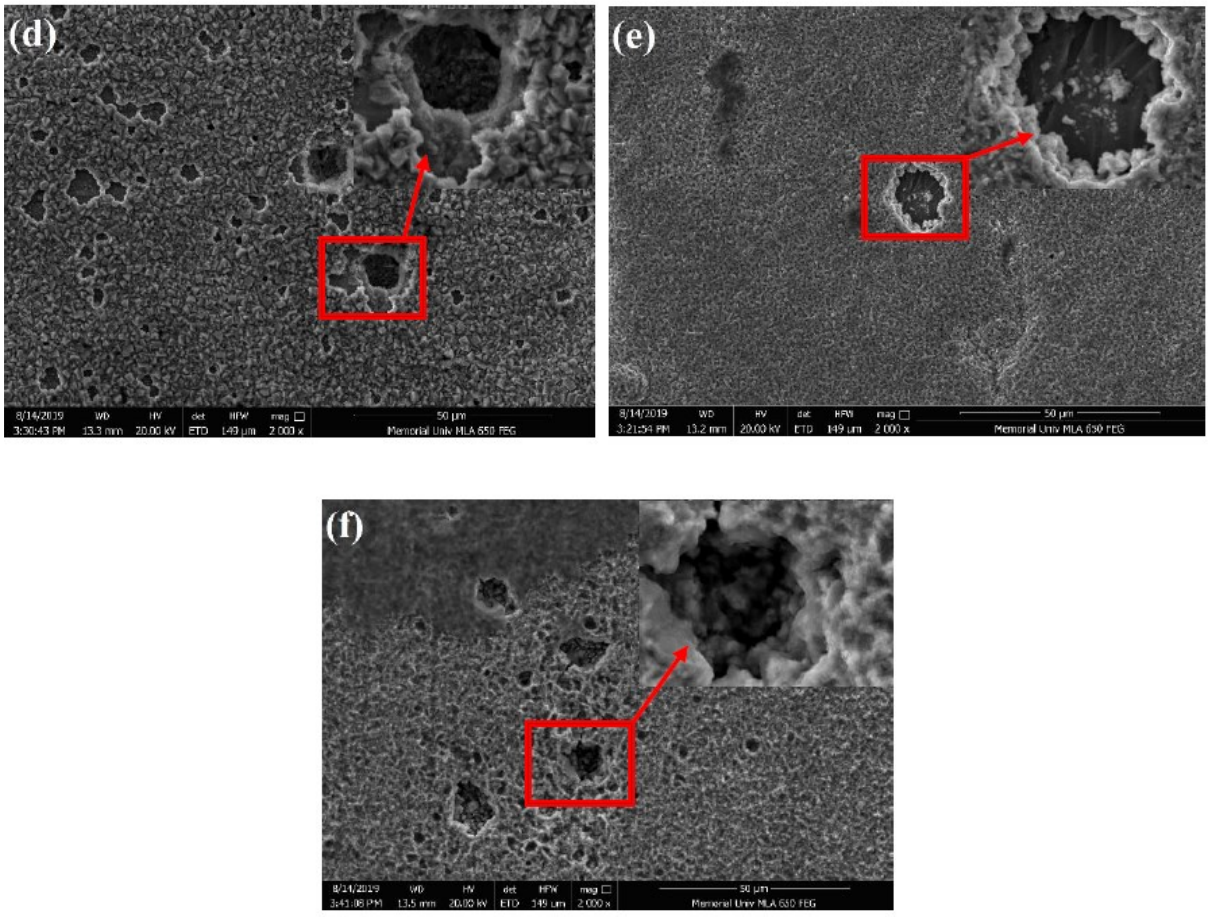

Figure 7.3 Pitting morphology of the corroded surface of (d) 0.35 mol/l of NaCl and pH = 3.0, (e) 0.35 mol/l of NaCl and pH = 7.0 and (f) 0.50 mol/l of NaCl and pH = 7.0 immersed at 4 hours (oxide layer removed in an ultrasonic bath)

Figure 7.4 (g), (h) and (i) of samples immersed at 6 hours respectively, the pits formed in the acidic solution with 0.35 mol/l of NaCl solution and neutral solution with 0.5 mol/l of NaCl concentration have many larger pits with the diameter in the range of 80 – 100 μm are observed in comparison to the pits formed from neutral solution with 0.35 mol/l of NaCl solution. The

similar result has been discussed by Wang et al. [14], Wint et al. [18], and Miao et al. [12]. In a solution with higher Cl^- concentration (0.5 mol/l of NaCl) have more intense pitting corrosion with larger pit growth. The impedance spectroscopy of the neutral solution with higher 0.5 mol/l of NaCl concentration as confirmed through SEM images is persistence with the high impedance in the Nyquist plots due to the formation of corrosion products (Figure 7.10 (c)). Afterward, corrosion product layer on Zn-Ni alloy from 0.50 mol/l of NaCl and pH = 7.0 is easily damaged due to the higher Cl^- concentration and the impedance value is decreased in comparison to the 0.35 mol/l of NaCl and pH = 7.0 samples.

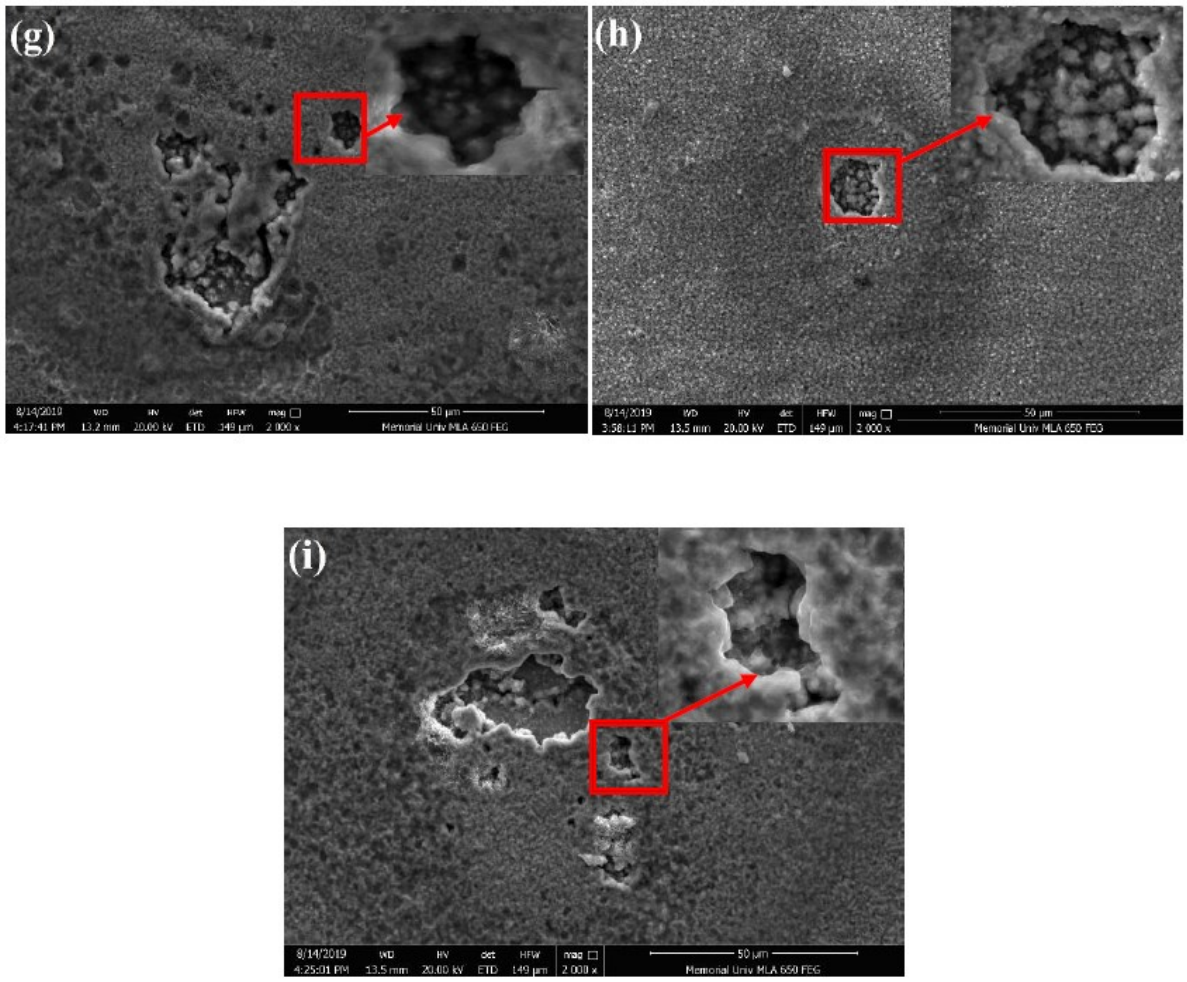

Figure 7.4 Pitting morphology of the corroded surface of (g) 0.35 mol/l of NaCl and pH = 3.0, (h) 0.35 mol/l of NaCl and pH = 7.0 and (i) 0.50 mol/l of NaCl and pH = 7.0 immersed at 6 hours (oxide layer removed in an ultrasonic bath)

Figure 7.5 (j), (k), and (l) samples immersed at 8 hours respectively, the pits formed in the acidic solution with 0.35 mol/l of NaCl solution have larger pits with the diameter in the range of 100 – 120 µm are observed in comparison to the pits formed from neutral solution with 0.35 mol/l of NaCl solution. When the Cl^- concentration is high, the pitting corrosion is more intense and denser on the sample surface where the developed pits covered by the plenty of corrosion products as shown in Figure 7.6 (l). Thus, the pit depth is small, and micro-crevice can form between the corrosion products and coated samples and heterogenous texture with many holes are observed.

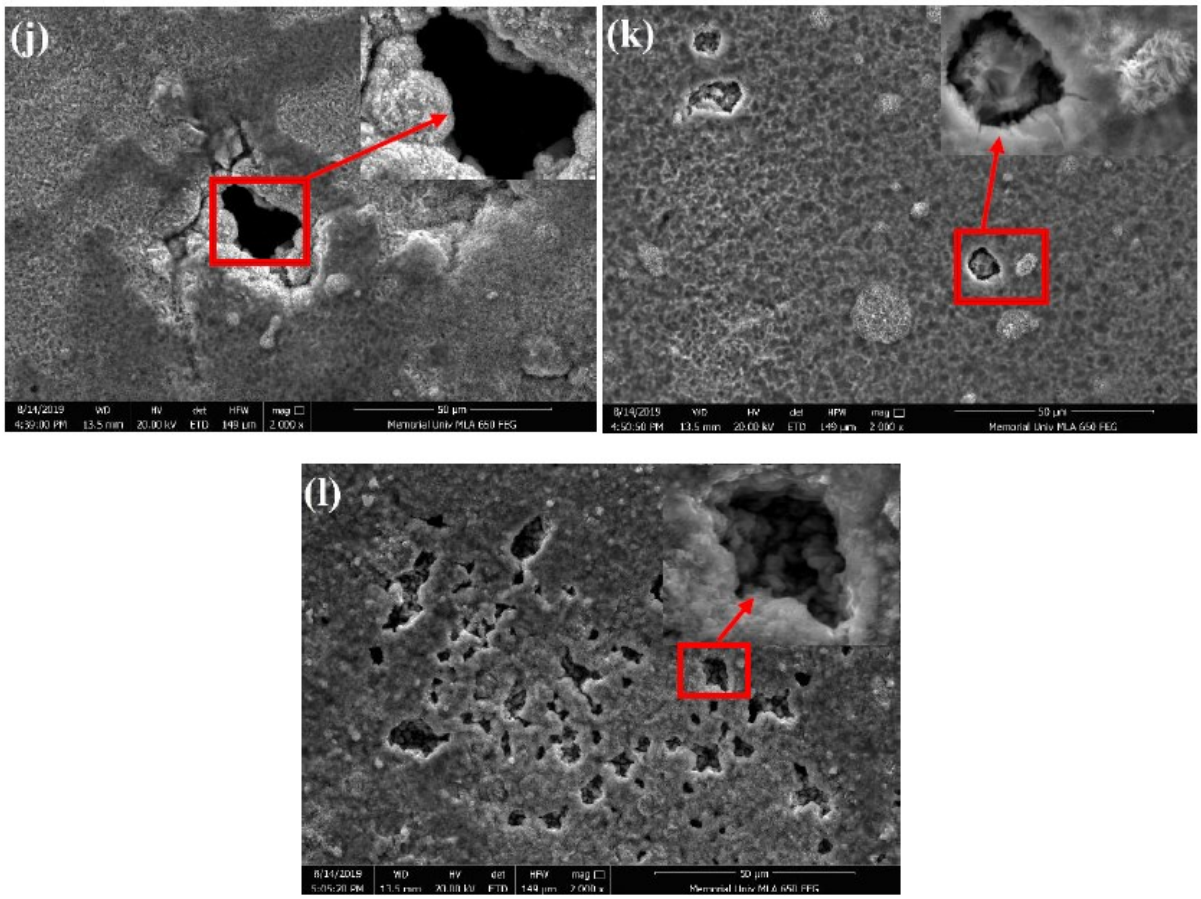

Figure 7.5 Pitting morphology of the corroded surface of (j) 0.35 mol/l of NaCl and pH = 3.0, (k) 0.35 mol/l of NaCl and pH = 7.0 and (l) 0.50 mol/l of NaCl and pH = 7.0 immersed at 8 hours (oxide layer removed in an ultrasonic bath)

The authors have also measured the corrosion pits depth by using an optical microscope. Figure 7.6 (a) and (b) shows the 2D image of the large pit which can be considered as the typical morphology of a fully developed pit. The corresponding cross-sectional profile of the giant pit of runs 7 and 8 is an acidic and neutral solution with low and high NaCl concentration are shown in Figure 7.6 (a') and (b'). As it can be seen from Figure 7.6 (a') and (b') that there is a difference between the pit depth and diameter of 0.35 mol/l of NaCl and pH = 3.0, and 0.35 mol/l of NaCl and pH = 7.0, samples in 8 hours immersion tests. The pit depth of samples in acidic medium (pH = 3.0) and low NaCl concentration (0.35 mol/l) have around 9 μm whereas, the samples in neutral medium (pH = 7.0) and low NaCl concentration (0.35 mol/l) have around 3 μm. In this way, the horizontal and vertical propagation process of pits in acidic solution is demonstrated. Similar large pits phenomenon has been reported by Tsutsumi [20] and Wang et al. [14] for the pitting corrosion of 304 stainless steel and high strength pipeline under the simulated chloride solution. More active corrosion products and low pH can also enhance the pit depth [21][22]. Since large pits formation is observed only in low pH solutions, it is concluded that the pH of the solution plays an active role in the propagation of the pits. A similar result has been stated by Wint et al [18].

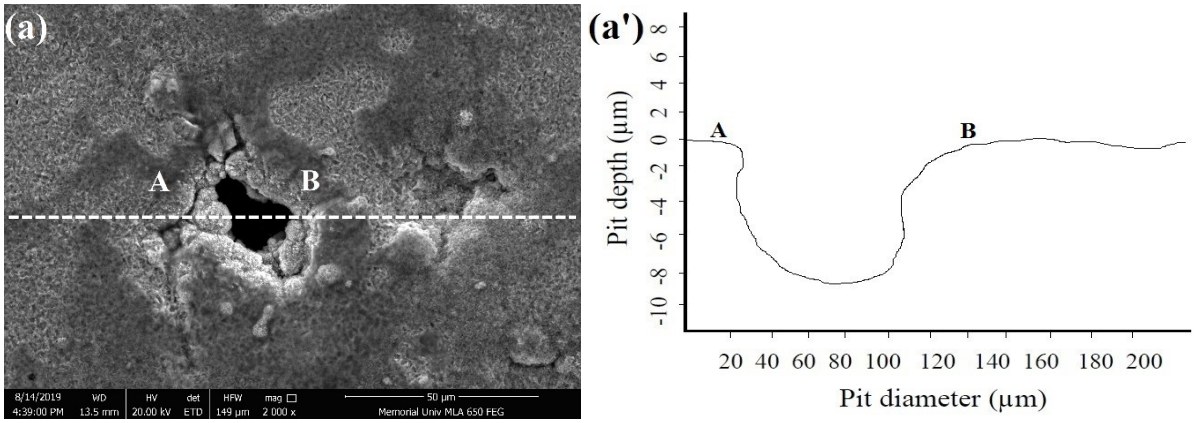

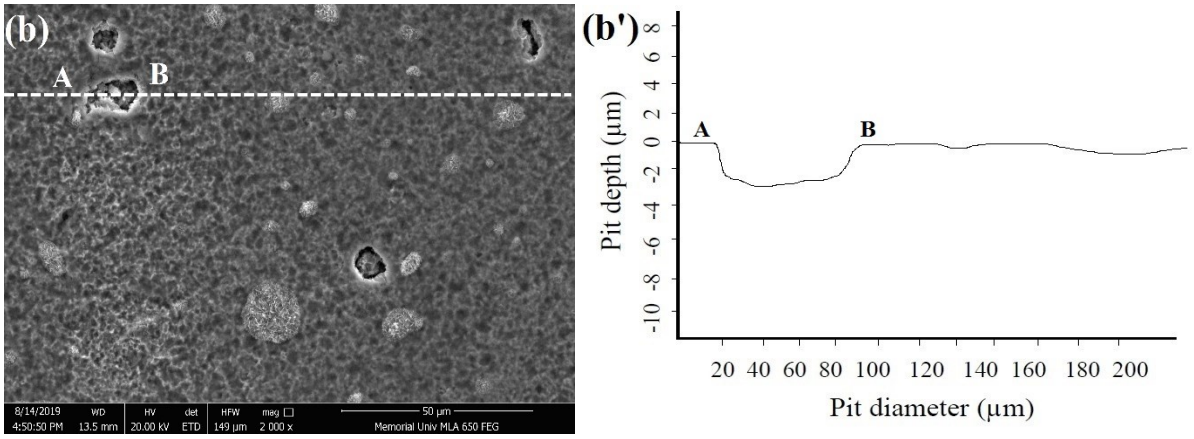

Figure 7.6 2D images of a pits immersed at 8 hours for (a) 0.35 mol/l of NaCl and pH = 3.0, (b) 0.35 mol/l of NaCl and pH = 7, and fully developed pitting depth cross section profiles for (a') 0.35 mol/l of NaCl and pH = 3.0 and (b') 0.35 mol/l of NaCl and pH = 7.

The mechanism of the pitting corrosion process is proposed as follows:

At the initial stage of the pitting, the metastable pits formed which is smaller in size and after some time it will either re-passivate or pits keep propagate. At the beginning of the propagation, the wall of the small pits are the anodic sites on which the metal dissolution occurs. Afterwards, Cl^- ions migrate from the corrosive electrolyte into the pits region to keep the electric neutrality of the corrosion process. Therefore, the Cl^- ions slowly gathered around the anodic sites of the pits, at which the chloride concentration is high on the pit mouth. A portion of the Cl^- ions may form a salt layer with the Zn^{+2} ions while the remaining diffuse away. The Cl^- ions passed in the horizontal direction influenced with chloride concentration difference and the places where the Cl^- ions reach will instantly become an anodic site due to the low pH (pH < 5.0) of the solution (Figure 7.8 (a)). The diffusion of Cl^- ions toward all directions from the pit mouth gives a reasonable explanation for the exceptionally regular shape of the large pits and pits keep growing. When the concentration of Cl^- ions is high then it formed more intense pits on the Zn-Ni coated surface, however, the pits are covered by the immense amount of the corrosion products. Zn^{+2} ions diffused and moved close to the cathodic sites precipitated as zinc oxides (ZnO), hydroxides ($Zn(OH)_2$) and simonkolleite $Zn_5(OH)_8Cl_2.H_2O$ [23]. (corroded

area on Figure 7.7 (b)). The suggested pitting mechanism has been reported and illustrated from Miao et al. [12], and reactions is determined in Figure 7.7.

$$Zn + OH^- \longrightarrow Zn(OH) + e^- \quad (1)$$

$$Zn(OH) + 2OH^- \longrightarrow Zn(OH)_3^- + e^- \quad (2)$$

$$Zn(OH)_3^- + OH^- \longrightarrow Zn(OH)_4^{2-} \quad (3)$$

$$Zn(OH)_4^{2-} \longrightarrow Zn(OH)_2 + 2OH^- \quad (4)$$

$$Zn + 2OH^- \longrightarrow Zn(OH)_2 + e^- \quad (5)$$

$$Zn + 2OH^- \longrightarrow ZnO + H_2O + 2e^- \quad (6)$$

$$Zn + Cl^- + H_2O \longrightarrow Zn(OH)Cl + H^+ + 2e^- \quad (7)$$

$$Zn(OH)Cl + Cl^- + H_2O \longrightarrow Zn_5(OH)_8Cl_2 \quad (8)$$

Where, Zn(OH) presumed to be absorbed on the Zn-Ni coated surface and equation (2) is the rate-determining step. The zinc hydroxide and zinc oxide has been proposed to be the passive film on the specimen surface. The numerous species i.e. Zn^{+2}, $ZnCl^+$, $Zn(OH)^+$, ZnO and $Zn_5(OH)_8Cl_2$ may exist under present experimental conditions; however, it is reported from [24] [12] and it could be the formation a multilayer structure of passive layer on the cathode surface.

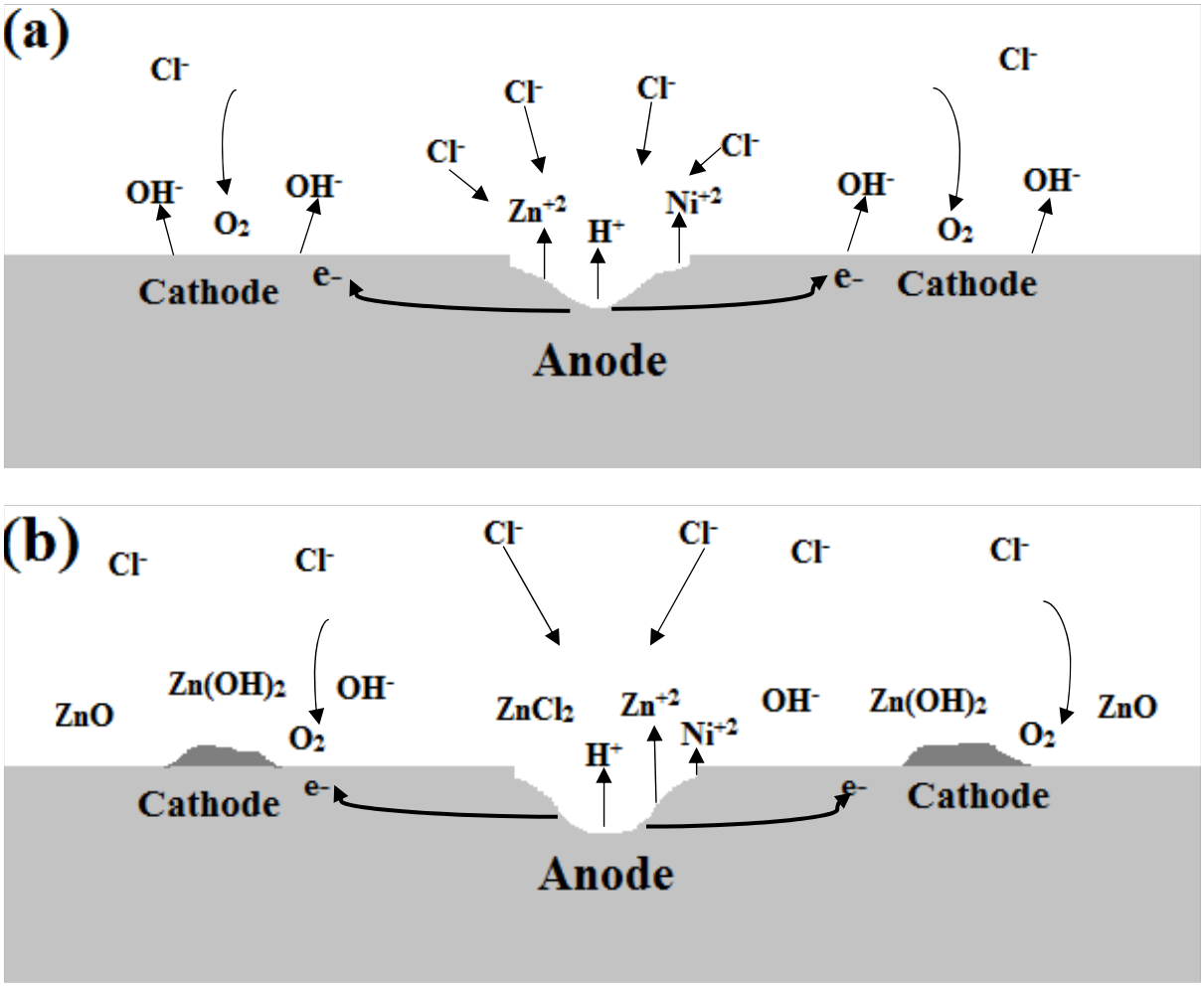

Figure 7.7 Schematic diagram for the Zn-Ni alloy pitting corrosion mechanism under electrolyte (a) migration of Cl^- towards anodic sites and (b) migration and diffusion of metal ions into metal oxide and hydroxide

Energy dispersive spectroscopy (EDS) analysis was used to measure the composition of corrosion products and it shows that the passive layers contain zinc (Zn), nickel (Ni), carbon (C), oxygen (O) and chlorine (Cl) on the Zn-Ni coated samples which is consistent with the formation of zinc oxide (ZnO), zinc hydroxide ($Zn(OH)_2$), simonkolleite $Zn_5(OH)_8Cl_2.H_2O$ [23][12]. The formation of corrosion products for the samples immersed in 0.35 mol/l of NaCl and pH = 3.0; 0.35 mol/l of NaCl and pH = 7.0; and 0.50 mol/l of NaCl and pH = 7.0 at 2, 4, 6, and 8 hours are shown in Table 7.6. The Zn-Ni deposits of run 8 at 2 hours of immersion

tests have the highest percentage of Zn contents (92.80) on the coating in comparison to the other immersed samples leads to decrease the corrosion rate of the coated samples. The sample with 4 hours of immersion shows significant amount of C, O, and Cl contents on the coated surface. The immersion time increase leads to increased C, O, and Cl contents. Moreover, it is observed that corrosion products film covered the coated surface after 2 hours of immersion time. It should be noted as well that the thickness of the corrosion product layer is increased as the immersion time increases. The increasing oxygen and chlorine contents on the coated surface is an evidence of the corrosion and reducing the Zn and Ni contents in the deposits. Afterward, increasing the chloride concentration and low pH lead to break the layer and increase the corrosion rate with increasing the pit growth.

Table 7.7. Chemical composition of the corrosion products immersed at 2, 4, 6 and 8 hours of 0.35 mol/l of NaCl and pH = 3.0, 0.35 mol/l of NaCl and pH = 7.0, and 0.50 mol/l of NaCl and pH = 7.0

Samples immersed at	**Composition (at%)**					
	Immersion time (h)	Zn	Ni	C	O	Cl
0.35 mol/l of NaCl and pH = 3.0 (run 7)	2	92.20	3.13	1.89	1.50	1.28
	4	89.50	2.83	3.09	3.08	1.50
	6	87.24	2.13	4.06	4.56	2.01
	8	82.25	2.09	4.82	8.01	2.84
0.35 mol/l of NaCl and pH = 7.0 (run 8)	2	92.80	2.29	1.90	1.99	1.01
	4	86.46	2.25	4.47	4.65	2.16
	6	80.25	2.28	6.01	8.72	2.75
	8	78.58	2.39	6.65	9.07	3.31
	2	89.73	3.16	2.71	3.22	1.18
	4	87.08	3.08	3.61	4.03	2.20

0.50 mol/l of NaCl	6	85.06	2.88	4.60	4.80	2.66
and	8	79.06	1.98	6.03	10.23	3.10
pH = 7.0 (run 9)						

7.6 Open Circuit Potentials (OCP)

Open Circuit potential (OCP) of 0.35 mol/l of NaCl and pH = 3.0 (run 7); 0.35 mol/l of NaCl and pH = 7.0 (run 8); and 0.50 mol/l of NaCl and pH = 7.0 (run 9) at 8 hours of immersion tests are presented in Figure 7.8. The OCP values are stabilized within 60 minutes, therefore time = 60 minutes is used to compare these three results. It can be seen from Figure 7.9 that OCP values shifts in the negative direction at 0.35 mol/l of NaCl and pH = 7.0, indicating to decrease the corrosion rate. However, the OCP values of 0.50 mol/l of NaCl and pH = 7.0 is shifted towards the positive potentials lead to an increase in the corrosion rate. It implies that that the 0.35 mol/l of NaCl concentration and neutral pH level (pH = 7) has lower corrosion rate in comparison to 0.5 mol/l of NaCl concentration and neutral pH level (pH = 7) of the electrolyte.

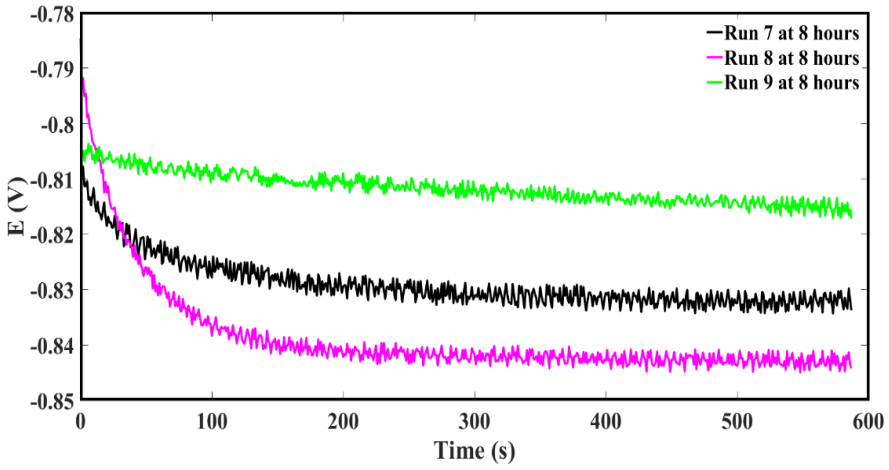

Figure 7.8 Open circuit potential (OCP) of 0.35 mol/l of NaCl and pH = 3.0 (run 7); 0.35 mol/l of NaCl and pH = 7.0 (run 8); and 0.50 mol/l of NaCl and pH = 7.0 (run 9) at 8 hours of the immersion tests

7.7 Potentiodynamic Polarization and Impedance Spectroscopy

The potentiodynamic polarization of the samples immersed in 0.35 mol/l of NaCl and pH = 3.0 (run 7); 0.35 mol/l of NaCl and pH = 7.0 (run 8); and 0.50 mol/l of NaCl and pH = 7.0 (run 9) at 8 hours are shown in Figure 7.9. It can be seen that the corrosion potentials shift towards the negative direction of the potential axis and anodic current density decreases for run 8, which concluded that the corrosion rate decreased by reducing the acidity of the solution (0.35 mol/l of NaCl concentration and neutral pH level (pH = 7)).

It can be seen from Figure 7.11 that the critical potential exists for each plot at which the current density increases rapidly. Most studies on pitting corrosion emphasis on metals and alloys that will be spontaneously passivated or under anodic polarization such as aluminum immersed in NaCl solution [25][26][27], stainless steel in NaCl solution [28][29][30] and carbon steel in $NaHCO_3$/NaCl environment[31][14]. The critical potential is also known as the pitting potential (E_{pit}). E_{pit} is stated as the potential at which the anodic current density increases abruptly[32]. The anodic current density increases seemingly above E_{pit} and pitting corrosion only occurs at the above E_{pit} potential, lead to the breakdown of the passive layer on the Zn-Ni surface. The E_{pit} of run 7 increases by reducing the pH of the solution (pH = 3.0). A similar result has been reported by Miao et al. [12]. However, the E_{pit} in the neutral solution (pH = 7.0) decline vary slightly, as shown in Figure 7.9. When the Cl^- concentration is increased from 0.35 mol/l to 0.5 mol/l lead to abruptly increase the anodic corrosion current due to the attack of Cl^- ions, increases the corrosion rate. The analogous result has been reported by Wang et al. [14].

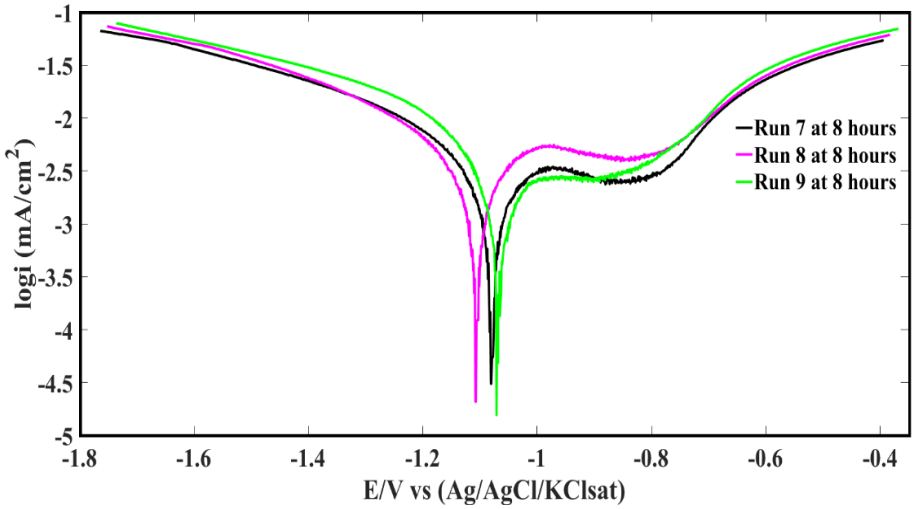

Figure 7.9 Potentiodynamic polarization of 0.35 mol/l of NaCl and pH = 3.0 (run 7); 0.35 mol/l of NaCl and pH = 7.0 (run 8); and 0.50 mol/l of NaCl and pH = 7.0 (run 9) at 8 hours of immersion tests

7.8 Electrochemical Impedance Spectroscopy (EIS) analysis

The results of the electrochemical impedance spectroscopy (EIS) tests on the 0.35 mol/l of NaCl and pH = 3.0 (run 7); 0.35 mol/l of NaCl and pH = 7.0 (run 8); and 0.50 mol/l of NaCl and pH = 7.0 (run 9) immersed samples are presented in Figure 7.10. The time evolution of impedance characteristics at 2, 4, 6, and 8 hours of immersion tests are shown in Figure 7.10 (a), (b), (c) and (d). As can be seen, the Nyquist diagram of run 8 at 2 hours of immersion tests have a bigger radius of the semi-circular arc of the impedance values in comparison to the other plots (Figure 7.10 (a)) led to decrease the corrosion rate. As the pH of the solution reduces to the acidic region (run 7) and Cl^- concentration of the solution increases to 0.5 mol/l (run 9) led to increasing the corrosion rate of the coated samples.

Figure 7.10 (b) shows the analogous characteristics at 4 hours of the immersion tests, run 8 at 4 hours of the immersion reported highest radius of the semi-circular arc led to increasing the impedance modulus values in comparison to the run 7 and 9 samples. Figure 7.10 (c) demonstrated the dissimilar behavior at 6 hours of the immersion tests, run order 8 shown depressed semi-circular arc at the high-frequency zone. However, the radius of the semi-

circular arc is decreased at the lower frequency zone due to the higher concentration of Cl^- ions (run 9), indicating accelerated corrosion rate caused by the addition of Cl^- ions.

Figure 7.10 (d) indicates that the similar characteristics at 8 hours of the immersion tests, run 8 at 8 hours of the immersion shows the highest radius of the semi-circular arc in comparison to the run 7 and 9 samples. However, run 7 sample radius of the semi-circular arc is increased at the lower frequency zone due to the enhanced concentration of Cl^- ions (run 9), indicating accelerated corrosion rate caused by the addition of Cl^- ions.

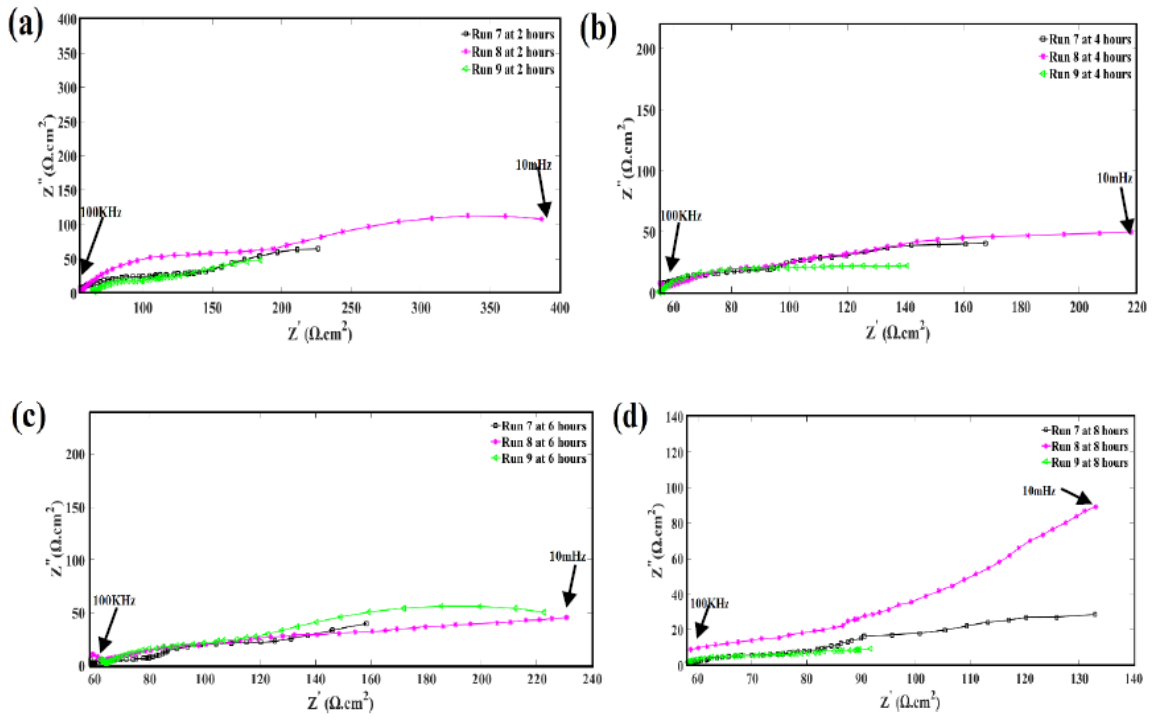

Figure 7.10 Nyquist plots for the Zn-Ni alloy coated samples immersed in (a) the 0.35 mol/l of NaCl and pH = 3.0 (run 7), 0.35 mol/l of NaCl and pH = 7.0 (run 8), and 0.50 mol/l of NaCl and pH = 7.0 (run 9) at 2 hours; (b) run, 7, 8 and 9 at 4 hours; (c) run, 7, 8 and 9 at 6 hours; and (d) run, 7, 8 and 9 at 8 hours.

The shape analysis of the impedance spectroscopy with the fitted electrical alternative circuit data assists in identifying the complete electrochemical activity exists on the coated surface when it contacts with the corrosive environment. However, the shape of the spectroscopy is significantly persuaded by the electrochemical process at the surface and by the geometric components of the working electrode [33][34]. The obtained EIS results are fitted with the

electrical equivalent circuit R(CR)(C[R(CR)]), and the circuit diagram is shown in Figure 7.11. The authors have fit the experimental impedance spectroscopy data (Nyquist plots) to the various arrangements of resistors (R) and the constant phase element (C). The equivalent circuit comprehend to address three capacitive loops in the impedance spectroscopy. It was demonstrated that the electrical equivalent circuit selected in this research work was the best fit for all the generated plots and the parameter results produced from the fit were regularly changing for the progress of the electrochemical systems. The generated results of the fits are shown in Table 7.7. R_s represents the salt solution resistance between the reference electrode and the working electrode. The (C_1R_1) corresponds the electrical properties for the formation of naturally occurring passive layer on the surface of Zn-Ni alloy coatings. R_2 represents the electrolyte resistance in pores and defects of the corrosion products and, C_2 is their capacitance. Lastly, R_3 represents charge transfer resistance of the anodic corrosion reaction occurring at the surface of Zn-Ni alloy coating and C_3 corresponds to the electrical double layer capacitance of the Zn-Ni alloy coatings surface.

Meng et a.l [23] reported the formation of corrosion products in a 0.9% NaCl solution on pure Zn coating and identified that there is a transition impedance response that can be fitted by using R(CR)(CR) electrical equivalent circuit to an R(C[R(CR)]) circuit when the immersion time is increased till 48 hours. To validate the selected electrical equivalent circuit is reasonably appropriate, the author has also calculated the double layer pseudocapacitance according to the formula proposed by Brug et al.[35].

$$C_{dl} = C_3^{\frac{1}{n3}} \left(\frac{1}{R_s} + \frac{1}{R_3}\right) \qquad (3)$$

By using the equation (3), it can be seen that the values of C_{dl} for all the samples immersed at different conditions are in μFcm^2 and it shows that the electrical equivalent circuit fitting data seem to be adequate.

The R_1 values of run 7 samples are increasing from 2 to 6 hours of the immersion tests lead to an increase in the passive layer on the specimen. At 8 hours of immersion, the R_1 value decrease due to the destruction of the passive layer by the growth of corrosion products. Similarly, for run 8 samples, the R_1 values increased until 4 hours of the immersion tests and then decreased due to the damage of the passive layer. For the run 9 samples the R_1 values at 2 hours of immersion tests is high; however, as the immersion time increase lead to a decrease in the passive layer strength on the coated surface.

The R_2 values of run 7 samples are decreasing as the immersion time increases lead to penetrating the electrolyte on the pores and defects of the corrosion product. However, for run 8 and 9 the electrolyte resistance increases until 4 hours of the immersion tests and then it decreases due to the accumulation of white rust on the sample and the limitation of surface availability for the penetration of electrolyte. The R_3 values of run 7 samples is quite stable throughout the immersion tests due to the formation of uniform, denser, and compact corrosion product layers. This behavior is related to the decrease in the corrosion rate on the coated surface. The similar action has been seen for all the coated samples exhibits the same behavior reported by Maciej et al. [36].

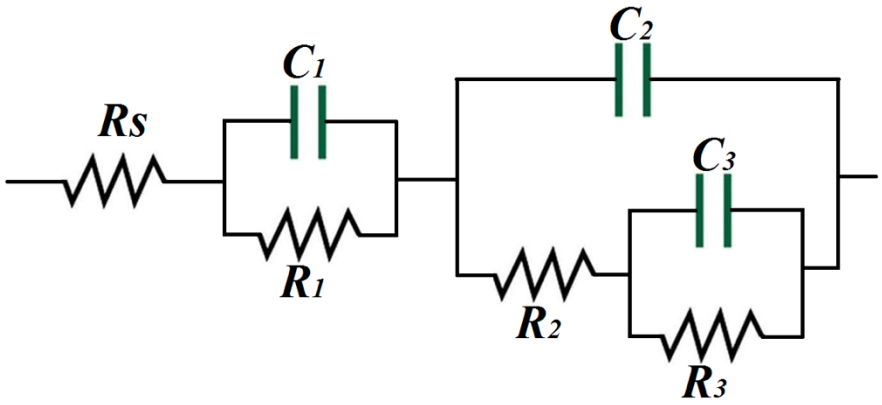

Figure 7.11 The electrical equivalent circuit used for the electrochemical impedance spectroscopy analysis

Table 7.8. Electrochemical impedance spectroscopy fitting results the electrical equivalent circuit from Figure. 13 of the Zn-Ni alloy coating immersed at 2, 4, 6 and 8 hours of the 0.35 mol/; of NaCl and pH = 3.0 (run 7), 0.35 mol/l of NaCl and pH = 7.0 (run 8) and 0.50 mol/l of NaCl and pH = 7.0 (run 9)

Zn-Ni samples Immersed at	Immersion time (hours)	R_s (Ωcm^2)	R_1 (Ωcm^2)	C_1 ($s^{-n}{}_2$. Ωcm^2)	n_1	R_2 (Ωcm^2)	C_2 ($s^{-n}{}_2$. Ωcm^2)	n_2	R_3 (Ωcm^2)	C_3 ($s^{-n}{}_2$. Ωcm^2)	n_3
	2	49.1	15.8	13.1	0.85	106.2	25.5	0.50	284.5	8.6	0.62
0.35 mol/l	4	31.9	74.4	18.6	0.74	104.4	41.5	0.55	235.1	5.3	0.57
of NaCl	6	36.1	81.0	58.6	0.56	50.1	44.3	0.65	203.7	9.6	0.77
and pH =	8	30.1	60.0	70.1	0.64	41.1	48.1	0.78	190.1	11.2	0.62
3.0 (run 7)											
	2	17.0	40.8	17.3	0.80	44.2	36.8	0.55	489.7	2.0	0.71
0.35 mol/l	4	34.7	72.8	66.7	0.77	57.4	15.1	0.67	409.5	6.6	0.67
of NaCl	6	24.8	39.3	95.3	0.60	39.2	21.8	0.78	394.7	3.8	0.56
and pH =	8	14.5	29.3	98.5	0.78	25.5	32.8	0.66	175.1	7.8	0.77
7.0 (run 8)											
	2	50.2	73.6	113.1	0.75	50.3	102.7	0.50	283.1	5.1	0.40
0.50 mol/l	4	53.4	16.8	119.3	0.60	64.4	145.8	0.40	189.3	11.0	0.55
of NaCl	6	55.3	10.2	113.1	0.78	32.2	141.8	0.60	295.1	8.0	0.34
and pH =	8	45.5	9.07	118.1	0.88	20.1	145.1	0.75	125.5	12.0	0.66
7.0 (run 9)											

7.9 Conclusions

The important deposition factors and levels influencing the pitting corrosion activity of the Zn-Ni alloy deposits are NaCl concentration and pH of the electrolyte. The pit depth of samples immersed in acidic medium (pH = 3.0) and low NaCl concentration (0.35 mol/l) have around 9 μm whereas, for samples in neutral medium (pH = 7.0) and low NaCl concentration (0.35 mol/l) have around 3 μm. In this way, the horizontal and vertical propagation process of pits in

acidic solution is demonstrated. The samples immersed at 0.35 mol/l of NaCl and pH = 3.0 solution has higher E_{pit} values. However, the E_{pit} in the neutral solution (pH = 7.0) decline very slightly. When the Cl^- concentration is increased from 0.35 mol/l to 0.5 mol/l lead to abruptly increase the anodic corrosion current due to the attack of Cl^- ions increases the corrosion rate. The pitting corrosion in neutral solution as confirmed through SEM images is persistence with the high impedance in the Nyquist plots with low Cl^- concentrations. The electrochemical results and SEM images show that the passivity of Zn-Ni alloy from low to high NaCl concentration and neutral to acidic pH solutions are easily damaged and pitting corrosion is initiated in the presence of acidic solution and higher Cl^- ions.

Acknowledgments

The authors thankfully acknowledge the financial support provided by the Natural Science and Engineering Council of Canada (NSERC) and the Canada Research Chair (CRC) Tier I Program.

References

[1] M. Fischer, "Possible models of the reaction mechanism of the function of passivating additions during the chemical passivation of iron in weakly acid, neutral and basic pH ranges," Werkst. Korros., vol. 29, p. 188, 1978.

[2] G. S. Frankel, "Pitting Corrosion of Metals," J. Electrochem. Soc., vol. 145, no. 6, p. 2186, 1998.

[3] R. C. Newman and W. R. Whitney, "understanding the corrosion of stainless steel," Corrosion, vol. 57, pp. 1030–1041, 2001.

[4] H. B. Li, J. Z.H., C. Y., and Z. R. Zhang, "Fabrication of high nitrogen austenitic stainless steels with excellent mechanical and pitting corrosion properties," J. Met. Mater., vol. 16, pp. 517–524, 2009.

[5] Y. Kim and R. G. Buchheit, “A characterization of the inhibiting effect of Cu on metastable pitting in dilute Al-Cu solid solution alloys,” Electrochim. Acta, vol. 52, no. 7, pp. 2437–2446, 2007.

[6] O. S. I. Fayomi and A. P. I. Popoola, “An Investigation of the Properties of Zn Coated Mild Steel,” Int. J. Electrochem. Sci, vol. 7, pp. 6555–6570, 2012.

[7] R. Fratesi, G. Roventi, G. Giuliani, and C. R. Tomachuk, “Zinc-cobalt alloy electrodeposition from chloride baths,” J. Appl. Electrochem., vol. 27, no. 9, pp. 1088–1094, 1997.

[8] V. G. Roev, R. A. Kaidrikov, and A. B. Khakimullin, “Zinc – Nickel Electroplating from Alkaline Electrolytes Containing Amino Compounds,” vol. 37, no. 7, pp. 756–759, 2001.

[9] D. Blejan, D. Bogdan, M. Pop, A. V. Pop, and L. M. Muresan, “Structure, morphology and corrosion resistance of Zn-Ni-TiO_2 composite coatings,” Optoelectron. Adv. Mater. Commun., vol. 5, no. 1, pp. 25–29, 2011.

[10] I. H. Karahan and H. S. Güder, “Electrodeposition and properties of Zn, Zn–Ni, Zn–Fe and Zn–Fe–Ni alloys from acidic chloride–sulphate electrolytes,” Trans. IMF, vol. 87, no. 3, pp. 155–158, 2009.

[11] T. Jin, W. Zhang, N. Li, X. Liu, L. Han, and W. Dai, “Surface characterization and corrosion behavior of 90/10 copper-nickel alloy in marine environment,” Materials (Basel)., vol. 12, no. 11, 2019.

[12] W. Miao, I. S. Cole, A. K. Neufeld, and S. Furman, “Pitting Corrosion of Zn and Zn-Al Coated Steels in pH 2 to 12 NaCl Solutions,” 2007.

[13] K. R. Sriraman, S. Brahimi, J. A. Szpunar, J. H. Osborne, and S. Yue, “Characterization of corrosion resistance of electrodeposited Zn-Ni Zn and Cd coatings,” Electrochim. Acta, vol. 105, pp. 314–323, 2013.

[14] Y. Wang, G. Cheng, W. Wu, Q. Qiao, Y. Li, and X. Li, “Effect of pH and chloride on the micro-mechanism of pitting corrosion for high strength pipeline steel in aerated NaCl solutions,” Appl. Surf. Sci., vol. 349, pp. 746–756, 2015.

[15] Y. Wang, G. Cheng, and Y. Li, “Observation of the pitting corrosion and uniform corrosion for X80 steel in 3.5 wt.% NaCl solutions using in-situ and 3-D measuring microscope,” Corros. Sci., vol. 111, pp. 508–517, 2016.

[16] W. Tian, N. Du, S. Li, S. Chen, and Q. Wu, “Metastable pitting corrosion of 304 stainless steel in 3.5% NaCl solution,” Corros. Sci., vol. 85, pp. 372–379, 2014.

[17] Shams Anwar, Yahui Zhang, Faisal Khan, and Susan Caines, “Optimization of Zinc-Nickel Film Electrodeposition for Better Corrosion Resistant Characteristics,” Can. J. Chem. Eng., pp. 1–14, 2019.

[18] N. Wint, “Concentration Effects on the Spatial Interaction of Corrosion Pits Occurring on Zinc in Dilute Aqueous Sodium Chloride,” vol. 166, no. 11, pp. 3028–3038, 2019.

[19] Shams Anwar, Yahui Zhang, Faisal Khan, and Susan Caines, “Optimization of Zinc-Nickel Film Electrodeposition for Better Corrosion Resistant Characteristics,” Can. J. Chem. Eng.

[20] Y. Tsutsumi, A. Nishikata, and T. Tsuru, “Pitting corrosion mechanism of Type 304 stainless steel under a droplet of chloride solutions,” Corros. Sci., vol. 49, no. 3, pp. 1394–1407, 2007.

[21] R. P. Vera Cruz, A. Nishikata, and T. Tsuru, “Pitting corrosion mechanism of stainless steels under wet-dry exposure in chloride-containing environments,” Corros. Sci., vol. 40, no. 1, pp. 125–139, 1998.

[22] S. Hastuty, A. Nishikata, and T. Tsuru, “Pitting corrosion of Type 430 stainless steel under chloride solution droplet,” Corros. Sci., vol. 52, no. 6, pp. 2035–2043, 2010.

[23] Y. Meng et al., “Initial formation of corrosion products on pure zinc in saline solution,”

Bioact. Mater., vol. 4, no. 1, pp. 87–96, 2019.

[24] P. Marcus and J.-M. Herbelin, “The entry of chloride ions into passive films on nickel studied by spectroscopic (ESCA) and nuclear (36Cl radiotracer) methods,” Corros. Sci., vol. 34, no. 7, pp. 1123–1145, 1993.

[25] H. Böhni and H. H. Uhlig, “Environmental factors affecting the critical pitting potenial of aluminum,” J. Electrochem. Soc., pp. 906–910, 1969.

[26] I. L. Muller and J. R. Galvele, “Pitting potential of high purity binary aluminium alloys—II. Al Mg and Al Zn alloys,” Corros. Sci., vol. 17, pp. 995–1007, 1977.

[27] P. Chong, Z. Liu, P. Skeldon, and G. Thompson, “Large area laser surface treatment of aluminium alloys for pitting corrosion protection,” Appl. Surf. Sci., vol. 208, pp. 399–404, 2003.

[28] H. Leckie and H. Uhlig, “Environmental factors affecting the critical potential for pitting in 18–8 stainless steel,” J. Electrochem. Soc., vol. 113, pp. 1262–1267., 1966.

[29] M. Srivastava, A. Srinivasan, and V. K. William Grips, “Influence of Zirconia Incorporation on the Mechanical and Chemical Properties of Ni-Co Alloys,” Am. J. Mater. Sci., vol. 1, no. 2, pp. 113–122, 2012.

[30] S. A. M. Refaey, F. Taha, and A. M. A. El-Malak, “Inhibition of stainless steel pitting corrosion in acidic medium by 2-mercaptobenzoxazole,” Appl. Surf. Sci., vol. 236, pp. 175–185., 2004.

[31] Y. F. Cheng and J. L. Luo, “A comparison of the pitting susceptibility and semiconducting properties of the passive films on carbon steel in chromate and bicarbonate solutions,” Appl. Surf. Sci., vol. 167, pp. 113–121, 2000.

[32] G. T. Burstein, C. Liu, R. M. Souto, and S. P. Vines, “Origins of pitting corrosion,” Corros. Eng. Sci. Technol., vol. 39, no. 1, pp. 25–30, 2004.

[33] M. K. Punith Kumar, T. V. Venkatesha, M. K. Pavithra, and A. N. Shetty, “A Study on

Corrosion Behavior of Electrodeposited Zn-Rutile TiO $_2$ Composite Coatings," Synth. React. Inorganic, Met. Nano-Metal Chem., vol. 42, no. 10, pp. 1426–1434, 2012.

[34] F. La Mantia, J. Vetter, and P. Novák, "Impedance spectroscopy on porous materials: A general model and application to graphite electrodes of lithium-ion batteries," Electrochim. Acta, vol. 53, no. 12, pp. 4109–4121, 2008.

[35] G. . Brug, A. L. Van Deen Adeen, M. Sluyters-Rehbach, and J. . Sluyters, "The Analysis of the Electrode Impedance Complicated by the presence of a Constant Phase Element," J Electroanal Chem, vol. 176, pp. 275–295, 1984.

[36] A. Maciej et al., "Improvement of corrosion resistance of Zn-Ni alloy coatings by anodizing in selected alcoholic solutions," Corros. Sci., vol. 158, no. July, p. 108107, 2019.

APPENDIX

General Factorial Regression: Pit diameter (μm) at 4 hours versus A, B

Table A.1. Analysis of Variance (ANOVA) for 2^{2-1} FFD

Source	Dfi	SSi	MSi	*F-value	P-value
Model	8	7536	942.0	5.55	0.010
Linear	4	5360	1340.1	7.90	0.005
A	2	3930	1965.1	11.58	0.003
B	2	1430	715.0	4.21	0.051
AB	4	2176	543.9	3.21	0.068
Error	9	1527	169.7		
Total	17	9063			

*R^2 (adj.) = 0.90

The combination of the experimental factors' effect and ANOVA data, a fitted polynomial model with statistical significance can be generated as follows:

Pit diameter (μm) at 4 hours = $52.49 + 20.44\ A_1 - 6.43\ A_2 - 14.00\ A_3 - 3.87\ B_1 + 12.33\ B_2 - 8.45\ B_3 - 0.55\ A_1{*}\ B_1 + 17.22\ A_1{*}\ B_2 - 16.67\ A_1{*}\ B_3 - 4.64\ A_2{*}\ B_1 + 0.03\ A_2{*}\ B_2 + 4.61\ A_2{*}\ B_3 + 5.19\ A_3{*}\ B_1 - 17.25\ A_3{*}\ B_2 + 12.06\ A_3{*}\ B_3$

General Factorial Regression: Pit diameter (μm) at 6 hours versus A, B

Table A.2. Analysis of Variance (ANOVA) for 2^{2-1} FFD

Source	Dfi	SSi	MSi	*F-value	P-value
Model	8	8071	1008.9	4.83	0.015
Linear	4	5206	1301.5	6.23	0.011
A	2	3995	1997.3	9.57	0.006
B	2	1211	605.7	2.90	0.107
AB	4	2865	716.3	3.43	0.058

Error	9	1879	208.8
Total	17	9950	

*R^2 (adj.) = 0.90

The combination of the experimental factors' effect and ANOVA data, a fitted polynomial model with statistical significance can be generated as follows:

Pit diameter (μm) at 6 hours = 59.95 + 19.85 A_1 – 3.81 A_2 – 16.04 A_3 + 0.92 B_1 + 10.47 B_2 – 9.56 B_3 - 2.18A_1* B_1 + 20.95 A_1*B_2 – 18.77 A_1* B_3 + 1.49 A_2*B_1 - 2.97 A_2*B_2 + 1.47 A_2*B_3 + 0.68 A_3*B_1 – 17.98 A_3* B_2 + 17.30 A_3* B_3

General Factorial Regression: Pit diameter (μm) at 8 hours versus A, B

Table A.3. Analysis of Variance (ANOVA) for 2^{2-1} FFD

Source	**Dfi**	**SSi**	**MSi**	***F-value**	**P-value**
Model	8	8074	1009.3	5.92	0.008
Linear	4	3845	961.3	5.63	0.015
A	2	2813	1406.5	8.24	0.009
B	2	1032	516.1	3.03	0.099
AB	4	4229	1057.2	6.20	0.011
Error	9	1536	170.6		
Total	17	9610			

*R^2 (adj.) = 0.95

The combination of the experimental factors' effect and ANOVA data, a fitted polynomial model with statistical significance can be generated as follows:

Pit diameter (μm) at 8 hours = 67.32 + 16.92A_1 – 4.03 A_2 – 12.89 A_3 + 0.20 B_1 + 9.18 B_2 – 9.37 B_3 + 0.35A_1* B_1 + 20.95 A_1* B_2 – 21.30 A_1* B_3 + 1.31 A_2* B_1 + 2.65 A_2* B_2 - 3.96 A_2*B_3 - 1.66 A_3* B_1- 23.60 A_3*B_2 + 25.26 A_3* B_3

8.0 Conclusions and Discussions

8.1 Optimization of Zinc-Nickel Film Electrodeposition for Better Corrosion Resistant Characteristics

In this study, the most important deposition factors influencing the corrosion resistant activity of the Zn-Ni deposits is experimentally designed and divided into four parts (1) a two-level fractional factorial design (FFD), (2) a response surface design the steepest ascent analysis, (3) a central composite design (CCD), and (4) corrosion behaviour test to achieve the optimized factors for Zn-Ni deposition. To analyse the optimized samples in step 4 the following analytical techniques were used (a) Electrochemical Impedance Spectroscopy (EIS) was employed to study the corrosion resistant property of the optimized Zn-Ni alloy coatings, (b) XRD was to analyze the phase compositions in deposit Zn-Ni films and found the relationship between film phase compositions and corrosion resistant properties, (c) SEM was used to analyze the microstructure of the Zn-Ni deposits and its effect on the corrosion resistant properties of the deposits. Moreover, energy dispersive spectroscopy (EDS) is used to measure the corrosion product chemical compositions of the optimized samples. To achieve the corrosion resistance of the optimized Zn-Ni alloy coating are concluded as follows:

The most important deposition factors influencing the corrosion resistant activity of the Zn-Ni deposits are citrate concentration, bath temperature and plating time from the FFD Study. Through the path of the steepest ascent study, the vicinity of the optimal electroplating settings for electroplating the Zn-Ni samples with the minimum activity of corrosion current density (I_{corr}) leads to exhibit better corrosion resistant properties. The optimal settings are Zn/Ni molar concentration ratio = 0.66, electroplating time = 13 minutes, electroplating current density = 60 mA/cm^2 and bath temperature = 28^{0}C and citrate concentration 0.062 mol/l , for the Zn-Ni samples with the with the highest.

1. activity of corrosion surrent density (I_{corr}) obtained by the regression model through CCD coupled with the surface response method.
2. The morphological structure the Zn-Ni deposits at optimum conditions from citrate baths exhibited uniform, compact and dense deposits which is favourable for corrosion resistance. The γ-Ni_2Zn_{11} phase with (330) plane orientation exhibit higher intensity than those of other γ-phases, i.e., γ-$NiZn_3$ and Ni_3Zn_{22}, demonstrating that γ-Ni_2Zn_{11} phase with (330) plane orientation plays an assertive role in the Zn-Ni alloy corrosion resistant coatings. This demonstrates that the co-deposition of different zinc and zinc-nickel phases will help to form a uniform and dense deposit.

8.2 (a) Electrochemical Behavior and Analysis of Zn and Zn-Ni Alloy Anti-Corrosive Coating Deposited from Citrate Baths

In this study, the electrochemical behaviour of pure Zn and Zn-Ni alloy coating from citrate and non-citrate bath and the stability of the electrolyte bath has been studied in this work. According to the above analysis, the following conclusions can be made as follows:

- Stabilized plating baths and complexing agents such as potassium citrate are employed for Zn-Ni alloy electrodeposition. This extends the precipitation of nickel hydroxide ($Ni(OH)_2$), and zinc monoxide ($Zn(OH)_2$) to a higher pH and the hydrogen evolution reaction is suppressed.
- The potentiodynamic polarization results reveal that the sample (b) coating possesses a lower I_{corr} value and more positive corrosion potential than the other two coated samples. The least I_{corr} is due to the stable citrate bath Zn-Ni coated samples with decreased HER, which exhibited uniform and higher corrosion resistance and the SEM images showed the formation of denser and more uniform coating. The phase structure

of the Zn-Ni deposits from citrate bath has the highest intensity of γ-phase (γ-$NiZn_3$) (815), and γ-Ni_2Zn_{11} (330) (631) plane orientation exhibits better corrosion resistance.

- The EIS measurement of the sample (b) deposited from citrate bath shown higher impedance modulus than the other coated samples. Further EIS measurements carried out for the sample (a) and sample (c) deposited from the non-citrate bath showed less impedance modulus in comparison to samples (b). The best coating with the maximum impedance modulus is found at 60 mA/cm^2 for sample (b). The electrical equivalent circuit modelling data best fit the generated Nyquist plot demonstrated that the Zn-Ni alloy coating on steel substrate deposited from citrate bath had maximum coating resistance (R_2) with minimum capacitance (CPE_2). This behaviour indicates that the addition of the complexing agent ($K_3(C_6H_5O_7)$) in a bath is a simple and effective process to improve the corrosion resistance of Zn-Ni alloy coating.
- The higher current density also leads to the reduced grain size and provides less coarse stronger and more uniform coating. The development of film microhardness shows an increase in the hardness from 154 HV for pure Zn (sample (a)) and 223 HV for Zn-Ni coating deposited from non-citrate (sample (c)) to (sample (b)) prepared from citrate bath.

8.2 (b) Electrochemical behavior and pH analysis of Zn-Ni alloy coating deposited from citrate bath

In this study, the electrochemical behavior of Zn-Ni alloy coating from citrate and non-citrate bath at acidic and neutral pH of the bath solution are concluded as follows:

1. The EIS measurement of sample (a) deposited from 0.0326 mol/l of citrate bath at acidic pH shown higher impedance modulus than the non-citrate bath coated samples.
2. The electrical equivalent circuit modelling data best fit the generated Nyquist plot demonstrated that the Zn-Ni alloy coating on steel substrate deposited from citrate bath

had maximum coating resistance (R_2) with minimum capacitance (CPE_2) of 879 Ωcm^2 and 28.2 μFcm^2. This behaviour indicates that the addition of the complexing agent ($K_3(C_6H_5O_7)$) in a bath is a simple and effective process to improve the corrosion resistance of Zn-Ni alloy coating.

3. The equivalent electrical circuits obtained from the experimental fitted data also demonstrated the drastic change in charge transfer (R_1) and polarization resistance (R_2) occurring on the Zn-Ni alloy coated surface deposited from citrate in comparison to a non-citrate bath.
4. The sample (a) Zn-Ni alloy coating at a plating current density equal to 60 mA/cm^2 exhibits smaller and more uniform grain sizes, and no swelling is found on the coatings.
5. The phase structure of the Zn-Ni deposit obtained from an acidic citrate bath having the highest intensity of γ-$NiZn_3$ (815) and γ-Ni_2Zn_{11} (330) (631) planes exhibits better corrosion resistance.

8.3 EDTA stabilized bath for electrodeposition of Zn-Ni alloy coatings and corrosion resistant analysis in 3.5 wt.% NaCl solutions

In this study, Zn-Ni alloy electroplating deposited from EDTA bath at various operating conditions to determine the optimal concentration of EDTA, plating current density, and bath composition are concluded as follows:

1. Potentiodynamic polarization result revealed that the Zn-Ni deposited from 0.119 mol/l of EDTA bath exhibited lowest I_{corr} and more positive E_{corr} values. The least I_{corr} was due to the Zn-Ni coating deposited from a stable EDTA bath with decreased HER, which showed a uniform and better corrosion resistance coating.
2. At 12 hours of immersion test, all samples have lower R_1, C_1, R_{ct}, and C_{dl} values. In contrast, at 24 hours of immersion time, the samples exhibit higher corrosion resistance leads to the formation of strong corrosion product layers.

3. SEM and AFM images showed that the sample (a), Zn-Ni coating from non-EDTA bath had cracks, holes, and non-uniformity on the coating due to the formation and release of hydrogen bubbles. However, Zn-Ni coating from EDTA bath (sample (b) and (c)) increase microhardness and exhibit more uniform grain sizes with γ-Ni_2Zn_{11} plane orientation and no holes are found on the coatings due to the stability of the bath solution and the occurrence of less hydrogen evolution reactions.

8.4 Corrosion Behavior of Zn-Ni alloy and Zn-Ni-nano-TiO_2 composite coatings electrodeposited from ammonium citrate baths

This study focuses on the deposition of Zn-Ni alloy and Zn-Ni-nanoTiO_2 films to enhance an anti-corrosion performance and mechanical properties of the coated samples. The polarization result revealed that stable citrate bath helped to deposit uniform coating with decreased hydrogen evolution reaction (HER). The least I_{corr} values and small grain or crystal size, compactness and homogeneous texture exhibited better anti-corrosion properties. The electrochemical and corrosion behaviour of coatings are concluded as follows:

1. The potentiodynamic polarization results reveal that the Zn-Ni-0.0033 mol/l of TiO_2 coating deposited from citrate bath possesses a lower I_{corr} value and more positive corrosion potential than the other coated samples. The least I_{corr} is due to the stable citrate bath Zn-Ni coated samples with decreased HER which exhibited uniform and higher corrosion resistance and the SEM images showed the formation of denser and more uniform coating.
2. The crystalline phase texture of the Zn-Ni alloy deposits from citrate bath has the maximum intensity of γ-phase (γ-$NiZn_3$) (815), γ-Ni_2Zn_{11} (330) (631) and Ni_3Zn_{22} plane orientation lead to increase the performance of corrosion resistance of the coating.
3. The impedance measurement of the Zn-Ni-0.0033 mol/l of TiO_2 coating deposited from citrate bath increase impedance modulus than the other coated samples. The excellent

coating with the maximum impedance modulus is Zn-Ni-0.0033 mol/l of TiO_2, and it exhibited compact and robust corrosion products at after 48 hours' immersion test.

4. The electrical circuit data showed that the Zn-Ni-nanoTiO_2 composite coating deposited from 0.033 mol/l of TiO_2 at 12 hours exhibit higher R_1 and R_{ct} value than other coatings. The incorporation of TiO_2 and complexing agent in a bath is an effective process to corrosion resistance and mechanical properties of the coating.
5. Increasing the immersion time lead to increase the composition of simonkolleite and zinc oxide (ZnO). The corrosion resistance performance decreased at 12 hours of immersion time due to the formation of the maximum amount of ZnO. This is also accompanied by the growth of the porous corrosion products. Furthermore, the corrosion resistance increases at 24 hours and 48 h hours, due to the disposition of robust and compact corrosion product layers.

8.5 Influence of Chloride and pH on the Pitting-Mechanism of Zn-Ni alloy Coating in Sodium Chloride Solutions

In this study, electrochemical and morphological analyses of pitting corrosion have been implemented on Zn-Ni alloy coated samples. To investigate the pitting corrosion behavior of Zn-Ni alloy coating on mild steel. In this paper, the effects of chloride and pH on the pitting-mechanism of Zn-Ni alloy coatings in NaCl solutions have been investigated and analyzed. Optical microscope and scanning electron microscope (SEM) were used to measure the pits depth/diameter and visualization of pits behavior. To achieve pitting corrosion mechanism and corrosion behaviour of the Zn-Ni alloy coating at different pH and chloride concentration are concluded as follows:

1. The important deposition factors and levels influencing the pitting corrosion activity of the Zn-Ni alloy deposits are NaCl concentration and pH of the electrolyte. The pit depth of samples immersed in acidic medium (pH = 3.0) and low NaCl concentration (0.35

mol/l) have around 9 μm whereas, for samples in neutral medium (pH = 7.0) and low NaCl concentration (0.35 mol/l) have around 3 μm. In this way, the horizontal and vertical propagation process of pits in acidic solution is demonstrated.

2. The samples immersed at 0.35 mol/l of NaCl and pH = 3.0 solution has higher E_{pit} values. However, the E_{pit} in the neutral solution (pH = 7.0) decline very slightly. When the Cl^- concentration is increased from 0.35 mol/l to 0.5 mol/l lead to abruptly increase the anodic corrosion current due to the attack of Cl^- ions increases the corrosion rate.
3. The pitting corrosion in neutral solution as confirmed through SEM images is persistence with the high impedance in the Nyquist plots with low Cl^- concentrations. The electrochemical results and SEM images show that the passivity of Zn-Ni alloy from low to high NaCl concentration and neutral to acidic pH solutions are easily damaged and pitting corrosion is initiated in the presence of acidic solution and higher Cl^- ions.

Future Recommendation

1. Comparing the mechanical and electrochemical properties of the different Zn-Ni composite coatings.
2. Understand the fact of the phase formation, grain size and the other microstructure parameters to find the relationship between microstructure parameters for future composite film design/tailoring.

   To develop stable commercial plating bath for uniform deposits to produce high quality composite films.